

Aus dem Walther-Straub-Institut  
für Pharmakologie und Toxikologie  
der Ludwig-Maximilians-Universität München

Vorstand Prof. Dr. med. Thomas Gudermann

Etablierung und Implementierung eines  
elektrophysiologischen Screening Assays zur Untersuchung  
der Wirkung rezeptoraktiver Substanzen an nikotinischen  
Acetylcholinrezeptoren

- Therapeutika bei Organophosphatvergiftungen -

Establishment and implementation of an  
electrophysiological screening assay for the assessment of  
the effect of receptor-active substances on nicotinic  
acetylcholine receptors

- Therapeutics in organophosphate poisoning -

Dissertation  
zum Erwerb des Doktorgrades der Humanbiologie  
der Medizinischen Fakultät der  
Ludwig-Maximilians-Universität zu München

vorgelegt von  
Corinna Melanie Scheffel

aus

München

2018



Aus dem Walther-Straub-Institut  
für Pharmakologie und Toxikologie  
der Ludwig-Maximilians-Universität München

Vorstand Prof. Dr. med. Thomas Gudermann

Etablierung und Implementierung eines  
elektrophysiologischen Screening Assays zur Untersuchung  
der Wirkung rezeptoraktiver Substanzen an nikotinischen  
Acetylcholinrezeptoren

- Therapeutika bei Organophosphatvergiftungen -

Establishment and implementation of an  
electrophysiological screening assay for the assessment of  
the effect of receptor-active substances on nicotinic  
acetylcholine receptors

- Therapeutics in organophosphate poisoning -

Dissertation  
zum Erwerb des Doktorgrades der Humanbiologie  
der Medizinischen Fakultät der  
Ludwig-Maximilians-Universität zu München

vorgelegt von  
Corinna Melanie Scheffel

aus

München

2018

Mit Genehmigung der Medizinischen Fakultät  
der Universität München

Berichterstatter:	Prof. Dr. Franz Worek
Mitberichterstatter:	Prof. Dr. Bernd Sutor Prof. Dr. Ludwig von Meyer Prof. Dr. Stefan Engelhardt
Mitbetreuung durch den promovierten Mitarbeiter:	Dr. Thomas Seeger
Dekan:	Prof. Dr. med. dent. Reinhard Hickel

Tag der mündlichen Prüfung: 11.Dezember 2018

## Abstract

The primary toxic action of organophosphorus (OP) compounds including pesticides and highly toxic nerve agents is the irreversible inhibition of acetylcholinesterase (AChE), impairing hydrolysis of acetylcholine (ACh). Accumulation of ACh within cholinergic synapses gives rise to overstimulation of nicotinic (nAChR) and muscarinic (mAChR) receptors causing a cholinergic syndrome and finally leads to respiratory arrest due to paralysis of the respiratory muscles and the central respiratory system. Medical countermeasure of OP poisoning comprises reactivation of inhibited AChE by mono- or bisquaternary pyridinium oximes and competitive antagonism at mAChR by atropine. Thereby, the currently available pharmacotherapy mitigates only muscarinic and does not directly target nicotinic effects. Accordingly, direct intervention at nAChR may be a promising generic approach against OP intoxications to complement oxime-therapy. The need of such a therapeutic strategy is urged in cases of nerve agents resistant to reactivation by oximes (e.g. soman, tabun) and in case of suicidal high load pesticide poisoning as no broad-spectrum oxime has been identified yet. In this context, compounds acting as positive allosteric modulators (PAM) that reduce or reverse nAChR desensitization became of increasing therapeutic relevance wherein the bispyridinium (BP) non-oxime MB327 found to mediate a positive therapeutic effect *in vitro* although not to a sufficiently high degree was used as a lead structure for the synthesis of a series of structural BP analogues.

In this study, functional activities of these BP, so called PTM compounds, were identified by establishing a whole-cell patch clamp method performed under voltage-clamping conditions applied with planar electrodes in an automatic system (Nanion Technologies GmbH, Munich) to record human  $\alpha 7$ -nAChR (h $\alpha 7$ -nAChR) stably expressed in a CHO-K1 cell line (CHO/RIC-3/h $\alpha 7$ -nAChR). To this end, elucidation of basic electrophysiological characteristics of two mammalian cell lines, GH<sub>4</sub>C<sub>1</sub> and CHO-K1 for use as host cell system of h $\alpha 7$ -nAChR showed that CHO-K1 cell line was well suited verified by its low voltage- and ligand-gated conductance. In contrast, moderate voltage-gated conductance detected in GH<sub>4</sub>C<sub>1</sub> may cause interference in voltage clamped screening method for the investigation of nAChR function. The seal success rate was optimized for the establishment of an efficient screening method of h $\alpha 7$ -nAChR function in CHO-K1/RIC-3/h $\alpha 7$ -nAChR cells by adjusting cellular parameters and settings including adjustment of the pressure applied to capture and to hold the cells, cell passage range used and addition of a Ca<sup>2+</sup> rich solution serving as a “seal enhancer” prior to measurement. Moreover, investigation of flow rate of compound solution application revealed most pronounced nicotine-induced current signal intensity at a flow rate of 171  $\mu$ l/s exposing the cells for 233 ms to a test solution. Considering recovery of receptors from desensitization, a time interval of 3 min and two washing steps between the next test solution application was required to ensure full regeneration of the desensitized state of h $\alpha 7$ -nAChR into a conductible state.

Fast kinetics of  $\alpha 7$ -nAChR activation demonstrated biphasic dose response curves ascending at low and descending at high agonist concentrations revealing the conformational states of receptors including activation at low, inactivation and desensitization of  $\alpha 7$ -nAChR at high agonist concentrations. Positive allosteric modulation of agonist-induced responses by PNU-120596 yielded an amplification of nicotine-induced peak current amplitude as well as a prolonged duration of the evoked response representing an elongated mean open channel conformation. Current-voltage relations of CHO-K1/RIC-3/ $\alpha 7$ -nAChR cells under control and upon agonist-induced activation and allosteric modulation by PNU-120596 as well as specific  $\alpha 7$ -nAChR antagonization with methyllycaconitine verified specific  $\alpha 7$ -nAChR expression and electrophysiological properties with respect to selective ion permeability of  $\alpha 7$ -nAChR to  $\text{Na}^+$  and  $\text{Ca}^{2+}$ . In the following screening method, the effect of BP compounds on  $\alpha 7$ -nAChR activation was investigated to identify structure-activity relations and revealed two different intrinsic activities of BP compounds on  $\alpha 7$ -nAChR activation comprising a potentiation of  $\alpha 7$ -nAChR activation by MB327 and five symmetrical PTM compounds bearing a *tert*-butyl or a methoxy-group at 2-,3- and 4-position of both pyridinium rings. In contrast, residual PTM compounds including those with a dimethylamino-group at 3-position, isopropyl-group at 2-,3- and 4-position or more than one substituted group at both pyridinium rings inhibited nAChR function. Elucidation of structure-activity yielded that potentiation was most pronounced with MB327 and was dependent on the position and chemical structure of substituted groups as BP compounds carrying a *tert*-butyl group or a methoxy-group showed a higher amplification of current response with a substitution at position 3 and 4 compared to position 2. By corresponding activity-relations of BP compounds, MB327 and PTM compounds bearing a *tert*-butyl or a methoxy-group were able to restore desensitized  $\alpha 7$ -nAChR. Because these compounds did not activate  $\alpha 7$ -nAChR by themselves without agonist and current response profile of activated and desensitized nAChR reflected the one obtained with the representative type II PAM PNU-120596, the underlying mechanism of action by these compounds was indicative for a type II allosteric mechanism able to prevent and recover receptors from desensitization. In summary, this study served to develop a stable screening method to identify structural requirements of test compounds to prevent and reverse  $\alpha 7$ -nAChR desensitization to unravel promising lead structures capable to convey a positive pharmacological effect after OP poisoning.

## Zusammenfassung

Die primäre Wirkung von phosphororganischen (OP) Verbindungen, zu denen Pestizide und Nervenkampfstoffe gehören, beruht auf der irreversiblen Hemmung der Acetylcholinesterase (AChE) sodass die katalytische Hydrolyse von Acetylcholin (ACh) ausbleibt. ACh akkumuliert unkontrolliert im synaptischen Spalt und verursacht infolge einer Überstimulation und anschließender Desensitisierung nikotinischer (nAChR) Rezeptoren und Überstimulation muskarinischer (mAChR) Rezeptoren eine cholinerge Krise welche unbehandelt zum Tod durch zentrale und periphere Atemlähmung führen kann. Die derzeitige Standardtherapie umfasst die Reaktivierung OP-gehemmter AChE durch mono- oder bisquaternäre Pyridiniumoxime und kompetitive Antagonisierung von mAChR durch Atropin. Dabei werden durch die derzeitig verfügbare Pharmakotherapie ausschließlich muskarinische Symptome behandelt wohingegen nikotinerge Effekte am nAChR nicht direkt adressiert werden. Dementsprechend stellt die direkte Intervention an nAChR einen innovativen und generischen therapeutischen Ansatz gegen OP Verbindungen dar, um die Oxim-Therapie zu ergänzen. Da es bisher noch kein Breitband-Oxim gibt und insbesondere bei Vergiftungen mit Soman oder Tabun die Reaktivierung mit Oxim nicht ausreichend ist, wird die Notwendigkeit einer solchen alternativen Therapiestrategie deutlich. Daher sind Verbindungen, die als positive allosterische Modulatoren (PAM) wirken und die Desensitisierung der nAChR vorbeugen bzw. diese wieder aufheben können von großer therapeutischer Bedeutung. Die Bispyridinium (BP) Verbindung MB327, welche einen positiven therapeutischen Effekt vermittelte, aber keine ausreichend hohe Effektivität zeigte, diente in dieser Studie als Leitstruktur für die Synthese einer Reihe strukturell analoger BP-Verbindungen (PTM Verbindungen). In dieser Arbeit wurde die Wirkung der sogenannten PTM Verbindungen auf die Funktion der nAChR mittels der Etablierung eines automatisierten Ganzzell-Patchclamp-Verfahrens an CHO-K1-Zellen untersucht, die mit dem humanen  $\alpha 7$ -nAChR ( $h\alpha 7$ -nAChR) stabil transfiziert wurden (CHO/RIC-3/ $h\alpha 7$ -nAChR). Die CHO-K1 Zelllinie wurde anstelle der GH<sub>4</sub>C<sub>1</sub> Zelllinie für die stabile Transfektion von  $h\alpha 7$ -nAChR verwendet, da grundlegende elektrophysiologische Eigenschaften der Membranen beider Säugerzelllinien zeigten, dass die CHO-K1 Zelllinie aufgrund der niedrigen spannungs- und ligandengesteuerten Leitfähigkeit gut geeignet war im Gegensatz zur GH<sub>4</sub>C<sub>1</sub> Zelllinie, welche eine gemäßigte spannungsgesteuerte Leitfähigkeit besaß, die die Untersuchung der nAChR Funktion mit der Patch Clamp Methode stören könnte. Die Erfolgsrate der Sealbildung wurde für die Etablierung eines effizienten Screening-Verfahrens optimiert, indem die zellulären Parameter und Einstellungen angepasst wurden, einschließlich der Einstellung des Ansaugdrucks der Zelle und des Drucks auf die Zelle während der Messung, der Festlegung des Bereichs der Zellpassagen für die Messung sowie die zusätzliche Verwendung einer Ca<sup>2+</sup>-reichen Lösung, die dazu diente die Sealbildung unmittelbar vor der Messung zu verstärken. Zudem wurde die Applikation der Testlösung mit einer

Durchflussrate von 171  $\mu\text{l/s}$  zugegeben sodass die Zellen für 233 ms gegenüber der Testlösung exponiert wurden. Im Falle der Desensitisierung von nAChR waren ein Zeitintervall von 3 Minuten und zwei Waschschriffe erforderlich, um vor der nächsten Applikation der Testlösung eine vollständige Regeneration des leitfähigen Zustands der Rezeptoren zu gewährleisten.

Die schnell verlaufende Reaktionskinetik der nAChR Aktivierung zeigte einen biphasischen Verlauf der Dosis-Wirkungsbeziehungen mit verschiedenen klassischen Agonisten, sodass sich bei niedrigen Agonist-Konzentrationen die Aktivierung erhöhte und bei hohen Konzentrationen die Aktivierung gehemmt wurde. Dadurch wurden die verschiedenen Konformationszustände der Rezeptoren durch klassische orthosterische Agonisten aufgezeigt, welche die  $\alpha 7$ -nAChR bei niedrigen Konzentrationen aktivierten und bei hohen Konzentrationen die Inaktivierung bzw. Desensitisierung induzierten. Die positiv allosterische Modulation von Agonisten-induzierter Aktivierung durch PNU-120596 ergab eine Verstärkung der Agonist-induzierten Stromamplitude sowie eine verlängerte Dauer der Stromantwort, welche eine Verlängerung der durchschnittlichen Öffnungsdauer der  $\alpha 7$ -nAChR anzeigte. Durch Strom-Spannungs-Beziehungen von CHO-K1/RIC-3/ $\alpha 7$ -nAChR-Zellen ohne und mit Agonist-induzierter Stimulierung und allosterischer Modulation durch PNU-120596, sowie spezifische  $\alpha 7$ -nAChR Antagonisierung mit Methylllycaconitin konnte die spezifische  $\alpha 7$ -nAChR Expression und elektrophysiologische Eigenschaften bezüglich der selektiven Ionenpermeabilität der  $\alpha 7$ -nAChR für  $\text{Na}^+$  und  $\text{Ca}^{2+}$  nachgewiesen werden.

Bei der folgenden Screening-Methode wurde die Wirkung von BP-Verbindungen auf die nAChR-Aktivierung untersucht, um Struktur-Wirkungs-Beziehungen zu identifizieren. Dabei wurden durch BP-Verbindungen zwei verschiedene intrinsische Aktivitäten auf die AChR-Aktivierung aufgezeigt. Die erste umfasste die Potenzierung der nAChR-Aktivierung durch PNU-120596, MB327 und fünf symmetrische PTM-Verbindungen mit einer *tert*-Butyl oder einer Methoxy Gruppe an der Position 2, 3 und 4 beider Pyridiniumringe. Die zweite zeigte dass die PTM-Verbindungen mit einer Dimethylaminogruppe an der Position 3, einer Isopropylgruppe an der Position 2, 3 und 4 oder mehr als einer substituierten Gruppe an beiden Pyridiniumringen die nAChR-Aktivierung inhibierten.

Die Bestimmung von Struktur-Aktivitäts-Beziehungen ergab, dass die Potenzierung der nAChR-Aktivierung von der Position und der chemischen Struktur und der substituierten Gruppe der Testsubstanz abhängt, da BP-Verbindungen, die eine *tert*-Butyl-Gruppe oder eine Methoxy-Gruppe an der Position 3 und 4 tragen, eine höhere Amplifikation der Stromantwort zeigten als eine solche Substitution an der Position 2. Untersuchungen zur Wiederherstellung der Rezeptorfunktion nach Desensitisierung zeigten, dass diese BP-Verbindungen die Desensitisierung aufhoben und dabei vergleichbare Struktur-Aktivitäts-Beziehungen in ihrer Effektivität wie zuvor bei den Aktivierungsprofilen zeigten. Stromantwortprofile der nAChR-Aktivierung sowie der nAChR Desensitisierung unter Einfluss der BP-Verbindungen waren weniger ausgeprägt aber analog zu PNU-



1204596 Stromantwortprofilen, einem bekannten PAM, und die Rezeptoren waren alleine durch BP-Verbindungen in Abwesenheit des Agonisten Nikotin nicht aktivierbar. Demnach war die zugrundeliegende Wirkungsweise der BP-Verbindungen durch eine Typ II allosterische Wechselwirkung mit den Rezeptoren naheliegend, die durch eine Vorbeugung sowie der Aufhebung der nAChR Desensitisierung gekennzeichnet ist.

Zusammenfassend konnte in dieser Studie eine stabile Screening-Methode entwickelt werden, um strukturelle Anforderungen an Testverbindungen zu identifizieren, die die nAChR-Desensitisierung vorbeugen und aufheben können, um vielversprechende Leit-Strukturen zu identifizieren, die eine positive pharmakologische Wirkung nach OP-Vergiftung vermitteln um diese effizient behandeln zu können.

## Eidesstattliche Versicherung

Ich erkläre hiermit an Eides statt, dass ich die vorliegende Dissertation mit dem Thema „Etablierung und Implementierung eines elektrophysiologischen Screening Assays zur Untersuchung der Wirkung rezeptoraktiver Substanzen an nikotinischen Acetylcholinrezeptoren - Therapeutika bei Organophosphatvergiftungen - “ selbständig verfasst, mich außer der angegebenen keiner weiteren Hilfsmittel bedient und alle Erkenntnisse, die aus dem Schrifttum ganz oder annähernd übernommen sind, als solche kenntlich gemacht und nach ihrer Herkunft unter Bezeichnung der Fundstelle einzeln nachgewiesen habe.

Ich erkläre des Weiteren, dass die hier vorgelegte Dissertation nicht in gleicher oder in ähnlicher Form bei einer anderen Stelle zur Erlangung eines akademischen Grades eingereicht wurde.

München, den 15.01.2018

---

(Corinna M. Scheffel)

## Preface

The present thesis was conducted during my work as a research assistant at the Bundeswehr Institute of Pharmacology and Toxicology in collaboration with the Department of Pharmacy at the LMU in Munich under the supervision of Prof. Dr. Franz Worek. My sincere gratitude goes to him for his great supervision, guidance and continuous support in all aspects with his immense experience and invaluable advice throughout, and for evaluation and examination of my thesis. He gave me the freedom to pursue my own ideas and created an excellent research environment. His support has significantly contributed to the success of my work.

I am very thankful to Prof. Dr. Horst Thiermann for giving me the opportunity to conduct the project of my dissertation in a very interesting environment at the Bundeswehr Institute of Pharmacology and Toxicology. I feel grateful for having had the opportunity to work on such an interesting and challenging project.

I would like to thank Prof. Dr. Klaus Wanner as the Chair of Pharmaceutical/Medicinal Chemistry of the Department of Pharmacy of the LMU and Karin Niessen as the project lead of the collaborative project for the opportunity to carry out my projects for this PhD thesis in an inspiring and productive cooperation and working environment. I am also very grateful to Katharina Heimberger for her assistance and administrative support throughout.

I owe special thanks to Dr. Thomas Seeger as my direct supervisor for his permanent support in everyday laboratory work and numerous scientific discussions throughout this project. This thesis would not have been possible without his long experience and great in-depth know-how about electrophysiology and his great scientific input and advice have been invaluable.

In addition, I am very grateful to Christoph Wübekke, Sarah Kirchner and Natalie Boos for excellent technical assistance, help and support as well as great working atmosphere over the last years.

Moreover, I wish to express my gratitude to my colleagues and friends for the great working atmosphere, valuable discussions, sport activities, abundant help and support in all situations: Amelie Tsoutsouloupoulos, Andreas Kranawetvogl, Andreas Wosar, Anne Bierwisch, Cathi Schäfers, Georg Menacher, Isabel Weimer, Jens von der Wellen, Markus Siegert, Robert Giesche, Simon Lang, Simone Rothmiller, Tamara Hannig, Tilo Kliemt, and Wolfgang Schmeißer.

Special gratitude goes to my family, and in particular, I deeply thank Jan Clauberg for his huge support throughout, continuous patience, encouragement and faith in me.

*Corinna Scheffel*

# Publications

## A. Publikationen:

1. Scheffel C, Niessen KV, Rappenglück S, Thiermann H, Worek F, Wanner KT, Seeger T.  
Electrophysiological investigation of the effect of structurally different bispyridinium non-oximes on human  $\alpha 7$  nicotinic acetylcholine receptor activity – an *in vitro* structure-activity analysis. Toxicology Letters. Accepted 2017; in press; DOI: 10.1016/j.toxlet.2017.11.025.
2. Scheffel C, Niessen KV, Rappenglück S, Thiermann H, Worek F, Wanner KT, Seeger T.  
Counteracting desensitization of human  $\alpha 7$ -nicotinic acetylcholine receptors with bispyridinium compounds as an approach against organophosphate poisoning. Toxicology Letters. Accepted 2017; in press; DOI: 10.1016/j.toxlet.2017.12.005.
3. Scheffel, C; Thiermann, H.; Worek, F.  
Effect of reversible ligands on oxime-induced reactivation of sarin- and cyclosarin-inhibited human acetylcholinesterase. Toxicology Letters. 2015; 232: 557-565;  
DOI: 10.1016/j.toxlet.2014.12.009.

Folgende der oben genannten Publikationen sind als Teile der Doktorarbeit veröffentlicht: A1, A2.

## B. Abstracts:

1. Scheffel, C.; Rappenglück, S.; Niessen, K.V.; Worek, F.; Thiermann, H.; Wanner, K.T.; Seeger, T.  
Electrophysiological drug screening of bispyridinium-non-oxime-compounds on human nicotinic  $\alpha 7$  acetylcholine receptors – an alternative approach for the treatment of nerve agent poisoning. Abstracts of the 82<sup>nd</sup> Annual Meeting of the German Society for Experimental and Clinical Pharmacology and Toxicology (DGPT). Naunyn-Schmiedeberg's Arch Pharmacol. 2016; 389: 42.
2. Scheffel, C.; Niessen, K.V.; Rappenglück, S.; Worek, F.; Thiermann, H.; Wanner, K.T.; Seeger, T.  
Effect of biypyridinium compounds on the activity of human  $\alpha 7$  acetylcholine receptors using an automated patch clamp system. Abstracts of the 83<sup>rd</sup> Annual Meeting of the German Society for Experimental and Clinical Pharmacology and Toxicology (DGPT). Naunyn-Schmiedeberg's Arch Pharmacol. 2017; 390: 42.

# Content

Abstract .....	iii
Zusammenfassung.....	v
Publications .....	x
List of Figures.....	xiii
List of Tables.....	xv
Abbreviations .....	xvii
1. Introduction.....	19
1.1. Organophosphorus compounds – general background.....	19
1.2. Classification and toxicokinetic aspects of organophosphorus compounds.....	21
1.3. Molecular mechanisms of organophosphorus compounds.....	22
1.4. Toxicological signs and symptoms of organophosphorus compounds.....	26
1.5. Current therapeutic regimen against organophosphate poisoning.....	30
1.6. Novel medical countermeasures against organophosphate poisoning .....	32
1.6.1 Novel oximes .....	32
1.6.2 Catalytic scavengers .....	33
1.7. Nicotinic receptors as targets for nerve agent therapy .....	34
1.7.1 Potential benefits .....	34
1.7.2 Nicotinic receptors .....	35
1.7.3 Ligands, allosteric transitions and implications in organophosphate poisoning .....	38
1.7.4 Preliminary work and state of the art .....	42
1.8. Aim of the present subject matter .....	44
2. Materials & Methods .....	47
2.1. Devices and supplies .....	47
2.2. Chemicals and reagents.....	49
2.3. Cell culture.....	56
2.4. Patch clamp technique .....	61
2.4.1 Theoretical background – ionic theory.....	61
2.4.2 Basic principle of the patch clamp technique .....	64
2.4.3 Automated planar patch clamp.....	66
2.4.4 Current- versus voltage-clamp mode.....	70
2.4.5 Cell handling for patch clamp experiments.....	71
2.4.6 Determination of the resting membrane potential .....	72
2.4.7 Seal success rate and current signal.....	72
2.4.8 Assessment of voltage-activated currents .....	75

2.4.9	Assessment of non-voltage-activated currents.....	76
2.4.10	Investigation of the effect of bispyridinium compounds on nAChR function.....	77
2.5	Data analysis.....	79
3.	Results .....	81
3.1.	Transmembrane potentials of GH <sub>4</sub> C <sub>1</sub> and CHO-K1 cells .....	81
3.2	Current-voltage relationships of GH <sub>4</sub> C <sub>1</sub> and CHO-K1 cells.....	81
3.3	Assessment of endogenous ligand-gated ion channels of GH <sub>4</sub> C <sub>1</sub> and CHO-K1 cells .....	87
3.4	Optimization of seal success rate and current signal .....	88
3.5	Activation, desensitization and modulation of human $\alpha 7$ -nAChR .....	95
3.6	Current-voltage relations of CHO/RIC-3/h $\alpha 7$ -nAChR cells and inhibition of human $\alpha 7$ -nAChR 99	
3.7	Structure-activity relations of bispyridinium compounds on nicotine-induced human $\alpha 7$ - nAChR activation .....	104
3.8	Effect of bispyridinium compounds on desensitization of human $\alpha 7$ -nAChR .....	110
4.	Discussion .....	115
4.1	Determination of the resting membrane potential of GH <sub>4</sub> C <sub>1</sub> and CHO-K1 cells .....	116
4.2	Assessment of voltage-gated and ligand-gated ion channels of GH <sub>4</sub> C <sub>1</sub> and CHO-K1 cells..	117
4.3	Establishment of a screening method for the investigation of human $\alpha 7$ -nAChR function	124
4.3.1	Seal success rate - cellular parameters and settings of making a seal.....	124
4.3.2	Current signal rate - Perfusion and application procedures .....	126
4.4	Conformational transitions and positive allosteric modulation of human $\alpha 7$ -nAChR.....	128
4.5	Electrophysiological characteristics of CHO/RIC-3/h $\alpha 7$ -nAChR cells .....	131
4.6	Effect of structurally different bispyridinium non-oximes on human $\alpha 7$ -nAChR function .	133
4.6.1	Structure-activity relations of bispyridinium compounds on activation of human $\alpha 7$ - nAChR	135
4.6.2	Recovery from desensitization of h $\alpha 7$ -nAChR by bispyridinium compounds.....	137
5.	Conclusion and future considerations.....	141
	References.....	cxliii
	Curriculum vitae .....	clxvii

## List of Figures

<b>Figure 1:</b> Principal reactions of inhibition of AChE by an OP compound, subsequent aging and oxime-induced reactivation of OP-inhibited AChE.....	24
<b>Figure 2:</b> Overview of the cholinergic neurotransmission at the neuronal cholinergic synapse and at the endplate of the neuromuscular junction under physiological conditions and in the presence of OP compound. ....	27
<b>Figure 3 A-D:</b> Schematic representation of the nAChR structure, heterogeneity of subtypes and conformational transitions of nAChR.....	38
<b>Figure 4:</b> General structure of a BP compound and of lead structure MB327 .....	50
<b>Figure 5:</b> Mammalian expression vector pBudCE4.1 (4595 pb) (Invitrogen distributed by LifeTechnologies, Darmstadt, Germany) for stable transfection of $\alpha 7$ -nAChR subunit and h-RIC3 cDNA into CHO-K1 cells (CHO/RIC-3/ $\alpha 7$ -nAChR) and open reading frames of $\alpha 7$ -nAChR subunit and h-RIC3 cDNA.....	58
<b>Figure 6:</b> Diagram of electrochemical equilibrium and charge for $\text{Na}^+$ , $\text{K}^+$ , $\text{Cl}^-$ and proteins ( $\text{A}^-$ ) across the semipermeable cellular membrane (Image adapted from [2]).....	62
<b>Figure 7:</b> The automated planar patch clamp workstation of a Patchliner <sup>®</sup> using NPC-16 chips for parallel recordings in the cell-attached and whole-cell configuration .....	67
<b>Figure 8 A-C:</b> Current response to a command test pulse with a cell approaching the aperture in the recording chamber. ....	69
<b>Figure 9:</b> Schematic of a cross-section of one chip chamber showing the arrangements of solutions, chip and cell.....	70
<b>Figure 10:</b> Simplified schematic of a circuit of a patch clamp amplifier for a cell under whole-cell patch clamp recording configuration and electric properties of the cell membrane.....	71
<b>Figure 11 A-B:</b> Currents of whole-cell current-clamp recordings for the assessment of resting membrane potentials (RMP) of CHO-K1 (A) and $\text{GH}_4\text{C}_1$ (B) cells.....	81
<b>Figure 12 A-F:</b> Current-voltage relations of CHO-K1 and $\text{GH}_4\text{C}_1$ cells using 200 ms and 2 s voltage-ramp protocols.....	84
<b>Figure 13 A-G:</b> Current-voltage relation of $\text{GH}_4\text{C}_1$ and CHO-K1 using voltage-step protocols. A. Schematic representation of the voltage-clamp step protocol with voltage-step length of 200 ms and increments of 20 mV per step from -60 to + 60 mV .....	86
<b>Figure 14 A-D:</b> Concentration-response relation of $\text{GH}_4\text{C}_1$ and CHO-K1 using continuous voltage-clamp protocols upon activation with acetylcholine (A), carbamoylcholine (B) and nicotine in the absence (C) and presence of the positive allosteric modulator PNU-120596 (D) .....	87
<b>Figure 15 A-D:</b> Modification and adjustment of cellular parameters for optimization of seal success rate in stably transfected CHO/RIC-3/ $\alpha 7$ -nAChR cells including increase in gigaseal formation, stability of seals and reduction of run down on an automated patch clamp platform .....	90

<b>Figure 16 A-B:</b> Variation of flow rate of stacked compound application for investigation of current signal intensity by $\alpha 7$ -nAChR activation in stably transfected CHO/RIC-3/ $\alpha 7$ -nAChR cells .....	92
<b>Figure 17 A-B:</b> Variation of time and washing steps for the full recovery of $\alpha 7$ -nAChR function after desensitization in stably transfected CHO/RIC-3/ $\alpha 7$ -nAChR cells .....	94
<b>Figure 18:</b> Time rate of decay ( $\tau$ ) of agonist-induced and PNU-120596 modulated $\alpha 7$ -nAChR activation in stably transfected CHO/RIC-3/ $\alpha 7$ -nAChR cells .....	97
<b>Figure 19 A-L:</b> Concentration-response relations of $\alpha 7$ -nAChR activation, desensitization and positive allosteric modulation in stably transfected CHO/RIC-3/ $\alpha 7$ -nAChR cells .....	98
<b>Figure 20 A-G:</b> Current-voltage relations of $\alpha 7$ -nAChR activation by agonists and modulation by PNU-120596 in stably transfected CHO/RIC-3/ $\alpha 7$ -nAChR cells using voltage-step protocols.....	101
<b>Figure 21 A-C:</b> Inhibition of $\alpha 7$ -nAChR activation by agonists and modulation by PNU-120596 in stably transfected CHO/RIC-3/ $\alpha 7$ -nAChR cells with methyllycaconitine (MLA) .....	102
<b>Figure 22 A-H:</b> Concentration-response relations of nicotine-induced $\alpha 7$ -nAChR activation potentiated by PNU-120596, MB327, PTM0001, PTM0002, PTM0008, PTM0009 and PTM0010 in stably transfected CHO/RIC-3/ $\alpha 7$ -nAChR cells .....	105
<b>Figure 23 A-B:</b> Comparison of the effect of two different counterions of test compounds on nicotine-induced $\alpha 7$ -nAChR activation potentiated by 4- <i>tert</i> -butyl and 2- <i>tert</i> -butyl bispypyridinium compounds containing trifluoromethanesulfonate (Tfo <sup>-</sup> ) or iodide (I <sup>-</sup> ) .....	107
<b>Figure 24:</b> Time constants of decay ( $\tau$ ) of potentiation of nicotine induced $\alpha 7$ -nAChR activation by MB327 and by PTM compounds in the presence of 100 $\mu$ M nicotine in stably transfected CHO/RIC-3/ $\alpha 7$ -nAChR cells.....	107
<b>Figure 25 A-D:</b> Concentration-response relations of nicotine-induced $\alpha 7$ -nAChR activation inhibited by PTM compounds (PTM0003 - PTM0007, PTM0013 - PTM0022) in stably transfected CHO/RIC-3/ $\alpha 7$ -nAChR cells .....	108
<b>Figure 26 A-D:</b> Concentration-response relations of recovery of nicotine-induced $\alpha 7$ -nAChR desensitization by PNU-120596, MB327 and PTM compounds (PTM0001, PTM0002, PTM0003, PTM0008, PTM0009, PTM0010, PTM0013 and PTM0014) in stably transfected CHO/RIC-3/ $\alpha 7$ -nAChR cells.....	111
<b>Figure 27 A-C:</b> Time-dependent decay of current responses after recovery of nicotine induced $\alpha 7$ -nAChR desensitization by PNU-120596, MB327 and by PTM compounds (PTM0001, PTM0002, PTM0008, PTM0009, PTM0010) in the presence of 1 mM of nicotine recorded after 10, 50 and 100 ms of exposure.....	113
<b>Figure 28:</b> Schematic representation of the sequential undulatory passing test solution at a CHO/RIC-3/ $\alpha 7$ -nAChR cell (right) in the recording chamber of a planar patch clamp set-up (left).....	127



## List of Tables

<b>Table 1:</b> Signs and symptoms of OP poisoning at various sites in the body (adapted from [199]).....	29
<b>Table 2:</b> Distribution of nAChR subunit mRNA and protein expression found in the human central nervous system (adapted from [117, 148]) .....	36
<b>Table 3:</b> Laboratory devices, equipment and software .....	47
<b>Table 4:</b> Consumables and supplies .....	48
<b>Table 5:</b> Ligands of nAChR.....	50
<b>Table 6:</b> BP compounds referred to as PTM compounds .....	50
<b>Table 7:</b> Buffers and solutions for patch clamp experiments .....	53
<b>Table 8:</b> Reagents for cell culture and handling .....	54
<b>Table 9:</b> Elements of pBudCE4.1 (4595 bp) (Invitrogen, distributed by Life Technologies, Darmstadt, Germany).....	59
<b>Table 10:</b> Composition of cell culture media for different cell lines .....	60
<b>Table 11:</b> Variation of cellular parameters and settings for investigation of seal success rate including cell capture and hold pressure and cell passages used for patch clamp investigations .....	75
<b>Table 12:</b> Variation of flow rate of compound solution application and of time interval and washing steps between solution application for investigation of intensity of current signal .....	75
<b>Table 13:</b> Current-clamp recordings and voltage-clamp voltage-ramp pulse protocols (200 ms, 2 s) in CHO-K1 and GH <sub>4</sub> C <sub>1</sub> cells for the determination of basic electrophysiological characteristics .....	85
<b>Table 14:</b> Adjustment and modification of cellular parameters and settings of making a seal including capture and holding pressure, addition of seal enhancer, cell passages for optimization of seal success rate .....	91
<b>Table 15:</b> Relation of flow rate of test compound application (40 µl of 100 µM nicotine) to current response .....	93
<b>Table 16:</b> Influence of time interval and washing steps on the recovery of hα7-nAChR of CHO/RIC-3/hα7-nAChR cells .....	95
<b>Table 17:</b> Means ± SD (n = 8-10) of maximum current amplitudes relative to EC <sub>100</sub> of nicotine set to 1, half-maximum efficacy (EC <sub>50</sub> ), inhibitory potency (IC <sub>50</sub> ) and time constants of decay (τ) of agonist-induced hα7-nAChR activation and potentiation by PNU-120596 in the presence of agonist.....	99
<b>Table 18:</b> Voltage-clamp recordings including voltage-step protocol in CHO/RIC-3/hα7-nAChR cells and continuous recording at a holding potential at – 70 mV for the determination of basic electrophysiological characteristics.....	103

**Table 19:** Means  $\pm$  SD ( $n = 8 - 10$ ) of maximum current amplitude ( $I_{max}$ ) relative to  $EC_{100}$  of nicotine set to 1 and time constant of decay ( $\tau$ ) of 100  $\mu$ M nicotine-induced  $\alpha 7$ -nAChR activation potentiated by bispyridinium (BP) compounds including MB327 and PTM compounds ..... 108

**Table 20:** Means  $\pm$  SD ( $n = 8-10$ ) of half-maximum inhibitory potency ( $IC_{50}$ ) of  $\alpha 7$ -nAChR activation inhibited by bispyridinium PTM compounds ..... 109

**Table 21:** Means  $\pm$  SD ( $n = 8-10$ ) of half-maximum efficacy ( $EC_{50}$ ), maximal current amplitudes ( $I_{max}$ ), slope coefficients ( $n_H$ ) and current amplitudes at different time points (10, 50 and 100 ms) of nicotinic signal (control) and after recovery from desensitization by test compounds (PNU-120596, MB327, PTM0001, PTM0002, PTM0008, PTM0009 and PTM0010) were determined ..... 114

# Abbreviations

## A

A	acetate
ACh	acetylcholine
AChE	acetylcholinesterase
ATP	adenosine triphosphate
AUC	area under the curve

## B

BChE	butyrylcholinesterase
BGH	bovine growth hormone
BP	bispyridinium

## C

CaE	carboxylesterase
Ch	choline
ChAT	choline acetyltransferase
ChE	cholinesterase
CHO	chinese hamster ovary
CMV	cytomegalovirus
CNS	central nervous system
CoA	coenzyme A
CWC	Chemical Weapons Convention

## D

DMSO	dimethyl sulfoxide
------	--------------------

## E

EC <sub>50</sub>	half-maximum effective concentration
ECD	extracellular domain
EF-1 $\alpha$	elongation factor 1 $\alpha$
EGFR	epidermal growth factor

## F

FCS	foetal calf serum
-----	-------------------

## G

GA	tabun
GABA <sub>A</sub>	$\gamma$ -aminobutyric acid A
GB	sarin
GD	soman
GF	cyclosarin
GH	growth hormone

## H

5-HT <sub>3</sub>	5-hydroxytryptamine 3
HEPES	2-(4-(2-hydroxyethyl)-1- piperazinyl)-ethane sulfonic acid
h $\alpha$ 7-nAChR	human $\alpha$ 7- nicotinic acetylcholine receptor

## I

IMS	intermediate syndrome
I <sup>-</sup>	iodide
IC <sub>50</sub>	half-maximum inhibitory concentration
I <sub>max</sub>	maximum current amplitude
IS	Islamic State

## L

LGIC	ligand-gated ion channel
LC/MS	liquid chromatography/ mass spectrometry

**M**

mAChR	muscarinic acetylcholine receptor
MLA	methyllaconitine
MMB-4	methoxime

**N**

nAChR	nicotinic acetylcholine receptor
NAM	negative allosteric modulator
$n_H$	slope coefficient
NMDG	N-methyl-D-glucamine
NTE	neuropathy target esterase

**O**

OP	organophosphorus
OPA	operational amplifier
OPCW	Organization for the Prohibition of Chemical Weapons
OPIDN	organophosphate induced delayed neuropathy
ORF	open reading frame

**P**

PAM	positive allosteric modulator
2-PAM	pralidoxime
PBS	phosphate buffered saline
PNS	peripheral nervous system
PON-1	paraoxonase-1
POX	phosphyloxime
PTE	phosphotriesterase

**R**

$R_F$	feedback resistor
RIC-3	resistance to inhibitors of cholinesterase-3
RMP	resting membrane potential

**S**

SLUDGE	salivation, lacrimation, urination, defecation, gastric cramps, emesis
--------	--

**T**

$\tau$	time constant of decay
TEPP	tetraethyl pyrophosphate
TMB-4	trimedoxime
Tfo <sup>-</sup>	trifluoromethanesulfonate

**V**

$V_c$	command voltage
VGIC	voltage-gated ion channel
$V_m$	membrane potential
$V_{out}$	output voltage

**W**

WHO	World Health Organization
WWII	World War II

# 1. Introduction

## 1.1. Organophosphorus compounds – general background

*Discovered by accident, abandoned by the Chemical Weapon Convention (CWC), used until today –  
Organophosphorus (OP) compounds*

Throughout history, extremely toxic chemicals served as weapons used in wars, conflicts, terrorists', extremists' and dictators' activities [195, 231, 255, 319]. The earliest form of chemical warfare agents can be traced back to the use of so called "arrow poisons", natural toxins from plants or animals used to coat arrowheads [35, 126]. With advancements in science and chemistry, a wide variety of organophosphorus (OP) compounds were developed and left their footprints since their initial development as insecticides and later as highly toxic warfare nerve agents by the turn of the 21<sup>st</sup> century [55, 78, 126, 143, 178, 287]. Beginning in the mid-19<sup>th</sup> century, literally hundreds of OP-based compounds were synthesized most importantly O-ethyl *N,N*-diethyl phosphoramidocyanidate, a close tabun analogue described by the chemist Michaelis, and tetraethyl pyrophosphate (TEPP) described by the French chemist Jean Lassaigue and Philip De Clermont [78, 213]. Nearly 80 years later, in 1932, the history of nerve agents began when Lange and Krueger discovered that alkyl phosphorofluoridates evoke miosis and difficulty in breathing probably leading the German chemist Gerhard Schrader to isolate a series of fluorine-containing esters while he was engaged in his program to develop new insecticides at the conglomerate I.G. Farben [178, 287]. Besides commonly used insecticides parathion, O,O-diethyl S-(4-nitrophenyl) phosphate, and its oxygen analog paraoxon, O,O-diethyl O-(4-nitrophenyl) phosphate, Schrader identified, rather accidentally than by intention, a series of considerably more toxic esters denoted as G-type nerve agents comprising tabun (GA), O-ethyl *N,N*-dimethyl phosphoramidocyanidate, and later toward the end of world war II (WWII) sarin (GB), isopropyl methyl phosphonofluoridate (Figure 1) [36, 142, 143, 199, 205, 286, 287]. These agents showed very high mammalian toxicity and were thus unsuitable for the use as insecticides. However, prior to WWII, the German military recognized the military value of the discovered G-agents and their potential to be used as chemical warfare agents [345]. In the wake of war, the nerve agents like tabun were manufactured in quantity and weaponized in bombs, shells and rockets [199]. Large stocks held by Germany were discovered and captured by the Allies by the end of WWII [199]. In spite of fears to the contrary, no proven incidents of the use of chemical nerve agents in Europe was recorded during WWII [199, 348]. In the war period, the nerve agent soman (GD), pinacolyl methyl phosphonofluoridate, was discovered in the course of Dr. Richard Kuhn's work on the pharmacology of tabun and sarin at the German Army (Figure 1) [130]. Further, intense research on OP compounds

out of studies of putative insecticides continued in the post-war period and led to the development of the V-agents in 1952 long after studies on the G-agents were underway [26, 110, 323]. Toxicity of VX, *O*-ethyl *S*-2-*N,N*-diisopropylaminoethyl methyl phosphonothioate, was shown to be manifold greater than toxicity of nerve agents of the G-series (Figure 1) [72, 113, 300, 302]. It was not until the incidents in Japan during the 1990s that dissemination of these deadly V-agents was used in a moderate scale [344]. Nozaki reported that members of the Aum Shinrikyo religious cult were involved in an incident of VX poisoning of an attempted assassination of individuals in 1994 in Tokyo and, in the same year, this group disseminated vaporized sarin in Matsumoto city targeting judges in their apartments [231, 318, 343, 344]. Reportedly, the nerve agent sarin deployed in the Tokyo subway terrorist attack in March of 1995 was released by the same politico-religious group [223, 226, 231, 236, 319]. Further global incidents of exposure, such as of sarin deployed in Iraq in the conflict with Iran from 1980-1988 and also against its indigenous Kurdish population in 1988 caused mass casualties of death and thus have received increasing attention since the post-war period [131, 195, 239]. The awareness of the need to control the persistent threat coming from chemical warfare agents and the existence of stockpiles of military-grade chemical weapons, e.g., sarin and VX in the USA, soman and Russian VX (VR, *O*-isobutyl *S*-*N,N*-diethylaminoethyl methyl phosphonothioate), in the former Soviet Union culminated in the conclusion of the Chemical Weapons Convention (CWC) in April 1997 embracing the prohibition of the development, production, stockpiling and use of chemical weapons [200, 204, 244, 246, 320, 349]. According to the Organization for the Prohibition of Chemical Weapons (OPCW) verifying the implementation of the CWC program, 192 State Parties covering 98 % of the global population joined the Convention since its entry-into-force and declared to meet the obligations to disarm the world of chemical weapons [243]. This treaty is considered to be a very successful development with respect to the OPCW's vision to achieve complete disarmament of chemical weapons and prevent their re-emergence worldwide and thus to contribute to international security and stability [242, 245]. Every five years, the implementing body of the CWC is assessed and evaluated by the State Parties in a review conference and focuses on the necessity of the State Parties to respond to rapid advances in scientific and technological developments and to shifts in the international environment [241]. According to this, such changing needs may concern the management of treatment of a large number of casualties such as in the intentional incident conducted in the Ghouta district near Damascus in Syria on the 21<sup>st</sup> of August 2013 [255, 353]. Moreover, to further build on the success of the CWC in the attempt to prevent future use of chemical warfare agents, the need to respond to the growing terrorist activities that may use chemical warfare nerve agents throughout the world is urgent [255, 386]. Indeed, international news reports surmised that the terrorist group Islamic State (IS) may be capable of both acquiring and deploying chemical warfare agents supported by the fact that highly

technical information regarding chemical weapons and raw materials for making them are readily accessible [73, 359].

In contrast to the military intention to find OP compounds with enhanced human toxicity, the course of the proceeding intense research on OP compounds yielded also numerous compounds developed for use as pesticides, such as phosphorylated thiocholine derivatives [55, 87]. These OP pesticides were increasingly used as pest-control agents in the agricultural industry. However, some of them were found to possess mammalian toxicity exerted through the same mechanism as nerve agents and accounted for over 300.000 accidental, suicidal and homicidal case fatalities per year worldwide, especially in the third world [32, 125]. Although widely banned in many developing countries, OP pesticide consumption is still in the range of multiple kilotons per year and thus OP pesticide poisoning is still an ongoing major concern [32, 93, 125]. Since more than one hundred different OP compounds are active ingredients in pesticides formulations, the possibility of escalating exposure of OP pesticides most toxic to humans underscore the need to restrict the use of these pesticides as approached by the World Health Organization (WHO) [59, 90, 91, 270]. To conclude, it is indicated that effective medical treatment is mandatory when faced with the high risk of exposure to OP pesticides and even more important when faced with the possibility of further terrorist attacks at present [47, 336, 386].

## **1.2 Classification and toxicokinetic aspects of organophosphorus compounds**

All OP compounds are encountered as viscous, colorless liquids at moderate temperature and pressure [199]. They share a similar generic formula characterized by a tetrahedral phosphorus atom bonded to four different groups. These groups constitute ester-, amide- or thiol-derivatives of phosphoric, phosphonic or phosphinic acids, two alkyl substituents (R and R') and a leaving group (X: OR, SR, F, CN) with varying combinations of oxygen, carbon, sulfur, or nitrogen (Figure 1) [307, 366]. In contrast to nerve agents, classical OP pesticides like parathion and malathion comprise phosphorothioates which exert their toxicity after metabolization into their oxon analog via oxidative desulfuration [56, 87]. Compared to pesticides, OP nerve agents possess a unique phosphorus carbon bond and exert a significantly superior mammalian toxicity [199]. The OP nerve agents are generally divided into G- and V-agents [365]. The common G-agents are sarin, soman, cyclosarin (GF, O-cyclohexyl methyl fluorophosphonate) and tabun while within the V-agents VX is the most remarkable due to its extremely high toxicity [7, 68, 112]. The physicochemical properties of OP nerve agents are highly variable and essential for hazard assessment and determination for the mode of use [354].

G-agents produce a moderate to high vapor pressure and are highly volatile [255, 354]. Sarin is one of the most volatile and therefore dangerous agents as it can be effectively disseminated and inhaled [255, 354]. In contrast, due to the low volatility and vapor pressure, V-agents may persist for weeks in the environment [157]. According to their high lipophilicity, percutaneous absorption through skin penetration is perceived to be their main hazard rather than inhalation as in case for the non-persistent G-agents [199, 354]. In addition, most G-type and V-type nerve agents possess chirality at the phosphorus atom (P). The resulting stereoisomers differ in their toxicological properties [29, 30]. (±)-sarin, (±)-cyclosarin, (±)-tabun and (±)-VX have a stereogenic (chiral) phosphorus atom and consist of an equimolar mixture of P(-)- and P(+)- stereoisomers, whereas C(±)P(±)-soman, with two different chiral centers (at the phosphorus and carbon atom), exists as four isomers [29, 30]. Thereby, it is documented that the P(-)-isomers of sarin, tabun and VX as well as the C(-)P(-)-isomer of soman appear to be more toxic *in vivo* compared to their corresponding P(+)-isomers [29, 30]. Besides physicochemical properties, toxicokinetic and toxicodynamic properties are determining factors for the development of appropriate drug treatment [30, 386]. Investigations of distinct toxicokinetic properties after different routes of nerve agent exposure at several systemic, organ and tissue doses were conducted [30, 354, 386]. These studies deliver important indications for the assessment of the time period of acute intoxication by nerve agents which is in turn essential for the development of strategies for timely administration of antidotes [354]. For example, absorption and distribution of volatile G-agent exposure is very rapid leading to a fast onset of acute symptoms and the need of an immediate therapeutic intervention [354]. In contrast, percutaneous exposure to less volatile VX develops acute toxic effects more slowly and persists over a longer period of probably due to a subcutaneous depot from which the agent is distributed [97, 264, 355]. Thus, with respect to VX poisoning, therapeutic intervention has to be adapted to systemic signs of poisoning occurring after a time lag [216, 354]. For obvious reasons, toxicokinetic data of OP poisoned humans are very scarcely documented, but especially due to the high variability in toxicology of nerve agent poisoning, these data are of ultimate importance for the design of new pharmaco-therapeutical strategies against intoxication with nerve agents [132, 267, 301, 386].

### 1.3 Molecular mechanisms of organophosphorus compounds

In 1937, Eberhard Gross, while studying the OP compounds synthesized by Gerhard Schrader, detected that the pathophysiological major reaction of OP nerve agents is exerted through inhibition of the enzyme acetylcholinesterase (AChE). AChE (3.1.1.7) is a serine protease that belongs to the carboxylase family and plays a key role in the termination of transmission impulse at cholinergic synapses and the neuromuscular endplate by degradation of the neurotransmitter acetylcholine (ACh) [143, 181, 286,



287]. The monomer of AChE is an ellipsoidal protein found in various types of conducting tissue involved in cholinergic synaptic transmission, such as nerves and muscles, central and peripheral tissues, motor, sensory and cholinergic fibers. It is encoded by a single gene in humans and most other vertebrates and occurs in multiple molecular forms, such as homodimer or tetramer, either soluble or attached to the cell surface [180, 332]. Each monomer contains twelve  $\beta$ -sheets surrounded by 14  $\alpha$ -helices and has an active site located close to the bottom of a gorge-like fold penetrating halfway into the enzyme and widening out close to its base [317]. The active site is composed of two conserved domains: the esteratic subsite comprising the catalytic triad and the anionic subsite (Figure 1) [317]. Both sites are involved in the extremely rapid hydrolyzation of ACh into acetate and choline [249]. The anionic subsite, uncharged and lipophilic, consists of Trp<sup>84</sup>, Phe<sup>330</sup>, and Phe<sup>331</sup> and interacts with the positive quaternary amine of the choline moiety of ACh, whereas the orientation of the substrate that enters the gorge is mainly mediated by Trp<sup>84</sup> [259, 317]. As indicated by the name, the catalytic triad defined by the three amino acid residues Ser<sup>200</sup>, His<sup>440</sup>, and Glu<sup>327</sup> contains the catalytic machinery of the enzyme. It mediates the nucleophilic attack of the serine oxygen at the active site of the enzyme with the electrophilic carbon of the carboxyl ester of ACh resulting in the formation of an acyl-enzyme and free choline [19]. The native enzyme is subsequently regenerated by aqueous hydrolysis [69]. The liberated choline from the ACh destruction is taken up again by the presynaptic nerve and is recycled by a one-step reaction with acetyl coenzyme A through catalysis with choline acetyltransferase, to regenerate ACh (Figure 2) [69]. The regenerated ACh is stored into vesicles that take up ACh through an energy-dependent pump acidifying the vesicle (Figure 2) [234]. During neurotransmission, ACh is released into the synaptic cleft by fusion of the vesicles with the presynaptic membrane and transmits the signal from the nerve by binding to postsynaptic cholinergic ACh receptors (Figure 2) [11, 260, 331].



interactions of an OP compound with the active site of AChE comprising the esteratic subsite with the catalytic triad consisting of the amino residues serine, histidine and glutamate and the anionic subsite. After covalent binding of the phosphate group of the OP compound to the hydroxyl group of the serine residue, the leaving group (X) is released and thereby partially stabilizes the intermediate. The phosphorylated AChE is reactivated by a nucleophilic attack by an oxime via hydrolysis of the ester bond resulting in the formation of a phosphyl-AChE-oxime-conjugate and subsequently in a removal of the phosphyl residue from the intermediary complex which is transferred to the oxime ( $S_N2$  mechanism). Reaction products include the free enzyme and phosphyloxime (POX). Depending on the nature of the leaving group, the phosphorylated AChE may undergo dealkylation, a process comprising the loss of an alkyl group leading to the formation of a stable AChE-OP complex that is resistant to reactivation by oximes, such as in poisoning with soman ("aging"). Structures of general OP compounds and oximes are included. Figure was adapted from [353].

ACh was the first neurotransmitter discovered and is mainly present in the autonomous nervous system [259, 325]. Within the central nervous system (CNS), ACh is mainly found in interneurons and serves as the excitatory neurotransmitter in the preganglionic and parasympathetic neurons [259]. In the peripheral nervous system (PNS), ACh is the neurotransmitter at the neuromuscular junction between the motor nerve and the skeletal muscle [69]. Considering the abundant expression sites of ACh, the major involvement of ACh in numerous cholinergic pathways becomes clear so that it is indicative that impairment of ACh hydrolysis by AChE involves grave pathological consequences [260]. As proposed by Burgen, the main principle of irreversible AChE inhibition is the phosphorylation (denotes phosphorylation and phosphonylation; the latter being more common with nerve agents) of the hydroxyl group of serine in the active site of the enzyme (Figure 1) [50, 90]. Until today, the anticholinesterase toxicology of OP nerve agents is considered to account for their primary action of toxic mechanism [143, 170, 181, 199, 233, 365]. Since OP compounds function as substrate for AChE by interacting with its substrate binding domain, binding and subsequent hydrolyzation of ACh is prevented resulting in complete failure of AChE activity [11, 265]. Chemically, this reaction is conveyed by a nucleophilic attack ( $S_N2$  mechanism) of the hydroxyl group of the serine residue with the electrophilic phosphorus atom of the OP compound resulting in the formation of a transient intermediate complex (Figure 1) [11, 199]. This intermediate chemical transition state is stabilized via coupled proton transfer by the release of the leaving group (Figure 1) [11, 199]. As described for the reaction of ACh, the covalently bound phosphate group at the hydroxyl group of the serine residue is analogous to the acylated intermediate in substrate hydrolysis [11, 199, 332, 341].

In case of some G-agents, the OP-AChE complex may undergo a rapid secondary dealkylation of the phosphate group known as "aging", a time-dependent, post-inhibitory process causing severe

problems in clinical treatment (Figure 1) [29, 101, 214, 383]. The rate of aging varies depending on the nature of the inhibiting OP compound, in particular the chemical structure of the substituted alkoxy chain that is dealkylated [101, 293, 299, 383]. In this context, aging half-life rates of AChE-nerve agent adducts range from a few minutes for soman, which has a bulky branched chain promoting rapid aging, to many hours for tabun and VX allowing for a longer lasting period of therapeutic intervention [101, 293, 299, 383]. The mechanism of the dealkylating aging reaction involves cleaving of the alkoxy moieties from the central phosphorus atom of the OP compound (Figure 1) [218]. The remaining P-OH function of the alkylphosphonylated AChE will undergo deprotonation thus leaving a negatively charged phosphorus moiety that is stabilized by the organophosphoryl-AChE bond (Figure 1) [218].

#### **1.4 Toxicological signs and symptoms of organophosphorus compounds**

Toxicology of OP compounds has been extensively researched predominantly by referring to casualty reports of OP pesticide poisoning and by extrapolating animal data to human since cases of human exposure to chemical warfare agents are rare [199, 265]. The primary routes of nerve agents' exposure are inhalation and absorption through the skin and OP compounds exert their main toxic action by inhibiting AChE in the PNS and CNS [11, 29, 142]. Consequently, excessive amounts of the neurotransmitter ACh at the synaptic cleft lead to overstimulation of cholinergic receptors as well as depolarization blockage at cholinergic synapses and neuromuscular junctions resulting in diverse symptoms and signs involved in the cholinergic crisis (Figure 2) [11, 29, 142].

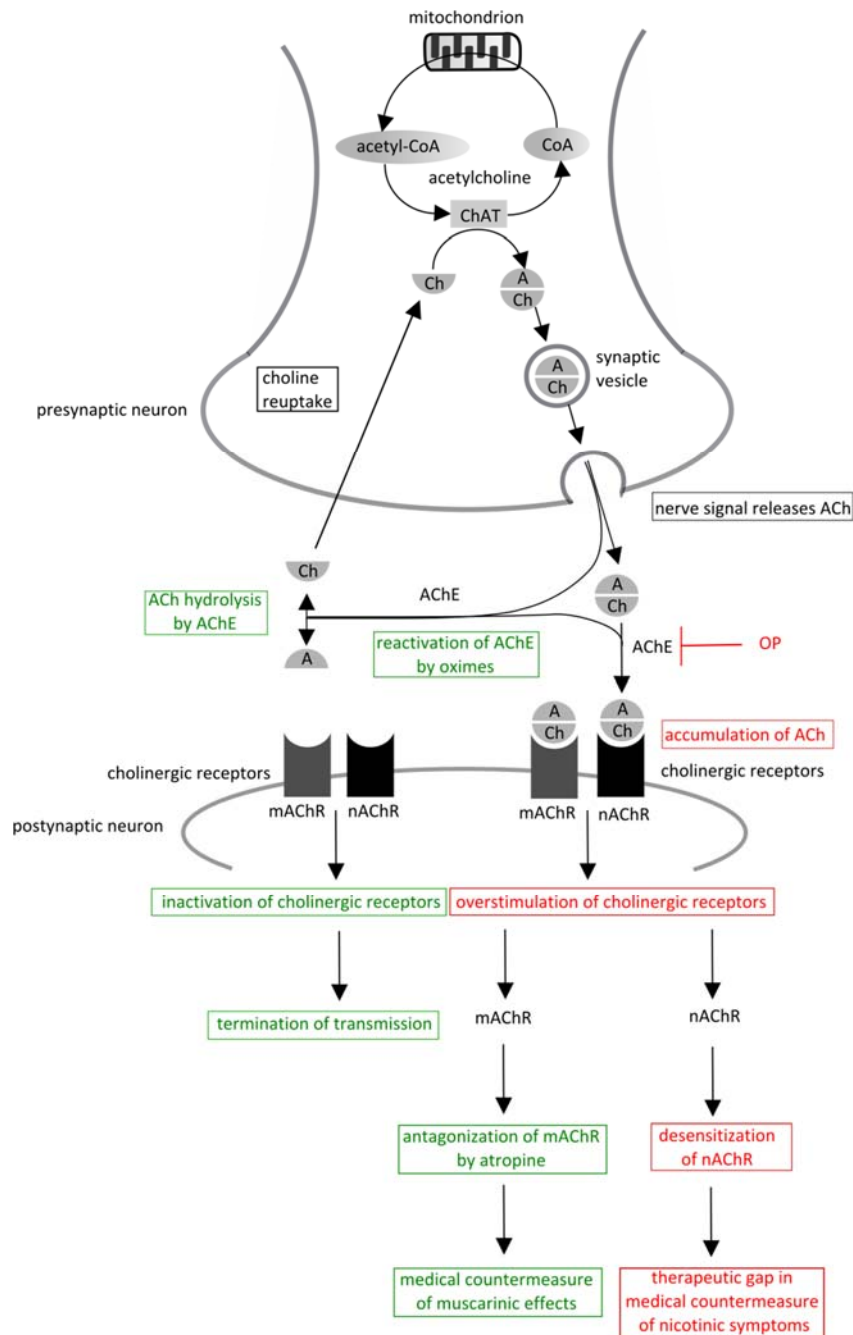


**Figure 2: Overview of the cholinergic neurotransmission at the neuronal cholinergic synapse and at the endplate of the neuromuscular junction under physiological conditions and in the presence of OP compound.** The nerve impulse is transmitted to the postsynaptic cell or effector (muscle) cell by release of the neurotransmitter acetylcholine (ACh) from the presynaptic membrane of the axon terminal by fusion of the synaptic vesicle containing ACh with the presynaptic membrane. In the synaptic cleft, ACh diffuses across the cleft and binds to and activates cholinergic receptors at the postsynaptic membrane including muscarinic (mAChR) and nicotinic acetylcholine receptors (nAChR), thereby causing depolarization of the postsynaptic cell. Under physiological conditions, ACh is hydrolyzed by the serine hydrolase acetylcholinesterase (AChE) into choline (Ch) and acetate (A) and thereby terminates the neuronal and neuromuscular transmission. Ch is transported back into the

axon terminal by a  $\text{Na}^+$ -dependent membrane choline transporter and ACh is regenerated from acetyl coenzyme A (CoA) and Ch through the catalytic action of the enzyme choline acetyltransferase (ChAT). In the presence of OP compound, AChE is irreversibly inhibited resulting in accumulation of ACh and overstimulation of mAChR and nAChR. Muscarinic effects are treated with atropine. Nicotinic effects involving initial overstimulation followed by desensitization which may lead to life endangering central and peripheral respiratory arrest can not be treated and leave a therapeutic gap.

Depending on the route of exposure, poison load, chemical nature and solubility of the OP compound, a wide range of toxic effects on muscle, glands and nerves is caused [4, 237, 254, 301]. The acute signs and symptoms of the cholinergic crisis occur within minutes to hours and have centered on (1) muscarinic, (2) nicotinic and (3) central manifestations (Table 1) [121, 142, 199, 249, 254, 332, 360]. Thereby, the most severe symptoms are provoked by desensitization of nAChR due to continued overstimulation which causes central and peripheral depression of the respiratory system if untreated [76, 142, 389]. In detail, the peripheral nicotinic effects of initial overstimulation are associated with skeletal muscle fasciculation and are followed by subsequent desensitizing neuromuscular blockade, causing weakness of the respiratory muscles and paralysis of the respiratory center (Table 1). Acute central symptoms deriving from nicotinic effects comprise restlessness, agitation, confusion and sometimes convulsions compromising airway and breathing, increasing aspiration risk and hypoxia (Table 1) [60, 254, 299, 360]. As suggested by a more complete clinical list of acute symptoms, respiratory failure, resulting from both diaphragm paralysis and failure of central respiratory drive ultimately accounts for the usual cause of death (Table 1) [199, 266]. Concerning muscarinic effects of this receptor-based classification, a common toxidrome of acute OP poisoning concerns the relevant glands and causes the peripheral SLUDGE (Salivation, Lacrimation, Urination, Defecation, Gastric cramps, Emesis) symptoms whereas muscarinic effects in the central nervous system causes confusion, coma and convulsions (Table 1) [254, 360]. Initially dominating muscarinic symptoms of salivation and bronchorrhea may give rise to life-threatening effects on the heart (bradycardia, hypotension) and may further cause drowsy patients to drown in their secretions [254, 360].

**Table 1:** Signs and symptoms of OP poisoning at various sites in the body (adapted from [199]).

cholinergic receptors				
muscarinic		nicotinic		central nervous system
target organ	signs & symptoms	target organ	signs & symptoms	signs & symptoms
<i>glands</i>		autonomic ganglia	sympathetic effects, including pallor, tachycardia, hypertension, weakness	giddiness, anxiety, restlessness, headache, tremor, dizziness, drowsiness, confusion, slurred speech, failure to concentrate, convulsions, ataxia, psychosis and respiratory depression
nasal mucosa	rhinorrhea			
bronchial mucosa	bronchorrhea			
sweat	sweating			
lachrymal	lachrymation			
salivary	salivation			
		skeletal muscle	twitching of fine muscles, hyperreflexia, fasciculations, muscle weakness, reduced tendinous reflexes, paralysis affecting diaphragm and respiratory muscles	
<i>smooth muscle</i>				
iris	miosis			
ciliary muscle	failure of accommodation			
gut	abdominal cramp, diarrhea,			
bladder	involuntary defecation frequency,			
heart	involuntary micturition bradycardia			

In addition to these acute symptoms which are categorized by receptor- (muscarinic and nicotinic) and organ-specific (cardiovascular, respiratory or neurological manifestations) means, a time-based approach may also be considered, wherein symptoms and signs are categorized as acute (minutes to hours) and delayed or late (days to weeks) [43, 86, 116]. In contrast to the acute syndromes where the ascribed cholinergic syndrome develops within minutes to hours after exposure of nerve agents, delayed and long term health effects including the intermediate syndrome (IMS) and organophosphate induced delayed neuropathy (OPIDN) may occur days to weeks following exposure either after an initial period of intense cholinergic symptoms and signs or after a period of minimal or no clinical features [5, 77, 305]. For instance, it was reported that about 60.000 Persian Gulf War veterans

suffered from such delayed adverse health effects after nerve agent exposure. This syndrome was referred to as the “Gulf War Illness” and was possibly due to low-dose exposure of nerve agents [127]. However, apart from some epidemiological studies, the etiology of this syndrome is still controversially discussed [68, 207]. With respect to the IMS, the classical late onset constitutes paralysis of proximal limb muscles, neck flexors, motor cranial nerves and respiratory muscles with weakness lasting for up to 18 days and may proceed in a delayed onset coma [254, 292]. The neurotoxic effect of OPIDN involves cramping pain and paresthesia of the extremities followed by weakness of the distal limb muscles, especially in the legs [86, 191]. Both delayed manifestations are thought to derive from delayed phosphorylation of neuropathy target esterase (NTE) at nerve tissues which leads to degeneration of long and large diameter motor and sensory axons of both peripheral nerves and spinal cord [86, 190, 191, 224]. However, since delayed manifestations have been more comprehensively described in association with OP pesticides poisoning, most attention of signs and symptoms of OP intoxication has been given to the acute syndrome of nerve agents [199, 386].

## 1.5 Current therapeutic regimen against organophosphate poisoning

While inhibition of cholinesterases is an important common feature of OP pesticides and highly toxic OP nerve agent poisoning, their physicochemical, toxicodynamic and toxicokinetic properties are highly variable [11, 354]. For these reasons, pharmacotherapy presents a major challenge for toxicologists, intensive care units, medical doctors and medical personnel [335]. Nevertheless, stepwise understanding of toxicokinetic and -dynamic properties of nerve agent compounds by studies conducted in the last two decades of the last century contributed to today’s therapeutic regimen to treat nerve agent poisoning [29, 91, 307, 354]. Current therapy comprises the administration of a nucleophilic agent, so called oxime, to reactivate phosphorylated AChE and of the muscarinic cholinergic antagonist, atropine, to counteract muscarinic effects (Figure 2) [29, 91, 307, 354]. Atropine is a racemic hyoscyamine and constitutes the main active component in *Atropa belladonna* (deadly nightshade), *Datura stramonium* (thorn apple) and *Hyoscyamus niger* (henbane) [44, 334]. It was introduced in the early 1950s as initial first-line antidote against OP pesticide and nerve agent poisoning and is classified as a symptomatic anticholinergic drug competitively antagonizing mAChR by competing with ACh for a common binding site at muscarinic receptors (M1-M5) [43, 44, 334]. Thus, rapid atropine administration of a recommended dose (2 mg in patients with mild symptoms, 4 mg with moderate symptoms and 6 mg with severe symptoms) to OP poisoned patients mitigates muscarinic effects of ACh hyperstimulation at neuroeffector sites on smooth muscle, heart muscle, glands, peripheral ganglia and in the CNS and thus prevent life-threatening airway secretions, and airway spasm deriving from muscarinic symptoms (rhinorrhea, bronchorrhea) (Table 1) [43]. The



usefulness of atropine is virtually undisputed but, as the antidotal mechanism is based on competition, the atropine dose has to be carefully adjusted to clinical signs in order to avoid adverse side effects [133, 208, 335]. However, larger doses of atropine are required to obtain appreciable concentrations of atropine into the CNS [208, 210, 298]. Apart from effectively antagonizing ACh at most peripheral and partly at central mAChR, atropine is unable to counteract the nicotinic signs of intoxication (e.g. muscle fasciculation, muscle fatigue, weakness) [91, 133]. Here, reversal of nicotinic signs of intoxication is therapeutically accomplished via oximes acting as reactivators of phosphorylated AChE [76, 164].

The history of oximes dates back to the early 1950s, starting with the compound 2-pyridine aldoxime methyl chloride, called pralidoxime (2-PAM), which was researched and published independently by Wilson and Ginsburg in the United States and Childs and coworkers in the UK in 1955 [64, 374]. The initial focus of research programs was to identify an oxime that effectively counteracts soman poisoning. As mentioned earlier, soman-inhibited AChE is dealkylated rapidly leading to an aged OP-AChE complex that is resistant to oxime reactivation and thus presents a major challenge to therapy [101, 214, 283]. Furthermore, in the last several decades, numerous studies of next generation oximes have focused on the development of broad spectrum oximes able to effectively reactivate structurally diverse nerve agents [64, 137, 139, 256, 374]. Unfortunately, none of such oxime derivatives that have emerged were effective against all nerve agents [25, 79, 89, 171, 189, 192, 238, 309].

Extensive research over the last decades of oxime reactivators yielded that the antidotal potency of these nucleophilic compounds is attributed to their ability to displace the phosphorus atom from the active site of the enzyme and thereby regenerating the physiological enzyme function (Figure 1) [22, 91, 139, 192, 217, 256, 374]. This reaction is conveyed via a nucleophilic attack of the oxime on the phosphyl group of the OP-inhibited AChE leading to a pentacoordinate transition state of the intermediate phosphyloxime [88, 370]. Subsequently, the phosphyl residue is removed from the intermediary complex and transferred to the oxime, resulting in formation of the reaction products phosphyloxime and the free enzyme with its restored enzyme activity after dissociation of phosphyloxime [158, 217]. The dissociation reaction is facilitated by the polarization of the phosphorus oxygen bond which is mediated by a charge transfer from the phosphorus to the double bonded oxygen of the phosphate ester [91]. Efficacy of oximes to restore AChE activity depends on the nucleophilicity and the architecture of the oxime, the decay rate of the phosphyloxime, and the concentration of oxime which is present at the active site and the rate of post-inhibitory dealkylation known as aging [91]. In particular, it is apparent that rather stable phosphorylated oximes comprising those of 4-pyridinium aldoximes rather than those of unstable 2-substituted pyridinium compounds could be potent re-inhibitors of the reactivated enzyme after the reactivation process [21, 168, 379, 380]. Moreover, efficacy of oximes in the CNS is impaired since penetration of mono- and bispyridinium

compounds across the blood-brain barrier is limited [54, 120]. Although it was shown that soman may open the blood-brain barrier in a seizure related manner, higher oxime concentrations are required to enable to passage the brain barrier [54, 120]. In context of oxime concentration, therapeutic window is narrow since an appropriate initial dose is required in treatment because oximes are rapidly cleared from the body [217]. If the dose is too low oximes may not be sufficiently persistent and effective after a time lag when another cycle of inhibition such as with slow flooding of VX may succeed [217]. In such cases, clinical improvement can only be achieved by repeated or persistent oxime administration as long as needed [217]. However, the treatment of soman poisoning is particularly fraught because of the rapid “aging” process of the conjugate that is usually faster and untraceable for the oxime-induced dephosphorylation reaction [101, 333]. Therefore, oximes are of little value in such cases if not given instantaneously [22, 91]. In addition to rapid aging, inefficient oxime treatment of OP-inhibited AChE is associated with limited access of oximes to the gorge due to spatial constraints of the gorge in combination with the steric limitations of bulky oximes as well as steric hindrance by some OP compounds (e.g. tabun) bound to the enzyme [22, 91]. From the above, it is apparent that research efforts developing innumerable oximes did not result in oximes that can be considered as broad spectrum antidotes with superior efficacy against structurally diverse OP compounds, in particular against rapid “aging” by soman [283]. Moreover, the synthesis of new, unknown structures of OP compounds can be easily adopted and modified since synthesis routes are readily accessible exemplified by former modification of VX to Chinese or Russian VX. The risk of exposure to agents that are hard to treat with current regimen complicates the development of such oximes [164, 174, 217]. In addition to the lack of a broad-spectrum therapy option, the current treatment regimen comprising oxime and atropine does not counteract symptoms mediated by overstimulation of nAChR. Thus patients are not sufficiently protected from nicotinic effects causing central and peripheral respiratory arrest representing the main cause of death after OP poisoning [24, 272, 283, 386]. Therefore, calls for alternative therapeutic approaches implicated with the prevention of respiratory arrest covering a wide range of OP compounds may be of great promise [24, 283, 386].

## **1.6 Novel medical countermeasures against organophosphate poisoning**

### **1.6.1 Novel oximes**

Many scientific institutions around the world are engaged in the development of improved medical countermeasures against chemical warfare agents and this ongoing progress culminated in the development of some oximes with superior efficacy when compared to pralidoxime, the first oxime therapeutically used [82, 101, 179, 283]. Hereby, symmetric bispyridinium compounds such as

methoxime (MMB-4), trimedoxime (TMB-4) and obidoxime as well as asymmetric bispyridinium compounds of the H-series, such as HI-6 and HLö7, which were developed in the laboratory of Professor Hagedorn, were of great interest [25, 79, 89, 171, 189, 192, 238, 309]. Although not yet commercially available, HI-6 is probably the most promising oxime under development in many countries since it was shown to have superior efficacy to VX compared to 2-PAM and very good action with sarin, but a poor or no response when treating tabun exposures [58, 66, 150, 194, 198, 212, 238]. At present, apart from the huge number of further oximes developed that are far away from commercial use, a few oximes including pralidoxime are in clinical use in the USA and Asia while in several European countries obidoxime is the oxime of choice [335, 336]. TMB-4 is only licensed in Israel for use in autoinjectors [335]. Further progress on oxime research led to numerous reviews dealing with novel oximes. However, since there is still no broad-spectrum reactivator and the complexity for the development of such an oxime is high, the research of novel promising oximes hampers. Instead, new trends to improve the conventional medical countermeasure for treatment of OP poisoning are starting to emerge [24, 283].

### 1.6.2 Catalytic scavengers

At the end of the 1980s, research programs were initiated to develop bioscavengers for human use in order to sequester and inactivate highly toxic chemicals in circulation before they reach their biological targets [376]. Endogenous candidate bioscavenger proteins including enzymes such as cholinesterases (ChE) and carboxylesterases (CaE) that stoichiometrically catalyze cleavage of OP compounds were investigated extensively [102, 134, 263]. Thereby, plasma-derived human butyrylcholinesterase (BChE) was envisioned as a prophylactic treatment in humans due to its rapid reaction with nerve agents, a prolonged circulatory residence time in humans, expected absence of undesirable immunological responses and its physiologically innocuous in the absence of nerve agent [80, 183, 225, 279, 283]. To allow a constant source of BChE of reproducible purity and activity, research investigations prompted production of recombinant human BChE [146, 147, 280]. However, catalytical activities of these mutants are too slow for practical use and thus, these research efforts continue to improve OP-hydrolyzing activity of the enzyme and to reduce immunogenicity by site-directed mutagenesis [283]. Moreover, a high dose of the stoichiometric bioscavenger is needed and the high costs involved producing recombinant BChE limit their applicability [201].

Hence, pseudo-catalytic scavengers co-administered with an oxime were examined for their ability to potentially produce greater extent to degrade OP compounds by using smaller quantities of chemical scavengers [201, 283]. Similar to pseudo-catalytic scavengers, the value of synthetic catalytic scavengers was discovered capable of trapping and catalytically hydrolyzing OP compounds with a higher turnover number than found with naturally occurring catalytic enzymes [81, 160, 161, 202, 346].

Conceived as pretreatment and/or post exposure treatment, this concept of fast and efficient degradation of OP compounds in the bloodstream by catalytic scavengers concentrated primarily on bacterial phosphotriesterases (PTE) and paraoxonase-1 (PON-1), but also on human BChE [34, 201, 272, 342, 382]. The recent unprecedented progress made in the development of bioscavengers for human use justifies the success of this novel approach [84, 114]. In the near future, optimized OP compound degrading enzymes by re-design of known enzymes applying new techniques used currently for drug design could be implemented [100, 201]. Among them, molecular modeling/docking techniques, quantum chemical/molecular mechanics calculations could be applied to reach this target of this promising research [167, 201].

## **1.7 Nicotinic receptors as targets for nerve agent therapy**

### **1.7.1 Potential benefits**

The anticholinesterase effect of nerve agents and other OP esters elicit toxicity through accumulation of ACh in the synaptic cleft and subsequent overstimulation of postsynaptic cholinergic receptors in the central and peripheral system, resulting in a syndrome referred to as the cholinergic crisis [11, 29, 142]. Medical research led to the development of the current therapeutic regimen consisting of the combined administration of an oxime to reactivate AChE, atropine to symptomatically antagonize muscarinic effects and later to the development of promising alternative therapeutic approaches, for instance catalytic scavengers that degrade OP compounds [23, 80, 133, 183, 225, 279, 283, 374]. Ongoing research on these therapeutic interventions together with medical assessment of OP-poisoned casualties contributed to a better understanding and reappraisal of therapeutic needs necessary to optimize current treatment [283, 384]. In this regard, previous casualty reports showed that OP-poisoned individuals suffering from severe clinical signs and symptoms of fasciculation and paralysis of the respiratory muscle deriving from dysfunction of nicotinic receptors could not be sufficiently recovered by the standard therapy [24, 272, 283, 335].

However, if untreated, such nicotinic symptoms arising from uncontrolled ACh accumulation and overstimulation of receptors may lead to subsequent desensitization in case of continued overstimulation. Desensitization is a transitional receptor state in which the receptor cannot be immediately reactivated is formed. Thus paralysis is caused by disruption of the respiratory centers in the brain and transmission failure at neuromuscular junctions of the respiratory muscles [60, 76, 142, 254, 299, 360, 389]. Although nicotinic effects can be counteracted indirectly by oximes, these previous casualties dying from respiratory depression have proven that oxime based therapy may be insufficient

[24, 208, 237, 272, 283, 335]. In addition to these acute symptoms, delayed manifestations that have been observed after the Gulf War period were presumed to be at least partly attributed to nicotinic effects [13, 369]. Prior to the role of nicotinic receptors in nerve agent poisoning, dysfunction of nicotinic receptors was already shown to be implicated in neurodegenerative diseases such as Alzheimer's disease, Parkinson's disease, schizophrenia and also myasthenia gravis [6]. Due to their involvement in several important pathologies, nAChR were studied extensively with regard to their molecular structure, pathological mechanisms and different ligands binding to various sites of the receptor [117, 148, 182, 322].

### **1.7.2 Nicotinic receptors**

Investigations on nicotinic acetylcholine receptors (nAChR) started in the beginning of the 20<sup>th</sup> century with studies of the effect of alkaloids muscarine and nicotine on cholinergic receptors carried out by Sir Henry Dale and gave origin to classification of acetylcholine receptors into muscarinic and nicotinic receptors [57, 75]. The two types of receptors are fundamentally different. While metabotropic muscarinic receptors which are coupled via guanosine triphosphate-binding proteins (G-proteins) to the enzymes adenylate cyclase or phospholipase C, are using second messenger systems, nAChR are part of the ligand-gated ion channel family [57, 247]. To date, five subtypes of muscarinic receptors designated M1 to M5 have been cloned and are found in parasympathetic effector organs, and, prejunctionally at the neuromuscular junction whereas nicotinic acetylcholine receptors are found in both the PNS at the neuromuscular junction and in the autonomic system as well as in the CNS (Table 2) [38, 39, 159, 172, 173, 199, 251].

**Table 2:** Distribution of nAChR subunit mRNA and protein expression found in the human central nervous system (adapted from [117, 148]).

CNS	CNS subunits							
	$\alpha 3$	$\alpha 4$	$\alpha 5$	$\alpha 6$	$\alpha 7$	$\beta 2$	$\beta 3$	$\beta 4$
<b>cortex</b>			○				○	○
frontal	○	○●			○●	○		
parietal	○	○●			○	○●		
occipital		○			○			
temporal	○●	○●			○●	○●		
insular	○	○				○		
<b>thalamus</b>	○	○	○		○	○	○	○
anterior					○			
lateral nuclei	○				○	○		
dorsomedial	○				○	○		
lateral geniculate					○			
reticular	○				○	○		
<b>midbrain</b>	○	○●	○		○	○●	○	○
<b>brainstem</b>					○			
<b>hippocampus</b>	○●	○●	○		○●	○●	○	○
entorhinal cortex	○●	○●			○●	○●		●
subiculum	○	○			○	○		
pyramidal cells	●	●			●	●		●
dentate gyrus	○●	○●			○●	○●		●
<b>basal ganglia</b>	○	○	○		○	○	○	○
caudate	○	○			○*	○		
putamen	○●	○●	●	●	○●	○●	●	
globus pallidus		○						
<b>cerebellum</b>	○●	○●	○	●	○*●	●	○	○●

mRNA (○), protein expression (●). Asterix (\*) indicates that mRNA was observed in deep cerebellar nuclei but not in cerebellar cortex, globus pallidus or caudate.

Nicotinic receptors belong to the Cys-loop family, a family of ligand-gated ion channels (LGIC) that also include  $\gamma$ -aminobutyric acid A (GABA<sub>A</sub>) receptors, glycine receptors and 5-hydroxytryptamine 3 (5-HT<sub>3</sub>) receptors [247]. A unique common characteristic feature of these integral membrane proteins is the presence of a conserved disulfide bridge flanked by two covalently bonded cysteine residues in the N-terminal extracellular domain of each subunit (Figure 3 A). In addition to the large N-terminal extracellular domain, each subunit comprises a transmembrane domain with four hydrophobic segments named M1-M4 with M2 lining the inner pore lumen of the channel, and a hydrophilic cytoplasmic domain carrying a phosphorylation site (Figure 3 A) [162].

Furthermore, they share a common structural pentameric pattern composing five subunits which are arranged symmetrically and build a central pore. The pore is permeant to the following cations: Na<sup>+</sup>, K<sup>+</sup>, or Ca<sup>2+</sup> (Figure 3 B) [276, 322]. The structure of the nAChR has been reviewed revealing some differences between receptors expressed at the neuromuscular junction and those in neuronal tissue (Figure 3 C) [40, 322, 350]. Historically, the muscle-type nicotinic receptor was the first studied when it was extracted and purified from the Torpedo electric ray [261]. It is formed by four different subunits with a stoichiometry of  $(\alpha)_2 \beta \epsilon \delta$  whereas in adult mammalian muscle tissue, the  $\epsilon$  subunits is replaced by a  $\gamma$  subunit (Figure 3 C) [220, 375]. The neuronal nAChR include both homopentamers, which are formed by five identical subunits, and heteropentamers that result from the combination of different subunits (Figure 3 C) [61, 63, 105, 277]. In total, eleven neuronal nAChR subunits have been identified in mammals ( $\alpha 2$ - $\alpha 7$ ,  $\alpha 9$ ,  $\alpha 10$ ,  $\beta 2$ - $\beta 4$ ), with the combination of  $\alpha 2$ - $\alpha 6$  and  $\beta 2$ - $\beta 4$  forming heteromeric nAChR [61, 63, 105, 277]. More precisely, heteromeric receptors are commonly composed of a single  $\alpha$  and a single  $\beta$  subunit with a stoichiometry of  $(\alpha)_2$  and  $(\beta)_3$  (Figure 3 C) [276]. Subunit composition of homomeric receptors are formed by  $\alpha$  (7-10) subunits (Figure 3 C) [276]. Notably, the bridged cysteines are only present in the  $\alpha$  subunit in the N-terminal extracellular domain and bear a sequence of 13 residues which form the Cys-loop located between the ligand-binding domain and the ion-channel domain [303]. With respect to expression sites of nAChR, the classical distribution in muscle and neuronal receptors appears to be outdated since apart from neuronal tissues, neuronal nAChR were also reported to be present in non-neuronal tissues such as lymphocytes, macrophages, lungs, keratinocytes, vascular endothelium, and others [70, 104, 117, 119, 166, 196, 250, 361]. The broad spectrum of various assemblies of neuronal nAChR subtypes reveals receptors that deviate with respect to their permeability of a specific cation species, with respect to their activation and desensitization kinetic profiles, and, moreover, display a distinct ligand pharmacology [152].

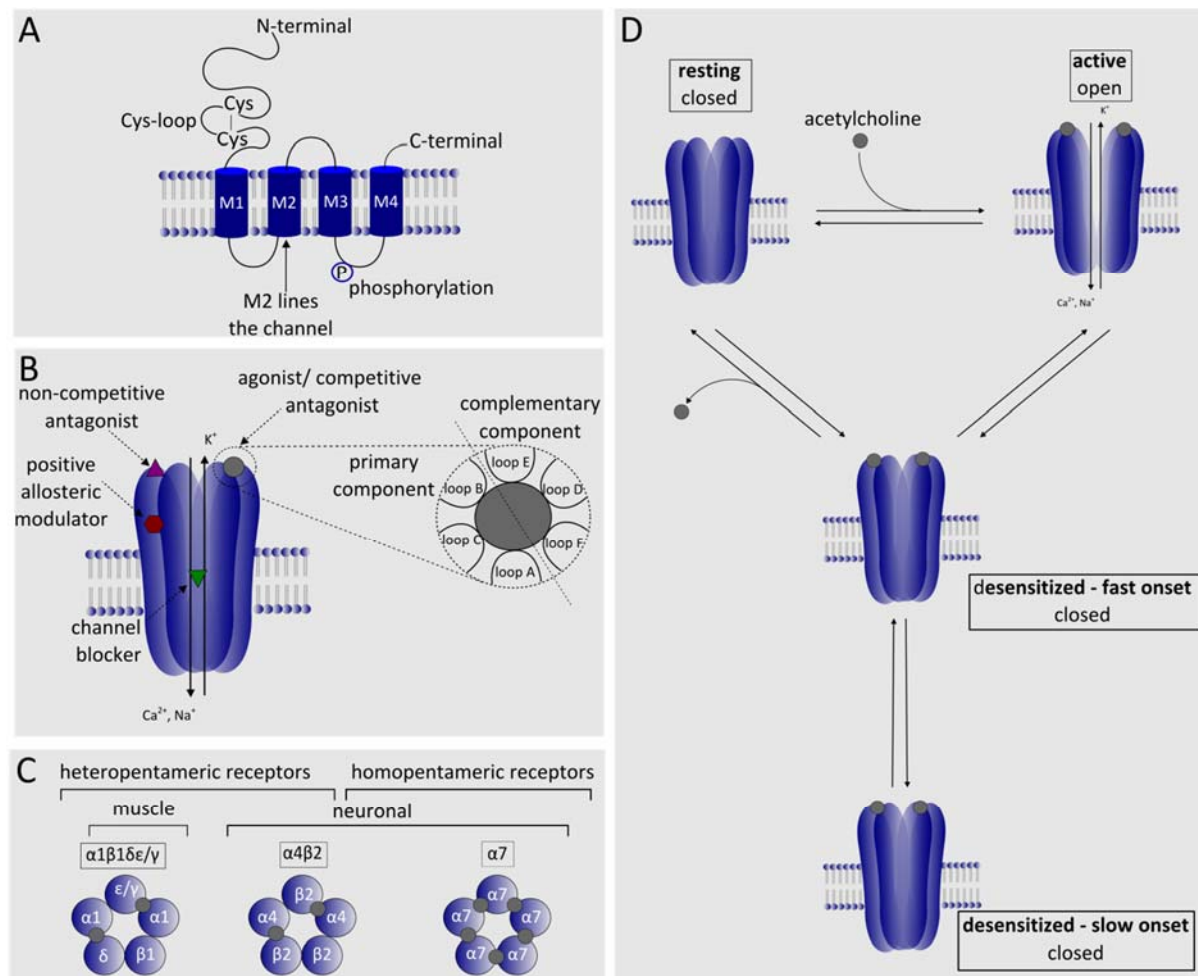


**Figure 3 A-D: Schematic representation of the nAChR structure, heterogeneity of subtypes and conformational transitions of nAChR.** A. Topography of a single nAChR subunit in the cell membrane. B. Schematic side view of a nAChR in the cell membrane with one subunit removed to reveal the ion channel lumen. Shown are notional sites of action for agonists including top view of the agonist binding site loop model, competitive and non-competitive antagonists and positive allosteric modulators. The agonist binding site is enlarged grouping the contributing polypeptide loops into the primary (loop A, B and C) and complementary components (loops D, E and F). C. Classification of nAChR are shown by exemplary major subunit combinations present in the CNS and the periphery with putative agonist binding sites indicated by grey circles at subunit interfaces. D. Model of conformational states of nAChR including resting, active and desensitized states (fast and slow onset). Figure was adapted from [377].

### 1.7.3 Ligands, allosteric transitions and implications in organophosphate poisoning

On the basis of binding studies, invaluable information of several ligands binding to nAChR was provided to advance the understanding of the binding domain and rational design of nAChR ligands



[49, 186, 193]. Besides the endogenous agonist ACh activating all nAChR subtypes, a diverse array of plant and animal toxins that target nAChR was identified as agonists with varying subtype-selectivity. The most prominent ones are naturally occurring agonists such as (-)-nicotine, (-)-cytisine, (+)-anatoxin A, (+)-epibatidine, anabasine and anabaseine [275, 377]. The perceived validity of nAChR as therapeutic target in particular in neurodegenerative diseases has stimulated the design of synthetic ligands with specific subtype-selectivity using agonists of natural source as lead structure [152, 153, 215, 273, 274, 281, 316, 377]. This culminated in a diverse array of agonists including carbamoylcholine derived from a modification of ACh to a carbamate, varenicline (Chantix<sup>TM</sup> (USA); Champix<sup>TM</sup> (EU)) which is a cytosine congener developed to exploit the properties of cytosine as an aid to smoking sensation and A-85380 recapitulating the chemical properties from epibatidine [152, 153, 215, 273, 274, 281, 316, 377]. In the last few years, several publications have reviewed a high number of nicotinic ligands, however, since the large number of agonists identified is beyond the scope of this study, the reader is referred to the aforementioned studies [148, 162, 275, 276, 377].

The available data suggest that the primary binding site of ACh and other agonists is positioned at the interface between two adjacent subunits wherein the  $\alpha$  subunit in the N-terminal domain constitutes the principal component of the binding site and the adjacent subunit the complementary site (Figure 3 B) [118, 303].

In case of homomeric nAChR, such as  $\alpha 7$ -nAChR, each subunit has both primary and complementary faces of the agonist binding site, hence, the  $\alpha 7$ -nAChR possesses five instead of two agonist binding sites as in case with heteromeric nAChR (Figure 3 C) [118, 303]. Notably, amino acid residues that contribute to the agonist binding site consist of highly conserved, through the LGIC family, aromatic residues that are referred to as loop A, B and C of the principal component and loop D, E and F of the complementary component (Figure 3 B) [118, 303]. These loops form a compact cavity in the center of the interface of the extracellular domain (ECD) of the nAChR [15, 71, 124, 163].

X-ray studies revealed that upon agonist binding a conformational transition of the loop C is triggered to form a closed conformation by the capping of loop C [83, 322]. In contrast, the ligand-free resting state is associated with a more open loop C conformation [83, 275]. This conformational shift involves a sequence of rearrangements of the subunit transmembrane regions following ligand binding [83, 275]. Upon binding, the channel pore opens, which leads to an increase in Na<sup>+</sup> conductance, depolarization of the cell membrane and neuronal and neuromuscular transmission, respectively [322, 377]. The transition from the resting to the open state upon activation occurs within a few milliseconds and inactivates rapidly which is due to the low affinity of the ligand causing fast dissociation from the binding site [377]. During sustained exposure of moderate ACh concentrations, controlled synaptic transmission constitutes repeatedly transition of the receptor from the agonist-bound open conformation to a non-conducting state, the deactivation, as the ACh dissociates from the receptor

(Figure 3 D) [148]. However, high concentrations of accumulated ACh results in increased binding of the neurotransmitter to the receptor. Thus, the probability of the receptor to transition to a non-conducting state, known as desensitization, a conformational state wherein the receptor is not susceptible for immediate re-activation, increases (Figure 3 D) [148]. Receptor desensitization is associated with high ligand affinity of ACh to the ligand binding site and induces a depolarization block of the endplate at the neuromuscular junction and interruption of neuronal transmission, thereby leading to muscle weakness and paralysis [148, 377]. Following nerve agent exposure, hyperstimulation of cholinergic receptors including mAChR and nAChR is followed by desensitization of nAChR leading to toxic signs of poisoning as evident in casualties from the terrorist attack in Tokyo, Japan, where respiratory distress was observed in approximately 63 % of the casualties [237, 266, 387]. Where death occurred, it was caused by a combination of effects at both central (loss of respiratory drive) and peripheral (weakness at intercostal muscles) levels [209]. In compliance with this notion, it would seem appropriate to develop nicotinic antagonists as therapeutic agents for patients displaying nicotinic-dominant signs in order to mitigate the effects of excessive ACh at nAChR [296].

Thereby, competitive antagonists bind at or near the orthosteric site preventing access for agonists and stabilizing the receptor in a conformation with the channel closed [42, 135, 148]. The use of such a nicotinic antagonist in the same way as atropine antagonizing the muscarinic effects in OP poisoning is currently not considered as a therapeutic approach because nAChR function and conformational changes differ from those in mAChR [278, 306, 330]. In this context, a major problem of such competitive antagonists to be applied as therapeutic agents is that very high concentrations of antagonist are needed to overcome the effects of excessive ACh stimulation of nicotinic receptors [330]. The main challenge hereby is to envisage a competitive range dosage that is not so high that the now normalized function itself becomes compromised by excess antagonism and thus causing serious adverse side effects in unpoisoned individuals [296]. Moreover, many nicotinic antagonists are of highly toxic nature such as tubocurarine, which is the principal component of an arrow poison used in South America, named curare [35]. Hence, clinical use of competitive nicotinic antagonists is not feasible to address the nicotinic effects of OP poisoning [296, 330].

A more attractive proposition would be to use non-competitive nAChR antagonists binding to other regions than the orthosteric site so that their block would not be overcome by increasing concentrations of ACh [330, 377]. Their inhibitory effect could be used to reduce nAChR overstimulation and agonist-evoked depolarization block caused by continued excess of ACh. Hereby, non-competitive nAChR antagonists bind distinct from orthosteric agonist binding sites and exert their function through a steric mechanism or through allosteric conformational changes of the channel upon binding [33, 61, 330, 377].

Such an antagonist that inhibits nAChR activity via an allosteric modulation of the receptor is referred to as a negative allosteric modulator (NAM) and a typical representative example is progesterone, which inhibits  $\alpha 4\beta 2$  nAChR [33]. The underlying mechanism of action to reduce ligand-induced response upon negative allosteric modulation of the receptor is associated with changes in the energy barrier between transition states [33, 62]. According to Hurst and colleagues, binding of NAM evokes an increase of the energy barrier between the resting and open state. Given this, these compounds should have no effect in healthy individuals because of their low intrinsic activity as their action is contingent upon prior nAChR activation by an agonist [148, 330]. In this regard, it should selectively inhibit nAChR activity in the face of increasing ACh concentrations in a use dependent manner so that the proportion blocked is maintained irrespective of the concentration of ACh in the synapse [330].

In addition to NAM, nAChR modulation can also be carried out via positive allosteric modulation by increasing the probability of channel opening induced by ACh and, additionally, by decreasing receptor desensitization via interactions with sites distinct from classical ACh binding sites [33, 85]. These positive allosteric modulators (PAM) represent a pharmacological class of molecules that reduce the energy barrier from the resting to the activated state and thereby increase the agonist response and/or enhance the energy barrier between the activated and the desensitized state [33, 62]. In respect of their mechanistic profile, PAM are categorized into type I and type II PAM depending on whether they only enhance agonist response (type I) or, in addition, reduce agonist-induced desensitization (type II). Hereby, types I PAM reduce the energy barrier between the resting and the active state (type I) amplifying agonist response. Type II PAM reduce agonist-induced desensitization by increasing the energy level of the desensitized state, thus destabilizing the desensitized state and promoting re-opening of receptors from the desensitized state (type II) [149]. Numerous compounds acting as PAM at nAChR have been described in literature, such as  $\alpha 7$ -nAChR specific type II PAMs PNU-120596 and NS-1738 [148, 149, 337]. So far, PAM of nAChR have not progressed to full development yet, but the ongoing progress in understanding nAChR functional properties will provide a considerable number of opportunities for the development of novel therapeutic applications [276, 322]. For instance, evidence has been provided that the reversible cholinesterase inhibitors physostigmine and galanthamine activate muscle and neuronal nAChR by a nicotinic allosteric action [235, 252, 253, 288, 294, 295, 314]. Both compounds were found to reverse desensitized receptors even at high agonist concentrations and were detected to be insensitive to inhibition by competitive antagonists of nAChR [235, 252, 253, 288, 294, 295, 314]. Furthermore, galanthamine is currently approved for treatment of cognitive dysfunctions in Alzheimer's disease. Its benefit is contributed to its effectiveness in improving synaptic transmission in the brain cholinergic system and protection of neurons from neurodegeneration [107, 188, 197, 282]. Symptoms deriving from compromise of the cholinergic system are not only evident in such neurological disorders but also observed in individuals intoxicated with nerve agents and other

OP [6, 289]. In particular, those symptoms include muscle weakness and fatigue observed in OP poisoned patients and are also evident in myasthenia gravis, an autoimmune disease characterized by muscle weakness deriving from destruction of nAChR at the neuromuscular junction [6, 289]. This consideration leads to the assumption that drugs intended for treatment of neurodegenerative diseases such as myasthenia gravis, Alzheimer's or Parkinson's disease may also be interesting in protection of central and peripheral nicotinic effects in OP poisoning [6, 10]. In this respect, a study by Albuquerque and colleagues has shown a superior therapeutic effect of galanthamine in soman and other nerve agent intoxications [10]. The possible utility of these PAM in Alzheimer's disease may also be a promising concept for an alternative therapeutic approach against OP poisoning. The potential benefit of the use of nAChR PAM in OP poisoning is the generic based approach for the development broad spectrum antidote. In this context, effects of PAM on nAChR are conveyed downstream from AChE inhibition and thus its efficacy does not depend on a specific nerve agent structure [268, 296].

#### **1.7.4 Preliminary work and state of the art**

During the search of a broad spectrum oxime that is more effective than presently available and clinically used oximes, in particular with improved efficacy related to soman, data derived from soman intoxicated non-human primates has indicated that oxime HI-6 exerts a positive therapeutic effect other than AChE reactivation. This is based on the observation that low AChE activities were found in blood of these primates which can be explained by the rapid aging of the enzyme resistant to reactivation [128]. From these data and subsequent data confirming these positive pharmacological effects of HI-6, it was concluded that processes other than AChE reactivation are important for the survival of soman intoxicated primates [66, 128, 177, 356, 357]. In a continuation of the *in vivo* experiments on the pharmacological effects, it was shown that even compounds that lack the oxime reactivating group (SAD-128, 1,1'-oxybis(methylene) bis 4-(1,1-dimethylethyl) pyridinium dichloride) have efficacy in treatment of OP poisoning resulting in a recovery of the neuronal transmission in the respiratory centers in the brain and recovery of neuromuscular transmission [123, 150, 238, 285]. A number of different explanations of this surprising non-activating effect by these bispyridinium (BP) compounds were suggested including reversible AChE inhibition, decreasing the rate of rapid aging, inhibition of muscarinic receptors in a competitive or allosteric manner, or interactions with nAChR [123, 129, 169, 175, 285]. Of all these possible explanations, it is the effect on the nAChR associated with a modulation of the postsynaptic response of nAChR that is of particular interest for new therapeutic interventions in OP poisoning [12, 65, 297, 315, 329]. Thereby, modulation of nicotinic ion channels by allosteric modulators so that in case of ACh accumulation, nAChR are rendered less sensitive to overstimulation in a use-dependent manner, became a promising approach in OP poisoning [229, 230]. Thus life endangering failure of neuronal transmission in the respiratory centers

of the brain and neuromuscular transmission in the respiratory muscles after OP poisoning may be restored sufficiently in cases where AChE activity appeared to be insufficient to be treated by oximes [330].

As a starting point of this new concept to maintain nAChR function by pharmacological interactions using potential allosteric modulators, the bispiridinium (BP) structure which is also present in HI-6 and SAD-128 served as a template to synthesize a series of structurally related derivatives [262, 329, 363]. The anti-nicotinic potency and effectiveness in recovering neuromuscular function of these compounds has been evaluated *in vitro* by measuring the muscle force production of the guinea pig phrenic nerve hemidiaphragm via direct and indirect stimulation tested with the field stimulation technique [321, 329]. Under basal conditions, controlled muscle contractions of these preparations occurred whereas after treating these with soman, a rapidly decaying contraction occurred [321, 329]. This so called tetanic fade could be reversed by adding increasing concentrations of the bispiridinium compound MB327 (1,1'-(propane-1,3-diyl)bis(4-*tert*-butylpyridinium) diiodide), a symmetrical bispiridinium compound with a *tert*-butyl group at position 4 at both pyridinium rings [138, 329]. MB327 was the most effective in a series of BP compounds with recovery of response of approximately 30 % measured at 100  $\mu$ M MB327 determined by the area under the curve (AUC) of the response compared to the control tetanic stimulation [329, 330]. Following animal studies using an identical compound to MB327, named P62 (diiodide salt), Schoene and coworkers found that mice poisoned with soman ( $LD_{95}$ ) and pretreated with atropine showed decreased toxic effects when P62 was administered by a dose of  $1.76 \times 10^{-5}$  mol  $kg^{-1}$  [285]. Furthermore, protection of animals by non-competitive ligands was further confirmed by a correlating study by Timperley and colleagues, using the water soluble di(methansulfonate) salt of MB327 named MB399 given at  $3.30 \times 10^{-5}$  mol  $kg^{-1}$  [338]. Both compounds, MB327 and MB399, have been observed to have no effect on soman inhibited AChE, thus indicating that therapeutic efficacy is associated with interactions at nicotinic receptors [285, 330]. Considering the development of therapies for nerve agent poisoning, it has to be considered whether experimental settings in animal studies can be extrapolated to the situations in humans. Unfortunately, enormous species differences with respect to sensitivity and oxime effectiveness have been found so that translation into humans is complicated [378, 379, 381, 385]. Because clinical investigations in humans are obviously not possible, one approach for instance to estimate appropriate concentrations of oximes to be applied in humans can be obtained from data of toxico- and pharmacodynamic studies investigating interactions of OP compound, oximes and AChE [29, 91, 157, 355, 383].

Based on these kinetic data, Seeger and colleagues used human intercostal muscle preparations to investigate the effect of therapeutically estimated concentrations of HI-6 and whether this effect is associated with an enhancement of muscle AChE activity [291]. Moreover, corresponding to the study

by Tattersall and coworkers, Seeger and colleagues studied the ability of MB327 to recover neuromuscular transmission using human preparations [290, 329]. Thereby, an increase of muscle force in soman exposed human muscles by pharmacological mechanisms other than AChE reactivation could not be observed with HI-6 in contrast to earlier studies using rodent and marmoset respiratory muscle. However, testing of MB327 verified a concentration dependent recovery that was not related to AChE reactivation as seen in guinea pig respiratory muscles [51, 211, 290, 329, 356, 357]. Therefore, convincing evidence is provided by this study that the effect of HI-6 appears to be without relevance for human therapy whereas therapeutic effects of MB327 found in animal studies can be translated to humans [330]. Although further promising *in vitro* and *in vivo* experiments have confirmed the beneficial pharmacological effect with MB327, the potency required for human application is too weak and insufficient in the concentration range needed for therapeutic administration [165, 257, 290, 329, 347]. Within the framework of this study, the medicinal chemistry program at hand has been started to develop more potent substances by using MB327 as a lead structure to develop analogues of symmetrical BP compounds bearing different substituted groups at varying positions by efficient synthetic routes [262]. By application of new techniques for rational drug design, among them prediction of new structures using chemometric tools, click chemistry, radioligand and liquid chromatography - mass spectrometry (LC-MS) binding studies in combination with functional assays to establish structure - activity relations, this alternative approach is used to identify promising candidates able to efficiently recover desensitized nAChR and thus providing the closure of a therapeutic gap in the therapy of OP poisoning [363].

## 1.8 Aim of the present subject matter

Increasing risk of terrorist attacks and homicidal use of OP compounds calls for improvement of medical countermeasures. The development of ligands interacting with nAChR as therapeutic agents against OP poisoning has raised much interest in recent years. In particular, ligands acting as positive allosteric modulators (PAM) of nAChR represent an important class of potential therapeutic drugs as they bind to a site distinct from the orthosteric binding site of ACh and thus may preserve nAChR desensitization by stabilizing its open state configuration and may “resensitize” the receptor by destabilizing the desensitized state. The current therapeutic regimen of oxime administration to reactivate AChE and atropine to counteract muscarinic effects provides efficient treatment against some OP compounds but not against all kinds of OP compounds, i.e. soman due to rapid “aging”. Accordingly, this alternative therapeutic approach could provide a broad-spectrum antidote because the effect of nicotinic PAM is effective downstream of AChE inhibition. Moreover, this generic approach is a promising strategy to close the therapeutic gap in OP poisoning which is induced by

nicotinic effects that may cause death if untreated due to severe central respiratory depression and paralysis of respiratory muscles. Previous *in vivo* and *in vitro* studies demonstrated partial recovery of the neuromuscular transmission with the bispyridinium (BP) non-oxime compound MB327 (4-*tert*-butyl bispyridinium) by a proposed allosteric interaction with nAChR rather than a classical reactivation of the inhibited AChE. However, the potency of MB327 is not sufficient enough to be applied at therapeutic concentrations and thus a deeper understanding of the structure-activity relation is required for a better understanding of the structural determinants for this beneficial effect. In this context, the aim of this study comprised the establishment of a patch clamp screening method to investigate the ability of BP compounds (denoted as PTM compounds), which were structural analogues to MB327, to prevent and to recover human acetylcholine receptors of the subtype  $\alpha 7$  ( $\alpha 7$ -nAChR) from desensitization. For this purpose, stably transfected Chinese hamster ovary (CHO) cells expressing the  $\alpha 7$ -nAChR (CHO/RIC-3/ $\alpha 7$ -nAChR cell line) were used and investigated by an automated planar patch clamp system.

Structure-activity-relations of such PTM compounds on  $\alpha 7$ -nAChR function were determined to identify structural determinants mediating a positive allosteric mechanism on  $\alpha 7$ -nAChR. Moreover, response profiles of such PTM compounds were compared to the effect by the lead structure MB327 and the well prescribed positive PAM PNU-120596 in order to gain inside into the mode of action.

Prior to such screening, basic electrophysiological properties of wildtype CHO-K1 and GH<sub>4</sub>C<sub>1</sub> cell line were elucidated in order to select a host cell line most suitable for stable transfection of  $\alpha 7$ -nAChR in order to investigate  $\alpha 7$ -nAChR function by an electrophysiological method. In the end, CHO cells were used as host system for stable transfection of  $\alpha 7$ -nAChR (CHO/RIC-3/ $\alpha 7$ -nAChR cell line) and electrophysiological properties of these stably transfected cells were investigated. For the subsequent establishment of the screening method, optimization of cellular parameters and settings to obtain a higher seal success rate of patch clamp recordings was examined including adjustment of the under-pressure applied to capture and to hold the cells at a fixed position, addition of a Ca<sup>2+</sup> rich solution serving as a “seal enhancer” and adjustment of the cell passage range used. Furthermore, the flow rate of test compound application was adjusted to increase signal intensity, which was essential due to the fast conformational change of  $\alpha 7$ -nAChR. Then, amount of time and number of washing steps between each test compound application were adjusted to ensure full recovery of receptors from desensitization prior to the next test compound application. Different transition states of the receptor were investigated by application of agonists and a prescribed allosteric modulator. In addition, inhibition of  $\alpha 7$ -nAChR activity by an antagonist in the absence and presence of a prescribed allosteric modulator was essential to confirm subtype specific expression of  $\alpha 7$ -nAChR. In conclusion, this study served to develop a screening method to investigate functional activities of these so called PTM compounds on  $\alpha 7$ -nAChR function in order to identify structural requirements of test compounds

that prevent and reverse nAChR desensitization. Based on the findings of the present study, identification of promising lead structures capable to convey a positive pharmacological effect after OP poisoning may testify to the utility of PAM of the h $\alpha$ 7-nAChR as a novel therapeutic principle for treating acute OP poisoning.



## 2. Materials & Methods

### 2.1 Devices and supplies

**Table 3:** Laboratory devices, equipment and software.

laboratory devices	
analytical balance	MSE324S (Sartorius AG, Göttingen, Germany)
autoclave	VX-150 (Systec GmbH Labortechnik, Linden, Germany)
automatic cell counting and analyzing system	Casy® TTC (Roche, Mannheim, Germany)
incubator	BBD 6220 (Thermo Electron LED GmbH, Langenselbold, Germany)
laminar flow sterile bench	KS 12 HERAsafe (Thermofisher Scientific GmbH, Bonn, Germany)
automated planar patch clamp system	Patchliner® Octo (Nanion Technologies GmbH, Munich, Germany)
ultra-microbalance	MSA6.6S (Sartorius AG, Göttingen, Germany)
equipment	
centrifuge with cooling, pre-cooling and different rotors	Rotina 420R (Hettich Zentrifugen, Tuttlingen, Germany)
deep freezer	Innovau 725-G, - 80 °C (New Brunswick/Eppendorf, Hamburg, Germany)
freezer	LGUEX1500, - 20 °C (Liebherr, Ochsenhausen, Germany )
liquid nitrogen tank with accessories	LS 3000 (Taylor-Wharton, Theodore, USA)
magnetic stirrers with accessories	Mr Hei-Tec (Heidolph Electro GmbH, Kehlheim, Germany)
microscope with external heating plate, digital camera and control unit	Invers TS100-F (Nikon GmbH, Düsseldorf, Germany) T 3500 (Nikon GmbH, Düsseldorf, Germany) DS-Vi 1 (Nikon GmbH, Düsseldorf, Germany)
pH-meter	LR 325 (WTW GmbH, Weilheim, Germany)
refrigerator	LKUexv 1610 MedLine (Liebherr, Ochsenhausen, Germany)
ultrapure water system	Synergy® UV-R (Millipore, Darmstadt, Germany)

vortexer	Vortex 3 (IKA-Werke GmbH & Co.KG, Staufen, Germany)
water bath	SW 22 (Julabo Labortechnik, Seelbach, Germany)
amplifier quadro patch clamp	EPC-10 Quadro patch clamp amplifiers (HEKA Elektronik Lambrecht/Pfalz, Germany)
<b>software</b>	
PatchControlHT	Nanion Technologies, Munich, Germany
PatchMaster	HEKA Elektronik GmbH, Lambrecht/Pfalz, Germany
GraphPad Prism 5.0	San Diego, CA, USA
IGORPro, Version 6.2.2.2	Lake Oswego, Oregon, USA

**Table 4:** Consumables and supplies.

<b>consumables</b>	
aspiration pipette	2 ml, catalog No. 357558 (Falcon distributed by VWR, Darmstadt, Germany)
coverslips	catalog No. 631-0168 (VWR, Darmstadt, Germany)
cell culture flask	T-75, catalog No. 734-0965 (Falcon distributed by VWR, Darmstadt, Germany)
measurement chip for patch clamp experiments	NPC® -16 Chips medium resistance (Nanion Technologies GmbH, Munich, Germany)
microscope slides	Superfrost Plus Gold, catalog No. K5800AMNZ (Thermo Scientific, Darmstadt, Germany)
pipette tips	0,5-20 µl, catalog No. 0030 000.854 2-200 µl, catalog No. 0030 000.870 50-1000 µl, catalog No. 0030 000.919 500-5000 µl, catalog No. 0030 000.978 (Eppendorf, Hamburg, Germany)
cryovials	polypropylene (PP) cryovials 1,5 ml, catalog. No 479-3221 (Nalgene distributed by VWR, Darmstadt, Germany)
reaction vessels	polypropylene (PP) reaction vessels,

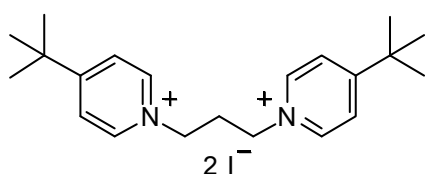
	1.5 ml, sterile, catalog No. 0030 108.081
	0.5 ml, catalog No. 0030 108.094
	1.5 ml, catalog No. 0030 108.116
	(Eppendorf, Hamburg, Germany)
serological pipettes	non-pyrogenic, sterile
	1 ml, catalog No. 357521,
	5 ml, catalog No. 357543,
	10 ml, catalog No. 357551,
	25 ml, catalog No. 357525,
	50 ml, catalog No. 357750,
	100 ml, catalog No. 357600,
	(Falcon distributed by VWR, Darmstadt, Germany)
tubes for cell counting	cell analyzer PP-tube, „CASY® cups“ , catalog No. 05 651 794 001 (Roche, Mannheim, Germany)
cellulose membrane	nitro cellulose (Millipore, Darmstadt, Germany)
<b>supplies</b>	
amber glass bottles	1000 ml (VWR, Darmstadt, Germany)
beakers	different sizes (VWR, Darmstadt, Germany)
measuring cylinder	1000 ml (VWR, Darmstadt, Germany)
volumetric flask	1000 ml (VWR, Darmstadt, Germany)
glas vials	4 ml (Zinsser Analytics GmbH, Frankfurt am Main, Germany)

## 2.2 Chemicals and reagents

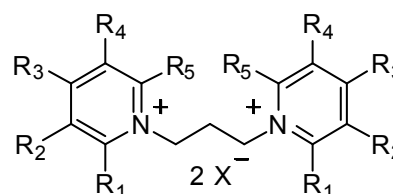
All chemicals and reagents used in this study were of a commercial grade and, unless further details have been provided, were obtained from the companies Merck KGa (Darmstadt, Germany), Carl Roth GmbH + Co. KG (Karlsruhe, Germany), Sigma Aldrich (Taufkirchen, Germany), Tocris Bioscience (Wiesbaden-Nordenstadt, Germany), GIBCO distributed by Life Technologies (Darmstadt, Germany) and Roche (Mannheim, Germany) (Table 5, Table 7, Table 8).

**Table 5:** Ligands of nAChR.

nicotine	(-)-nicotine, CAS No. 54-11-5 (Sigma Aldrich, Taufkirchen, Germany)
methyllycaconitine	methyllycaconitine citrate (MLA), CAS No. 112825-05-5 (Tocris Bioscience, Wiesbaden-Nordenstadt, Germany)
carbamoylcholine	carbamoylcholine chloride, CAS No. 51-83-2 (Sigma Aldrich, Taufkirchen, Germany)
acetylcholine	acetylcholine iodide, CAS No. 60-31-1 (Sigma Aldrich, Taufkirchen, Germany)
epibatidine	(±) – epibatidine dihydrochloride, CAS No. 148152-66-3 (Tocris Bioscience, Wiesbaden-Nordenstadt, Germany)
PNU 120596	1-(5-chloro-2,4-dimethoxyphenyl)-3-(5-methylisoxazol-3-yl)urea, CAS No. 501925-31-1 (Sigma Aldrich, Taufkirchen, Germany)
MB327	1,1'-(propane-1,3-diyl)bis(4-tert-butylpyridinium) diiodide/ trifluoromethanesulfonate (Centre of Pharma Research, Department of Pharmacy, Ludwig-Maximilians-Universität, Munich, Germany)



MB327



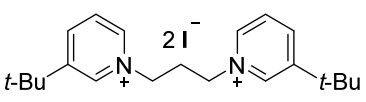
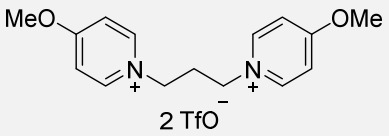
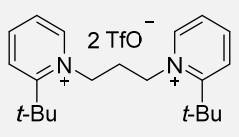
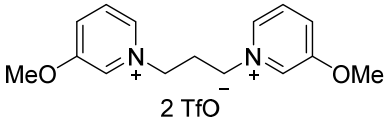
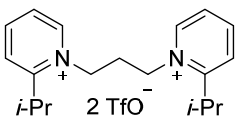
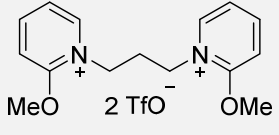
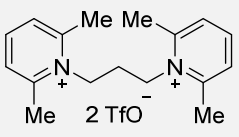
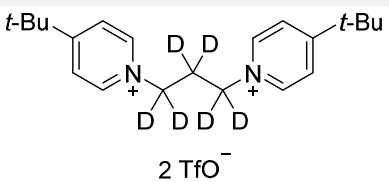
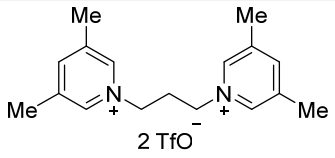
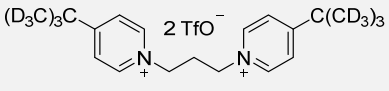
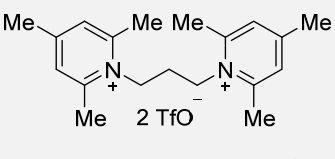
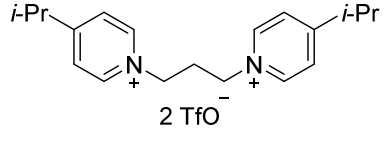
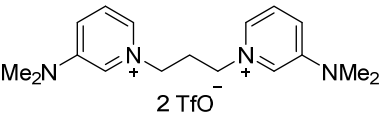
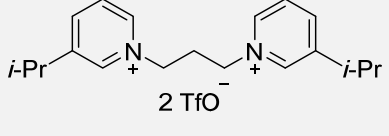
General structure of a substituted BP compound

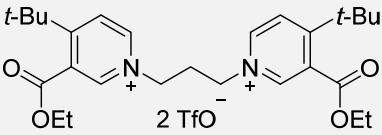
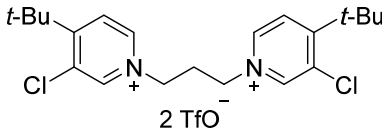
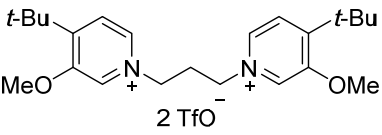
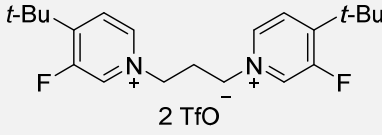
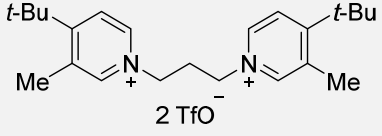
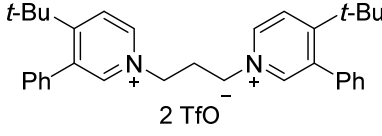
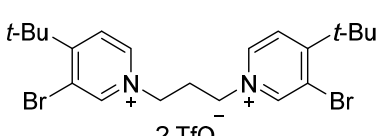
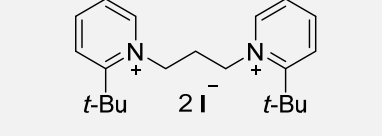
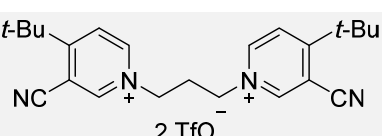
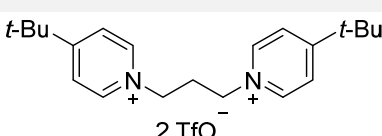
**Figure 4:** General structure of a BP compound and of lead structure MB327.

Test compounds used for electrophysiological screening using the bispyridinium (BP) non-oxime MB327 as a lead structure comprised novel structural BP analogues referred to as PTM compounds which were synthesized at the Centre of Pharma Research, Department of Pharmacy, Ludwig-

Maximilians-Universität, Germany, and were available as iodide ( $I^-$ ) and trifluoromethanesulfonate ( $TfO^-$ ) salts (Figure 4; Table 6) [262].

**Table 6:** BP compounds referred to as PTM compounds.

PTM code	structural chemical formula	PTM code	structural chemical formula
PTM0001	 $C_{21}H_{32}I_2N_2$ : 566.30 g/mol	PTM0008	 $C_{17}H_{20}F_6N_2O_8S_2$ : 558.47 g/mol
PTM0002	 $C_{23}H_{32}F_6N_2O_6S_2$ : 610.63 g/mol	PTM0009	 $C_{17}H_{20}F_6N_2O_8S_2$ : 558.47 g/mol
PTM0003	 $C_{21}H_{28}F_6N_2O_6S_2$ : 582.58 g/mol	PTM0010	 $C_{17}H_{20}F_6N_2O_8S_2$ : 558.47 g/mol
PTM0004	 $C_{19}H_{24}F_6N_2O_6S_2$ : 554.52 g/mol	PTM0011*	 $C_{23}H_{26}D_6F_6N_2O_6S_2$ : 616.55 g/mol
PTM0005	 $C_{19}H_{24}F_6N_2O_6S_2$ : 554.52 g/mol	PTM0012*	 $C_{23}H_{14}D_{18}F_6N_2O_6S_2$ : 628.74 g/mol
PTM0006	 $C_{21}H_{28}F_6N_2O_6S_2$ : 582.58 g/mol	PTM0013	 $C_{21}H_{28}F_6N_2O_6S_2$ : 582.57 g/mol
PTM0007	 $C_{19}H_{26}F_6N_4O_6S_2$ : 584.55 g/mol	PTM0014	 $C_{21}H_{28}F_6N_2O_6S_2$ : 582.57 g/mol

PTM0015	 $C_{29}H_{40}F_6N_2O_{10}S_2$ : 754.75 g/mol	PTM0020	 $C_{23}H_{30}Cl_2F_6N_2O_6S_2$ : 679.51 g/mol
PTM0016	 $C_{25}H_{36}F_6N_2O_8S_2$ : 670.68 g/mol	PTM0021	 $C_{23}H_{30}F_8N_2O_6S_2$ : 646.61 g/mol
PTM0017	 $C_{25}H_{36}F_6N_2O_6S_2$ : 638.68 g/mol	PTM0022	 $C_{35}H_{40}F_6N_2O_6S_2$ : 762.82 g/mol
PTM0018	 $C_{23}H_{30}Br_2F_6N_2O_6S_2$ : 768.42 g/mol	PTM0045	 $C_{21}H_{32}I_2N_2$ : 566.31 g/mol
PTM0019	 $C_{25}H_{30}F_6N_4O_6S_2$ : 660.65 g/mol	PTM0061	 $C_{23}H_{32}F_6N_2O_6S_2$ : 610.63 g/mol

\* deuterated PTM compounds were synthesized for use in liquid chromatography - mass spectrometry (LC-MS) binding studies and were not analyzed in this study [363].

Stock solutions were prepared as 10 mM solutions of ACh, nicotine, epibatidine, carbamoylcholine and methyllycaconitine (MLA) in external recording solution (Table 7). PTM compounds were freshly prepared in external recording solution (Table 7) and diluted to appropriate concentrations for electrophysiological measurements. PNU-120596 stock solutions were prepared as 1 mM solution in 10 % aqueous DMSO and stored at - 80 °C until use.

**Table 7:** Buffers and solutions for patch clamp experiments.

internal solution		
KCl	50 mM	potassium chloride (KCl), catalog No. 7447-40-7 (Carl Roth GmbH, Karlsruhe, Germany)
NaCl	10 mM	sodium chloride (NaCl), catalog No. 7681-52-9 (Carl Roth GmbH, Karlsruhe, Germany)
KF	60 mM	potassium fluoride (KF), catalog No. 7789-23-3 (Carl Roth GmbH, Karlsruhe, Germany)
EGTA	20 mM	ethyleneglycolbis(aminoethyl ether) -N, N, N', N'-tetraacetic acid (EGTA), CAS No. 67-42-5 (Sigma Aldrich, Taufkirchen, Germany)
HEPES	10 mM	2-(4-(2-hydroxyethyl)-1-piperazinyl)-ethane sulfonic acid (HEPES), CAS No. 75277-39-3 (Sigma Aldrich, Taufkirchen, Germany)
KOH	internal solution adjusted to pH 7.4	potassium hydroxide (KOH), CAS No. 1310-58-3 (Merck KGa GmbH, Darmstadt, Germany)
external solution		
NaCl	140 mM	sodium chloride (NaCl), catalog No. 7681-52-9 (Carl Roth GmbH, Karlsruhe, Germany)
KCl	3 mM	potassium chloride (KCl), catalog No. 7447-40-7, Carl Roth GmbH, Karlsruhe, Germany)
MgCl <sub>2</sub>	1 mM	magnesium chloride hexahydrate (MgCl <sub>2</sub> · H <sub>2</sub> O), catalog No. 7791-18-6 (Carl Roth GmbH, Karlsruhe, Germany)
CaCl <sub>2</sub>	2 mM	calcium chloride dehydrate (CaCl <sub>2</sub> · H <sub>2</sub> O), catalog No. 10035-04-8 (Carl Roth GmbH, Karlsruhe, Germany)
glucose	5 mM	D-(+)-glucose, catalog No. 14431-43-7 (Carl Roth GmbH, Karlsruhe, Germany)
HEPES	10 mM	2-(4-(2-hydroxyethyl)-1-piperazinyl)-ethane sulfonic acid (HEPES), CAS No. 75277-39-3 (Sigma Aldrich, Taufkirchen, Germany)
NaOH	external solution adjusted to pH 7.4	sodium hydroxide (NaOH), catalog No. 1310-73-2 (Carl Roth GmbH, Karlsruhe, Germany)
seal enhancer		

NaCl	80 mM	sodium chloride (NaCl), catalog No. 7681-52-9 (Carl Roth GmbH, Karlsruhe, Germany)
KCl	3 mM	potassium chloride (KCl), catalog No. 7447-40-7 (Carl Roth GmbH, Karlsruhe, Germany)
MgCl <sub>2</sub>	10 mM	magnesium chloride hexahydrate (MgCl <sub>2</sub> · H <sub>2</sub> O), catalog No. 7791-18-6 (Carl Roth GmbH, Karlsruhe, Germany)
CaCl <sub>2</sub>	35 mM	calcium chloride dehydrate (CaCl <sub>2</sub> · H <sub>2</sub> O), catalog No. 10035-04-8 (Carl Roth GmbH, Karlsruhe, Germany)
HEPES	10 mM	2-(4-(2-hydroxyethyl)-1-piperazinyl)-ethane sulfonic acid (HEPES), CAS No. 75277-39-3 (Sigma Aldrich, Taufkirchen, Germany)
HCl	seal enhancer adjusted to pH 7.4	0.1 mol/l, CAS No. 7647-01-0 (Carl Roth GmbH, Karlsruhe, Germany)

For the preparation of aqueous buffer solutions, deionized water, which was additionally freshly distilled, was used. All buffers were filtered through a cellulose membrane ( $\varnothing$  0.2  $\mu$ m) and stored at - 20 °C. Prior to an experiment, buffers were freshly thawed and hold at room temperature during an experiment.

**Table 8:** Reagents for cell culture and handling.

DMSO	dimethyl sulfoxide (DMSO), sterile filtered, CAS No. 67-68-5 (Invitrogen, Darmstadt, Germany)
cell culture medium	DMEM/F-12 Media + GlutaMax™, catalog No. 10565018 (Gibco distributed by Life Technologies, Darmstadt, Germany) Ham's F-12 Nutrient Mix, GlutaMAX™, catalog No. 31765035 (Gibco distributed by Life Technologies, Darmstadt, Germany)
ethanol	dried SeccoSolv®, catalog No. 1.00990 (Merck KGa GmbH, Darmstadt, Germany)
liquid nitrogen	CAS No. 7727-37-9 (Air Liquide, Düsseldorf, Germany)

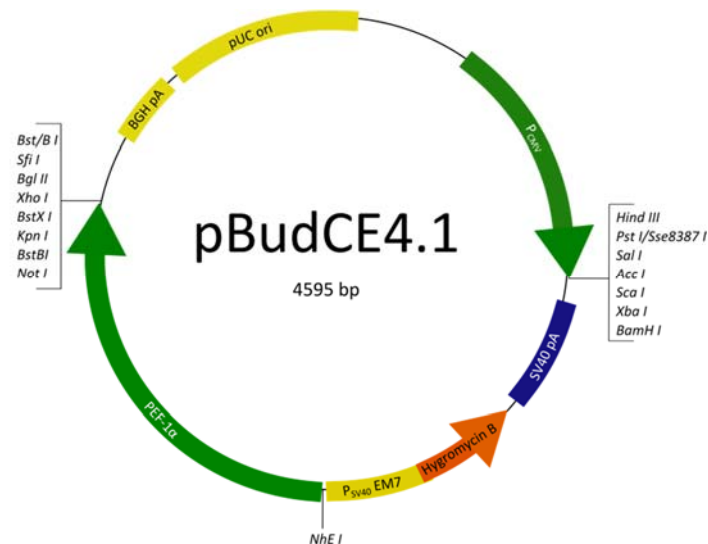


HEPES	2-(4-(2-hydroxyethyl)-1-piperazinyl)-ethane sulfonic acid (HEPES), CAS No. 75277-39-3 (Sigma Aldrich, Taufkirchen, Germany)
hygromycin B	60 mg/ml, catalog No. 10687-010 (Gibco distributed by Life Technologies, Darmstadt, Germany)
geneticin	50 mg/ml, catalog No. 10131019 (Gibco distributed by Life Technologies, Darmstadt, Germany)
sodium pyruvate	100 mM, catalog No. 11360070 (Gibco distributed by Life Technologies, Darmstadt, Germany)
isopropanol	catalog No. 100995 (Merck KGa GmbH, Darmstadt, Germany)
NMDG	M2004, N-methyl-D-glucamine (NMDG), CAS No. 6284-40-8 (Sigma Aldrich, Taufkirchen, Germany)
PBS	phosphate buffered saline (PBS), sterile, 280-315 mOsm/kg, pH 7,4, catalog No. 1001015 (Gibco distributed by Invitrogen, (Darmstadt, Germany)
cell dissociation reagent	„TrypLE™ Express“, catalog No. 12605010 (Gibco distributed by Invitrogen, Darmstadt, Germany) cell dissociation buffer, enzyme-free, PBS-based, catalog No. 13151014 (Gibco, distributed by Invitrogen, Darmstadt, Germany)
“CASY® ton“	isotonic measurement buffer for cell counting with an automatic cell counting and analyzing system, catalog No. 05 651 808 001 (Roche, Mannheim, Germany)
“CASY® clean“	capillary and system cleaning agent for cell counting with an automatic cell counting and analyzing system, catalog No. 05 651 786 001 (Roche, Mannheim, Germany)

“CASY® blue”	cytotoxic agent for viability determination and cell sizing, catalog No. 05 651 760 001 (Roche, Mannheim, Germany)
FBS	fetal bovine serum (FBS), catalog No.: 16000036 (Gibco, distributed by Life Technologies)

## 2.3 Cell culture

Immortalized mammalian cells deriving from rat pituitary tumor cells (*Rattus norvegicus*), GH<sub>4</sub>C<sub>1</sub>, and CHO-K1 cells deriving from Chinese hamster ovary (*Cricetulus griseus*) were obtained from Genionics (Schlieren, Switzerland). CHO-K1 cells were stably transfected with cDNA of human  $\alpha$ 7-nicotinic acetylcholine receptor (h $\alpha$ 7-nAChR) and the acetylcholine receptor chaperone RIC-3 also known as resistance to inhibitors of cholinesterase-3 (RIC-3) expediting the transport of the receptor to the cell membrane (Figure 5) [176]. These cells were denoted as CHO/RIC-3/h $\alpha$ 7-nAChR cells and were obtained from Genionics (Schlieren, Switzerland). The following h $\alpha$ 7-nAChR subunit cDNA and h-RIC3 cDNA with start and end codons highlighted in blue in Figure 5 were applied for insertion into the mammalian expression vector pBudCE4.1 (Invitrogen distributed by Life Technologies, Darmstadt, Germany) which was designed for simultaneous expression of two genes in mammalian cell lines.



### NCBI open reading frame (ORF) sequence of human $\alpha 7$ -nAChR subunit (NM\_000746 version 2)

ATGCGCTGCTCGCCGGGAGGCGTCTGGCTGGCGCTGGCCGCTCGCTCCTGCACGTGTCCCTGCAAGGCG  
 AGTTCCAGAGGAAGCTTTACAAGGAGCTGGTCAAGAACTACAATCCCTTGGAGAGGCCCGTGGCCAATGA  
 CTCGCAACCACTCACCGTCTACTTCTCCCTGAGCCTCCTGCAGATCATGGACGTGGATGAGAAGAACCAA  
 GTTTTAACCACCAACATTTGGCTGCAAATGTCTTGGACAGATCACTATTTACAGTGGAATGTGTGAGAAT  
 ATCCAGGGGTGAAGACTGTTTCGTTTCCCAGATGGCCAGATTTGGAAACCAGACATTCTTCTCTATAACAG  
 TGCTGATGAGCGCTTTGACGCCACATTCCACACTAACGTGTTGGTGAATTCTTCTGGGCATTGCCAGTAC  
 CTGCCTCCAGGCATATTCAAGAGTTCCTGCTACATCGATGTACGCTGGTTTCCCTTTGATGTGCAGCACT  
 GCAAACCTGAAGTTTGGGTCTTGTCTTACGGAGGCTGGTCTTGGATCTGCAGATGCAGGAGGCAGATAT  
 CAGTGGCTATATCCCCAATGGAGAATGGGACCTAGTGGGAATCCCCGGCAAGAGGAGTGAAAGGTTCTAT  
 GAGTGCTGCAAAGAGCCCTACCCCGATGTACCTTCACAGTGACCATGCGCCGAGGACGCTCTACTATG  
 GCCTCAACCTGCTGATCCCTGTGTGCTCATCTCCGCCCTCGCCCTGCTGGTGTTCCTGCTTCTGCAGA  
 TTCCGGGGAGAAGATTTCCCTGGGGATAACAGTCTTACTCTCTCTTACCGTCTTCATGCTGCTCGTGGCT  
 GAGATCATGCCCAGCAACATCCGATTCCGTACCATTTGATAGCCAGTACTTCGCCAGCACCATGATCATCG  
 TGGGCCTCTCGGTGGTGGTGACAGTGATCGTGCTGCAGTACCACCACCACGACCCCGACGGGGGCAAGAT  
 GCCCAAGTGGACCAGAGTCATCCTTCTGAACTGGTGCGCGTGGTTCTTGCGAATGAAGAGGCCCGGGGAG  
 GACAAGGTGCGCCCGGCCTGCCAGCACAAGCAGCGGCGCTGCAGCCTGGCCAGTGTGGAGATGAGCGCCG  
 TGGCGCCGCCCGCCCGCCAGCAACGGGAACCTGCTGTACATCGGCTTCCGCGGCCTGGACGGCGTGCACTG  
 TGTCCCGACCCCCGACTCTGGGGTAGTGTGTGGCCGCATGGCCTGCTCCCCCACGCACGATGAGCACCTC  
 CTGCACGGCGGGCAACCCCCGAGGGGGACCCGACTTGGCCAAGATCCTGGAGGAGGTCCGCTACATTG  
 CCAACCGCTTCCGCTGCCAGGACGAAAGCGAGGCGGTCTGCAGCGAGTGGAAGTTCGCCGCTGTGTGGT

GGACCGCCTGTGCCTCATGGCCTTCTCGGTCTTCACCATCATCTGCACCATCGGCATCCTGATGTCGGCT  
CCCAACTTCGTGGAGGCCGTGTCCAAAGACTTTGCGTAA

#### NCBI open reading frame (ORF) sequence of human RIC-3 (NM\_001206671 version 2)

ATGGCGTACTCCACAGTGCAGAGAGTCGCTCTGGCTTCTGGGCTTGTCTGGCTCTGTCGCTGCTGCTGC  
CCAAGGCCTTCTGTCCCGCGGAAGCGGCAGGAGCCGCCGACACCTGAAGGAAAATTGGGCCGATT  
TCCACCTATGATGCATCATCACCAGGCACCCTCAGATGGCCAGACTCCTGGGGCTCGTTTTCCAGAGGTCT  
CACCTTGCCGAGGCATTTGCAAAGGCCAAAGGATCAGGTGGAGGTGCTGGAGGAGGAGGTAGTGGAAGAG  
GTCTGATGGGGCAGATTATTCCAATCTACGGTTTTGGGATTTTTTTATATATACTGTACATTCTATTTAA  
GCTCTCAAAGGGGAAAACAACTGCAGAGGATGGGAAATGCTATACTGCCATGCCTGGAAACACCCACAGG  
AAAATTACCAGTTTTGAGCTTGCTCAACTGCAAGAAAACTGAAGGAGACAGAAGCAGCCATGGAAAAAT  
TAATCAACAGAGTGGGACCTAATGGTGAGAGCAGAGCACAGACTGTGACTTCTGACCAAGAGAAAACGGTT  
GCTACATCAGCTCCGAGAAATCACCAGGGTCATGAAAGAAGGAAAATTCATTGACAGATTTTCTCCAGAG  
AAAGAAGCTGAGGAGGCCCTTACATGGAGGACTGGGAAGGTTACCCTGAAGAGACTTACCCAATTTATG  
ACCTTTTCAGACTGTATCAAGCGTAGGCAAGAAACAATCTTGGTGGATTACCCTGACCCAAAAGAACTTTC  
TGCTGAAGAAATAGCTGAAAGAATGGGAATGATAGAAGAGGAAGAATCAGATCATTGTTGGGTTGGGAAAGT  
CTGCCCCTGACCCAGAGCCCAGGAAGATAATTCTGTTACCTCGTGTGATCCAAAGCCAGAAACATGTT  
CCTGCTGTTTTTCATGAAGACGAGGATCCTGCTGTCTTGGCAGAGAATGCTGGATTCAGTGCAGATAGCTA  
CCCTGAGCAAGAGGAAACCACCAAAGAAGAGTGGTCCCAAGACTTTAAAGATGAAGGGTTGGGCATCAGC  
ACCGATAAAGCATATACAGGCAGCATGCTGAGGAAGCGTAACCCCCAGGGTTTAGAGTGA

**Figure 5: Mammalian expression vector pBudCE4.1 (4595 pb) (Invitrogen distributed by LifeTechnologies, Darmstadt, Germany) for stable transfection of  $\alpha 7$ -nAChR subunit and h-RIC3 cDNA into CHO-K1 cells (CHO/RIC-3/ $\alpha 7$ -nAChR) and open reading frames of  $\alpha 7$ -nAChR subunit and h-RIC3 cDNA.** Elements of pBudCE4.1 designed for simultaneous expression of two genes in mammalian cell lines are described in Table 9 and start and stop codons of cDNA are shown in blue.

**Table 9:** Elements of pBudCE4.1 (4595 bp) (Invitrogen, distributed by Life Technologies, Darmstadt, Germany).

element	location (bases)	specification
human cytomegalovirus (CMV) immediate-early promoter/enhancer	7-594	permits high-level expression of recombinant protein
CMV forward priming site	544-564	permits sequencing through the insert from the 5' end
T7 promoter/priming site	638-657	permits sequencing through the insert from the 5' end. Allows for <i>in vitro</i> transcription in the sense orientation
CMV multiple cloning site	664-713	seven unique sites allow insertion of gene
SV40 polyadenylation signal	803-933	transcription termination and polyadenylation of mRNA
hygromycin B resistance gene	1063-1437 (complementary strand)	selection of transformants in <i>E. coli</i> and stable transfectants in mammalian cells
EM7 promoter	1456-1510 (complementary strand)	synthetic promoter based on the bacteriophage T7 promoter for expression of the hygromycin resistance gene in <i>E. coli</i>
SV40 early promoter and origin	1547-1869 (complementary strand)	permits high-level expression of the hygromycin B resistance gene and episomal replication in cells expressing the SV40 large T antigen
human elongation factor 1 $\alpha$ (EF-1 $\alpha$ ) promoter	1885-3051	permits high-level expression of recombinant protein
EF-1 $\alpha$ forward priming site	2999-3019	permits sequencing through the insert from the 5' end
EF-1 $\alpha$ multiple cloning site	3062-3126	seven unique sites allow insertion of the gene
bovine growth hormone (BGH) reverse priming site	3218-3235 (complementary strand)	permits sequencing through the insert from the 3' end

BGH polyadenylation signal	3224-3447	transcription termination and polyadenylation of mRNA
pUC origin	3521-4194	high-copy number replication and growth in <i>E. coli</i>

Transfection of the construct was performed according to the manufacture's protocol (Genionics, Schlieren, Switzerland) and stably transfected CHO/RIC-3/h $\alpha$ 7-nAChR cells were cultivated in the presence of the selection marker hygromycin B to separate transfected cells from not transfected cells. Functional properties of h $\alpha$ 7-nAChR were validated by patch clamp techniques in the whole-cell configuration according to the manufacture's protocol (Genionics, Schlieren, Switzerland). For long-term storage, GH<sub>4</sub>C<sub>1</sub>, CHO-K1 and CHO-K1/RIC-3/h $\alpha$ 7-nAChR cells were suspended in fresh freezing medium containing complete medium given in Table 10 supplemented with 10 % DMSO at a density of approx. of  $2 \times 10^6$  cells/ml. Aliquots of 0.5 ml of cell suspension were filled into cryovials and transferred to a liquid nitrogen tank.

**Table 10:** Composition of cell culture media for different cell lines.

cell line	cell culture medium	supplements
GH <sub>4</sub> C <sub>1</sub>	DMEM/F-12 Media + GlutaMax™	FCS, 10 % + natrium pyruvate, 1mM
CHO-K1	Ham's F-12 Nutrient Mix, GlutaMAX™	FCS, 10 %
CHO-K1/RIC-3/h $\alpha$ 7-nAChR	Ham's F-12 Nutrient Mix, GlutaMAX™	FCS, 10 % + hygromycin B, 300 $\mu$ g/ml

For cultivation, cells were thawed quickly at 37 °C and transferred into T-75 culture flasks containing 20 ml pre-warmed complete medium (Table 10) and were maintained at 37 °C in a humidified, 5 % CO<sub>2</sub> environment in supplemented cell culture media.

Cells were incubated at 37 °C for 24 h to allow cells to attach to the bottom of the flask before the medium was aspirated and replaced by fresh complete medium. When cells reached 70 - 80 % confluence, they were passaged. For this purpose, the culture medium was aspirated and washed once with 4 ml PBS. Subsequently, 3 ml cell dissociation buffer (enzyme-containing, trypsin-free) was added to the cells and the flask was tilt gently to distribute the solution evenly. Then, most of the solution was removed leaving only a thin film covering the cells. During incubation of cells for 3 min in the incubator (37 °C, 95 % O<sub>2</sub> and 5 % CO<sub>2</sub>) cells detached from the surface of the culture flask. Then, cells were resuspended in 10 ml pre-warmed complete culture medium and an aliquot of 2 ml containing approx.  $2 \times 10^6$  cells was transferred to a T-75 culture flask prefilled with 20 ml fresh pre-warmed

culture medium. For further cultivation, cells were routinely passaged after 3 days at 70 - 80 % confluence according to the prescribed procedure. For cell counting, 100  $\mu$ l of the cell suspension were added to 10 ml of CASY<sup>®</sup> ton prefilled in a CASY<sup>®</sup> cup and the cell number was determined by an automatic cell counting and analyzing system (Casy<sup>®</sup> TTC).

## 2.4 Patch clamp technique

### 2.4.1 Theoretical background – ionic theory

The electrical properties of a cell derive from the properties of the cell membrane. The cell membrane is selectively permeable to specific ion species through ion channels and transporters which determine the electrical potential difference between the interior and the exterior of a cell [8, 31]. This so called membrane potential is generated by the unequal concentrations of ions on opposite sides of the membrane due to the semipermeable property of the membrane of a cell. The membrane is in electrical terms a resistor or conductor because it is selectively permeable to specific ion species whereas it is a barrier for the flow of other ion species (Figure 6) [3, 310]. In this context, ions move through the semipermeable membrane by diffusion down their concentration gradient and their electrical force. In addition, ions move by active transport through integral membrane transporters and pump proteins that actively carry ions against their concentration gradient under the use of cellular energy adenosine triphosphate (ATP) (Figure 6) [52]. The most relevant ion pump for membrane potential that carry out active transport is the Na<sup>+</sup>-K<sup>+</sup> pump that uses energy derived from ATP to take three Na<sup>+</sup> ions outside the cell in exchange of two K<sup>+</sup> ions that are transported to the inside of the cell [140]. In that way, K<sup>+</sup> concentration is high inside the cell and low outside the cell whereas Na<sup>+</sup> is at low concentrations inside and at high concentrations outside the membrane (Figure 6) [310, 311]. The inside of the cell is slightly more negatively charged relative to the outside of the cell due to the high Na<sup>+</sup> concentration outside the cell and the excess of negatively charged ions and proteins inside the cell (Figure 6) [228, 388]. Hence, the ion gradient of a cell membrane consists of two components that determine the movement of ions across the membrane, an electrical component causing a charge difference and a chemical component causing a concentration difference of ions across the membrane and together this is called the electrochemical gradient [228, 394]. This gradient is determined by ion diffusion with the gradient through ion channels that can be classified into voltage-gated (VGIC) and ligand-gated ion channels (LGIC) besides other channels. These VGIC and LGIC open and close the channel pore selective for one type of ion, for example K<sup>+</sup> channels in response to the voltage or to the binding of a ligand molecule [367]. The ion species that is the main driving force for the formation of the membrane potential is K<sup>+</sup> due to its high permeability across the membrane,

but can also involve  $\text{Na}^+$ , whereas  $\text{Ca}^{2+}$  and  $\text{Cl}^-$  ions can be omitted [48]. Therefore, the electrochemical gradient of  $\text{K}^+$  constitutes the tendency of  $\text{K}^+$  ions to diffuse out of the cell due to the concentration difference of  $\text{K}^+$  between the two sides of the membrane. In contrast, the positive charge of the  $\text{K}^+$  ion leads to diffusion of  $\text{K}^+$  with the electrical gradient to the inside of the cell [228]. Consequently, the electrochemical gradient causes an unequal concentration of  $\text{K}^+$  at its equilibrium and causes a voltage difference between the inside and the outside of the cell (Figure 6) [48, 228, 388].

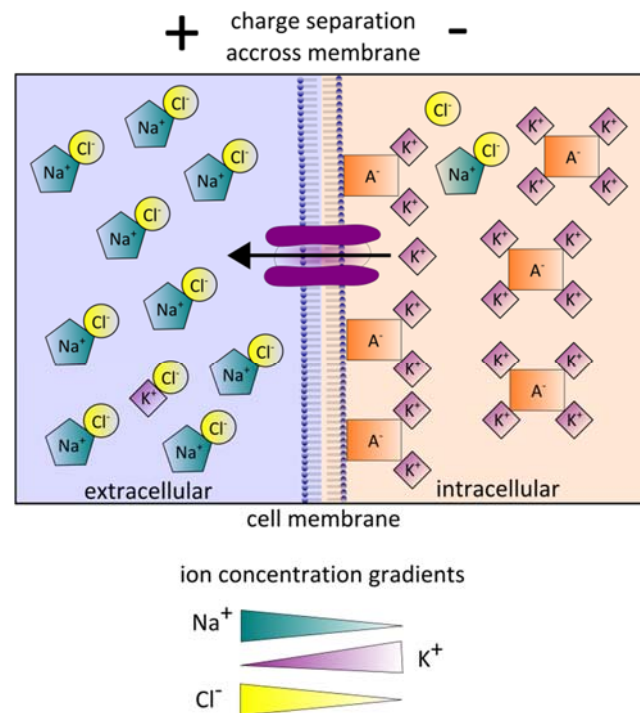


**Figure 6: Diagram of electrochemical equilibrium and charge for  $\text{Na}^+$ ,  $\text{K}^+$ ,  $\text{Cl}^-$  and proteins ( $\text{A}^-$ ) across the semipermeable cellular membrane (Image adapted from [2]).**



When the concentration of an ion is equilibrated on both sides of the membrane, the reversal potential of that ion is reached which is the equilibrium potential of an ion at which diffusive and electrical forces counterbalance [48]. Thus, the chemical gradient equals the electrical gradient at the reversal potential and can be calculated for single ions by using the Nernst equation [48]:

---


$$E_A = \frac{RT}{zF} \ln \frac{[A]_o}{[A]_i}, \quad \text{equation 1}$$

with  $\ln(x) = -2.3 \log_{10}(x)$ :

$$E_A = -2.3 \frac{RT}{zF} \log_{10} \frac{[A]_o}{[A]_i}, \quad \text{equation 2}$$

with  $\ln(x) = -2.3 \log_{10}(x)$ :

and  $RT/F = 25.2 \text{ mV}$  (at  $20^\circ \text{C}$ ):

$$E_A = -2.3 \times 25.2 \text{ mV} \log_{10} \frac{[A]_o}{[A]_i} = -58 \text{ mV} \log_{10} \frac{[A]_o}{[A]_i} \quad \text{equation 3}$$

where  $R$  is the gas constant ( $8.314 \text{ V C K}^{-1} \text{ mol}^{-1}$ ),  $T$  is the absolute temperature ( $T = 273^\circ + \text{C}^\circ$ ),  $z$  is the charge of ion  $A$ ,  $F$  is Faraday's constant ( $9.648 \times 10^4 \text{ C mol}^{-1}$ ), and  $[A]_o$  and  $[A]_i$  are the concentrations of ion  $A$  outside the cell and inside the cell, respectively.

---

Considering the ion concentrations of the external and internal solution used in this study, the Nernst potential of the single type of ions were calculated for  $\text{K}^+$  and  $\text{Na}^{2+}$  by the following equations:

---

Nernst potential

$$E_{\text{K}^+} = -58 \text{ mV} \log_{10} \frac{[\text{K}^+]_o}{[\text{K}^+]_i} \quad E_{\text{K}^+} = -58 \text{ mV} \log_{10} \frac{3 \text{ mM}}{50 \text{ mM}} = -71 \text{ mV} \quad \text{equation 4}$$

$$E_{\text{Na}^+} = -58 \text{ mV} \log_{10} \frac{[\text{Na}^+]_o}{[\text{Na}^+]_i} \quad E_{\text{Na}^+} = -58 \text{ mV} \log_{10} \frac{140 \text{ mM}}{10 \text{ mM}} = +66 \text{ mV} \quad \text{equation 5}$$


---

By definition, the voltage generated by the gradient of single ions determined by the Nernst potential is based on charge and the interior and exterior concentration of the ion in question while the voltage generated by the gradient of all ions is reached when the net flow of current across the membrane is zero [221]. This so called resting membrane potential (RMP) is defined as the potential at the inner side of the membrane relative to the potential at the outer side of the membrane in a steady-state condition for a long period of time [3] and typically ranges between  $-40$  to  $-80 \text{ mV}$  inside the cell membrane of mammalian cells [48, 228, 388]. Thereby, the Goldman-Hodgkin-Katz equation describes

the averaged reversal potentials of all ion species and considers the permeability of the plasma membrane to each ion species (equation 6), in order to calculate the RMP [48]. The equation gives the weighted, which means the ions relative permeability, average of the equilibrium potential considering all permeant ions [48]. Changes in membrane potentials and determinants of the RMP are determined by properties of semipermeable membranes through which ions move by diffusion, upon ion channel activation or active transport. Thus, the membrane potential changes with changes of the permeability of the membrane due to opening of ion channels and is directly proportional to the conductance of a cell [3, 48, 221, 228, 388].

---


$$E_m = \frac{RT}{zF} \ln \frac{P_{i_1}[A_1]_o + P_{i_2}[A_2]_o + P_{i_3}[A_3]_o}{P_{i_1}[A_1]_i + P_{i_2}[A_2]_i + P_{i_3}[A_3]_i} = \frac{RT}{zF} \ln \frac{P_K[K^+]_o + P_{Na}[Na^+]_o + P_{Cl}[Cl^-]_i}{P_K[K^+]_i + P_{Na}[Na^+]_i + P_{Cl}[Cl^-]_o} \quad \text{equation 6}$$

where  $R$  is the gas constant ( $8.314 \text{ V C K}^{-1} \text{ mol}^{-1}$ ),  $T$  is the absolute temperature ( $T = 273^\circ + C^\circ$ ),  $z$  is the charge of ion  $A$ ,  $F$  is Faraday's constant ( $9.648 \times 10^4 \text{ C mol}^{-1}$ ),  $[A]_o$  and  $[A]_i$  are the concentrations of ion [outside the cell and inside the cell] and  $P_i$  is the relative permeability of the ion type outside the cell and inside the cell, respectively.

---

Based on the facts that cells possess a distinct RMP due to unequal distribution of ions mediated by the electrochemical gradient of the semipermeable membrane and on the fact that the transmembrane potential changes upon activation of ion channels, the development of the patch clamp technique was intended to record the electrical currents deriving from ions flowing through single channels on a plasma membrane of a cell. This technique derived from the concept of a voltage-clamp described in section 2.4.4. By convention, currents induced by an inflow of positively charged ions into the cell are denoted as an inward current and are displayed as downward deflecting current whereas an efflux of positively charged ions is denoted as an outflux and is displayed as an upwards deflecting current in the patch clamp recordings. For negatively charged ions the opposite applies [232].

### 2.4.2 Basic principle of the patch clamp technique

Based on the work by Kenneth Cole and J. H. Curtis [67] on the technique of the voltage-clamp, the electrophysiological patch clamp technique was developed in 1976 by the pioneering work by Erwin Neher and Bert Sakmann who were awarded the Nobel Prize for the development of the patch clamp method in 1991 [227]. In principle, the patch clamp technique is used to investigate the properties of ion channels by recording electrical currents flowing through single channels on a plasma membrane of a cell [227]. In this technique, a glass micropipette called a patch pipette as a recording

microelectrode with a small opening is pressed against a cell that is floating in a physiological bath solution where a second electrode, a bath electrode, is placed as a reference ground electrode [221]. The pipette is filled with a solution corresponding the ionic composition of the bath solution and captures a surface area or so called patch of a cell that contains just one or a few ion channel molecules [232]. By application of slight under-pressure in the pipette, a portion of the membrane is suctioned into the pipette and forms tight sealing between the cell membrane and the rim of the glass pipette in terms of high resistance [221]. The high resistance of this seal creates a resistance of the order of several gigaohm, the so called “gigaseal” that electronically isolates the patch from the rest of the membrane and allows for direct measurement of electric current across the patched membrane [221]. Such currents are induced by activation of ion channels below the pipette opening. Achieving a gigaseal provides mechanical stability to the recording and low noise recordings and thus allows for resolving small currents, even at single channel level [232]. This gigaseal procedure allowed Neher and Sakmann and their co-workers to obtain the so called cell-attached patch clamp recording configuration which is used for the measurement of single channels. Hereby, it is assumed that the patch which is the membrane under the opening of the pipette contains just one ion channel molecule [227]. Moreover, three other measurement configurations beside the cell-attached configuration can be excised [232]. One of them is the inside-out patch where the pipette is pulled back to isolate the membrane patch and thus, the cytosolic side of the membrane is separated from the residual membrane and faces the external salt solution allowing modifications of the solution to test for intracellular factors that control membrane channel activity [232]. The most common mode is the whole-cell configuration which is achieved from the cell-attached configuration by briefly applying a suction pulse while maintaining the tight seal to rupture the cell membrane under the opening of the pipette in order to access the interior of the cell [232]. In this mode, the ionic continuity between the solution in the pipette and the interior of the cell is perfused, thus, the ionic composition of the pipette solution corresponds that of the cytoplasmic ionic composition when measuring in the whole-cell configuration [221]. The main difference of the whole-cell mode to cell attached mode is that electrical currents are recorded from the entire cell membrane in the whole-cell mode instead of from the membrane patch [221]. A modification of the whole-cell mode is the outside-out configuration. In this case, the pipette is retracted during the whole-cell configuration resulting in rupture and rearrangement of the membrane so that two pieces of membrane with the cytosolic site facing the pipette solution reconnect at the tip of the pipette to form a vesicular structure with the extracellular surface exposed to the extracellular site [221]. The outside-out configuration enables investigation of small populations of channels or single channels and allows modifying the extracellular medium by rapid perfusion [221]. In this study, the whole-cell configuration was used.

### 2.4.3 Automated planar patch clamp

The conventional patch clamp technique is considered as the state-of-the-art technology for obtaining highly resolved information in real time about ion channel function and regulation through direct measurement of ion flow across these membrane proteins [221]. However, patch clamping suffers from being extremely laborious and very labor intense since a skilled and highly trained experimenter and technical means to visually and mechanically control the pipette and to shield the recordings from vibrations and electromagnetic noise are required [94, 96]. Due to the serious throughput restrictions of conventional patch clamping, it is not feasible to be routinely employed in most phases of large scale ion channel drug screening and ion channel related research in industrial drug development programs [94, 96]. The development of automated patch clamp technology is aimed at removing this bottle neck and enabling the generation of high-quality data with efficient high throughput capabilities by automation and parallelization to facilitate the drug screening of ion channels active compounds [98, 313]. Such automated patch clamp platforms become increasingly used within areas of drug discovery as well as academic research and are pivotal for safety assessment, secondary screening and lead optimization [94, 96]. Many platforms have been launched and are commercially available such as NPC-16 Patchliner<sup>®</sup> and SyncroPatch<sup>®</sup> 96 (Nanion Technologies GmbH, Munich, Germany), CytoPatch<sup>™</sup> (Cytocentrics AG, Rostock, Germany), PatchXpress<sup>®</sup> 7000A, IonWorks<sup>®</sup> Quattro and IonWorks Barracuda<sup>™</sup> (Molecular Devices, LLC, Wals, Austria), Dynaflo<sup>®</sup> HT (Celletricon AB, Mölndal, Sweden), QPatch HT (Sophion A/S, Copenhagen, Denmark) and IonFlux HT (Fluxion Bioscience Inc, San Francisco, USA) [219, 313, 362]. Here we describe features of Nanion's Patchliner<sup>®</sup>, which is a fully automated patch clamp workstation supporting gigaseal recordings from up to eight cells simultaneously (Figure 7) [95]. This technology utilizes micro structured borosilicate glass chips with small perforations of a diameter of  $\sim 1 \mu\text{m}$  as seal forming substrates (NPC-chips) with 16 recording chambers (Figure 7) [45, 46]. These tiny holes mimic the geometry of an inverted patch pipette tip and replace the traditionally used, manually manipulated, glass micropipette for patch clamp recordings. In total, three NPC-16 chips can be mounted on the chip loading area at a time so that up to 48 experiments can be pre-programmed and executed in a row [95]. Each of the recording chambers is a three-part structure in which a rectangular glass plate is sandwiched between two pieces containing the microchannel structures, the upper one for the administration of external solution to the upper site, and the lower one for the administration of internal solutions (Figure 7) [45, 46, 95]. The whole system is integrated into a liquid handling environment enabling application of solutions, cell suspension and compounds on the chip by a robotic pipetting arm (Figure 7) [95]. The robot and thus the electrophysiological measurements were controlled using a graphical user interface with a user-determined protocol which was pre-programmed and computer controlled [95].

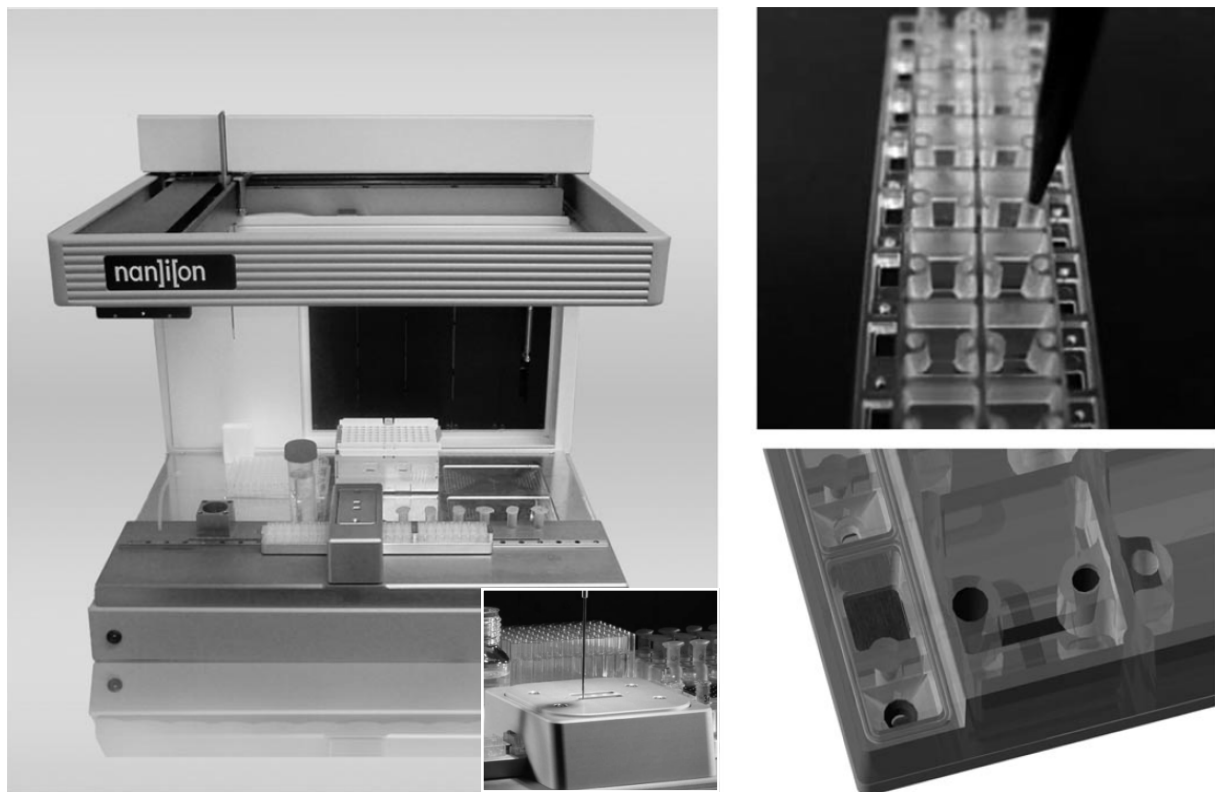


**Figure 7: The automated planar patch clamp workstation of a Patchliner® using NPC-16 chips for parallel recordings in the cell-attached and whole-cell configuration.** On the left, the patchliner platform is shown with the measurement head magnified in the right front corner which contains the pneumatic and electric contacts for recording. The chips are placed on a motorized stage, which slide automatically into the head station. On the upper right, the chip containing 16 recording channels with a solution delivery pipette inserted into the extracellular inlet of one chamber is shown. On the lower right, a schematic drawing of single recording site of the 16-well microfluidic cartridge with microfluidic cross-channel geometry with internal and external microfluidic perfusion channels is illustrated [46, 95].

Thereby, the software adapts two simultaneously running programs, PatchControlHT and Patchmaster [95]. The Patchmaster was used to control the settings of the amplifier and to conduct the recordings while in PatchControlHT the complete sequence of the experiment was defined which contained the user-determined experimental routine from cell catch, over sealing, gaining whole-cell access to the electrophysiological recordings and solution exchange [95]. Following the set-up of this sequential protocol, the chip was first filled with 35  $\mu\text{l}$  internal solution which was added to the lower compartment of the chip underneath the aperture (Figure 9). Then, 40  $\mu\text{l}$  external solution was added to the upper compartment above the aperture (Figure 9). Subsequently, an external and an internal coated silver chloride electrode were applied to both compartments, whereas the internal microelectrode corresponded the recording microelectrode and the external microelectrode the

reference ground electrode (Figure 9). Once the chambers were filled with internal solution in the lower and external solution in the upper chamber, the zero potential was set which is defined as the potential where no current flows between internal and external solution. Thus the zero potential was determined from the bath and the recording electrode [221]. After setting the zero potential controlled by the PatchControlHT and Patchmaster software, a repetitive rectangular command test pulse was induced signifying the resistance of the aperture (Figure 8) [221]. Thereby, a squared current response was observed on the monitor which was an important aid to monitor the process of making a seal (Figure 8) [3, 221]. Cells suspended in external solution were applied to the upper microchannel structure whereby one single cell was captured at the micro-sized aperture in the center of the recording chamber. By applying suction to place the cell on top of aperture created a strong seal between the cell membrane and the rim of the aperture so that a high electrical gigaseal was formed [46, 95]. The process of making a seal initiated by a cell approaching the aperture was monitored by a decrease of the current response as the resistance between the cell membrane and the opening of the aperture increased (Figure 8) [221]. If contact was stable, the outer membrane patch electrically isolated the internal from the external solution whereas resistance between the internal solution in the lower chamber and the external solution in the upper chamber was in the gigaohm range ( $G\Omega$ ,  $10^9$  Ohm, "gigaseal") [95, 221]. During the formation of a gigaseal, the current response approached the baseline until it was in line with the baseline with two capacitive artefacts shown as fast peaks visible at the start and the end of the pulse on the monitor (Figure 8) [3, 221].

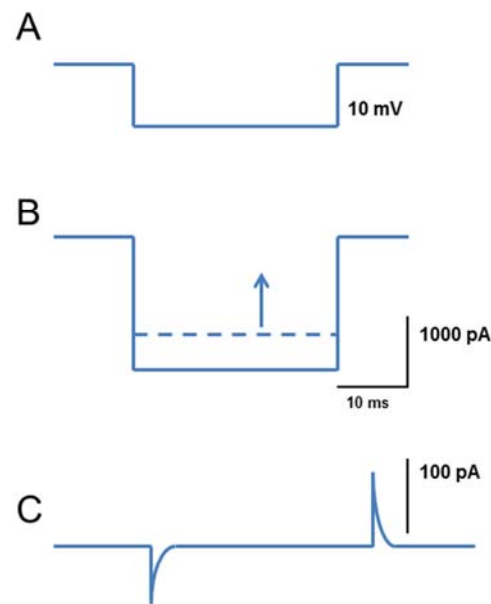


**Figure 8 A-C: Current response to a command test pulse with a cell approaching the aperture in the recording chamber.** The command test pulse (A), the current response of the internal and external solution to the command test pulse (solid line) and of the increasing resistance as the cell approached the aperture (dashed line) are shown (B). During seal formation, the decrease of the current response is indicated by the arrow moving towards the baseline of the command test pulse (B). Current response to the command test pulse after gigaseal formation is shown with two capacitive artefacts (C) [232].

The difference between the baseline and the current after seal formation gives the offset potential that equals the leakage current which derives from ion movement between the outer cell membrane and the rim of the aperture [221]. With establishment of a sufficiently high seal, leakage currents were very small. Such a leakage current would systematically generate excessively high compensating current of the voltage-clamp and also raise the proportion of the non-relevant currents, denoted as background noise [232].

From the cell-attached configuration, the patch could be modified and was thus accessible to other configurations as described in section 2.4.2. [232]. The experiments of this study were conducted in the whole-cell configuration. For this purpose, the membrane patch underneath the aperture was ruptured by application of a short negative impulse so that current pattern of the entire cell membrane and therefore an ion channel population of the cell were recorded [232]. Following the whole-cell configuration of a cell, the application of test solutions to the cell was initiated by using a specific liquid

application method [1]. This method comprises a stacked application approach, wherein external solution was aspirated first into the pipette, directly followed by aspiration of compound solution (Figure 9) [1]. Thereby, mixing of the two solutions was avoided by a tiny air gap between the two solutions. Using the stacked solution the patch clamped cells were exposed with solutions in reversed order at a user-determined flow rate and volume [1].

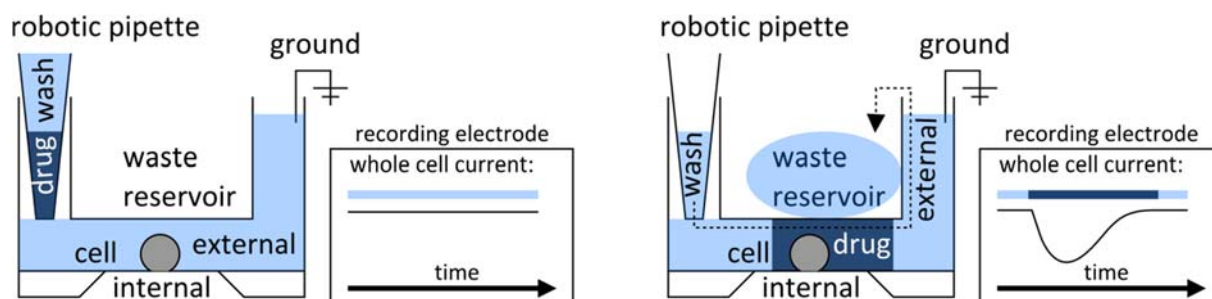


**Figure 9: Schematic of a cross-section of one chip chamber showing the arrangements of solutions, chip and cell.** In brief, a cell is automatically sealed to borosilicate glass chip and recordings can be performed in the cell-attached or whole-cell configuration. Drug application is carried out by using a double stacked solution. Thereby, the pipette first aspirates buffer, then compound. When expelling this stack, the cell is first exposed to ligand and then buffer and subsequently the liquid is spilled into a waste reservoir via the outlet. The path of the compound solution is indicated in the schematic. Representative recordings are shown next to the schematic cross-section. For more information, see [1].

#### 2.4.4 Current- versus voltage-clamp mode

Ion currents through the membrane of a cell arise from activation of ion channels induced by voltage changes or a selective ligand and can be analyzed by application of the voltage-clamp mode [232]. In a patch clamp experiment in the voltage-clamp mode, the membrane voltage and measurement of the transmembrane current was controlled by setting the desired command voltage, which is also referred to as the holding potential  $V_c$  to a constant potential [221]. The membrane potential  $V_m$  was measured iteratively by an amplifier connected to the internal recording electrode in the internal solution, and an external reference, or bath, electrode in the external solution (Figure 10) [232]. More specifically,  $V_c$  of the cell was maintained by using a negative feedback mechanism [232]. First, the operational amplifier (OPA) received an input from the signal generator that determined  $V_c$  and subtracted the membrane potential from the command potential ( $V_c - V_m$ ) [232]. If  $V_m$  was not equal to  $V_c$ , the output of the OPA generated a voltage which was proportional to the difference of the input voltages but extremely amplified [232]. This voltage was passed to the control output unit of the amplifier ( $V_{out}$ ),



and converted into current, which was equal to the voltage at the OPA output and opposite to the ionic current, with a corresponding calibration factor depending on the resistor of the feedback circuit called  $R_f$  [232]. Because of the different voltages between  $V_c$  (point 1 in Figure 10) and point 2 in Figure 10, a current flowed through  $R_f$  (Figure 10) [232]. Thus, a voltage proportional to the current flowed described by the Ohm's Law:  $U_f = R_f * I$  until the potential at point 1 ( $V_c$ ) was equal to  $V_m$  [232]. The current flowed into the electrode and not back into the OPA due to its high input resistance. This negative feedback circuit operated visually instantaneously and allowed to measure and record the required current to be applied to the cell to keep  $V_m$  equal to  $V_c$  [232]. In this means, the current generated by ion channels that open and close over time in response to changes in  $V_m$  could be measured and recorded [232]. In contrast to the voltage-clamp mode, the current-clamp mode recorded the membrane potential by injecting current into a cell [232]. Unlike in the voltage-clamp mode, where the membrane potential was kept at a set level determined by the experimenter and the compensating current was recorded, in the current-clamp mode the current was hold at a constant value and changes of the membrane potential were recorded [221]. The current-clamp mode was used to draw conclusions about the resting potential of a cell by setting the current flow to zero [3, 221].

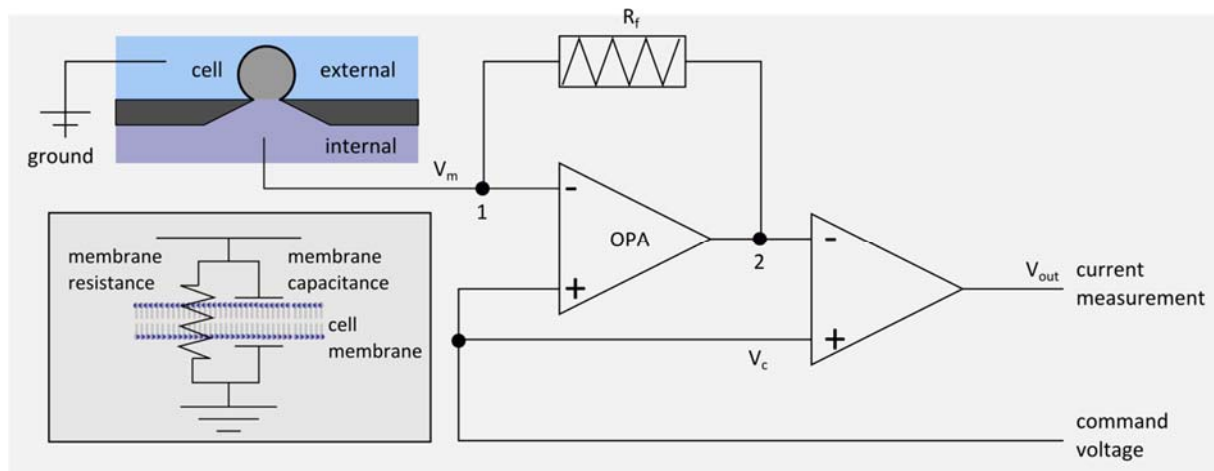


**Figure 10: Simplified schematic of a circuit of a patch clamp amplifier for a cell under whole-cell patch clamp recording configuration and electric properties of the cell membrane.** The definitions of the symbols are as follows: OPA: operational amplifiers,  $R_f$ : feedback resistor,  $V_c$ : command voltage,  $V_m$ : membrane potential,  $V_{out}$ : output voltage [232].

#### 2.4.5 Cell handling for patch clamp experiments

On the day of experiment, cells were harvested by removing the culture medium from the culture flask followed by one washing step with 5 ml PBS. Then, cells were detached from the bottom of the flask by applying and removing cell dissociation buffer so that a thin film remains on the cells while incubation for 3 min at 37 °C. Dissociation of the cells from the flask was mechanically supported by

gently tilting the flask before cells were resuspended in external solution (see section 2.3). Cells were centrifuged at room temperature for 5 min. The supernatant was discarded and the cell pellet was dissolved in external solution whereas the volume of external solution was adjusted to the recommended cell count between  $1 \times 10^5 - 5 \times 10^5$  cells/ml. Cell viability and cell number was controlled before each patch clamp experiment using the Casy<sup>®</sup> TTC, an automated cell counting and analyzing system. Cells were incubated at 4 °C for 1 h before transferred to a so called “cell-hotel”, a pre-cooled conical cell storage device which is integrated into the Patchliner workstation.

#### **2.4.6 Determination of the resting membrane potential**

The current clamp mode was used for determination of RMP of a quiescent cell, which is defined as the potential between the inside and outside of a cell where no impulse was conducted [221]. The RMP was recorded for wildtype CHO-K1 and GH<sub>4</sub>C<sub>1</sub> cells at a current level set to zero. For a total time of 4 s, the potential with no injected current ( $I = 0$  A) was recorded and plotted versus time. The RMP was determined by the means voltage measured for 4 s.

#### **2.4.7 Seal success rate and current signal**

The Patchliner is a flexible research platform since the user can interrupt and directly control the experiments at any time and protocols can be changed or extended on-the-fly, according to the user's judgment [95, 313]. Therefore, the Patchliner is preferable for academic purpose over other robotic systems, which run through predefined protocols and are thus designed to meet the needs of the pharmaceutical industry for secondary drug screening efforts and safety profile characterization [95, 96, 98, 313]. In this study, whole-cell patch clamp recordings were conducted on the Patchliner<sup>®</sup> using planar borsilicate chips as described in section 2.4.3. Cellular parameters and settings were modified from the original ones given in Table 11 in order to achieve an improved seal success rate of the cells. From the pre-cooled cell hotel, an aliquot of 20 µl of the cell suspension was aspirated and added to the chip after addition of external and internal solution to the cell described in section 2.4.3. A cell was caught randomly from the cell suspension and positioned at the aperture by application of under-pressure to capture and to hold the cell. Thereby, the under-pressure strength to capture and to hold the cell was modified (first modification) by varying the capture pressure to position the cell at the aperture and holding pressure was modified (second modification) to keep the cell at the aperture. The cell number successfully captured and hold at the aperture out of all cells tested was determined. After the whole-cell configuration was established, a seal enhancer solution was additionally applied to the cell (third modification). Seal enhancer was replaced by external solution just before starting recording and the number of cells achieving giga-seal formation and with a stable seal which means a

maintained gigaseal over a 5 point measurement by addition of seal enhancer was determined. Moreover, the number of cells achieving gigaseal formation and with a stable seal over a 5 point measurement was determined by using cells from passages 13 to 33 and was delimited to a specific cell range where gigaseals were observed to be stable (fourth modification) (Table 11). All in all, percentage seal success rate composed of gigaseal formation, stable seal rate and rate of run down over a five point measurement was determined for original setting (Table 11) and after step by step modification. The configuration showing the highest percentage gigaseal formation including configuration of cell capture and holding pressure, plus addition of seal enhancer and finally plus use of a cell within a distinct cell passage range where no significant reduction in sealing rate occurred was routinely applied. Thereby, the total improvement of the seal success rate, stable seals and run down over a 5 point measurement could be calculated using the following equations:

---


$$\text{gigaseal [\%]} = (\text{cell number of gigaseal formation rate of 1}^{\text{st}} \text{ step} / \text{total cell number}) * 100$$

*equation 7*

$$\text{stable seal [\%]} = (\text{cell number of gigaseal of 5}^{\text{th}} \text{ step} / \text{cell number of gigaseal formation rate of 1}^{\text{st}} \text{ step}) * 100$$

*equation 8*

$$\text{run down [\%]} = 100 - (\text{cell number of gigaseal of 5}^{\text{th}} \text{ step} / \text{cell number of gigaseal of 1}^{\text{st}} \text{ step}) * 100$$

*equation 9*

---

For determination if a stable seal was achieved or not, three threshold parameters comprising the seal resistance, membrane capacitance and series resistance were defined [232]. By this means, stable seals were achieved, if the resistance between the cell and the aperture was higher than 0.5 GΩ. Membrane capacitance deriving from the properties of a cell membrane that acts as a capacitor is a measure of the membrane to store charge and thus imparts a delay in changes of potential because the stored charge needs to be overcome by the cell membrane [221]. Thus, membrane capacitance should be kept to a minimum defining stable seals if the membrane capacitance was below 100 pA. Capacitance of the cell membrane deriving from the transient currents was compensated automatically when less or equal 100 pA to ensure that the set command test pulse was the actual voltage applied to the cell (see section 2.4.3). Moreover, changes in potential were affected by the series resistance which is the resistance of the membrane and was particularly increased when the cell entered the whole-cell configuration and membrane fragments and intracellular cell material accumulated in the internal solution increasing the series resistance [221]. Consequently, induced current dropped at the series resistance so that the actual command potential was reduced over the desired command potential [232]. As a result, a low series resistance was necessary and was set below

100 M $\Omega$  as threshold to discriminate stable from unstable seals [232]. All of these cell parameters comprising seal resistance, membrane capacitance and series resistance had to meet the above mentioned thresholds in order to be considered as a stable gigaseal in the whole-cell configuration.

Following whole-cell configuration of a stable seal, recording of cells was started and different flow rates of solution were tested in order to determine at which flow rate the most pronounced current signal was induced (Table 12). To achieve defined exposure times during recordings, compound solutions were stacked in the robotic pipettor as described before in section 2.4.3.

Thereby, a volume of 40  $\mu$ l of 100  $\mu$ M nicotine was applied in the stacked solution for investigation of the flow rate at which most pronounced current signal was induced (Table 12). Current amplitudes of current responses induced by 100  $\mu$ M nicotine were determined for each flow rate application and the flow rate at which the current amplitude was most pronounced was set as a routinely applied flow rate in the following experiments.

Prior to investigation of  $\alpha$ -nAChR function, it was essential to ensure that receptors were in a conductible state before each application of compound by stacked solution. This was particularly critical when receptors were in the desensitized state and thus, the time interval between each stacked solution exposure as well as the number of washing steps was adapted to the time and amount of washing steps needed to completely recover receptors from desensitization (see section 1.7.3). For determination of the number of washing steps and the time needed to recover receptors from desensitization, 100  $\mu$ M nicotine initially applied as control to activate receptors were followed by 1 mM nicotine exposed to the cells to induce complete desensitization of the receptors. Subsequently 100  $\mu$ M nicotine for receptor activation was applied after varying time intervals (1, 2 and 3 min) and washing steps (0, 1, and 2) to investigate recovery of  $\alpha$ -nAChR from desensitization (Table 12). By comparing the current amplitude induced by 100  $\mu$ M nicotine after desensitization to current amplitude induced by initially applied 100  $\mu$ M nicotine set to 100 %, the percentage recovery rate was determined for each additional time interval and washing step applied. The number of applied washing steps and applied time interval between stacked solution applications that fully recovered receptors was set as a standard setting for the measurement protocol of the following patch clamp experiments.

**Table 11:** Variation of cellular parameters and settings for investigation of seal success rate including cell capture and hold pressure and cell passages used for patch clamp investigations.

cellular parameters and settings	original setting	variation of configurations and settings
cell capture pressure [mbar]	- 150	- 100, - 125, - 150, - 175, - 200, - 225, - 250, - 275, - 300
cell hold pressure [mbar]	- 50	- 30, - 35, - 40, -45, - 50, - 55, - 60, -65, -70, - 75
cell passages	13-33	13, 15, 17, 19, 21, 23, 25, 27, 29, 31, 33

**Table 12:** Variation of flow rate of compound solution application and of time interval and washing steps between solution application for investigation of intensity of current signal.

settings of solution handling	variation of settings
flow rate [ $\mu\text{l/s}$ ]	16, 27, 57, 114, 171, 200, 257, 314
time interval [min]	1,2,3
washing steps	0,1,2

#### 2.4.8 Assessment of voltage-activated currents

Voltage-clamp protocols were applied to determine the voltage-gated ion channel (VGIC) conductance and to determine the reversal membrane potential of wildtype CHO-K1 and GH<sub>4</sub>C<sub>1</sub> cells as well as of stably transfected CHO-K1 cells. Currents were recorded in CHO-K1 and GH<sub>4</sub>C<sub>1</sub> cells using a linearly depolarizing fast (200 ms) and a slow (2 s) voltage ramp protocol from - 80 to + 80 mV depolarizing within 200 ms or 2 s, respectively. A holding potential of - 70 mV was applied prior to and after the voltage ramp protocols. The voltage ramp was initiated every 3 s and at least 20 runs were acquired to monitor the stability of the recorded currents over time. For quantification, the recorded currents in CHO-K1 and GH<sub>4</sub>C<sub>1</sub> cells were plotted versus voltage and linear regression analysis was carried out. Maximum current amplitudes ( $I_{\text{max}}$ ) of current-voltage relations of CHO-K1 and GH<sub>4</sub>C<sub>1</sub> cells by ramp protocols in the negative ( $-I_{\text{max}}$ ) and positive ( $+I_{\text{max}}$ ) direction were determined which were used as a measure for the overall conductance of a cell. From the linear regression line, the slope coefficient ( $n_H$ ) of the linear regression of the current-voltage relations by ramp protocols indicating the conductance of the membrane was determined. Moreover, the reversal potential was determined by the intersection of the linear regression of the current-voltage relation of CHO-K1 and GH<sub>4</sub>C<sub>1</sub> cells with the abscissa (voltage = 0 V). The area under the curve (AUC) of AUC<sub>current-voltage</sub> and AUC<sub>linear regression</sub> was determined and  $\Delta\text{AUC}$  was determined by the following equation:

$$\Delta\text{AUC} = (\text{AUC}_{\text{current voltage relation}} - \text{AUC}_{\text{linear regression}})$$

equation 10

Detection of pronounced  $\Delta$ AUC reflected activation of VGIC in 200 ms and 2 s voltage-ramp measurements.

In addition to voltage ramp protocols, voltage-step protocols were applied in CHO-K1, GH<sub>4</sub>C<sub>1</sub>, and CHO-K1/RIC-3/h $\alpha$ 7-nAChR cells to characterize VGIC more precisely and to determine the ion species that are permeant to VGIC [221]. In voltage-step protocols, depolarizing voltage-steps of a constant duration of 200 ms from holding potentials of - 60 mV to + 60 mV and - 100 mV to + 80 mV, respectively, increasing by 20 mV increments were recorded whereas a holding potential of - 70 mV was applied prior to and after the voltage-step protocol. After each test pulse the voltage was returned to the holding potential for 10 s to allow full VGIC deactivation before the next voltage step was applied. Detection of voltage-gated Na<sup>+</sup> channels was confirmed by antagonization with the specific voltage-gated Na<sup>+</sup> channel blocker ambroxol. Current-voltage relations by voltage-step protocols were determined for wildtype CHO-K1 and GH<sub>4</sub>C<sub>1</sub> cells by application of external solution, and, in case of CHO-K1/RIC-3/h $\alpha$ 7-nAChR cells, by application of external solution and, additionally, with 100  $\mu$ M of agonist (nicotine or acetylcholine) in the absence and presence of 10  $\mu$ M of the positive allosteric modulator PNU-120596. Solutions applied to a cell were exposed for 233 ms using a flow rate of 171  $\mu$ l/s of the stacked solution application. After each drug exposure cells were washed twice with external solution and an interval of at least 3 min was set before the next step to ensure recovery of receptors into the resting state. The AUC of the positive and negative current traces was determined and plotted versus voltage. Current-voltage relationships were established by non-linear regression analysis. Maximum current amplitudes induced in the negative (-  $I_{\max}$ ) and positive (+  $I_{\max}$ ) direction were determined in CHO-K1/RIC-3/h $\alpha$ 7-nAChR cells used as a measure for the overall conductance of a cell and the reversal potential of the cell determined by the intersection of the current traces with the abscissa (voltage = 0 V) was calculated.

#### **2.4.9 Assessment of non-voltage-activated currents**

Non-voltage activated currents were examined in CHO-K1, GH<sub>4</sub>C<sub>1</sub> and CHO-K1/RIC-3/h $\alpha$ 7-nAChR cells by continuous voltage measurements with a holding potential set to - 70 mV. All compounds applied to a cell were exposed for 233 ms using a flow rate of 171  $\mu$ l/s of the stacked solution. A maximum of five consecutive exposure circuits were applied to each cell. Thus, analysis of current responses was obtained from pooled data of several cells since single cells were not sufficiently stable to generate a complete dose-response-relation. Baseline current response was determined by an initial application of external solution in all experiments. After each drug exposure cells were washed twice with external solution and an interval of at least 3 min was set before the next step to ensure recovery of receptors into the resting state.

Wildtype CHO-K1 and GH<sub>4</sub>C<sub>1</sub> cells were exposed to agonists (acetylcholine, nicotine, carbamoylcholine) in increasing concentrations (50, 100, 250  $\mu$ M) to verify if endogenously expressed ligand gated ion channel (LGIC) sensitive to these agonists are expressed and activated. Furthermore, increasing nicotine concentrations (50, 100, 250  $\mu$ M) and 10  $\mu$ M of the  $\alpha$ 7-specific positive allosteric modulator PNU-120596 was co-applied to wildtype CHO-K1 and GH<sub>4</sub>C<sub>1</sub> cells for the detection of endogenous  $\alpha$ 7-nAChR activity. Current amplitudes were determined and plotted versus the respective compound concentration. CHO-K1/RIC-3/h $\alpha$ 7-nAChR cells were stimulated by agonists (acetylcholine, nicotine, carbamoylcholine, epibatidine) in increasing concentrations (1 – 1000  $\mu$ M). Afterwards, agonist concentrations evoking maximum current amplitudes were co-applied with increasing concentration of the  $\alpha$ 7-specific positive allosteric modulator PNU-120596 (1- 1000  $\mu$ M). Current amplitudes were determined and normalized relative to control concentration of 100  $\mu$ M nicotine set to 1. Means  $\pm$  SD of normalized current amplitudes was plotted versus the respective compound concentration. Dose-response curves were analyzed by non-linear regression analysis and EC<sub>50</sub> and IC<sub>50</sub> values, maximum current amplitude ( $I_{\max}$ ) relative to nicotine set to 1 as well as agonist concentrations inducing most pronounced current amplitudes were determined from dose-response-relations. Furthermore, the decay rate of the current response at the most pronounced current response was determined by  $\tau$  defined as the time constant of decay. Physically, the time constant represents the elapsed time required for current amplitude to decay in value to  $1/e = 36.8\%$  and used as a parameter of choice for the evaluation of current decay rate [232].

Specific  $\alpha$ 7-nAChR activation was verified by antagonization of nicotine-induced and positively modulated current signals using a specific  $\alpha$ 7-nAChR antagonist, methyllycaonitine (MLA). Therefore, increasing concentrations of MLA (0.1 nM – 10 nM) that specifically block  $\alpha$ 7-nAChR activation in the lower nanomolar range were applied to 100  $\mu$ M nicotine-induced h $\alpha$ 7-nAChR activation and to PNU-120596 modulated responses co-applied with 100  $\mu$ M nicotine. In this regard, complete inhibition of the current responses by MLA would indicate that no other nAChR subtypes are involved in agonist-induced receptor activation. Current amplitudes were determined and normalized relative to control concentration of 100  $\mu$ M nicotine set to 1. Means  $\pm$  SD of normalized current amplitudes were plotted versus MLA concentration. IC<sub>50</sub> values were determined from dose-response-relations of inhibition of nicotine-induced h $\alpha$ 7-nAChR activation and of PNU-120596 modulated responses.

#### **2.4.10 Investigation of the effect of bispyridinium compounds on nAChR function**

The effect of BP compounds was investigated with respect to the activated and desensitized  $\alpha$ 7-nAChR state using two separate protocols. The first protocol comprising the determination of the effect of BP compounds on the activated receptor was performed to analyze the ability of these compounds to prevent the fast onset of receptor desensitization. Thus, after the cell was initially exposed to 100  $\mu$ M

nicotine, increasing test compound concentrations (1 - 1000  $\mu$ M) were co-applied to 100  $\mu$ M nicotine inducing receptor activation. Current amplitudes were determined and normalized relative to control concentration of 100  $\mu$ M nicotine set to 1. Means  $\pm$  SD of normalized current amplitudes was plotted versus the respective compound concentration.

With respect to PTM compounds potentiating  $\alpha$ 7-nAChR activation, maximum current amplitude ( $I_{\max}$ ) relative to nicotine was set to 1 and concentrations inducing most pronounced current amplitudes were determined from dose-response-relations. Furthermore, the decay rate of the current response was determined by  $\tau$  known as the time constant of decay. With respect to PTM compounds inhibiting  $\alpha$ 7-nAChR activation induced by 100  $\mu$ M nicotine, dose-response curves were analyzed by non-linear regression analysis and  $IC_{50}$  values were determined from dose-response-relations of inhibition of nicotine-induced  $\alpha$ 7-nAChR activation.

The second protocol examined the ability of BP compounds and PNU-120596 to resensitize nAChR from the slow onset of desensitization. First, 100  $\mu$ M nicotine was applied to activate the receptors. Then, cells were exposed to 1 mM nicotine to induce complete desensitization of receptors. Subsequent exposure of cells to 1 mM nicotine followed by increasing concentrations of test compounds (1nM – 10 mM) was carried out while the cells were continuously maintained at 1 mM nicotine during test compound application to ensure complete desensitization and thus to avoid spontaneous conformational transition of the receptor into the active or closed, activatable state. Current amplitudes were determined and normalized relative to control concentration of 100  $\mu$ M nicotine set to 1. Means  $\pm$  SD of normalized current amplitudes was plotted versus the respective compound concentration. Dose-response curves were analyzed by non-linear regression analysis.  $EC_{50}$  values, slope coefficients ( $n_H$ ), maximum current amplitude ( $I_{\max}$ ) relative to nicotine set to 1 and concentrations inducing most pronounced current amplitudes were determined from dose-response relations. Since an exponential decay of current response was required for calculation of  $\tau$  and was not feasible with current traces of these experiments investigating recovery of receptors from desensitization, an alternative for determining the duration of current response and thus the decay rate of the current response was used. In this context, current amplitudes of current responses were determined at different time points following exposure (10 ms, 50 ms, 100 ms) and compared to current response by 100  $\mu$ M nicotine at 10 ms, 50 ms, 100 ms after exposure whereas current amplitudes were normalized relative to maximum current amplitude induced by 100  $\mu$ M nicotine set to 1.



## 2.5 Data analysis

As part of a standardized method, all continuous recordings were performed under the same conditions comprising a fixed number of compound exposure steps set to 5 with an initial application of external solution for baseline determination, 100  $\mu$ M of nicotine applied as control for receptor activation before increasing concentrations of test compounds were applied. Terminal application of 100  $\mu$ M nicotine was compared to initial application of 100  $\mu$ M nicotine to test full recovery of receptors over time which was critical after high agonist concentrations due to increased probability of desensitization. Thereby, a deviation of current amplitude by less than 15 % was considered as complete receptor activity. Generated current response amplitudes were subtracted from baseline induced by external solution. All current signals were recorded at 50 kHz and were filtered at 5 kHz prior to digitization and storage using the software PatchControlHT (Nanion Technologies GmbH, Munich, Germany). Original current traces were displayed using IgorPro software, Version 6.2.2.2 (Lake Oswego, Oregon, USA). Experimental data were expressed as Means  $\pm$  SD with the number of independent experiments provided in the Figures. All dose-response curves were fitted by linear or non-linear regression and analysis of experimental data was performed by GraphPad Prism 5.0 software (San Diego, CA, USA).



## 3. Results

### 3.1. Transmembrane potentials of GH<sub>4</sub>C<sub>1</sub> and CHO-K1 cells

For recording transmembrane potentials of GH<sub>4</sub>C<sub>1</sub> and CHO-K1 cells, whole-cell current-clamp experiments were conducted (see section 2.4.6). By setting the constant current level applied to the cell to zero ( $I = 0$  A), a net ion flux through the cell membrane was avoided so that the membrane potential of the unstimulated cell, denoted as the resting membrane potential (RMP) could be measured (see section 2.4.1). Thereby, the voltage was measured for 4 s to retrieve the RMP and, as displayed in Figure 11 A-B, the RMP was determined by the means of 13 independent experiments. In CHO-K1 cells, the RMP was recorded at  $-49.54 \pm 2.29$  mV and was slightly less negative than the RMP found in GH<sub>4</sub>C<sub>1</sub> cells, which was recorded at  $-57.05 \pm 3.52$  mV (Figure 11 A-B; Table 13).

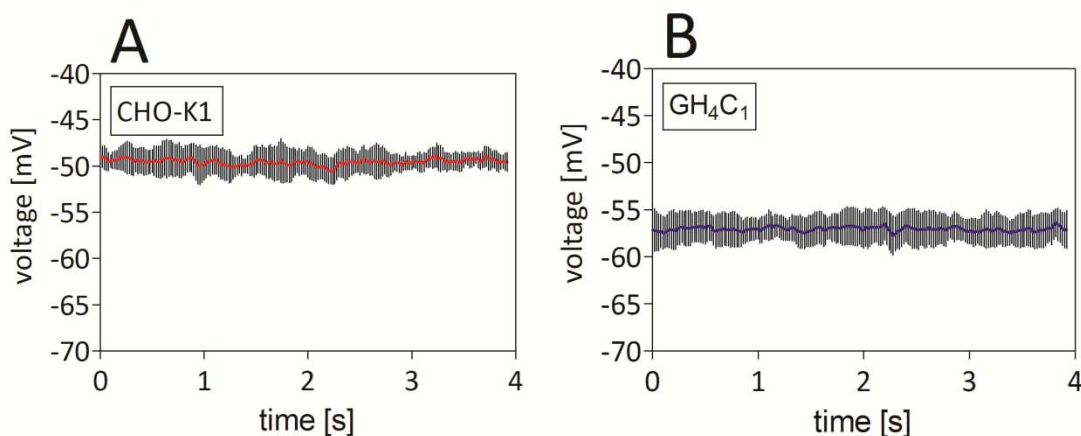


**Figure 11 A-B: Currents of whole-cell current-clamp recordings for the assessment of resting membrane potentials (RMP) of CHO-K1 (A) and GH<sub>4</sub>C<sub>1</sub> (B) cells.** Means  $\pm$  SD ( $n = 13$ ) of RMP was determined from voltage recordings for 4 s during exposure to external solution with a constant current level at zero ( $I = 0$  A).

### 3.2 Current-voltage relationships of GH<sub>4</sub>C<sub>1</sub> and CHO-K1 cells

The voltage-activated conductance was investigated in GH<sub>4</sub>C<sub>1</sub> and CHO-K1 cells by a voltage-clamp ramp protocol measured in the whole-cell voltage-clamp mode to determine the relation between membrane voltage and current in the cell lines GH<sub>4</sub>C<sub>1</sub> and CHO-K1 (see section 2.4.8). Currents of cells at different voltages were measured by applying two different ramp protocols which are illustrated in Figure 12 A-B. Both voltage protocols were initiated by recording currents at a constant holding

potential of  $-70$  mV, followed by continuously increasing voltage starting from a potential of  $-80$  mV and depolarizing the cell up to a potential of  $+80$  mV. Hereby, the first voltage ramp protocol was carried out by continuously increasing the voltage within a total time of  $200$  ms (Figure 12 A) and the second voltage ramp protocol was applied within a total time of  $2$  s (Figure 12 B). Current-voltage relations of both cell lines were generated from  $200$  ms and  $2$  s voltage ramp protocols and were fitted by linear regression analysis as shown in Figure 12 C-F. Assessment of the current-voltage relation of CHO-K1 cells revealed that cells were not stimulated significantly at increasing voltage by  $200$  ms and  $2$  s ramp showing very low inward and outward currents within approx. maximum currents at  $-100$  pA ( $-I_{\max}$ ) at  $-80$  mV to  $+200$  pA ( $I_{\max}$ ) at  $+80$  mV (Figure 12 C-D; Table 13). Compared to CHO-K1 cells, more pronounced current responses were evoked in GH<sub>4</sub>C<sub>1</sub> cells. Thereby, when applying the  $200$  ms voltage ramp in GH<sub>4</sub>C<sub>1</sub> cells, negative current responses starting at  $-157.75 \pm 13.84$  pA ( $-I_{\max}$ ) at  $-80$  mV up to  $+295.41 \pm 57.19$  pA ( $I_{\max}$ ) at  $+80$  mV were obtained (Figure 12 E; Table 13). Recordings in GH<sub>4</sub>C<sub>1</sub> cells using the  $2$  s ramp protocol showed current responses from  $-257.73 \pm 65.83$  pA ( $-I_{\max}$ ) at  $-80$  mV up to  $+798.87 \pm 73.90$  pA ( $I_{\max}$ ) at  $+80$  mV (Figure 12 F; Table 13). In general, current-voltage relations of both cell lines showed that by continuously increasing voltage from  $-80$  mV to  $+80$  mV, the current response continuously increased starting from negative currents at negative voltage to positive currents at positive voltage resulting in a linear rise (Figure 13 C-F).

For further analysis of the linearity of the current-voltage relation by voltage ramp protocols, linear regression analysis was performed and subsequently the slope coefficient ( $n_H$ ) of the linear regression was determined (Figure 12 C-F; Table 13). Comparing  $n_H$  of linear regression lines of the current-voltage-relations generated by  $200$  ms and  $2$  s ramp protocols in CHO-K1 and GH<sub>4</sub>C<sub>1</sub> cells, marked differences were detected between these cell types. In this context,  $n_H$  of the linear regression by  $200$  ms and  $2$  s voltage ramps revealed a considerably larger  $n_H$  and thus a steeper slope in GH<sub>4</sub>C<sub>1</sub> cells ( $n_H = 5.74 \pm 0.09$  A/V;  $2.71 \pm 0.03$  A/V) compared to the small  $n_H$  of the linear regression of  $200$  ms and  $2$  s voltage ramps in CHO-K1 cells indicating shallow slopes ( $1.44 \pm 0.02$  A/V;  $0.92 \pm 0.01$  A/V) (Table 13). The reversal potential of CHO-K1 and GH<sub>4</sub>C<sub>1</sub> cells was determined by the intersection of the current-voltage relation with the abscissa in  $200$  ms and  $2$  s voltage-ramp protocols and represented the potential where no net ion flux was conducted (Figure 12 C-F; Table 13) [48]. In brief, comparable reversal potentials of CHO-K1 cells in  $200$  ms and  $2$  s ramps were found at  $-23.28 \pm 4.25$  mV and  $23.23 \pm 2.93$  mV, respectively, while GH<sub>4</sub>C<sub>1</sub> cells displayed a more negative reversal potential at  $-31.01 \pm 3.52$  mV in  $200$  ms voltage ramp and a more depolarized reversal potential of  $-13.27 \pm 0.81$  mV in the  $2$  s voltage ramp measurement (Table 13). For determination of deviation of currents of the current-voltage relation from calculated currents of the linear regression analysis in CHO-K1 and GH<sub>4</sub>C<sub>1</sub> cells using  $200$  ms and  $2$  s voltage ramps recorded from  $-80$  to  $+80$  mV, the area under the curve (AUC) of AUC<sub>current-voltage</sub> was calculated and subtracted from the AUC<sub>linear regression</sub> resulting in  $\Delta$ AUC (AUC<sub>current voltage relation</sub>

–  $AUC_{\text{linear regression}}$ ) (equation 10). CHO-K1 cells showed no detectable deviation of currents from linear regression analysis with depolarization since the course of the current-voltage relation converged with linear regression throughout the voltage ramp measurement and thus  $AUC_{\text{current-voltage}}$  was approx. the same size as  $AUC_{\text{linear regression}}$ , resulting in a  $\Delta AUC$  of approx.  $0 \text{ A}\cdot\text{V}$  (Figure 12 C-D; Table 13). With respect to  $\text{GH}_4\text{C}_1$  cells,  $AUC_{\text{current-voltage}}$  was smaller than  $AUC_{\text{linear regression}}$  in both voltage ramp measurements whereas the difference ( $\Delta AUC$ ) was more pronounced by a factor of 10 in 200 ms ramp measurement ( $6.32 \pm 0.73 \cdot 10^{-5} \text{ A}\cdot\text{V}$ ) compared to the 2 s ramp measurement ( $7.63 \pm 1.25 \cdot 10^{-6} \text{ A}\cdot\text{V}$ ) (Figure 12 E-F; Table 13). As depicted in Figure 12 E and F, deviation of the currents of the current-voltage relation from linear regression in  $\text{GH}_4\text{C}_1$  cells was only found to be due to smaller currents of the current-voltage relation compared to those calculated by linear-regression analysis. The voltage range in which deviation of currents of the current-voltage relation from calculated currents of linear regression analysis occurred was found within a more negative voltage range between - 70 mV to + 19 mV in the 200 ms voltage-ramp compared to the voltage range found in 2 s voltage ramps from - 45 mV to + 40 mV (Figure 12 E-F). This voltage area was colored in grey in Figure 12 E-F in both ramp protocols.

Next, a voltage-step protocol was carried out as described in section 2.4.8 and schematically illustrated in Figure 13 A. Representative individual current responses at different pulses are demonstrated in Figure 13 B, D and F.  $AUC$  of the current responses were determined and plotted versus the voltage step as depicted in Figure 13 C, E and G. Positive currents were detected in both cell lines which increased proportional to the depolarizing voltage steps (- 60 mV to + 60 mV) (Figure 13 B-D). Regarding the positive current traces of both cell lines, currents did not inactivate over time during the voltage charge application and terminated by a sharp abortion of the current signal at the time the voltage returned to holding potential (Figure 13 B, D and F). Comparing current sizes in the positive direction expressed by  $AUC$  of the voltage-step protocol, current-voltage relations showed that only small current responses were obtained in CHO-K1 cells at increasing voltage steps and no negative currents were detectable while  $\text{GH}_4\text{C}_1$  cells revealed significantly enhanced positive currents that steadily increased with depolarization induced by increasing voltage steps (Figure 13 B-E). Additionally, current traces of voltage-step recordings of  $\text{GH}_4\text{C}_1$  cells displayed rapidly ascending and descending negative peak currents (Figure 13 D). Determination of  $AUC$  of the negative currents yielded a bell-shaped current-voltage relation of current responses with an increase in  $AUC$  from -60 mV to a maximum  $AUC$  at - 20 mV followed by a decrease with increasing voltage-steps (Figure 13 G). Reversal of the negative current direction was reached at approx.  $+ 38.5 \pm 2.78 \text{ mV}$  (Figure 13 G). Negative currents were completely blocked by applying an excess of  $50 \mu\text{M}$  of a voltage-gated  $\text{Na}^+$  channel blocker, named ambroxol (Figure 13 F-G).

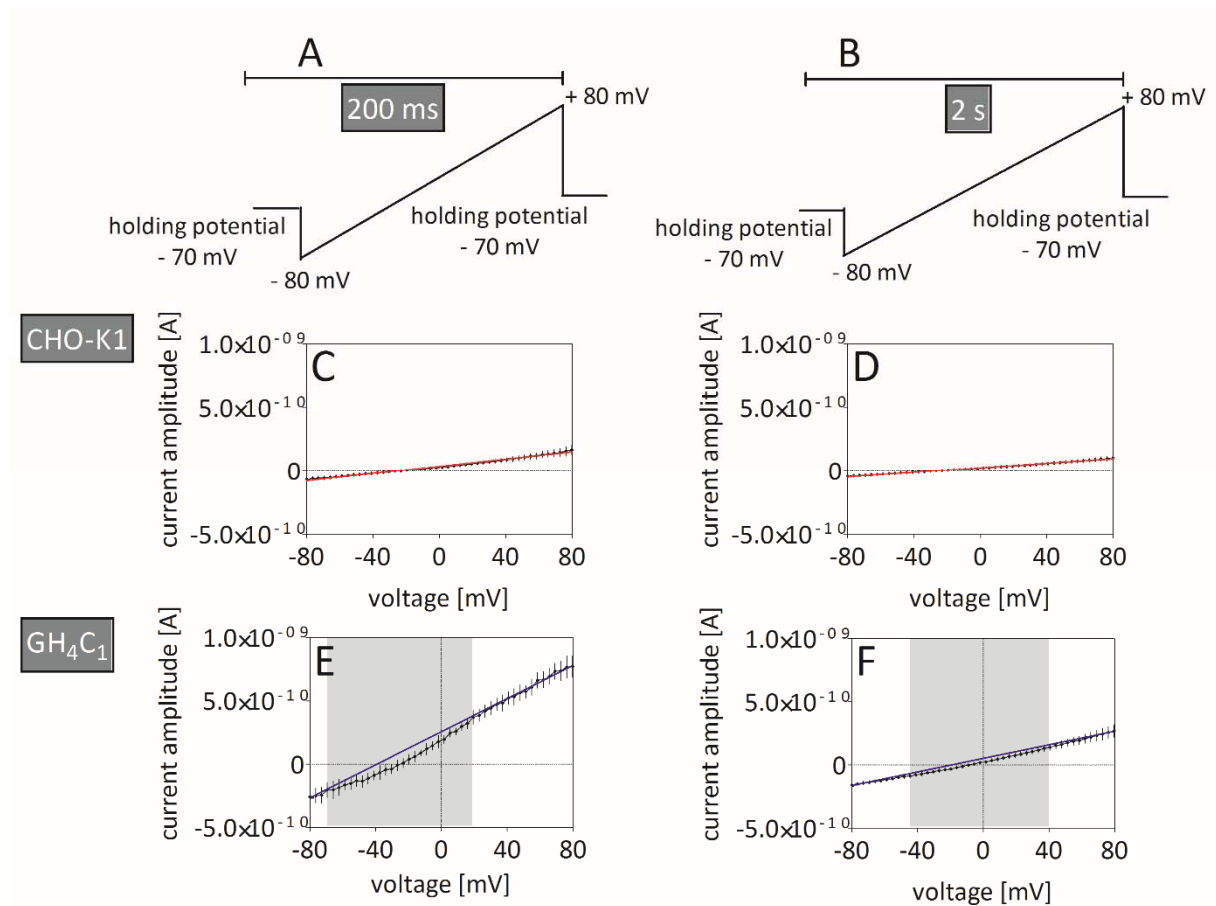


**Figure 12 A-F: Current-voltage relations of CHO-K1 and GH<sub>4</sub>C<sub>1</sub> cells using 200 ms and 2 s voltage-ramp protocols.** A-B. Schematic representation of the voltage-clamp ramp protocol with total time of ramp application of 200 ms (A) and 2 s (B). Holding potential was set to -70 mV and applied prior and after the voltage ramp. C-F. Means  $\pm$  SD (n = 7) of current amplitudes of CHO-K1 (C-D) and GH<sub>4</sub>C<sub>1</sub> cells (E-F) were determined by 200 ms and 2 s voltage ramp measurements and plotted versus voltage (-80 mV to +80 mV). Current-voltage relations were analyzed by linear regression analysis drawn in red for CHO-K1 cells and in blue for GH<sub>4</sub>C<sub>1</sub> cells. Grey area of current-voltage relations indicated the voltage range in which Means  $\pm$  SD (n = 7) of current amplitude did not converge with linear regression.

**Table 13:** Current-clamp recordings and voltage-clamp voltage-ramp pulse protocols (200 ms, 2 s) in CHO-K1 and GH<sub>4</sub>C<sub>1</sub> cells for the determination of basic electrophysiological characteristics. Elucidation of the membrane resting potential (RMP) and of voltage-gated conductance by determination of maximum current amplitude in the negative and positive direction ( $-I_{\max}/+I_{\max}$ ), slope coefficient ( $n_H$ ), reversal potential and determination of area under the curve ( $\Delta AUC$ ; equation 10). Means  $\pm$  SD were determined ( $n = 5-8$ ).

configuration	parameter	pulse protocol	cell line	
			CHO-K1	GH <sub>4</sub> C <sub>1</sub>
current clamp	RMP	$I = 0$ A	$-49.54 \pm 2.29$ mV	$-57.05 \pm 3.52$ mV
voltage ramp	$-I_{\max}/+I_{\max}$	200 ms	$-68.82 \pm 16.26$ pA/ $+174.52 \pm 37.53$ pA	$-157.75 \pm 13.84$ pA/ $+295.41 \pm 57.19$ pA
		2s	$-46.02 \pm 26.07$ pA/ $+106.58 \pm 53.92$ pA	$-257.73 \pm 65.83$ pA/ $+798.87 \pm 73.90$ pA
	$n_H$	200 ms	$1.44 \pm 0.02$ A/V	$5.74 \pm 0.09$ A/V
		2s	$0.92 \pm 0.01$ A/V	$2.71 \pm 0.03$ A/V
	reversal potential ( $I = 0$ A)	200 ms	$-23.28 \pm 4.25$ mV	$-31.01 \pm 3.52$ mV
		2s	$-23.23 \pm 2.93$ mV	$-13.27 \pm 0.81$ mV
	$\Delta AUC$	200 ms	n.d.*	$6.32 \pm 0.73 \cdot 10^{-5}$ A*V
		2s	n.d.*	$7.63 \pm 1.25 \cdot 10^{-6}$ A*V

\* n.d.: not detectable

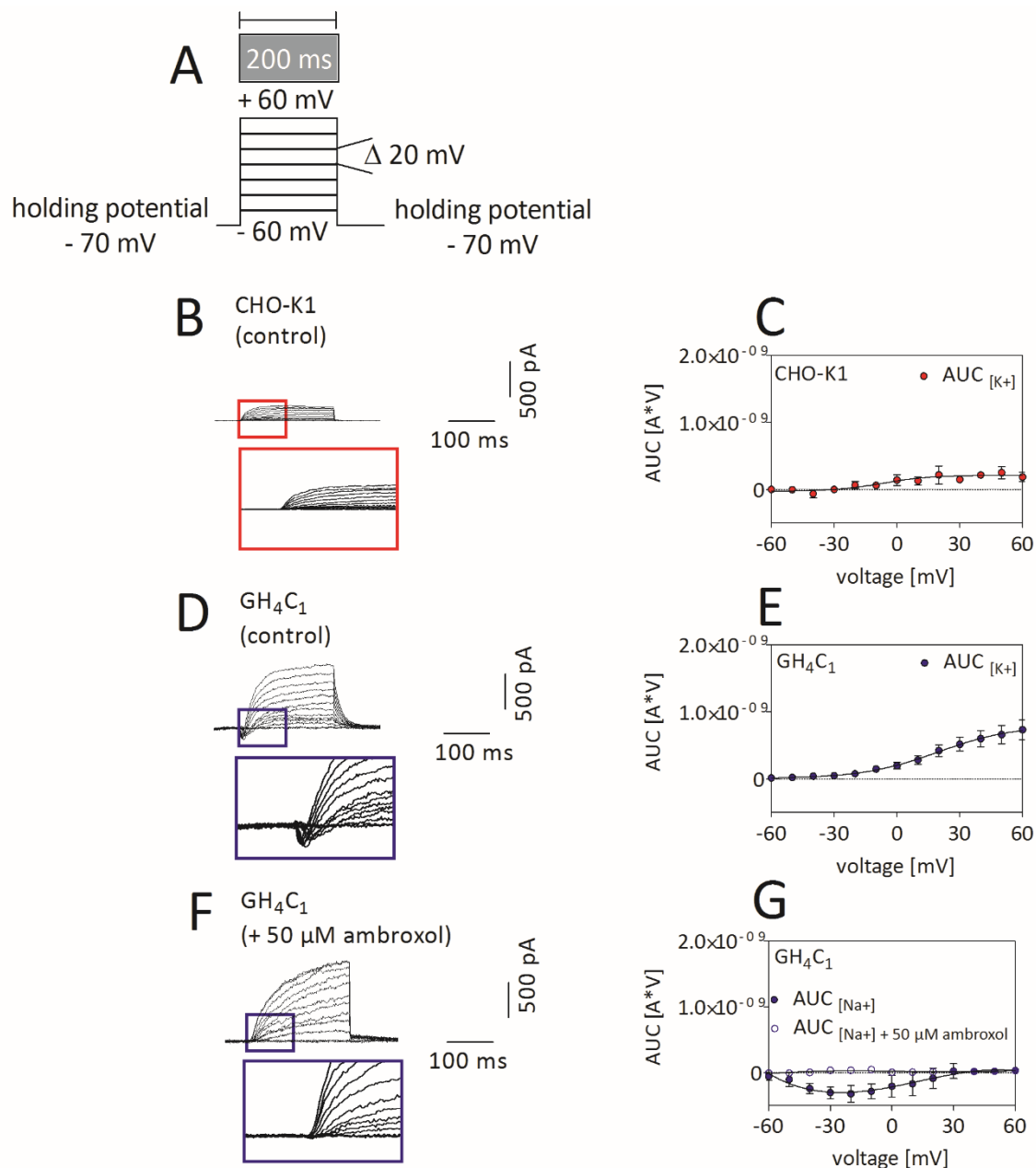


**Figure 13 A-G: Current-voltage relation of GH<sub>4</sub>C<sub>1</sub> and CHO-K1 using voltage-step protocols.** A. Schematic representation of the voltage-clamp step protocol with voltage-step length of 200 ms and increments of 20 mV per step from -60 to +60 mV. Holding potential was applied prior and after each step and was set to -70 mV. B-G. Representative current traces of voltage-steps in CHO-K1 (B) and in GH<sub>4</sub>C<sub>1</sub> cells in the absence (D) and presence of 50  $\mu$ M ambroxol (F) are shown and 4 x magnification of current onset was included. Current-voltage relation of CHO-K1 (C) and in GH<sub>4</sub>C<sub>1</sub> cells of positive currents (E) and of negative currents in the absence and presence of 50  $\mu$ M ambroxol (G) by application of voltage-steps were determined by the Means  $\pm$  SD of AUC and plotted versus voltage. Current-voltage relations were fitted using non-linear regression analysis (n = 5-7).



### 3.3 Assessment of endogenous ligand-gated ion channels of GH<sub>4</sub>C<sub>1</sub> and CHO-K1 cells

For investigation of voltage-independent ligand-gated activation of ion channels, continuous voltage-clamp recording was used by setting the holding potential of GH<sub>4</sub>C<sub>1</sub> and CHO-K1 cells to  $-70$  mV (see section 2.4.9). During recording, three different nAChR agonists comprising acetylcholine, carbamoylcholine and nicotine were exposed to the cell in increasing concentration (50, 100, 250  $\mu$ M) to test for endogenous expression of nAChR (Table 5). Maximum current amplitudes were determined from recordings and plotted against concentrations. As shown in Figure 14 A-C, control currents recorded during application of external solution to the cells were comparable in size with currents upon agonist application in the lower picoampere range.

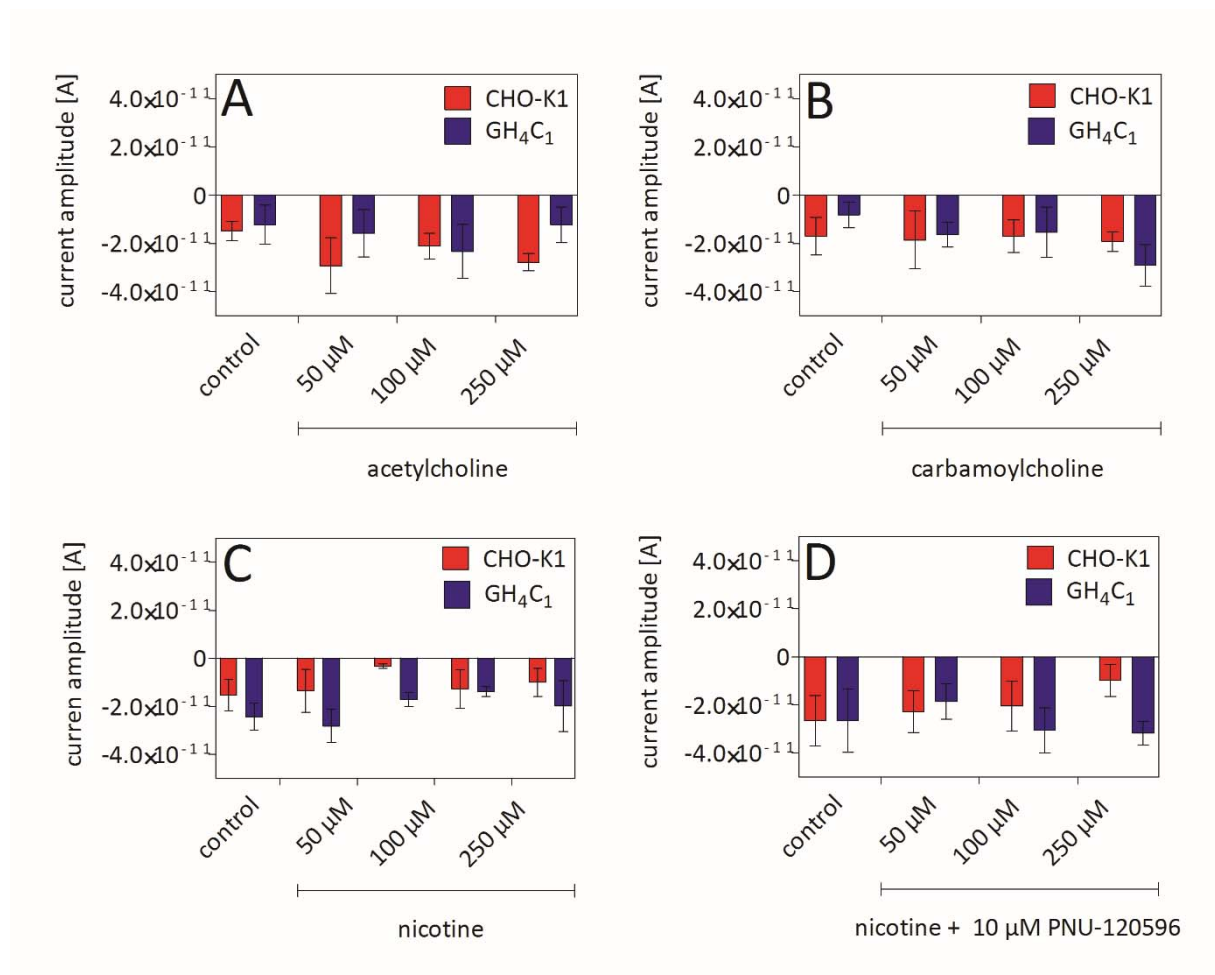


**Figure 14 A-D: Concentration-response relation of GH<sub>4</sub>C<sub>1</sub> and CHO-K1 using continuous voltage-clamp protocols upon activation with acetylcholine (A), carbamoylcholine (B) and nicotine in the absence (C) and presence of the positive allosteric modulator PNU-120596 (D).** Currents were recorded at a constant holding potential of  $-70$  mV with an at least 3 min interval between each drug exposure. Means  $\pm$  SD ( $n = 6-8$ ) of current amplitudes were determined and plotted versus concentration shown for GH<sub>4</sub>C<sub>1</sub> cells in blue and CHO-K1 cells in red.

In addition, a well-prescribed  $\alpha 7$ -specific positive allosteric modulator PNU-120596 was co-applied with increasing nicotine concentrations (50, 100, 250  $\mu$ M) to investigate particularly the activation of a particular subtype, the  $\alpha 7$ -nAChR, and revealed no detectable activation of currents (Figure 14 D) (Table 5) [148].

### 3.4 Optimization of seal success rate and current signal

The general set-up of a patch clamp experiment includes a planar borosilicate glass chip containing a micro-sized aperture which is encased in a cartridge forming the microfluidic channels through which solutions were added and in which the electrophysiological measurement was carried out as described in section 2.4.3. In brief, after internal and external solution were delivered to the chip, a fixed volume and concentration of cell solution was pipetted onto each upper compartment of the recording chamber of the chip and by application of gentle under-pressure, a random cell was positioned and captured on the aperture. In general, the overall procedure of establishing a seal is common to all forms of patch clamping, however, the parameters of the process of making a gigaseal on a cell membrane in the whole-cell configuration were optimized step by step in order to increase the seal success rate including gigaseal formation, seal stability and run down over time (see section 2.4.7). Since CHO-K1 cells were the cells of choice for stable transfection of the h $\alpha 7$ -nAChR for investigation, settings of patch clamp experiments were adapted to this cell line in the whole-cell configuration as described in the following.

The first step of modification served to increase the cell capture rate on the aperture for the establishment of a gigaseal. Thereby, suction strength or under-pressure to capture a cell was adjusted and cell capture rate was determined. Cell capture rates were slightly increased (8 %) by reducing initially applied suction strength of - 200 mbar to - 150 mbar (Figure 15 A).

After the cell was captured, the under-pressure for holding the cell to the aperture was reduced from - 70 mbar to -50 mbar increasing cell hold rate by 4 % (Figure 15 B; Table 11). Both, cell capture and cell hold rate increased gigaseal formation by 12 % and the cell capture and hold rate was diminished when suction strength was heightened or lowered from a cell capture pressure of - 200 mbar and from a cell holding pressure of - 50 mbar (Figure 15 A and B).

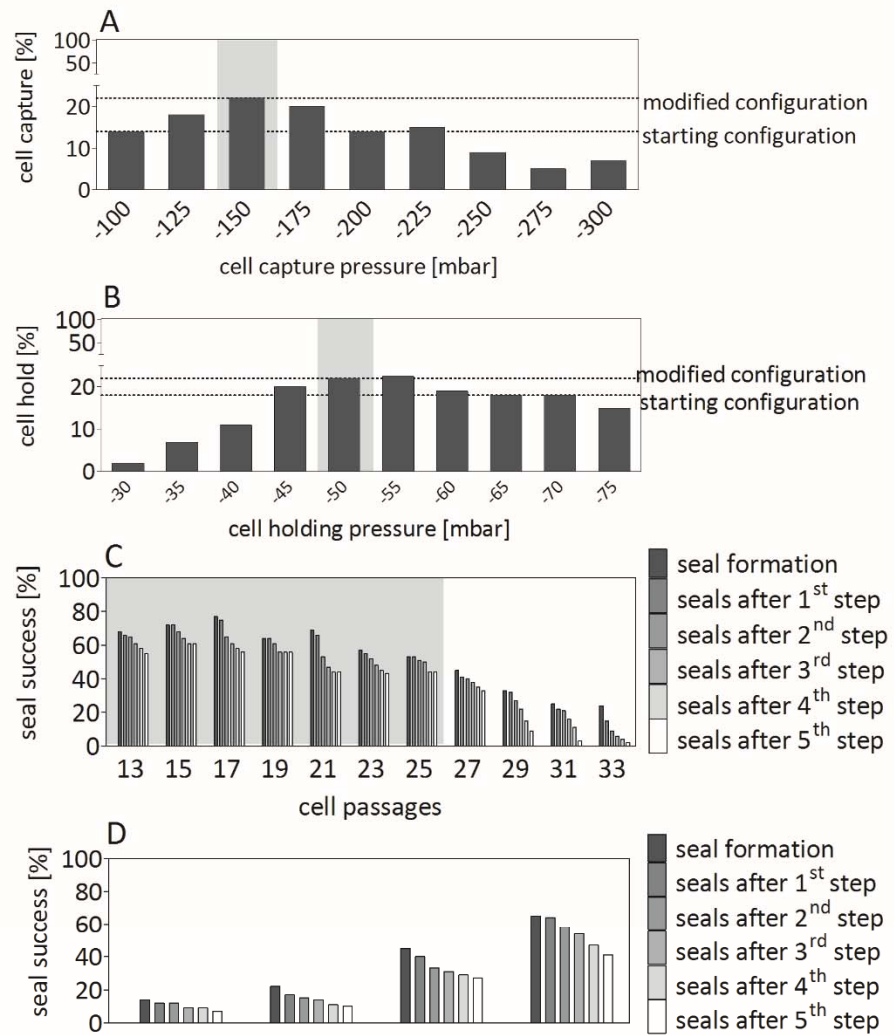
The next modification applied comprised an exchange of the external solution by an externally applied seal enhancing solution containing a high  $\text{Ca}^{2+}$  concentration which was added to the upper compartment of the recording chamber after establishment of the whole-cell configuration of the captured cell but prior to recording (see section 2.4.7). After the patched cell was stabilized for 30 s when dispensed in the seal enhancer, gigaseal formation and seal stability over a five point measurement increased significantly (Figure 15 D; Table 14). In this regard, establishment of a gigaseal

was achieved, if the resistance between the cell and the aperture was higher than 0.5 G $\Omega$ , cell capacitance below 100 pA and if the series resistance was below 100 M $\Omega$  (see section 2.4.7).

Prior to patch clamp recording, the seal enhancer solution was replaced with fresh external solution. Last, gigaseal formation and stability of seals of cells were tested with respect to the cell passage (13-33) used. Thereby, cells from passage 13 up to passage 25 showed a higher gigaseal formation with no significant run down of seal rate over a five point measurement compared to all cells exceeding passage 25 (Figure 15 C).

All in all, application of all modifications comprising adjustment of cell capture (- 150 mbar) and cell holding pressure (- 50 mbar), the use of seal enhancer and usage of cells between passage 13 to 25 increased gigaseal formation in the whole-cell configuration by a factor of 4.6 compared to original settings summarized in Table 11 (Figure 15 D; equation 7). In addition, when seal stability was analyzed by determining the seal success rate over a five point measurement, seals were found to be more stable by a factor of 1.3 compared to original settings (equation 8; Table 14). Vice versa, run down of seal success rate over a five point measurement was reduced by a factor of 0.7 (equation 9; Table 14). In conclusion these modifications were routinely used for the subsequent measurements.

CHO/RIC-3/h $\alpha$ 7-nAChR cell line was assessed for the intensity of current signal by h $\alpha$ 7-nAChR activity upon activation with 100  $\mu$ M nicotine using different flow rates (Table 12; see section 2.4.7). By application of a stacked solution, a volume of 200  $\mu$ l of external solution was aspirated first by the pipette followed by a volume 40  $\mu$ l of 100  $\mu$ M nicotine which was then exposed to the cell in reversed order with a constant flow rate so that the cell was exposed to the solution for a defined period of time depending on the flow rate applied. Flow rates between 16  $\mu$ l/s and 314  $\mu$ l/s of application of stacked solution were tested.



parameters	original settings	modifications and adjustments of settings		
		pressure [mbar]	seal enhancer	cell passages
cell capture pressure [mbar]	-200	-150	-150	-150
cell holding pressure [mbar]	-70	-50	-50	-50
seal enhancer	-	-	+	+
cell passages	13-31	13-31	13-31	13-25

**Figure 15 A-D: Modification and adjustment of cellular parameters for optimization of seal success rate in stably transfected CHO/RIC-3/h $\alpha$ 7-nAChR cells including increase in gigaseal formation, stability of seals and reduction of run down on an automated patch clamp platform.**

A-B. Percentage number of cell capture and cell hold rate obtained at different under-pressure applied for cell capture (A) (n = 64) and for holding the cell (B) (n = 84) are shown. Dotted lines indicate the cell capture and cell hold rate of the original settings (starting configuration) and of the modified settings with the most pronounced cell capture and cell hold rate (modified configuration) that are highlighted by grey background. C. Percentage gigaseal formation and stability of cells over a five point

measurement of cells at different passages (13-33) are shown with the most pronounced success rates highlighted by grey background (13-25) (n = 72). D. Percentage seal success rate including percentage gigaseal formation and stability of cells over a five point measurement of cells of the original settings and consecutively modified settings including adjustment of cell capture and cell holding pressure, addition of a seal enhancer and delimited usage of cell passages are shown (Table 11) (n=24 per modification).

**Table 14:** Adjustment and modification of cellular parameters and settings of making a seal including capture and holding pressure, addition of seal enhancer, cell passages for optimization of seal success rate. For determination of seal success rate, percentage of cell capture and hold rate, percentage of stable seals defined as percentage of recorded gigaseals in the whole-cell configuration over a 5 point measurement and run down denoted by the percentage of residual stable seal rate after 5 point measurement were analyzed (equation 7-9) (n = 24 per adjustment/modification).

cellular parameters & settings	seal success rate		
	gigaseal [%]	stable seal [%]	run down [%]
original settings	14	50	50
+ capture and hold pressure (150 mbar/50 mbar)	26	45	55
+ seal enhancer	45	60	40
+ cell passages (13-25)	65	63	37
seal success rate [fold]	4.6	1.3	0.7

Notably, variation in flow rates of a fixed volume of 40 µl of nicotine also resulted in different time span in which cells were exposed to the compound solution, i.e. the faster the application the shorter the time span cells were exposed to the cells (Table 15).

As displayed by representative current traces and current amplitudes determined at different flow rate in Figure 16 A-B, current amplitudes of current responses revealed no detectable currents up to 27 µl/s and an increase in current signal from 57 µl/s up to 171 µl/s. Faster flow rates than 171 µl/s yielded a decrease of the current amplitude (Figure 16 A-B). Subsequent patch clamp experiments using a stacked solution were standardized to a flow rate of 171 µl/s so that the cell was exposed to the 40 µl test solution for a total time period of 233 ms (Table 15). Besides variation of flow rate to find a sufficiently high current signal by  $\alpha 7$ -nAChR activation, the time and washing steps needed to convert

receptors in a conductible state before application of the next compound was investigated (see section 2.4.7).

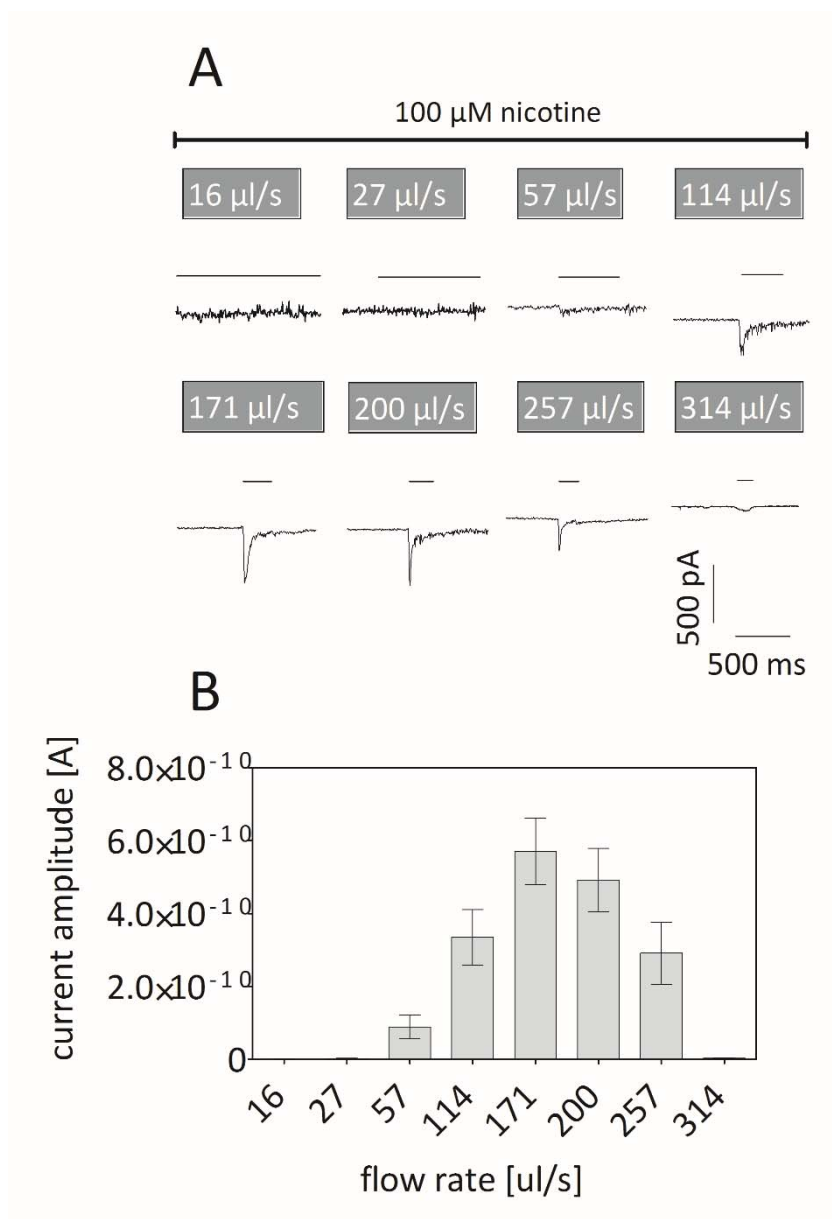


**Figure 16 A-B: Variation of flow rate of stacked compound application for investigation of current signal intensity by  $\alpha$ 7-nAChR activation in stably transfected CHO/RIC-3/ $\alpha$ 7-nAChR cells.**

A. Representative current traces of activation by 100  $\mu$ M nicotine at different flow rates. Currents were recorded at a constant holding potential of -70 mV with an at least 3 min interval between each drug exposure. Horizontal bars indicate exposure time (Table 15) of compound(s) to the cell. B. Means  $\pm$  SD ( $n = 5$ ) of current amplitudes induced by 100  $\mu$ M nicotine were determined and plotted versus flow rate ranging from 16  $\mu$ l/s to 314  $\mu$ l/s.

**Table 15:** Relation of flow rate of test compound application (40  $\mu$ l of 100  $\mu$ M nicotine) to current response. Means  $\pm$  SD ( $n = 5$ ) of current amplitudes were determined by  $\alpha 7$ -nAChR activation with 100  $\mu$ M nicotine at various flow rates between 16 and 314  $\mu$ l/s resulting in different time spans of test compounds exposed to CHO-K1/RIC-3/ $\alpha 7$ -nAChR cells.

application of 40 $\mu$ l of 100 $\mu$ M nicotine		
flow rate [ $\mu$ l/s]	exposure time [ms]	current amplitude [A]
16	2500	$7.41 \pm 0.5 * 10^{-13}$
27	1481	$1.36 \pm 0.7 * 10^{-12}$
57	701	$6.17 \pm 7.4 * 10^{-11}$
114	350	$3.42 \pm 2.07 * 10^{-10}$
171	233	$5.81 \pm 2.79 * 10^{-10}$
200	200	$5.44 \pm 2.29 * 10^{-10}$
257	155	$3.24 \pm 2.42 * 10^{-10}$
314	127	$2.57 \pm 0.31 * 10^{-12}$

Converting the receptors in a conductible state before the next test compound application was critical when receptors were priority desensitized and thus in a non-conductible state. In such a situation, the so called resensitization of  $\alpha 7$ -nAChR was affected by the time period and the number of washing steps applied between test compound exposures which were adjusted in the following (Table 12)[148, 221, 377].

Therefore, nAChR were first activated with 100  $\mu$ M nicotine, followed by complete depletion of current signal by an excess of 1 mM nicotine. Extinction of the latter current signal was due to slow onset desensitization [148, 377]. After desensitization, regeneration of receptors was assessed by application of 100  $\mu$ M nicotine after 1, 2 or 3 min without a washing step to activate receptors and the generated current amplitude was compared to the current amplitude induced by 100  $\mu$ M nicotine initially applied. Current responses determined by current amplitudes did not occur after 1 to 3 min of 100  $\mu$ M nicotine application indicating that receptors were not able to recover after 3 min (Figure 17 A-B; Table 16). Additional application of either one or two washing steps before the application of 100  $\mu$ M nicotine after desensitization was carried out to test the influence of the washing steps on the recovery of receptors after 1, 2 or 3 min. By adding one washing step, a small proportion of the desensitized receptor population returned from the non-conductible to the conductible state after 1-2 min which was indicated by a moderate current showing a partial recovery of  $54.7 \pm 20.9$  % at 2 min (Figure 17 A-B, Table 16). Initial current amplitude induced by 100  $\mu$ M nicotine was almost recovered when receptors were activated after one washing step and 3 min ( $72.9 \pm 21.8$  %) (Figure 17, Table 16). When applying two washing steps before verification of recovery, nicotine-induced current amplitude after

1 min was recovered by half ( $54.2 \pm 22.6 \%$ ) compared to initial current amplitude induced by  $100 \mu\text{M}$  nicotine, and showed comparable current amplitudes after 2 min ( $88.7 \pm 22.4 \%$ ) and 3 min ( $98.5 \pm 13.5 \%$ ) which could be considered as a full recovery after slow onset desensitization (Figure 17 A-B; Table 16).

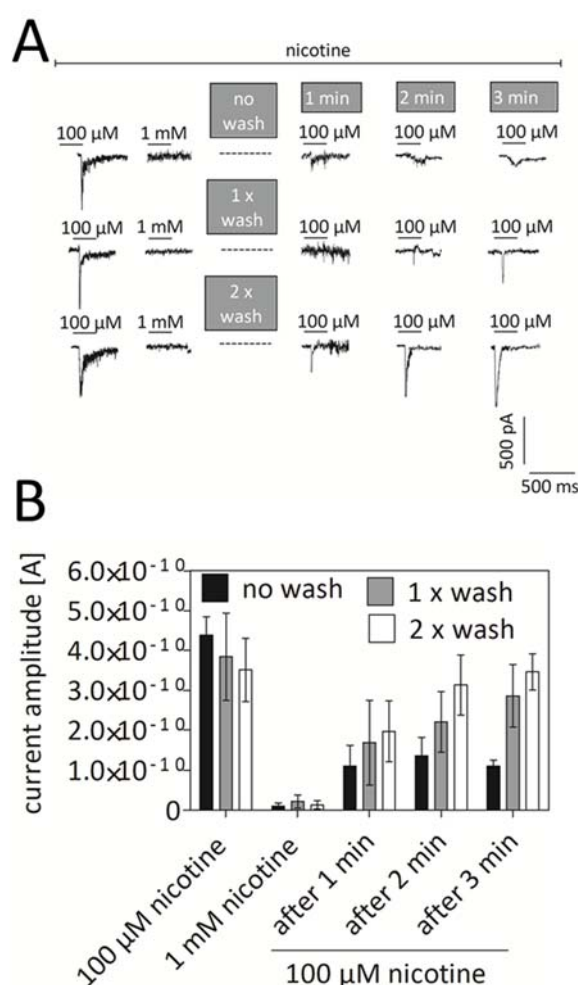


**Figure 17 A-B: Variation of time and washing steps for the full recovery of  $\text{h}\alpha 7\text{-nAChR}$  function after desensitization in stably transfected CHO/RIC-3/ $\text{h}\alpha 7\text{-nAChR}$  cells.** A. Representative current traces of  $\text{h}\alpha 7\text{-nAChR}$  activation ( $100 \mu\text{M}$  nicotine), desensitization ( $1 \text{ mM}$  nicotine) and recovery by application of  $100 \mu\text{M}$  nicotine after different time points and by variation of washing steps (Table 12). Currents were recorded at a constant holding potential of  $-70 \text{ mV}$ . Horizontal bars indicated exposure time (233 ms) of compound(s) to the cell. B. Means  $\pm$  SD ( $n = 5$ ) of peak current amplitudes were determined and plotted versus initially applied  $100 \mu\text{M}$  nicotine,  $1 \text{ mM}$  nicotine and application of  $100 \mu\text{M}$  nicotine after different time points (1 - 3 min) and by variation of washing steps (0, 1, 2).



**Table 16:** Influence of time interval and washing steps on the recovery of  $\alpha 7$ -nAChR of CHO/RIC-3/ $\alpha 7$ -nAChR cells. Means  $\pm$  SD ( $n = 5$ ) of percentage recovery from desensitization was determined by percentage current amplitude relative to activation of  $\alpha 7$ -nAChR induced by 100  $\mu$ M nicotine set to 100 % and desensitization of  $\alpha 7$ -nAChR induced by 1 mM nicotine set to 0 %.

		time interval [min]		
		1	2	3
number of washing steps	0	22.9 $\pm$ 12.3 %	29.2 $\pm$ 10.7 %	22.9 $\pm$ 3.6 %
	1	40.5 $\pm$ 29.2 %	54.7 $\pm$ 20.9 %	72.9 $\pm$ 21.8 %
	2	54.2 $\pm$ 22.6 %	88.7 $\pm$ 22.4 %	98.5 $\pm$ 13.5 %

### 3.5 Activation, desensitization and modulation of human $\alpha 7$ -nAChR

For determination of concentration-activity relations of agonist-induced  $\alpha 7$ -nAChR current responses and positively modulated currents evoked by co-application of a well-prescribed and  $\alpha 7$ -specific PAM, PNU-120596, voltage-clamp patch clamp experiments using continuous recording at a constant holding potential set to  $-70$  mV were performed (see section 2.4.9) [148]. Thereby, compound application was carried out by using the stacked solution method and a flow rate of 171  $\mu$ l/s of compound application was applied exposing the cell to 40  $\mu$ l compound solution for 233 ms. In addition, two washing steps between each compound application were acquired and the time until the next compound application was at least 3 min (see section 2.4.7 and 3.4). Agonists that were used for establishment of dose-response profiles of  $\alpha 7$ -nAChR function included classical nAChR agonists comprising nicotine, acetylcholine, carbamoylcholine and epibatidine (Table 5). A common feature of the individual current traces of all agonists tested was the progression of the current trace, which revealed a sharp current peak displayed by very rapid onset of current signal and fast decline of such (Figure 19 A-D; Table 17). As a measure of duration of current response, the time constant of decay denoted as  $\tau$  was determined for quantification. The time constant of decay represents the time of decay of response where the maximum current amplitude was reduced by  $1/e$  which corresponds to a decrease by 36.8 % and showed that agonist-induced current responses were reduced by that value after a few milliseconds (Figure 18; Table 17).

For establishment of dose-response profiles, agonist concentrations starting from 1  $\mu$ M up to 1000  $\mu$ M were exposed to the cells and revealed a dual concentration-activity relation of all current response profiles (Figure 19 I-J). Therefore, an initial increase in current amplitudes was observed at low agonist concentrations followed by a concentration-dependent decrease as agonist concentrations increased. From ascending dose-response curves,  $EC_{50}$  values were determined as a measure of the half-

maximum efficacy and  $IC_{50}$  values as a measure of the inhibitory potency were obtained from descending dose-response curves (Figure 19 I-J, Table 17). Determination of maximum current amplitudes ( $I_{max}$ ) relative to nicotine set to 1 served for the evaluation of compound efficacy. Acetylcholine, nicotine and carbamoylcholine yielded comparable dose-response profiles wherein  $EC_{50}$  value of carbamoylcholine at  $85.41 \pm 14.72 \mu M$  was slightly enhanced compared to that of nicotine at  $31.33 \pm 5.17 \mu M$  and acetylcholine at  $43.75 \pm 4.33 \mu M$  (Table 17). Maximum current amplitude ( $I_{max}$ ) relative to nicotine set to 1 was moderately reduced with acetylcholine at  $0.51 \pm 0.06$  fold compared to nicotine ( $1.00 \pm 0.14$  fold) and carbamoylcholine at  $0.92 \pm 0.10$  fold relative to nicotine (Table 17). Concentrations at which  $I_{max}$  was found were induced by  $100 \mu M$  nicotine and acetylcholine, respectively, and at slightly enhanced concentrations by carbamoylcholine at  $300 \mu M$  (Figure 19 I-J). With respect to inhibitory potency of these compounds at high agonist concentrations shown by the second section of the biphasic course of the dose-response relations, the  $IC_{50}$  values were found at the higher micromolar range of nicotine, acetylcholine and carbamoylcholine (Figure 19 I-J; Table 17).

In contrast to these agonists, the biphasic dose-response curve of epibatidine was shifted to the left resulting in a considerably reduced  $EC_{50}$  value of  $3.13 \pm 0.27 \mu M$  and a reduced  $IC_{50}$  value at  $35.5 \pm 0.32 \mu M$ .  $I_{max}$  of epibatidine found at a considerably low concentration of  $5 \mu M$  was slightly diminished ( $0.79 \pm 0.06$  fold) compared to nicotine and carbamoylcholine although revealing a higher  $I_{max}$  than acetylcholine (Figure 19 I-J; Table 17). When constant agonist concentration ( $EC_{100}(\text{nicotine}) = 100 \mu M$ ,  $EC_{100}(\text{acetylcholine}) = 100 \mu M$ ;  $EC_{100}(\text{carbamoylcholine}) = 300 \mu M$ ;  $EC_{100}(\text{epibatidine}) = 5 \mu M$ ) were co-applied with increasing concentration of the positive allosteric modulator (PAM) PNU-120596, all currents were enhanced in current amplitude as well as in duration of current response (Figure 18; Figure 19 E-H; Table 17). With respect to the course of the individual current traces, fast onset of current activation was followed by a distinctly elongated decay in the presence of modulator instead of rapid decline within a few milliseconds in the absence of modulator (Figure 18; Figure 19 E-H; Table 17). For comparison of duration of current responses in the absence and presence of modulator, the time constant of decay ( $\tau$ ) was determined for quantification of the duration of current traces inducing most pronounced current amplitudes by PNU-120596 modulated current responses of agonist-induced  $\alpha 7$ -nAChR activation (Figure 18; Table 17).

Agonist induced dose-response curves modulated by this PAM proceeded in a biphasic concentration-activity relation illustrated by an initial ascending curve at low PNU-120596 concentrations ( $\leq 10 \mu M$  when co-applied with nicotine, acetylcholine and epibatidine;  $\leq 100 \mu M$  when co-applied with carbamoylcholine) followed by a descending section of the curve at higher PNU-120596 concentrations ( $> 10 \mu M$  when co-applied with nicotine, acetylcholine and epibatidine,  $> 100 \mu M$  when co-applied with carbamoylcholine) which proceeded in a concentration-dependent manner (Figure 19 K-L). Hereby, current amplitudes of nicotine and carbamoylcholine-induced activation were substantially

potentiated and moderately in case of acetylcholine- and epibatidine-induced  $\alpha 7$ -nAChR activation in the presence of PNU-120596 (Figure 19 E-H and K-L; Table 17).

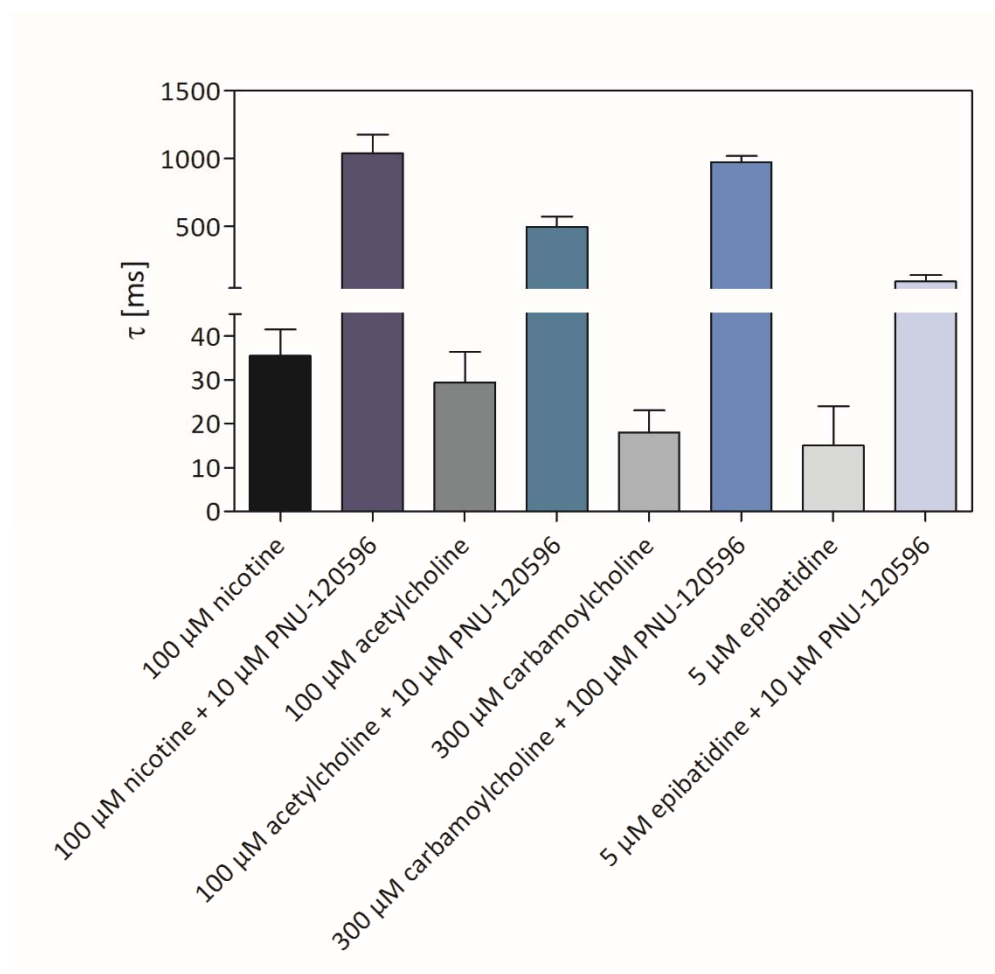


**Figure 18: Time rate of decay ( $\tau$ ) of agonist-induced and PNU-120596 modulated  $\alpha 7$ -nAChR activation in stably transfected CHO/RIC-3/ $\alpha 7$ -nAChR cells.** Time constants of decay were determined for current responses induced by 100  $\mu$ M nicotine, 100  $\mu$ M acetylcholine, 300  $\mu$ M carbamoylcholine and 5  $\mu$ M epibatidine in the absence and presence of PNU-120596. Currents were recorded at a constant holding potential of  $-70$  mV with an at least 3 min interval between each drug exposure. Means  $\pm$  SD ( $n = 8-10$ ) of the time constant of decay was plotted versus the corresponding test compound solution(s).

$EC_{50}$  values determined for the ascending section of dose response curves were similar in dose-response curves of PNU-120596 in the presence of nicotine, acetylcholine and epibatidine in the lower micromolar range (Table 17) while PNU-120596 dose response curves in the presence of carbamoylcholine was markedly shifted to the right showing a higher  $EC_{50}$  value and indicating a lower efficacy (Figure 19 L; Table 17). In case of co-application of PNU-120596 with nicotine, acetylcholine and epibatidine, the descending section of the dose-response curve revealed a similar inhibitory

potency in the lower micromolar range while with carbamoylcholine a markedly weaker inhibitory potency as shown by a higher  $IC_{50}$  value of PNU-120596 dose-response was found (Figure 19 K-L; Table 17).

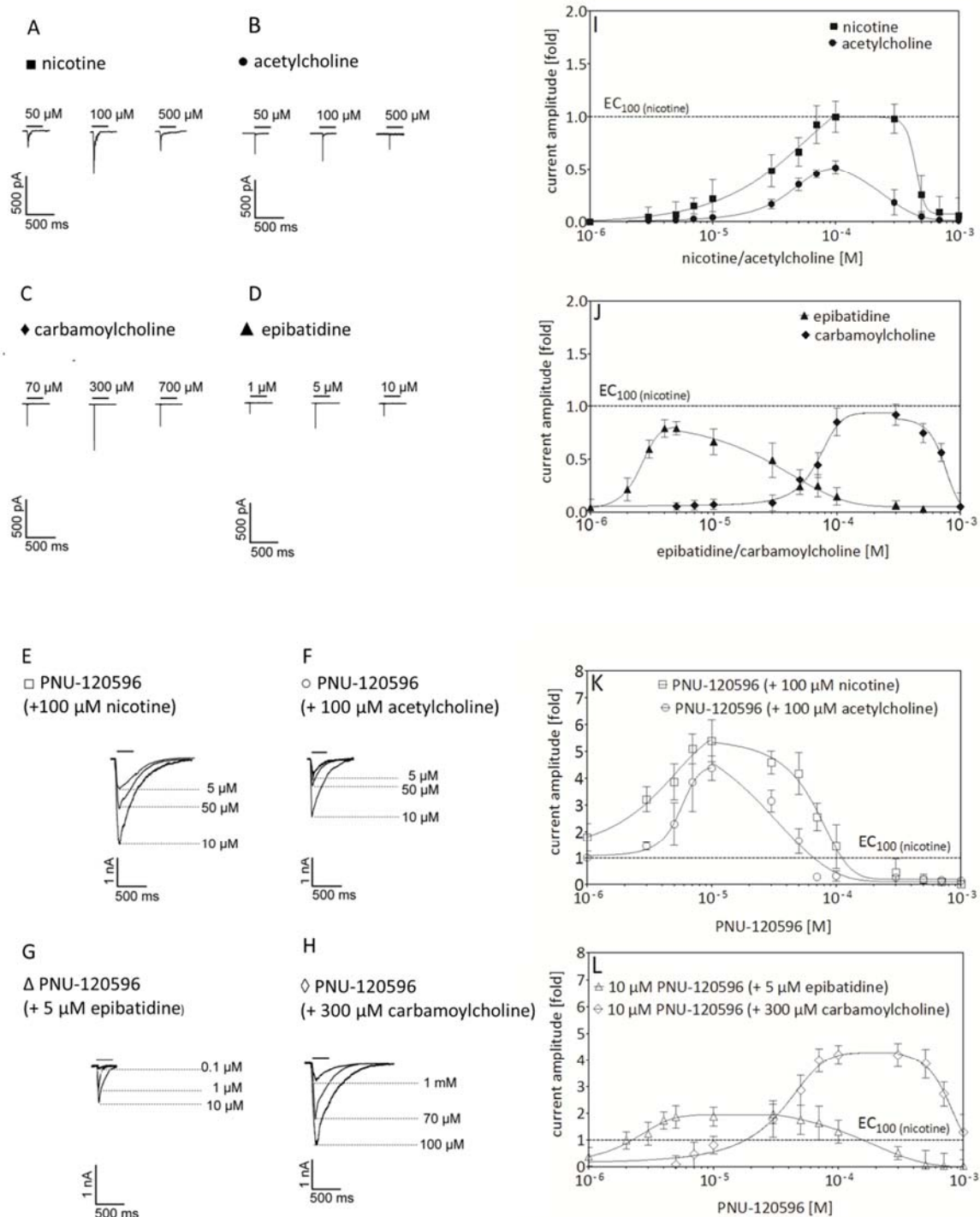


**Figure 19 A-L: Concentration-response relations of  $h\alpha 7$ -nAChR activation, desensitization and positive allosteric modulation in stably transfected CHO/RIIC-3/ $h\alpha 7$ -nAChR cells. Representative current traces (A-H) and biphasic dose-response relations (I-K) of agonist-induced activation and**

desensitization by nicotine (I), acetylcholine (I), carbamoylcholine (J), epibatidine (J) and of positive allosteric modulation by increasing concentrations of PNU-120596 co-applied with agonist ( $EC_{100}$ ) were recorded (K, L). Horizontal bars indicate exposure time (233 ms) of compound(s) to the cell. Currents were recorded at a constant holding potential of  $-70$  mV with an at least 3 min interval between each drug exposure. Current amplitudes were normalized relative to  $EC_{100}$  of nicotine set to 1 (dotted line). Means  $\pm$  SD ( $n = 8-10$ ) of normalized current amplitude was plotted and fitted using non-linear regression analysis.

**Table 17:** Means  $\pm$  SD ( $n = 8-10$ ) of maximum current amplitudes relative to  $EC_{100}$  of nicotine set to 1, half-maximum efficacy ( $EC_{50}$ ), inhibitory potency ( $IC_{50}$ ) and time constants of decay ( $\tau$ ) of agonist-induced  $\alpha 7$ -nAChR activation and potentiation by PNU-120596 in the presence of agonist. Concentrations of compounds were applied as indicated.

compound	current amplitude [fold]	$EC_{50}$ [ $\mu$ M]	$IC_{50}$ [ $\mu$ M]	$\tau$ [ms]
nicotine	$1.00 \pm 0.14^a$	$31.33 \pm 5.17$	$472.4 \pm 18.61$	$35.5 \pm 6.1^a$
acetylcholine	$0.51 \pm 0.06^a$	$43.75 \pm 4.33$	$282.4 \pm 20.42$	$29.4 \pm 7.3^a$
carbamoylcholine	$0.92 \pm 0.10^b$	$85.41 \pm 14.72$	$453.44 \pm 7.81$	$18.2 \pm 5.4^b$
epibatidine	$0.79 \pm 0.06^c$	$3.13 \pm 0.27$	$35.5 \pm 0.32$	$15.3 \pm 9.1^c$
PNU-120596 (+ 100 $\mu$ M nicotine)	$5.39 \pm 0.78^d$	$3.1 \pm 0.15$	$64.1 \pm 8.35$	$1037 \pm 141.2^d$
PNU-120596 (+ 100 $\mu$ M ACh)	$4.37 \pm 0.45^d$	$5.48 \pm 0.26$	$45.9 \pm 7.38$	$496.8 \pm 76.5^d$
PNU-120596 (+ 300 $\mu$ M carbamoylcholine)	$4.18 \pm 0.43^a$	$57.76 \pm 2.76$	$734.46 \pm 53.26$	$974.3 \pm 46.0^a$
PNU-120596 (+ 5 $\mu$ M epibatidine)	$1.97 \pm 0.36^d$	$2.20 \pm 0.18$	$76.36 \pm 3.84$	$97.8 \pm 45.4^d$

<sup>a</sup> at 100  $\mu$ M, <sup>b</sup> at 300  $\mu$ M, <sup>c</sup> at 5  $\mu$ M, <sup>d</sup> at 10  $\mu$ M

### 3.6 Current-voltage relations of CHO/RIC-3/ $\alpha 7$ -nAChR cells and inhibition of human $\alpha 7$ -nAChR

Electrophysiological properties of  $\alpha 7$ -nAChR expressed in a CHO-K1 host cell system (CHO/RIC-3/ $\alpha 7$ -nAChR cells) were examined by verification of VGIC conductance upon agonist-induced activation

(nicotine, acetylcholine) and modulation of  $\alpha 7$ -nAChR by PNU-120596 using a voltage-step protocol (see section 2.4.8). Moreover, verification of LGIC including nAChR subtypes other than  $\alpha 7$ -nAChR by inhibition of nicotine-induced  $\alpha 7$ -nAChR activation and PNU-120596 modulated current responses with methyllycaconitine (MLA) was investigated using continuous recording (see section 2.4.9).

For the electrophysiological investigation of voltage-activated conductance in CHO/RIC-3/ $\alpha 7$ -nAChR cells, current-voltage relations were established at different voltages starting from  $-100$  mV to  $+80$  mV increasing by  $20$  mV increments as schematically illustrated by Figure 20 A (see section 2.4.8). First, control currents were recorded when cells were exposed to external solution without stimulation by agonist or modulator. As shown in Figure 20 B-C, only minor negatively rectifying currents were detected in controls. Thereby, currents up to approx.  $-100$  pA in the negative voltage range ( $-80 - 0$  mV) were found while in the voltage range from  $0$  to  $+80$  mV currents increased slightly in the positive direction up to  $+200$  pA (Figure 20 B-C). When cells were stimulated with agonists, nicotine or acetylcholine, a negative current signal was induced at negative voltage which declined with increasing voltage (Figure 20 D-G). Thus, negative current amplitudes induced by  $100$   $\mu$ M nicotine were more than 2-fold more pronounced compared to those induced by  $100$   $\mu$ M acetylcholine and decreased with depolarization (Figure 20 D-G; Table 18). By application of depolarizing voltage steps, the reversal potential of agonist-induced currents showed no clear cut reversal potential but rather a range where voltage was zero which was reached at positive voltage charges between approx.  $0$  and  $+40$  mV (Figure 20 E, G; Table 18). Increasing depolarization above  $+40$  mV evoked markedly higher positive currents in the presence of agonists compared to control (Figure 20 C-G). In addition to agonist-induced currents, current-voltage relations of positively modulated currents which were generated by  $100$   $\mu$ M agonist, nicotine and acetylcholine, co-applied with the PAM PNU-120596, were established (Figure 20 D-G). As depicted in Figure 20 E and G, modulated current-voltage relations were directly proportional to agonist-induced current-voltage relations whereas current amplitudes and duration of current response were substantially potentiated compared to agonist-induced response without modulator (Figure 20 D-G; Table 18). Thereby, modulated currents activated with nicotine displayed more significant potentiation than modulated currents activated with acetylcholine (Figure 20 D-G; Table 18).

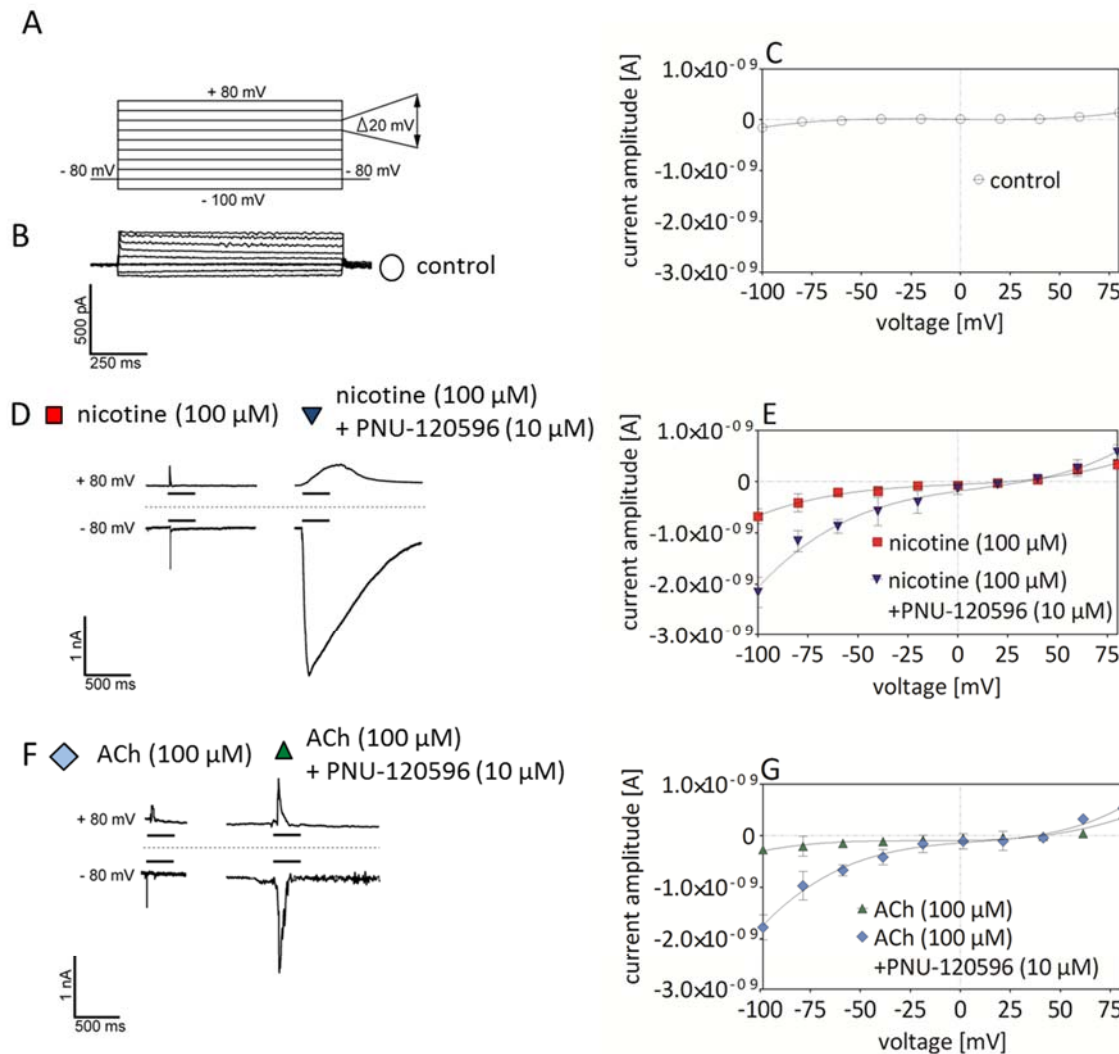


**Figure 20 A-G. Current-voltage relations of h $\alpha$ 7-nAChR activation by agonists and modulation by PNU-120596 in stably transfected CHO/RIC-3/h $\alpha$ 7-nAChR cells using voltage-step protocols.**

A. Schematic representation of the voltage-clamp step protocol with voltage step length of 200 ms and increments of 20 mV per step from - 100 to + 80 mV in steps of 20 mV with an at least 3 min interval between each drug exposure. Holding potential was applied prior and after each step and was set to - 70 mV. B-G. Representative current traces of voltage steps (B, D, F) and current-voltage-relations (C, E, G) of h $\alpha$ 7-nAChR of control exposed to external solution (B-C) and of h $\alpha$ 7-nAChR activation induced by nicotine or acetylcholine (ACh) in the absence and presence of PNU-120596 (D-G). Means  $\pm$  SD (n = 6-8) of current amplitudes were plotted and fitted using non-linear regression analysis. Horizontal bars indicate exposure time (233 ms) of compound(s) to the cell.

A common feature of current-voltage relations was that the range of reversal potential did not significantly deviate between agonist-induced and positively modulated currents and was thus found between approx. 0 and + 40 mV (Figure 20 D-G; Table 18).

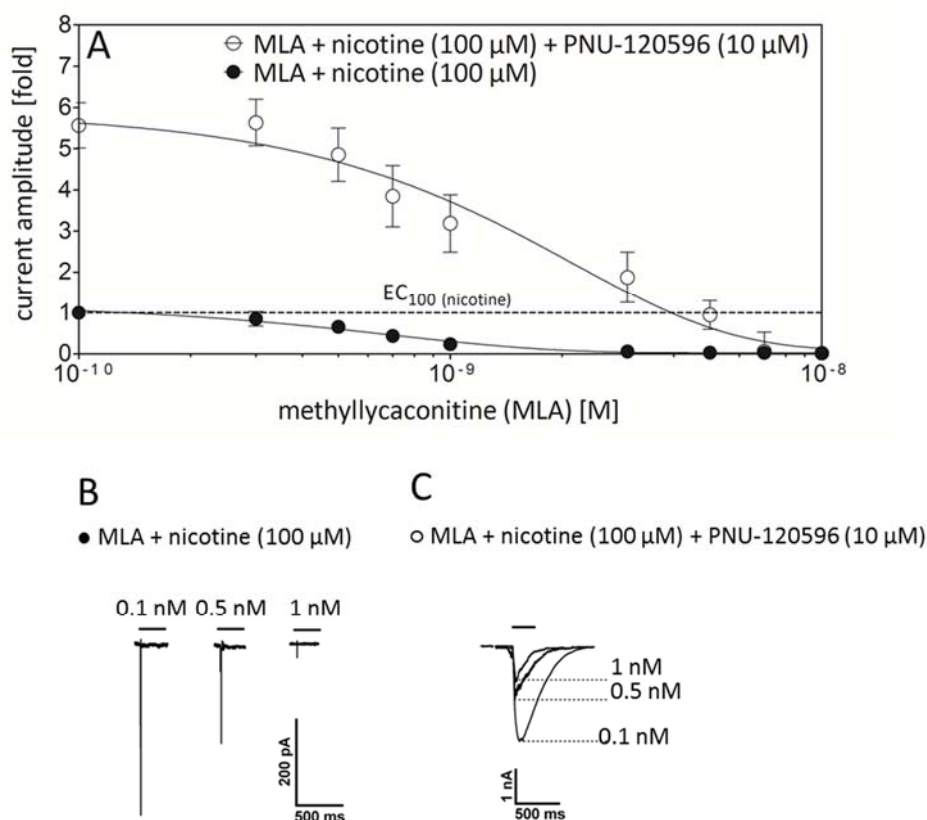


**Figure 21 A-C: Inhibition of  $\alpha 7$ -nAChR activation by agonists and modulation by PNU-120596 in stably transfected CHO/RIC-3/ $\alpha 7$ -nAChR cells with methyllycaconitine (MLA).** Dose-response relations (A) and representative current traces (B-C) of inhibition of nicotine-induced activation and of positive allosteric modulation by PNU-120596 (10  $\mu$ M) co-applied with nicotine (1-1000  $\mu$ M) were recorded. Horizontal bars indicate exposure time (233 ms) of compound(s) to the cell. Currents were recorded at a constant holding potential of – 70 mV with an at least 3 min interval between each drug exposure. Current amplitudes were normalized relative to  $EC_{100}$  of nicotine set to 1 (dotted line) and Means  $\pm$  SD ( $n = 8-10$ ) of normalized current amplitude was plotted fitted using non-linear regression analysis.

Current responses induced by 100  $\mu$ M nicotine in the absence and presence of 10  $\mu$ M PNU-120596 were inhibited by the  $\alpha 7$ -selective nAChR antagonist methyllycaconitine (MLA) (see section 2.4.9). Nicotine-induced responses were inhibited by MLA in a concentration-dependent manner revealing an inhibitory potency of dose-response curve in the lower nanomolar range ( $IC_{50} = 7.26 \pm 0.51 \cdot 10^{-10}$  M)



(Figure 21 A-B; Table 18). Furthermore, inhibition of PNU-120596-potentiated current responses co-applied with 100  $\mu$ M nicotine with increasing MLA concentrations was investigated. Inhibition of PNU-120596-potentiated current responses by MLA revealed a markedly weaker inhibitory potency than of inhibition of nicotine-induced activation without modulator ( $IC_{50} = 2.19 \pm 0.18 \cdot 10^{-09}$  M) (Figure 21 A and C; Table 18).

**Table 18:** Voltage-clamp recordings including voltage-step protocol in CHO/RIC-3/ $\alpha 7$ -nAChR cells and continuous recording at a holding potential at  $-70$  mV for the determination of basic electrophysiological characteristics. Elucidation of voltage-gated conductance of voltage-gated conductance by determination of maximum current amplitude in the negative and positive direction ( $-I_{max} / +I_{max}$ ), reversal potential and half-maximum inhibitory potency ( $IC_{50}$ ) of methyllycaconitine (MLA) of nicotine-induced and PNU-120596 potentiated current responses.

configuration	parameter	pulse protocol	CHO/RIC-3/ $\alpha 7$ -nAChR
voltage-step	$-I_{max} / +I_{max}$	100 $\mu$ M nicotine	- 100 mV: $-6.78 \pm 1.46 \cdot 10^{-10}$ A + 80 mV: $4.05 \pm 0.95 \cdot 10^{-10}$ A
		100 $\mu$ M acetylcholine	- 100 mV: $-2.68 \pm 0.73 \cdot 10^{-10}$ A + 80 mV: $2.39 \pm 0.22 \cdot 10^{-10}$ A
		100 $\mu$ M nicotine + 10 $\mu$ M PNU-120596	- 100 mV: $-2.16 \pm 0.29 \cdot 10^{-09}$ A + 80 mV: $5.75 \pm 1.38 \cdot 10^{-10}$ A
		100 $\mu$ M acetylcholine + 10 $\mu$ M PNU-120596	- 100 mV: $-1.78 \pm 0.24 \cdot 10^{-09}$ A + 80 mV: $5.33 \pm 3.38 \cdot 10^{-10}$ A
	reversal potential	100 $\mu$ M nicotine 100 $\mu$ M acetylcholine 100 $\mu$ M nicotine + 10 $\mu$ M PNU-120596 100 $\mu$ M acetylcholine + 10 $\mu$ M PNU-120596	$\sim 0$ mV - + 40 mV
voltage-clamp:	$IC_{50}$	nicotine	$7.26 \pm 0.51 \cdot 10^{-10}$ M
holding	[methyllycaconitine]	nicotine + PNU-120596	$2.19 \pm 0.18 \cdot 10^{-09}$ M
potential at - 70 mV			

### 3.7 Structure-activity relations of bispyridinium compounds on nicotine-induced human $\alpha 7$ -nAChR activation

For investigation of the functional effect of novel substituted bispyridinium (BP) compounds, so called PTM compounds and comparison of PTM compounds with the prescribed 4-*tert*-butyl BP compound MB327 on  $\alpha 7$ -nAChR activation (Figure 4; Table 6), increasing concentrations of PTM compounds and MB327 were co-applied to 100  $\mu$ M nicotine and exposed to  $\alpha 7$ -nAChR of stably transfected cells by a stacked solution in continuous voltage-clamp recording at a holding potential at  $-70$  mV (see section 2.4.10). Dose-response curves were determined from current amplitudes of increasing concentrations of MB327 and PTM compounds in the presence of 100  $\mu$ M nicotine whereas current amplitudes were normalized to the initially applied current amplitude induced by 100  $\mu$ M nicotine set to 1. With respect to the lead structure MB327, a biphasic dose-response relation yielded a pronounced concentration-dependent potentiation of nicotine-induced currents up to a concentration of 30  $\mu$ M MB327 and a consecutive reduction in current signal at higher MB327 concentration with the highest applied concentration revealing extinction of current signal (Figure 25 A and G). Considering representative current traces of 30  $\mu$ M MB327 co-applied to nicotine-induced currents yielded that potentiation of current responses represented an approx. 3.5 fold increase in current amplitude and pronounced elongation of nicotine-induced current responses (Figure 22 G; Table 19). Duration of response at 30  $\mu$ M MB327 evoking most pronounced potentiation was quantified by determination of the time constant of decay ( $\tau$ ) (Table 19). To test if MB327 or PTM compounds acted as an agonist on  $\alpha 7$ -nAChR, MB327 and PTM compounds were applied alone without agonist and failed to evoke current signal postulating that the mode of action by MB327 may be based on a positive allosteric mechanism (data not shown). Since MB327 was found to be a promising lead structure for the development of more potent PAM of nAChR, PTM compounds comprising analogues of MB327 bearing symmetrically substituted groups at the pyridinium rings were developed and tested for their ability to act as potent PAM in order to unravel structural determinants for this mode of action (see section 1.7.4; Figure 4; Table 6). Determination of current amplitudes used to generate dose-response relations showed that in total five of the tested PTM compounds (PTM0001, PTM0002, PTM0008, PTM0009, PTM0010) potentiated maximum current responses ( $I_{\max}$ ) induced by 100  $\mu$ M nicotine. These dose-response relations followed a comparable biphasic course of concentration-response relation as observed with MB327 although less pronounced than MB327 (Figure 22 A-H). Most significant enhancement in current amplitudes of BP compounds comprising 2-, 3- and 4-*tert*-butyl BP (PTM0002, PTM0001, MB327), 2-, 3- and 4-methoxy BP (PTM0010, PTM0009, PTM0008) was achieved with those carrying the substituted group at 3- (*tert*-butyl-, methoxy-,) and 4-position (*tert*-butyl-, methoxy-) compared to moderate potentiation by BP compounds with a substituted group at 2-position (*tert*-butyl-, methoxy-) (Figure 22 A-H; Table 19).

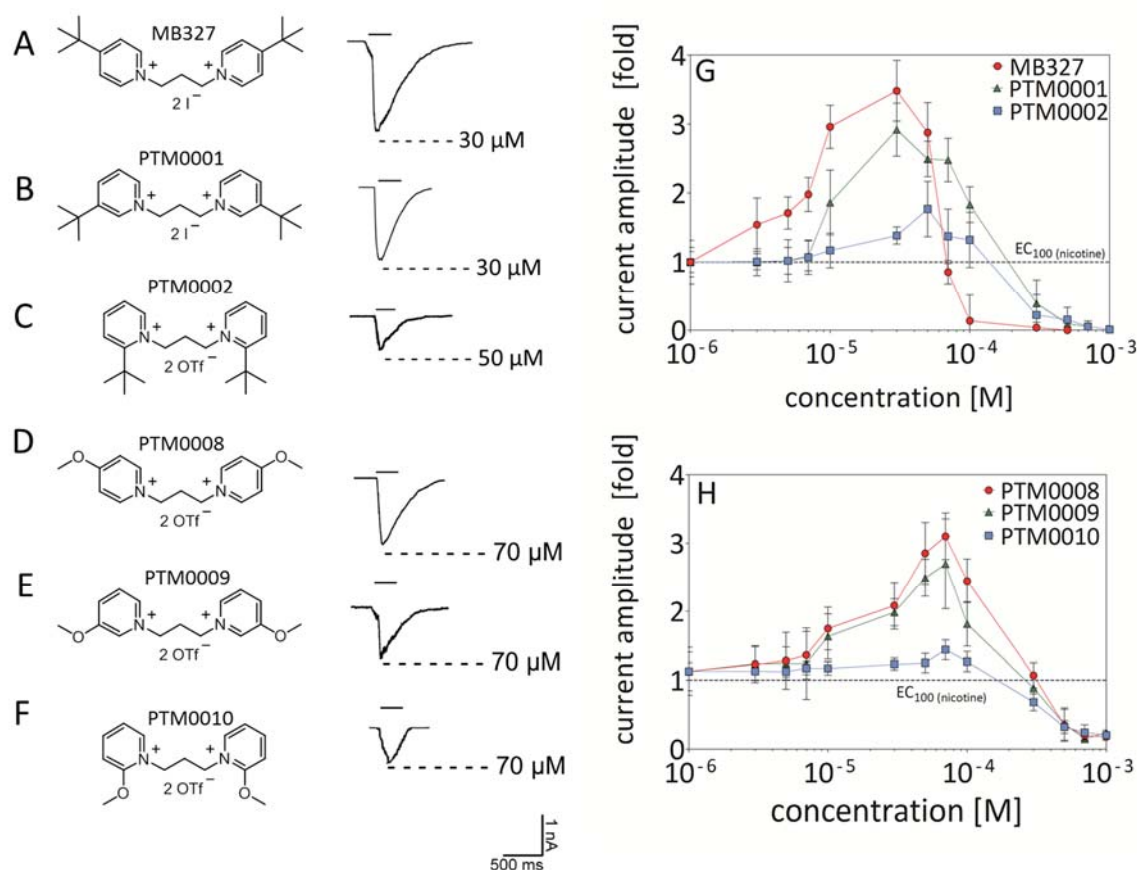


**Figure 22 A-H: Concentration-response relations of nicotine-induced  $\alpha 7$ -nAChR activation potentiated by PNU-120596, MB327, PTM0001, PTM0002, PTM0008, PTM0009 and PTM0010 in stably transfected CHO/RIC-3/ $\alpha 7$ -nAChR cells.** A-F. Chemical structures of PTM compounds potentiating nAChR activation are shown. A-H. Representative current traces of maximum current amplitudes (A-F) and biphasic dose-response relations (G-H) of  $\alpha 7$ -nAChR responses induced by nicotine in the presence of PNU-120596, MB327, PTM0001, PTM0002, PTM0008, PTM0009 and PTM0010 of maximum current amplitudes are shown. Horizontal bars indicate exposure time (233 ms) of compound(s) to the cell. Currents were recorded at a constant holding potential of -70 mV with an at least 3 min interval between each drug exposure. Current amplitudes were normalized relative to  $EC_{100}$  of nicotine set to 1 (dotted line) and Means  $\pm$  SD (n = 8-10) of normalized current amplitude was plotted.

Besides potentiation of current amplitudes by these test compounds, duration of current responses was substantially enhanced compared to nicotine-induced current response duration as depicted by Figure 22 A-F, which displayed representative current traces of PTM0001-PTM0002 and PTM0008-PTM0010 at concentrations evoking maximum peak current responses ( $I_{max}$ ) in the presence of 100  $\mu$ M nicotine (Table 19). Time constants of decay ( $\tau$ ) of current responses were determined at PTM concentrations inducing maximally potentiated peak currents whereas the degree of elongation of current response directly correlated with the degree of enhanced amplitude of current which was

more pronounced with PTM compounds with a substituted group at 3- and 4- position (*tert*-butyl-, methoxy-) and to a reduced extent with PTM compounds with a substituted group at 2-position (*tert*-butyl-, methoxy-) (Figure 24; Table 19). In concordance with this structure-activity relation of potentiated current amplitudes, time constant of decay ( $\tau$ ) of MB327 bearing a *tert*-butyl group at 4-position was significantly greater compared to PTM0001-PTM0002 and PTM0008-PTM0010 (Figure 24; Table 19).

Since test compounds contained either trifluoromethanesulfonate ( $\text{Tfo}^-$ ) or iodide ( $\text{I}^-$ ) as counterion and a functional interaction of these ions with  $\text{h}\alpha 7$ -nAChR could not be excluded, it was investigated if either of these counterions interacted functionally with the  $\text{h}\alpha 7$ -nAChR. For this purpose, two test compounds containing either of these counterions were tested for diverging effects on potentiation of  $\text{h}\alpha 7$ -nAChR activation. Thereby, a diverging effect of identical compounds carrying different counterions on  $\text{h}\alpha 7$ -nAChR activation would indicate a functional interaction of  $\text{Tfo}^-$  or  $\text{I}^-$  with the  $\text{h}\alpha 7$ -nAChR. Hereby, the 4-*tert*-butyl BP compound containing  $\text{Tfo}^-$  as counterion was denoted as PTM0061, and 4-*tert*-butyl BP compound containing  $\text{I}^-$  as counterion was denoted as MB327. The 2-*tert*-butyl BP compound containing  $\text{Tfo}^-$  as counterion was denoted as PTM0002 and the 2-*tert*-butyl BP compound containing  $\text{I}^-$  as counterion was denoted as PTM00045. Therefore, 100  $\mu\text{M}$  nicotine was co-applied with 5, 50 and 500  $\mu\text{M}$  of these compounds, a concentration range which covered the initial phase, the peak phase and the exhaustion of potentiation found with PTM0002 and MB327 (compare Figure 22 G). By comparison of the current amplitudes of identical compounds with either  $\text{Tfo}^-$  or  $\text{I}^-$  as counterion, currents did not show significant deviations of 4-*tert*-butyl BP or 2-*tert*-butyl BP induced-current responses confirming that a functional interaction of either  $\text{Tfo}^-$  or  $\text{I}^-$  could be excluded (Figure 23 A-B). Examination of structure-activity relations of further PTM compounds carrying an isopropyl-group (PTM0003, PTM0013, PTM0014), a dimethylamino-group (PTM0007), methyl-groups (PTM0004 – PTM0006) or an additional group at 3-position to the 4-*tert*-butyl group (PTM0015 – PTM0022) were found to antagonize activation of  $\text{h}\alpha 7$ -nAChR by 100  $\mu\text{M}$  nicotine in a concentration-dependent manner (Figure 25 A-D; Table 20). Inhibitory potency ( $\text{IC}_{50}$ ) by these test compounds did not strictly correlate with its substitution pattern. In this context, a weak inhibitory potency was induced by compounds with an isopropyl-group (PTM0003, PTM0013, PTM0014), but for instance inhibitory potency scattered widely from  $17.86 \pm 5.80 \mu\text{M}$  (PTM0005) to  $212.72 \pm 1.49 \mu\text{M}$  (PTM0004) by methyl-substituted BP compounds (PTM0004, PTM0005, PTM0006) (Figure 25 B; Table 20). Among the 4-*tert*-butyl BP compounds with an additional substituted group at 3-position of each pyridinium ring and the PTM compound carrying a dimethylamino-group (PTM0007), two distinct clusters with similar  $\text{IC}_{50}$  values were detected. Thereby, PTM compounds belonging to the same cluster were not linked to a common group of structural pattern as for instance inhibitory potency was weak with PTM0018

carrying a bromide and PTM0021 carrying a fluoride, but strong with PTM0020 carrying a chloride at 3-position (Figure 25 C-D; Table 20).

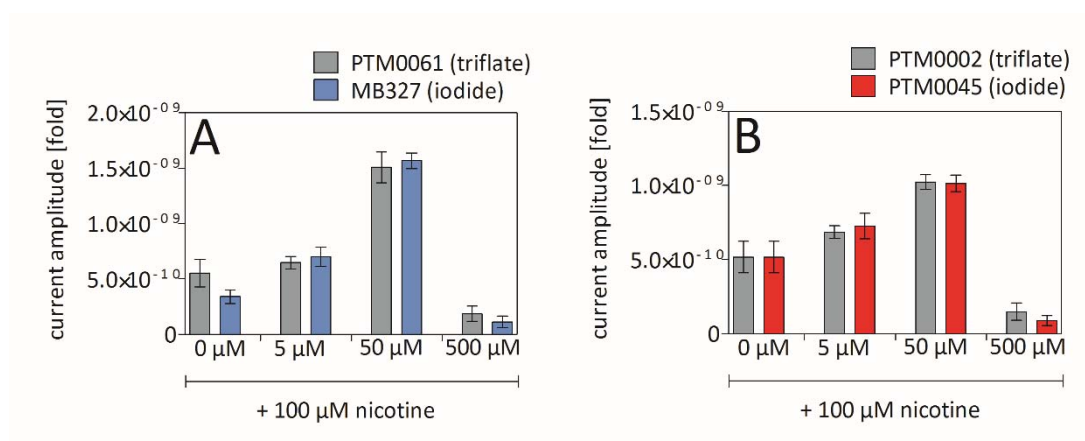


**Figure 23 A-B: Comparison of the effect of two different counterions of test compounds on nicotine-induced  $\alpha 7$ -nAChR activation potentiated by 4-*tert*-butyl and 2-*tert*-butyl bispyridinium compounds containing trifluoromethanesulfonate (Tfo<sup>-</sup>) or iodide (I<sup>-</sup>).** Current amplitudes induced by 5, 50 and 500  $\mu$ M of BP compound (4-*tert*-butyl and 2-*tert*-butyl BP) containing Tfo<sup>-</sup> or I<sup>-</sup> were recorded in the presence of 100  $\mu$ M nicotine. Currents were recorded at a constant holding potential of  $-70$  mV with an at least 3 min interval between each drug exposure. Means  $\pm$  SD ( $n = 8-10$ ) of current amplitude was plotted.

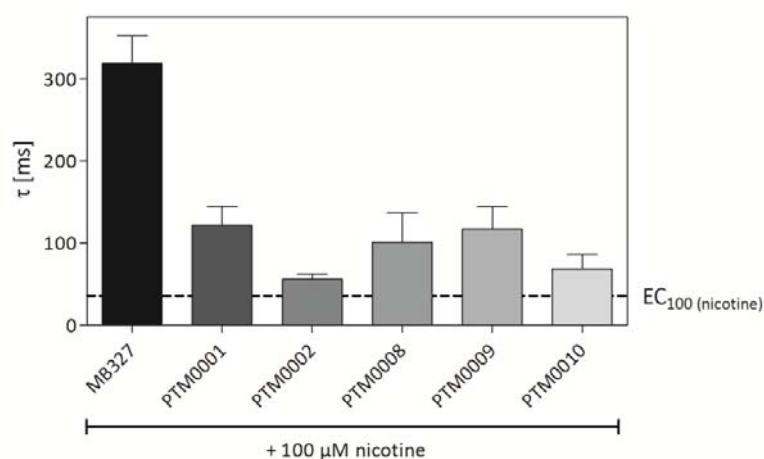


**Figure 24: Time constants of decay ( $\tau$ ) of potentiation of nicotine induced  $\alpha 7$ -nAChR activation by MB327 and by PTM compounds in the presence of 100  $\mu$ M nicotine in stably transfected CHO/RIC-3/ $\alpha 7$ -nAChR cells.** Currents were recorded at a constant holding potential of  $-70$  mV with an at least 3 min interval between each drug exposure and Means  $\pm$  SD ( $n = 8-10$ ) of time constants of decay ( $\tau$ ) versus PTM compounds were plotted and compared to  $\tau$  value at the  $EC_{100}$  of nicotine set to 1 (dotted line).

**Table 19:** Means  $\pm$  SD ( $n = 8-10$ ) of maximum current amplitude ( $I_{max}$ ) relative to  $EC_{100}$  of nicotine set to 1 and time constant of decay ( $\tau$ ) of 100  $\mu$ M nicotine-induced  $\alpha 7$ -nAChR activation potentiated by bispyridinium (BP) compounds including MB327 and PTM compounds. General chemical structures of PTM compounds are displayed in Figure 4 with the corresponding substituted group(s) given in Table 6. Concentrations of compounds were applied as indicated.

code	R <sub>1</sub>	R <sub>2</sub>	R <sub>3</sub>	compound	$I_{max}$ [fold]	$\tau$ [ms]
MB327	-	-	C(CH <sub>3</sub> ) <sub>3</sub>	4- <i>tert</i> -butyl BP	$3.48 \pm 0.44^a$	$319 \pm 33^a$
PTM0001	-	C(CH <sub>3</sub> ) <sub>3</sub>	-	3- <i>tert</i> -butyl BP	$2.92 \pm 0.38^a$	$122 \pm 2^a$
PTM0002	C(CH <sub>3</sub> ) <sub>3</sub>	-	-	2- <i>tert</i> -butyl BP	$1.76 \pm 0.40^b$	$56 \pm 6^b$
PTM0008	-	-	OCH <sub>3</sub>	4-methoxy BP	$2.56 \pm 0.65^c$	$101 \pm 36^c$
PTM0009	-	OCH <sub>3</sub>	-	3-methoxy BP	$2.97 \pm 0.34^c$	$117 \pm 27^c$
PTM0010	OCH <sub>3</sub>	-	-	2-methoxy BP	$1.31 \pm 0.14^c$	$68 \pm 18^c$

<sup>a</sup> at 30  $\mu$ M, <sup>b</sup> at 50  $\mu$ M, <sup>c</sup> at 70  $\mu$ M

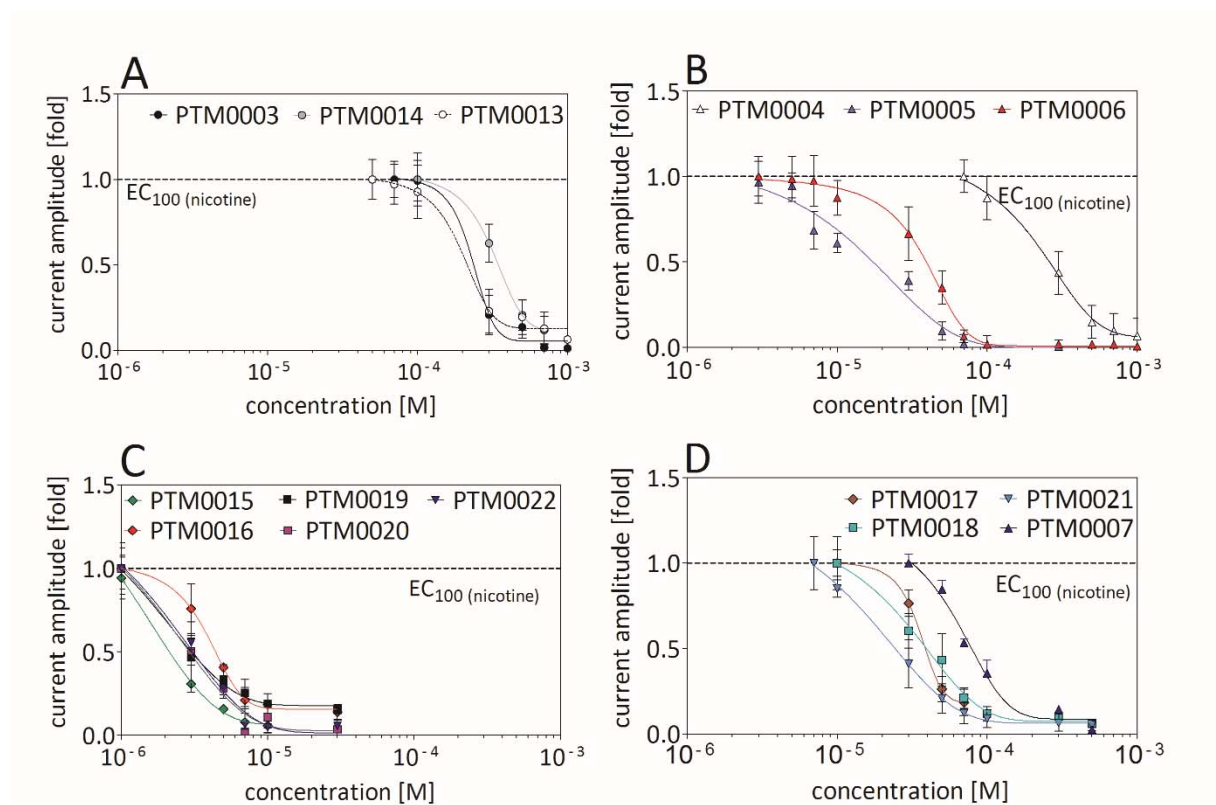


**Figure 25 A-D:** Concentration-response relations of nicotine-induced  $\alpha 7$ -nAChR activation inhibited by PTM compounds (PTM0003 - PTM0007, PTM0013 - PTM0022) in stably transfected CHO/RIC-3/ $\alpha 7$ -nAChR cells. Inhibitory dose-response relations of  $\alpha 7$ -nAChR responses induced by nicotine in the presence of PTM compounds (PTM0003 - PTM0007, PTM0013 - PTM0022) of maximum current amplitudes are shown. Currents were recorded at a constant holding potential of

- 70 mV with an at least 3 min interval between each drug exposure. Current amplitudes were normalized relative to EC<sub>100</sub> of nicotine set to 1 (dotted line) and Means  $\pm$  SD (n = 8-10) of normalized current amplitude was plotted and fitted using non-linear regression analysis.

**Table 20:** Means  $\pm$  SD (n = 8-10) of half-maximum inhibitory potency (IC<sub>50</sub>) of  $\alpha 7$ -nAChR activation inhibited by bispyridinium PTM compounds. General chemical structure of BP compounds is displayed in Figure 4 with the corresponding substituted group(s) given in Table 6.

code	R <sub>1</sub>	R <sub>2</sub>	R <sub>3</sub>	R <sub>4</sub>	R <sub>5</sub>	compound	IC <sub>50</sub> [ $\mu$ M]
PTM0014	-	CH(CH <sub>3</sub> ) <sub>2</sub>	-	-	-	3-isopropyl BP	312.61 $\pm$ 17.89
PTM0003	CH(CH <sub>3</sub> ) <sub>2</sub>	-	-	-	-	2-isopropyl BP	228.93 $\pm$ 8.73
PTM0004	CH <sub>3</sub>	-	-	-	CH <sub>3</sub>	2,6-dimethyl BP	212.72 $\pm$ 1.49
PTM0013	-	-	CH(CH <sub>3</sub> ) <sub>2</sub>	-	-	4-isopropyl BP	194.55 $\pm$ 24.93
PTM0007		N(CH <sub>3</sub> ) <sub>2</sub>				3-dimethylamino	73.14 $\pm$ 13.52
PTM0018	-	Br	C(CH <sub>3</sub> ) <sub>3</sub>	-	-	3-bromo-4- <i>tert</i> -butyl BP	42.78 $\pm$ 7.96
PTM0017	-	CH <sub>3</sub>	C(CH <sub>3</sub> ) <sub>3</sub>	-	-	4- <i>tert</i> -butyl-3-methyl- BP	38.56 $\pm$ 4.13
PTM0006	CH <sub>3</sub>	-	CH <sub>3</sub>	-	CH <sub>3</sub>	2,4,6-trimethyl BP	35.56 $\pm$ 3.96
PTM0021	-	F	C(CH <sub>3</sub> ) <sub>3</sub>	-	-	4- <i>tert</i> -butyl-3-fluoro-BP	21.31 $\pm$ 5.24
PTM0005	-	CH <sub>3</sub>	-	CH <sub>3</sub>	-	3,5-dimethyl BP	17.86 $\pm$ 5.80
PTM0016	-	OCH <sub>3</sub>	C(CH <sub>3</sub> ) <sub>3</sub>	-	-	4- <i>tert</i> -butyl-3-methoxy- BP	4.14 $\pm$ 0.38
PTM0022	-	Ph	C(CH <sub>3</sub> ) <sub>3</sub>	-	-	4- <i>tert</i> -butyl-3-phenyl- BP	3.77 $\pm$ 0.06
PTM0019	-	CN	C(CH <sub>3</sub> ) <sub>3</sub>	-	-	4- <i>tert</i> -butyl-3-cyano-BP	3.27 $\pm$ 0.10
PTM0020	-	Cl	C(CH <sub>3</sub> ) <sub>3</sub>	-	-	4- <i>tert</i> -butyl-3-chloro- BP	3.15 $\pm$ 0.56
PTM0015	-	C=O(EtO)	C(CH <sub>3</sub> ) <sub>3</sub>	-	-	4- <i>tert</i> -butyl-3-ethoxycarbonyl- BP	2.29 $\pm$ 0.10

### 3.8 Effect of bispyridinium compounds on desensitization of human $\alpha 7$ -nAChR

To examine the effect of PTM compounds on desensitized  $\alpha 7$ -nAChR of stably transfected cells by a stacked solution in continuous voltage-clamp recording at a holding potential at  $-70$  mV, receptors were first activated by  $100\text{ }\mu\text{M}$  nicotine followed by an excess of  $1\text{ mM}$  nicotine to induce complete desensitization of the receptor population. Subsequent augmenting PTM compound concentrations were exposed to cells together with  $1\text{ mM}$  nicotine to ensure that recovery of receptors by application of test compound was not accompanied by spontaneous regeneration of receptors from desensitization (see section 2.4.10). Using the same protocol as for testing of PTM compounds, the effect of MB327 from which this analogues series of PTM compounds derived and PNU-120596, chosen as a representative type II PAM, were compared to the effect of test compounds on desensitized receptors. Thereby, corresponding resemblance of response pattern would strengthen the hypothesis of a common mode of action by all compounds tested and was discussed hereinafter (see section 4.6.2). For determination of dose-response curves and evaluation of the proportional recovery by test compounds (including PNU-120596, MB327 and PTM compounds), current amplitudes were normalized to the initially applied current amplitude induced by  $100\text{ }\mu\text{M}$  nicotine set to 1, a threshold used as a benchmark of complete resensitization of nicotinic receptors. As depicted in Figure 26 A, dose-response curves revealed that PTM compounds PTM0003, PTM0014, PTM0013, bearing an isopropyl-group at 2-, 3- or 4-position were unable to retrieve nicotinic currents. As shown by previous experiments of this study investigating the effect of the PTM compounds on nAChR activation instead of desensitization, this group of compounds was priory found to inhibit nAChR activation induced by  $100\text{ }\mu\text{M}$  nicotine and thus it was expected that those PTM compounds would not be able to reverse desensitization of receptors (see section 3.7; Figure 25 A). In line to these data, PTM compounds with a *tert*-butyl or a methoxy-group substituted at 2-, 3- or 4-position of the pyridinium rings (PTM0002, PTM0001, MB327, PTM0010, PTM0009 and PTM0008) were found to have a potentiating effect on  $\alpha 7$ -nAChR activation and were observed also to promote recovery of nicotine-induced  $\alpha 7$ -nAChR desensitization (see section 3.7; Figure 22 A-H). With respect to recovery of receptors from desensitization, such PTM compounds resensitizing receptors concentration-dependently yielded similar  $\text{EC}_{50}$  values between  $0.45$  and  $3.24\text{ mM}$  (Table 21). The most pronounced current amplitudes were found at the highest PTM concentration applied at  $10\text{ mM}$  whereas merely less than half of the initial nicotine-induced current amplitude could be recovered by PTM0001, PTM0002 and PTM0008 (Figure 26 A-D; Table 21). Minor restoration of receptor function was found with PTM0009 and PTM0010 (Figure 26 A-D; Table 21).

Concerning dose-response curves of prescribed potentiating compound MB327 (compare Figure 22 A and G), a markedly superior effect was recorded with MB327 compared to the PTM



compounds by an almost full regeneration of initial nicotine-induced currents after desensitization (Figure 26 A and C; Table 21). With regard to the ability of PNU-120596 to recover desensitization, a full resensitization of the current amplitude was found when applied in the lower micromolar range ( $\leq 10 \mu\text{M}$ ), and, when applied at concentrations in the higher micromolar range ( $\geq 10 \text{ M} \leq 100 \mu\text{M}$ ), the nicotine-induced current amplitude was amplified in the presence of PNU-120596 by a factor of 1.3 (Figure 26 A and B; Table 21). Contrary to PTM compounds and MB327, PNU-120596 concentrations above  $100 \mu\text{M}$  reduced the amplified current signal concentration-dependently resulting in a bimodal dose-response relation of PNU-120596 when investigating recovery of desensitized receptors (Figure 26 A and B; Table 21).

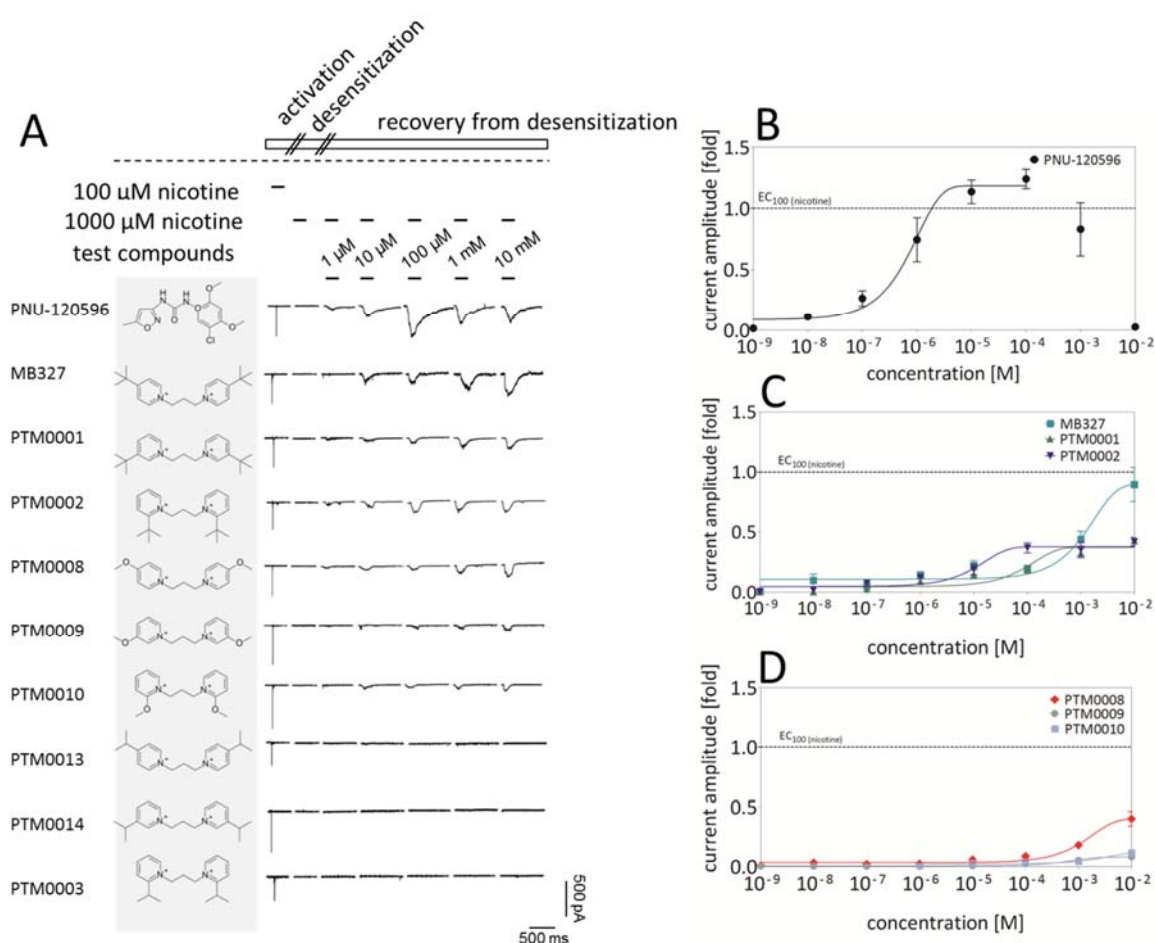


**Figure 26 A-D: Concentration-response relations of recovery of nicotine-induced hα7-nAChR desensitization by PNU-120596, MB327 and PTM compounds (PTM0001, PTM0002, PTM0003, PTM0008, PTM0009, PTM0010, PTM0013 and PTM0014) in stably transfected CHO/RIC-3/hα7-nAChR cells.** A. Chemical structures of PTM compounds tested for their ability to recover nAChR desensitization are shown. Representative current traces show initial nicotine-induced activation by  $100 \mu\text{M}$  followed by desensitization by  $1 \text{ mM}$  nicotine and application of increasing PTM compound concentrations in the presence of  $1 \text{ mM}$  nicotine. B-D. Dose-response relations of recovery of hα7-nAChR responses induced by  $1 \text{ mM}$  nicotine in the presence of PNU-120596 (B), MB327 (C) and PTM

compounds (PTM0001, PTM0002, PTM0008, PTM0009, PTM0010) (C-D) are shown. Horizontal bars indicate exposure time (233 ms) of compound(s) to the cell. Currents were recorded at a constant holding potential of -70 mV with an at least 3 min interval between each drug exposure. Current amplitudes were normalized relative to EC<sub>100</sub> of nicotine set to 1 (dotted line). Means  $\pm$  SD (n = 8-10) of normalized current amplitude was plotted and fitted using non-linear regression analysis.

Slopes determined by the coefficients ( $n_H$ ) from dose response curve revealed a steep  $n_H$  by PNU-120596 mediated nAChR recovery (Table 21). PTM compounds displayed relatively shallow  $n_H$  in contrast to MB327, which displayed a steep  $n_H$  although less pronounced than PNU-120596 (Table 21). A common feature of all compounds that contributed, either partly or fully, to resensitization of receptors was the prolongation of current responses to different degrees (Figure 26 A; Figure 27 A-C; Table 21). In this context, current amplitudes at all applied concentrations of compounds tested were determined at different time points following exposure (10 ms, 50 ms, 100 ms) (Figure 27 A-C; Table 21). This approach was used to illustrate the decay rate of the current response as an alternative to the determination of  $\tau$  used as a parameter of choice for the evaluation of current decay rate because an exponential decay of current response is required for calculation of  $\tau$  and was not feasible with current traces of this experiment. As shown in Figure 27 A-C, current amplitudes were expressed as fraction relative to the current amplitude induced by 100  $\mu$ M nicotine set to 1 and compared to reduced current amplitudes after 10, 50 and 100 ms of nicotine induced activation by 100  $\mu$ M (dotted line). In this context, after 10 ms nicotinic activation was reduced by  $0.78 \pm 0.09$  fold (Figure 27 A; Table 21). Only the current amplitude evoked with 10 and 100  $\mu$ M PNU-120596 exceeded nicotinic response after 10 ms (Figure 27 A; Table 21). Current amplitude with 10 mM MB327 was slightly reduced while current amplitudes of PTM0001, PTM0002 and PTM0008 were diminished by about half compared to nicotinic response after 10 ms (Figure 27 A; Table 21). Current amplitudes of 10 mM PTM0009 and PTM0010 were markedly decreased and only displayed small current amplitudes when compared to nicotinic induced current amplitudes after 10 ms (Figure 27 A; Table 21). After 50 ms, the current signal of nicotine was depleted while current amplitudes of PNU-120596, MB327 and PTM compounds were only marginally decreased and thus significantly superior to nicotinic response at high concentrations (Figure 27 B; Table 21). After 100 ms, the current signal of PTM0002, PTM0009 and PTM0010 was almost completely exhausted (Figure 27 C; Table 21). Current amplitudes by PNU-120596 were still clearly present, whereas small currents remained with MB327, PTM0001 and PTM0008 (Figure 27 C; Table 21). In conclusion, the size of current amplitude of PTM compounds recovering desensitized receptors revealed a direct correlation with the duration of prolonged whole cell currents of recovered nAChR (Figure 27 A-C; Table 21). All in all, when comparing PTM compounds to MB327 and PNU-120596, the resensitization showed a lower potency and efficacy of PTM compounds compared to MB327 and PNU-120596 (Figure 26 A-D; Figure 27 A-C; Table 21).

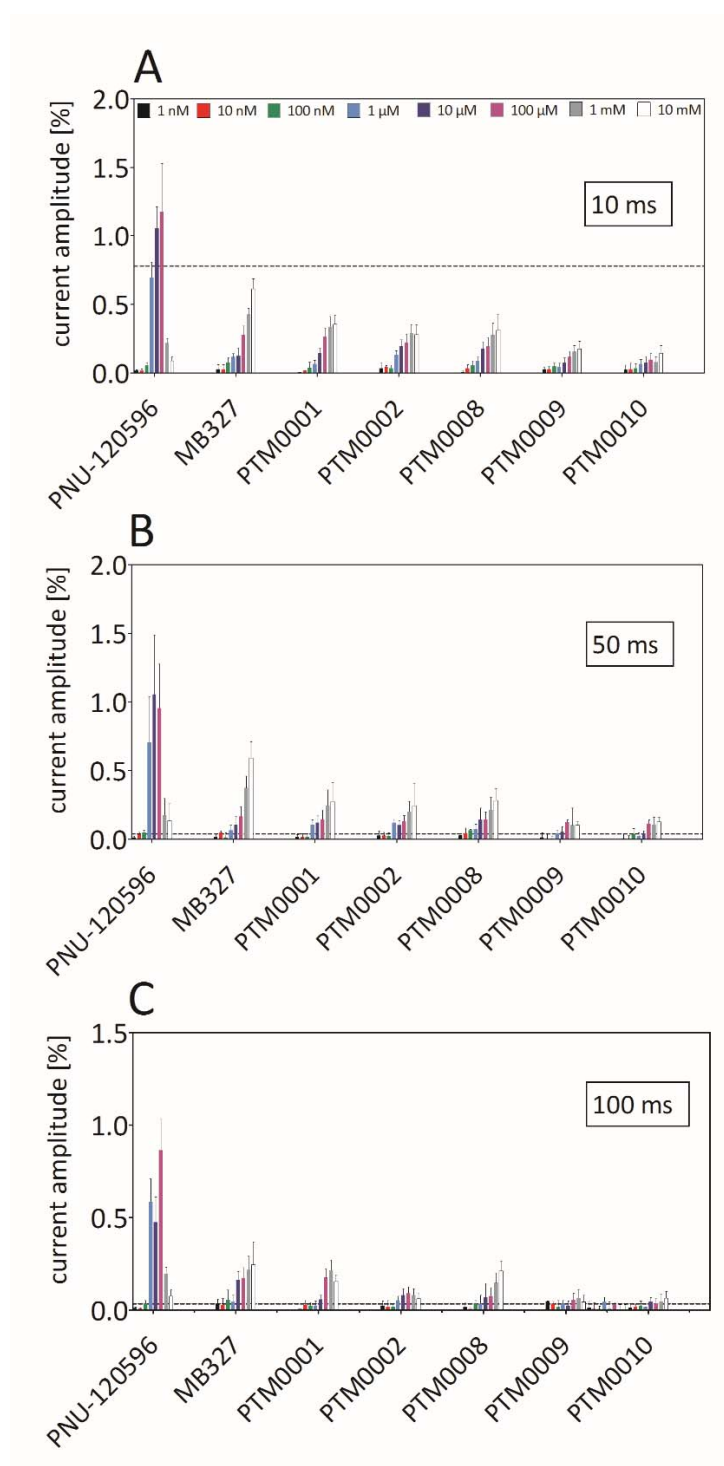


**Figure 27 A-C: Time-dependent decay of current responses after recovery of nicotine induced  $\alpha 7$ -nAChR desensitization by PNU-120596, MB327 and by PTM compounds (PTM0001, PTM0002, PTM0008, PTM0009, PTM0010) in the presence of 1 mM of nicotine recorded after 10, 50 and 100 ms of exposure.** Currents were recorded at a constant holding potential of  $-70$  mV with an at least 3 min interval between each drug exposure. Means  $\pm$  SD ( $n = 8-10$ ) of current responses of test compounds were normalized relative to  $EC_{100}$  of nicotine set to 1 and were compared to current

responses of EC<sub>100</sub> of nicotine determined after 10 (A) , 50 (B) and 100 ms (C) (dotted line) after exposure.

**Table 21:** Means  $\pm$  SD ( $n = 8-10$ ) of half-maximum efficacy (EC<sub>50</sub>), maximal current amplitudes ( $I_{max}$ ), slope coefficients ( $n_H$ ) and current amplitudes at different time points (10, 50 and 100 ms) of nicotinic signal (control) and after recovery from desensitization by test compounds (PNU-120596, MB327, PTM0001, PTM0002, PTM0008, PTM0009 and PTM0010) were determined. If not indicated otherwise,  $I_{max}$  and current amplitudes at different time points (10, 50 and 100 ms) were determined at the highest concentration applied (10 mM).

code	EC <sub>50</sub> [mM]	$I_{max}$ [fold]	$n_H$	current amplitudes		
				10 ms	50 ms	100 ms
nicotine	0.035 $\pm$ 0.005	1.00 $\pm$ 13.4	2.13 $\pm$	0.78 $\pm$	0.04 $\pm$	0.03 $\pm$
			0.37	0.09	0.02	0.02
PNU-120596	0.82 $\pm$ 0.005 $\times 10^{-3}$	1.23 $\pm$ 0.15 <sup>a)</sup>	3.14 $\pm$	1.17 $\pm$	0.95 $\pm$	0.86 $\pm$
(+ 100 $\mu$ M nicotine)			0.53	0.35 <sup>a</sup>	0.32 <sup>a</sup>	0.17 <sup>a</sup>
MB327	1.20 $\pm$ 0.091	0.89 $\pm$ 0.31	1.74 $\pm$	0.68 $\pm$	0.59 $\pm$	0.24 $\pm$
			0.42	0.07	0.11	0.13
PTM0001	0.52 $\pm$ 0.034	0.42 $\pm$ 0.06	0.65 $\pm$	0.35 $\pm$	0.27 $\pm$	0.15 $\pm$
			0.089	0.06	0.13	0.03
PTM0002	0.45 $\pm$ 0.011	0.42 $\pm$ 0.07	0.55 $\pm$	0.28 $\pm$	0.24 $\pm$	0.06 $\pm$
			0.071	0.07	0.16	0.04
PTM0008	1.744 $\pm$ 0.164	0.40 $\pm$ 0.01	0.79 $\pm$	0.31 $\pm$	0.28 $\pm$	0.21 $\pm$
			0.078	0.11	0.08	0.05
PTM0009	1.31 $\pm$ 0.181	0.08 $\pm$ 0.01	0.043 $\pm$	0.17 $\pm$	0.10 $\pm$	0.04 $\pm$
			0.0039	0.05	0.02	0.03
PTM0010	3.24 $\pm$ 0.105	0.11 $\pm$ 0.03	0.015 $\pm$	0.14 $\pm$	0.12 $\pm$	0.06 $\pm$
			0.0022	0.05	0.03	0.03

<sup>a</sup> 0.1 mM

## 4. Discussion

In the present study, a patch clamp screening method was established to investigate the ability of bispyridinium non-oximes to prevent and to recover human acetylcholine receptors of the subtype  $\alpha 7$  ( $\text{h}\alpha 7\text{-nAChR}$ ) from desensitization. Intrinsic activities and structure-activity-relations of PTM compounds were determined and compared to the effect by the lead structure MB327 and the well prescribed positive allosteric modulator (PAM) PNU-120596 in order to verify if the mode of action was based on a positive allosteric mechanism and to identify structural determinants of the structure-activity-relations mediating such a positive allosteric mechanism on  $\text{h}\alpha 7\text{-nAChR}$ .

Screening for such an effect by such compounds and establishment of structure-activity relations by an automated patch clamp technique using a cell line stably transfected with  $\text{h}\alpha 7\text{-nAChR}$  served as a starting point for synthetization of more potent nAChR PAM for the development of an alternative therapeutic option against organophosphorus (OP) poisoning [148, 149, 230, 290, 330].

First of all, basic electrophysiological properties of wildtype CHO-K1 and  $\text{GH}_4\text{C}_1$  cell were elucidated in order to identify a cell line most suitable for stable transfection of  $\text{h}\alpha 7\text{-nAChR}$ . In this regard, a suitable cell line should have a low expression of endogenous voltage-gated (VGIC) and ligand-gated (LGIC) ion channels on the cell membrane that may otherwise cause interference in investigations of the effect of PTM compounds on  $\text{h}\alpha 7\text{-nAChR}$  when activated. Moreover, resting membrane potentials (RMP), reversal potentials and ions permeant to voltage-gated ion channels as well as ligand-gated endogenous membrane sources in wildtype CHO-K1 and  $\text{GH}_4\text{C}_1$  cell line were determined (see section 3.1; 3.2; 3.3). Subsequently, the influence of modified cellular parameters and settings to obtain a higher seal success rate of patch clamp recordings of CHO-K1 cell line stably transfected with  $\text{h}\alpha 7\text{-nAChR}$  (CHO-K1/RIC-3/ $\text{h}\alpha 7\text{-nAChR}$ ) was examined. These modifications included adjustment of the under-pressure applied to capture and to hold the cells, addition of a  $\text{Ca}^{2+}$  rich solution serving as a “seal enhancer” and cell passage range used (see section 3.4).

Considering the fast conformational change of  $\text{h}\alpha 7\text{-nAChR}$ , the flow rate of test compound application was adjusted to increase signal intensity. In addition, the amount of time and number of washing steps between each test compound application were adjusted to ensure full recovery of receptors from desensitization prior the next test compound application (see section 3.4). Prior to screening of the effect test compounds on  $\text{h}\alpha 7\text{-nAChR}$  function, typical electrophysiological properties including conformational transition states and ion permeability of  $\text{h}\alpha 7\text{-nAChR}$  in CHO-K1 cells were elucidated by establishing dose-response curves and current-voltage relations, respectively, induced by different classical agonists and by modulation with the positively allosteric modulator PNU-120596. Furthermore, the specific expression of  $\text{h}\alpha 7\text{-nAChR}$  on CHO-K1 cells was verified by specific

antagonization of  $\alpha 7$ -nAChR activation and modulation with the  $\alpha 7$ -specific PNU-120596 (see section 3.5; 3.6).

All patch clamp experiments were carried out in the whole-cell configuration as described in section 2.4.2, wherein the behavior of the  $\alpha 7$ -nAChR population across the cell membrane of the entire cell was recorded [221]. More precisely, in the whole-cell configuration, the averaged open probability of multiple  $\alpha 7$ -nAChR upon changes in voltage was determined instead of the open probability on single channel level which is investigated using the cell-attached configuration [232].

#### **4.1 Determination of the resting membrane potential of GH<sub>4</sub>C<sub>1</sub> and CHO-K1 cells**

The RMP of a cell typically derives from a much higher permeability of K<sup>+</sup> compared to Na<sup>+</sup>, Ca<sup>2+</sup> or Cl<sup>-</sup> which causes a RMP that is normally near the Nernst potential of K<sup>+</sup> [48]. However, comparison of the Nernst potential of K<sup>+</sup> determined at - 71 mV with the RMP in GH<sub>4</sub>C<sub>1</sub> and CHO-K1 cells recorded by current-clamp whole-cell patch clamp experiments revealed that the RMP of CHO-K1 cells recorded at - 49.54 ± 2.29 mV and the RMP of GH<sub>4</sub>C<sub>1</sub> cells recorded at - 57.05 ± 3.52 mV had a more depolarized potential than the Nernst potential of K<sup>+</sup> (see section 2.4.1; Figure 11 A-B). It was conceivable that besides the main determining component of the RMP, the K<sup>+</sup> permeability, activation of voltage-gated ion channels (VGIC) mediating permeability of other ion species apart from K<sup>+</sup> shifted the RMP to a more depolarized potential [221]. Therefore, the RMP in GH<sub>4</sub>C<sub>1</sub> and CHO-K1 cells may have derived from a mixed composition of permeability of ion species that determined the RMP and resulted in a RMP that was between the Nernst potentials of the ion species involved [48]. Thus, the RMP was either closer or more far away from the Nernst potential of K<sup>+</sup> depending on the degree of permeability of further ions involved at the RMP [48]. Although dominated by K<sup>+</sup> permeability, the RMP is known to be typically also mediated at least partly by Na<sup>+</sup> permeability, so that a contribution of Na<sup>+</sup> permeability was likely and shifted the RMP minorly towards a more depolarized value due to the more depolarized reversal potential of Na<sup>+</sup> which was found at + 66 mV (see section 2.4.1) [48]. Accordingly, the slightly more depolarized RMP of CHO-K1 cells compared to the RMP of GH<sub>4</sub>C<sub>1</sub> may indicate a higher contribution of Na<sup>+</sup> permeability in the cell membranes of CHO-K1 cells at RMP than in GH<sub>4</sub>C<sub>1</sub> cells. In the following, endogenously expressed ion channels reported to be typically present in these cell lines were elucidated to unravel potential cell membrane components that may be responsible for the more depolarized RMP compared to the Nernst potential of K<sup>+</sup>.

In this regard, a study by Törnquist and Ekokoski [340] reported that the increase of intracellular Na<sup>+</sup> concentrations increased in GH<sub>4</sub>C<sub>1</sub> cells with depolarization indicating voltage-activated Na<sup>+</sup> channels.

Moreover,  $\text{Na}^+$  influx was significantly higher when a  $\text{Ca}^{2+}$ -free buffer was used compared to  $\text{Ca}^{2+}$  containing buffer postulating that  $\text{Ca}^{2+}$  acted as an inhibitor of  $\text{Na}^+$  channels [340]. They further surmised that  $\text{Na}^+$  may enter the cells through  $\text{Ca}^{2+}$  channels in the absence of  $\text{Ca}^{2+}$  in the external solution [340]. Transferring this to the composition of the recording solutions of the present study considers that due to the external solution containing a low  $\text{Ca}^{2+}$  concentration of 2 mM,  $\text{Na}^+$  channels were not substantially affected by blockage with  $\text{Ca}^{2+}$  leading to  $\text{Na}^+$  influx via  $\text{Na}^+$  and presumably  $\text{Ca}^{2+}$  channels in a voltage-dependent manner. Thus the RMP was shifted to a more depolarized value compared to a RMP that would be only dominated by  $\text{K}^+$  permeability [48].

With respect to CHO-K1 cells, RMP was depolarized to an even greater extent than the RMP of GH<sub>4</sub>C<sub>1</sub> cells (Figure 11 A-B). In general, expression of endogenous ion channels is reported to be very low in CHO-K1 cells [106, 151]. Consequently, voltage-operated  $\text{K}^+$  channels may only be present to a reduced level resulting in a reduced permeability of  $\text{K}^+$  at the RMP. Assuming that  $\text{K}^+$  permeability was more impaired than  $\text{Na}^+$  permeability at the RMP due to lower expression of voltage-operated ion channels, the proportional contribution of ion permeability by  $\text{K}^+$  to the RMP would be still dominant although to a reduced degree and thus a contribution by  $\text{Na}^+$  would be more pronounced inducing a greater shift of the RMP to a more depolarized value towards the Nernst potential of  $\text{Na}^+$  (see section 2.4.1). When comparing the RMP of GH<sub>4</sub>C<sub>1</sub> and CHO-K1 cells recorded by current-clamp measurements in this study with those reported by other studies, the obtained RMP agreed well with the range of the reported values of RMP in GH<sub>4</sub>C<sub>1</sub> cells (- 60 mV to - 40 mV) [28, 248, 324]. Accordingly, comparison of the RMP of CHO-K1 cells to reported values of RMP yielded good accordance with previous description of this cell line where measured potentials ranged from - 30 mV to - 50 mV [339].

For all following experiments in the voltage-clamp mode, the holding potential of GH<sub>4</sub>C<sub>1</sub> and CHO-K1 cells in voltage-clamp measurements was set to - 70 mV corresponding to the nearest whole number of the  $\text{K}^+$  Nernst potential (see section 2.4.1). In this way, the physiological environment of h $\alpha$ 7-nAChR was resembled by this holding potential as in human neuronal cells where h $\alpha$ 7-nAChR is endogenously expressed, typical values of the RMP range from - 70 mV to - 80 mV [48, 117, 228, 273, 388].

## **4.2 Assessment of voltage-gated and ligand-gated ion channels of GH<sub>4</sub>C<sub>1</sub> and CHO-K1 cells**

Prior to the electrophysiological screening of PTM compounds on the effect of h $\alpha$ 7-nAChR activity and desensitization using a cell line stably transfected with h $\alpha$ 7-nAChR, the suitability of the two mammalian cell lines, GH<sub>4</sub>C<sub>1</sub> and CHO-K1, for use as host cell system for the stable transfection of the channel under study, h $\alpha$ 7-nAChR, was verified (see section 3.2; 3.3).

The rat pituitary cell line GH<sub>4</sub>C<sub>1</sub> cell line found in the anterior pituitary of the rat (*Rattus norvegicus*) is commonly used for the study of the physiology of pituitary function with regard to hormone production because these cells originate from somatotrophic cells which produce and secrete growth hormones (GH) [240]. Some of the clonal strains of somatotropes also secrete prolactin by the regulated secretory pathway [20, 103], wherein GH<sub>4</sub>C<sub>1</sub> cells produce GH at a lower level but higher levels of prolactin than their primary clones from which the GH<sub>4</sub>C<sub>1</sub> cell line was derived [326–328].

The CHO cell line was developed in 1957 by Theodore T. Puck, who isolated them from the Chinese hamster ovary (CHO) (*Cricetulus griseus*) [106, 258]. Besides the original CHO cell line which is characterized by their deficiency of proline synthesis and lack of epidermal growth factor receptor (EGFR), several subclones most prominent CHO-K1 cell line derived from the parental strains [184, 393]. Today, this line of epithelial-like cells and subclones are commonly used as an expression system for the production of recombinant proteins frequently applied in biomedical research [108, 151].

Elucidation of basic characteristics of voltage-dependent and voltage-independent conductance of GH<sub>4</sub>C<sub>1</sub> and CHO-K1 cells served to identify expression of endogenous membrane sources that could interfere with current signal of  $\alpha 7$ -nAChR activation during patch clamp recordings, including activation of VGIC and LGIC such as nAChR subtypes other than  $\alpha 7$ -nAChR. To this end, activation of such ion channels in particular at or close to a holding potential of -70 mV would cause an overlap with the current signal of  $\alpha 7$ -nAChR activation during patch clamp recordings making the setting of the experimental parameters and interpretation of the results difficult [221]. Therefore, the cell line with the fewest voltage-dependent and voltage-independent conductance was favored for investigation of the effect of test compounds on  $\alpha 7$ -nAChR function.

Currents deriving from activation of VGIC were evoked by changes in holding potential [232]. The commonest pulse protocol used to record currents of VGIC is to apply a continuous change in voltage, a so called voltage ramp, or a series of voltage-steps of a set duration but varying amplitude, which is denoted as a voltage-step protocol [3]. In this study, both pulse protocols were initiated by application of a holding potential at -70 mV. Then, voltage was set to a more positive potential either by continuous (voltage ramp) or stepwise (voltage-step) increase resulting in depolarization of the cell and in ionic movement at a given voltage due to activation of VGIC (see section 2.4.8). During opening of VGIC, the net ion flow was measured and resembled the overall conductance of the cell at different potentials. After application of voltage ramp or voltage-steps, potential was set to the holding potential of -70 mV [232].

With respect to the voltage-ramp, this protocol is well suitable for determining activation of transient VGIC, overall conductance of a cell and the reversal potential [221]. Thereby, variation of the time period of continuously increasing voltage (200 ms and 2 s voltage-ramp) served to verify currents of VGIC characterized by fast (200 ms voltage-ramp) and slow (2 s voltage-ramp) activating components,



respectively [221]. Thereby, application of the 200 ms and 2 s voltage-ramps to the cell lines GH<sub>4</sub>C<sub>1</sub> and CHO-K1 revealed a common feature by a continuously increasing curve of the current-voltage relation with increasing voltage (Figure 12 A-F).

Thereby, negative current responses were found at negative voltage in both cell lines (Figure 12 C-F; Table 13). Considering the ionic composition of the internal and external solution determining the Nernst potential and the principle of the ionic theory, conductance by inwardly rectifying currents at negative voltage was presumably due to K<sup>+</sup> influx through VGIC [48, 388]. In this context, the electrochemical gradient of K<sup>+</sup> under physiological conditions as well as under experimental conditions displayed an equilibrium at – 71 mV and thus, a potential below the Nernst potential of K<sup>+</sup> indicated that it was most likely K<sup>+</sup> that diffused to the inside of the cell displayed by a negative current flow (see section 2.4.1) [48, 228, 232, 388]. Vice versa, outwardly rectifying currents detected by depolarization of both cell lines were driven by the electrochemical gradient of K<sup>+</sup> evoking a K<sup>+</sup> outflux via VGIC (Figure 12 A-F; see section 2.4.1) [48, 228, 232, 388].

With respect to CHO-K1 cells, conductance investigated by 200 ms and 2 s voltage ramps was low over the entire voltage range applied because only little currents postulated to be mediated by K<sup>+</sup> influx at negative and efflux at positive voltage were found (Figure 12 C-D; Table 13). In contrast, conductance of GH<sub>4</sub>C<sub>1</sub> cells was markedly higher because current amplitude, concerning both negatively and positively deflecting currents, was found to be profoundly larger compared to current amplitude of CHO-K1 cells (Figure 12 E-F; Table 13). Comparing the 200 ms and the 2 s voltage ramps of GH<sub>4</sub>C<sub>1</sub> cells, a 2-fold higher current amplitude was detected by 200 ms voltage ramps than in 2 s voltage ramps indicating that fast VGIC were activated to a higher level by the fast proceeding 200 ms voltage ramp than slow VGIC by the 2 s voltage ramp (Table 13) [221]. Those fast activating VGIC may include cationic influx through K<sup>+</sup> channels but also Ca<sup>2+</sup> and Na<sup>+</sup> channels which were reported to be expressed in GH<sub>4</sub>C<sub>1</sub> cells [28, 221, 324]. K<sup>+</sup> and Na<sup>+</sup> VGIC are typically open at negative voltage and may thus be responsible for the more negative current amplitude by cation influx whereas Ca<sup>2+</sup> VGIC have a moderately higher activating potential at around 0 mV [3, 48, 221, 228, 389]. As a measure of the conductance of the cell membrane over the entire voltage-range applied in the voltage ramp protocols, slope coefficients ( $n_H$ ) were determined from linear regression analysis of the current-voltage relation (Figure 12 C-F). Hence, a high  $n_H$  revealed a steep slope of the linear regression and indicated a high conductance of the cell whereas a small  $n_H$  was due to a shallow slope and a low conductance of the cell [232]. The  $n_H$  of linear current-voltage relations of both voltage ramps revealed a shallow rise and thus low conductance in CHO-K1 cells while significantly steeper slopes of linear current-voltage relations in GH<sub>4</sub>C<sub>1</sub> cells yielded a higher conductance (Table 13). From the linear current-voltage relations of voltage ramps, reversal potential was determined at  $I = 0$  A and thus denotes the equilibrium potential where no net ion flux was conducted by all permeant ions [3, 48, 221, 228, 388].

Thereby, the reversal potential gives insight into the ion species or composition of ion species permeability that determine the conductance of the cell membrane because those currents would reverse at the reversal potential [3, 48, 232]. Reversal potentials of CHO-K1 cells in 200 ms and 2 s ramps were found at very similar values at around - 23 mV whereas reversal potential of GH<sub>4</sub>C<sub>1</sub> cells during application of the 200 ms voltage ramp protocol was found to be more negative at  $-31.01 \pm 3.52$  mV compared to the reversal potential determined in the 2 s voltage ramp protocol at  $-13.27 \pm 0.81$  mV (Table 13). This difference of reversal potential in GH<sub>4</sub>C<sub>1</sub> cells depending on the time period of voltage ramp (200 ms or 2 s) may be due to an alternate pattern of permanent activation and inactivation of VGIC upon voltage changes shifting the reversal potential to an alternate value [221]. However, further elucidation for example by specifically blocking distinct ion specific VGIC would be needed to unravel these different interactions but go beyond the scope of this study [221, 232]. Nevertheless, due to the fact that the reversal potential of linear current-voltage relations of CHO-K1 and GH<sub>4</sub>C<sub>1</sub> cells was between the Nernst potential of K<sup>+</sup> ( $E_{K^+} = -71$  mV) and Na<sup>+</sup> ( $E_{Na^+} = +66$  mV) indicated that permeability of these ion species determined the equilibrium potential and mediated the conductance of both cell types (see section 2.4.1) [48].

Notably, the definition of the reversal potential denoted as the potential where the net current flow is zero may imply that the RMP defined by current-clamp recordings at the net current flow of zero ( $I = 0$  A) may be found at a comparable value to the reversal potential [3, 221].

However, reversal potentials were moderately less negative than the obtained RMP in both cell lines (Table 13). This deviation of reversal potential to RMP could be related to the influence of the transient voltage-activated conductance and to a temporally delayed onset of current response upon voltage increase in voltage ramp pulse protocols [221]. As a result of this timely delay, reversal potential in voltage ramps at which no net current was induced was shifted to the right and thus to a more depolarized potential whereas for the determination of RMP a constant long lasting potential at  $I = 0$  A was applied so that side effects by these transient VGIC were avoided [221].

With respect to voltage ramps, the linear current-voltage relation of CHO-K1 cells converged with the linear regression analysis over the entire voltage range applied in both voltage ramp protocols showing that no other VGIC apart from those permeant to K<sup>+</sup> were activated. In contrast, deviation of the course of the current-voltage relation from the linear regression analysis was noticeable in GH<sub>4</sub>C<sub>1</sub> cells with the course of the current-voltage-relation below the linear regression at a voltage range between - 70 mV to + 19 mV in the 200 ms voltage-ramp and between - 45 mV and + 40 mV in the 2 s voltage-ramp protocol (Figure 12 C-F).

Regarding that Na<sup>+</sup> and Ca<sup>2+</sup> VGIC were active within this voltage range, it could be that deviation from linear regression derived from a mixed activation of these VGIC leading to a cation influx that caused the more pronounced downward deflection of the current-voltage course compared to the linear-

regression [48, 232]. The degree of deviation of the current-voltage relation from the linear regression analysis in GH<sub>4</sub>C<sub>1</sub> cells was quantified by calculation of  $\Delta AUC$  ( $AUC_{\text{current voltage relation}} - AUC_{\text{linear regression}}$ ) to gain more insight into the relative impact of such channels on cell conductance. The determined  $\Delta AUC$  was higher in 200 ms voltage ramps of GH<sub>4</sub>C<sub>1</sub> cells than in 2 s voltage ramps by a factor of 10, indicating that fast activating VGIC detected by 200 ms voltage-ramp protocols had a higher impact on cell conductance. This is in line with the higher conductance of GH<sub>4</sub>C<sub>1</sub> cells observed in this study and further with previous reports claiming that mainly fast rather than slow activating voltage-gated channels in GH<sub>4</sub>C<sub>1</sub> cells were expressed (Figure 12 E-F; Table 13) [28, 324].

Due to the permanent changing activation and inactivation of different VGIC in continuously increasing voltages in ramp protocols, the identification of ion species or the composition of ion species that were permeant through VGIC of the cell membrane could only be roughly estimated and thus voltage ramps do not provide sufficient accuracy about the determination of these ion species [221]. Therefore, a voltage-step protocol using a constant voltage charge for a constant time interval was applied to avoid permanent changing activation and inactivation of different VGIC and enabling a more reliable and accurate identification of the ion species permeant through activated VGIC (see section 3.2) [221].

In compliance with the results of voltage-ramps, only small current responses were obtained in CHO-K1 cells at increasing voltage-steps confirming that VGIC were only expressed at a low level (Figure 13 B-C) [106]. Considering the electrochemical gradient of a cell membrane and physiological basic characteristics of ion permeability of a cell determined by the Nernst potential discussed in section 2.4.1, the generated current was due to a K<sup>+</sup> influx at negative and K<sup>+</sup> efflux at positive voltage [48]. Current-voltage relations of CHO-K1 cells obtained by voltage-step protocols showed that, although very low, current responses expressed as AUC of the current traces elevated consistently with rising voltage steps. This reflected results of voltage ramps showing that VGIC other than those permeant to K<sup>+</sup> were not activated (Figure 12 A-F; Figure 13 B-C) [106]. Although it is generally accepted by most studies that CHO-K1 cells lack most VGIC, it should be pointed out that considerable Ca<sup>2+</sup> conductance has been reported which may complicate experiments involving Ca<sup>2+</sup> [106, 304]. However, in this study only low Ca<sup>2+</sup> concentrations of 2 mM were contained in the external solution and Ca<sup>2+</sup> conductance was not observed by investigation of VGIC in CHO-K1 cells in this study so that side effects of Ca<sup>2+</sup> disrupting screening of the effect of test compounds on  $\alpha 7$ -nAChR function could be excluded (Figure 12 C-D; Figure 13 B-C). With respect to current traces of voltage-step measurement of GH<sub>4</sub>C<sub>1</sub> cells displayed in Figure 13 D-E, a significantly more pronounced K<sup>+</sup> efflux represented by upwards directed current traces increasing with depolarization was observed compared to K<sup>+</sup> efflux in CHO-K1 cells. This observation was consistent with voltage ramp protocols where total currents of GH<sub>4</sub>C<sub>1</sub> cells reflecting the conductance of the cell was markedly enhanced (Figure 12 E-F; Table 13). Current-voltage relations of GH<sub>4</sub>C<sub>1</sub> cells showed that positive current responses quantified by determination of

the AUC increased with depolarization induced by increasing voltage-steps (Figure 13 E). In addition to  $K^+$  efflux, slightly negatively rectifying currents were recorded in GH<sub>4</sub>C<sub>1</sub> cells and appeared just prior to  $K^+$  response (Figure 13 E). Current-voltage relations in Figure 13 F yielded that the size of the AUC of the downward current response proceeded in a bell shaped manner with a maximum current signal at  $-20$  mV and decreasing current signal with hyperpolarization up to  $-60$  mV and with depolarization up to  $+30$  mV. Interestingly, downwardly deflecting currents were detected within a voltage range that mainly corresponded to the voltage range of voltage ramp measurements in GH<sub>4</sub>C<sub>1</sub> cells where current-voltage relation deviated downwards from linear progression (compare Figure 12 E-F; Figure 13 E). This indicated that within this voltage range, activated VGIC were probably of the same nature in voltage ramp as in voltage-step protocols which seemed to be  $Na^+$  and  $Ca^{2+}$  VGIC [48, 232]. Consulting VGIC that are typically active at this voltage range of the voltage-step protocol, the negative current responses could be rather explained by a  $Na^+$  than a  $Ca^{2+}$  influx into the cell because  $Na^+$  channels are typically activated between  $-20$  and  $+20$  mV which is in line with the voltage range found in this study (Figure 13 D-E) [48, 232]. Moreover, the course of the negative current traces of the voltage-step protocol showed a peak-shaped current trace as displayed in Figure 13 D and reflected rapidly opening and closing of VGIC which was characteristic for VGIC permeant to  $Na^+$  and not to  $Ca^{2+}$  mediated responses by VGIC which typically open and close more slowly [3, 48, 52, 136, 156, 221, 308]. Furthermore, with regard to the potential at which the current direction of the negative current reversed found at  $+38.5$  mV, it was close to the Nernst potential of  $Na^+$  ( $E_{Na^+} = +66$  mV) and consolidated that these currents were mediated by  $Na^+$  permeability (Figure 13 D and G) [48]. Subsequent application of the voltage-step protocol in GH<sub>4</sub>C<sub>1</sub> cells in the presence of the specific  $Na^+$  channel blocker amiloride caused distinction of the negative currents confirming that these currents derived from activation of  $Na^+$  VGIC (Figure 13 F-G) [368]. In line with these results, GH<sub>4</sub>C<sub>1</sub> cells used in previous patch clamp studies were shown to be responsive to  $Na^+$ ,  $K^+$  and  $Ca^{2+}$  channels [28, 74, 111, 187, 222, 240, 324, 390–392].

In summary, investigation of voltage-gated conductance in CHO-K1 and GH<sub>4</sub>C<sub>1</sub> cells by voltage ramp recordings showed that activation of VGIC including both fast and slow components permeant to  $Na^+$  was only present in GH<sub>4</sub>C<sub>1</sub> cells and commonly present  $K^+$  permeability was more pronounced in GH<sub>4</sub>C<sub>1</sub> cells compared to CHO-K1 cells which showed only minor activation of VGIC permeant to  $K^+$  (Figure 12 A-F). Moreover, given the assumption that current responses by activation of voltage-gated  $Na^+$  ion channels in GH<sub>4</sub>C<sub>1</sub> cells were induced at a potential close to the holding potential set to  $-70$  mV verified by voltage-step recordings, it may reveal that  $Na^+$  VGIC activity covered current signal of  $\alpha 7$ -nAChR activation in investigation of the effect of test compounds on  $\alpha 7$ -nAChR function recorded at a holding potential of  $-70$  mV (Figure 13 D-E) [48, 221, 232]. The low conductance and the absence of VGIC at or close to the holding potential of  $-70$  mV in CHO-K1 cells revealed that the low background

noise of this cell line was favored for electrophysiological investigations of  $\alpha 7$ -nAChR function as current signal would not interfere by such endogenously expressed VGIC that may be active simultaneously to  $\alpha 7$ -nAChR at the holding potential of  $-70$  mV [106, 151].

Not only voltage-gated conductance that may disrupt investigations of  $\alpha 7$ -nAChR activity was essential to evaluate but also ligand-gated conductance, in particular of endogenously expressed ion channels of the same source as the channel under study. In this context, voltage-independent activation of LGIC was studied by using continuous voltage-clamp recordings at a holding potential at  $-70$  mV instead of variation in voltage charges (see section 2.4.9). Cells were exposed to various classical nAChR agonists including acetylcholine (ACh), nicotine and carbamoylcholine to activate nAChR of various subtypes. As depicted in Figure 14 A-C, no significant currents of LGIC, most likely nAChR, induced by these agonists were found in CHO-K1 and in GH<sub>4</sub>C<sub>1</sub> cells. In conclusion, these agonists did not detectably activate endogenously expressed nAChR or other channels sensitive to these agonists of these cells and thus would not interfere with the following measurement of nicotinic receptor function. Besides assessment of nAChR of various subtypes which were activated by these agonists, it was further analyzed if specifically  $\alpha 7$ -nAChR were naturally present and activated on the cell membrane by applying a well-prescribed  $\alpha 7$  specific positive allosteric modulator PNU-120596 with nicotine. As observed with ligands alone, no detectable activation of LGIC was found with modulation by PNU-120596 (Figure 14 D).

Although not detected in this study, it was proposed that GH<sub>4</sub>C<sub>1</sub> cells express native  $\alpha 7$ -nAChR [373]. Moreover, the chaperone RIC-3 (resistance to inhibitors of cholinesterase 3) which was shown to be expressed in pituitary cells is known to be essential for functional  $\alpha 7$ -nAChR expression on the cell membrane and thus it was conceivable that GH<sub>4</sub>C<sub>1</sub> cells endogenously express  $\alpha 7$ -nAChR [373]. Nevertheless, a study by Williams and colleagues [373] showed that  $\alpha 7$ -nAChR expression levels were too low and failed to verify detectable currents induced by  $\alpha 7$ -nAChR activation in patch clamp experiments which could explain that no currents were detectable in this study by whole-cell patch clamping.

As discussed above, the very low general expression level of endogenous ion channels in CHO-K1 cells resulted in low background conductance of VGIC and LGIC making CHO-K1 cells a widely used cell model in patch clamp electrophysiology [41, 106, 159, 271, 284]. Considering LGIC in CHO-K1 cells, it was reported that these cells endogenously express TRP channels and swelling activated Cl-channels [185, 352], but an impact of these channels in patch clamp recordings investigating  $\alpha 7$ -nAChR function was considered to be negligible as they were not sensitive to nAChR ligands (Figure 14 A-D). To conclude, as LGIC were not activated in both cell lines, it was conceivable that current signal of electrophysiological investigation of  $\alpha 7$ -nAChR using either GH<sub>4</sub>C<sub>1</sub> or CHO-K1 cells as host cell system

for stable transfection of h $\alpha$ 7-nAChR would not be accompanied by endogenously expressed nAChR or other LGIC (Figure 14 A-D).

Nevertheless, with regard of conductance including voltage-dependent and voltage-independent ones, GH<sub>4</sub>C<sub>1</sub> cells showed disadvantageous electrophysiological properties when considered as a host system for stable transfection of h $\alpha$ 7-nAChR and investigation of h $\alpha$ 7-nAChR function because, as analyzed in section 3.2, voltage-gated Na<sup>+</sup> channels detected in GH<sub>4</sub>C<sub>1</sub> cells were activated at voltage close to the holding potential at -70 mV. To this end, CHO-K1 cells did not display such Na<sup>+</sup> inward currents or other VGIC in the negative voltage range and displayed a generally low background noise considering voltage-dependent as well as voltage-independent conductance. Thus, CHO-K1 cells were detected to be well suited for the following experiments in this study and were therefore chosen as a host system for stable transfection of the receptor (Figure 12 C-D; Figure 13 B-C) [106].

### **4.3 Establishment of a screening method for the investigation of human $\alpha$ 7-nAChR function**

As obtained from the section 4.2 assessing the voltage-dependent and voltage-independent conductance of GH<sub>4</sub>C<sub>1</sub> and CHO-K1 cells, CHO-K1 cells denoted as CHO-K1/RIC-3/h $\alpha$ 7-nAChR cells were selected as a host system for stable transfection of h $\alpha$ 7-nAChR cotransfected with the chaperone RIC-3 to promote transportation of receptor to the cell membrane [373]. Prior to examine h $\alpha$ 7-nAChR function in CHO-K1/RIC-3/h $\alpha$ 7-nAChR cells, seal success rate was optimized by a stepwise modification of cellular parameters and settings. Thereby, pressure applied to capture and to hold the cells in the gigaseal configuration was adjusted, a Ca<sup>2+</sup> rich solution was added after the whole-cell configuration was established and served as a seal enhancer, and finally the cell passages used for patch clamp recordings were delimited to a passage range where no significant reduction in seal rate occurred (Figure 15 A-D; Table 11).

Moreover, considering the fast conformational change of h $\alpha$ 7-nAChR, the flow rate of test compound application was adjusted to increase signal intensity. In addition, the amount of time and number of washing steps between each test compound application were adjusted to ensure full recovery of receptors from desensitization prior the next test compound application (see section 3.4).

#### **4.3.1 Seal success rate - cellular parameters and settings of making a seal**

A detailed description of the procedure of making a gigaseal on a cell membrane and establishing the whole-cell configuration using an automated planar patch clamp platform was given in section 2.4.3. In brief, the basic elements of the planar patch clamp set-up are composed of eight recording

chambers encased in a planar borosilicate glass chip. Each of the recording chambers consists of an upper and lower compartment separated by a planar surface containing a micro-sized aperture where the cell was captured [46]. In this context, when a cell of a cell suspension in the upper compartment approached the aperture, some delicate suction was applied to carefully capture a membrane patch of the cell at the aperture so that a direct contact between surface of the cell membrane and the rim of the aperture was established [99].

To generate a gigaseal with low leakage current, an appropriate suction strength was required which was strong enough to efficiently capture the cell with high stability, but not too strong to avoid mechanical damage of the membrane [221]. The minimal suction strength that can be applied to a cell is dependent of the cell type, opening diameter of the aperture and the composition of the internal and external solution [232]. In this regard, the suction strength to capture a cell was adjusted by reducing the standard parameter of - 200 mbar to - 150 mbar enhancing the cell capture rate by 8 % (Figure 15 A). When the pressure of suction strength was higher than -150 mbar to capture a cell, cell capture rate decreased which was probably caused by aforementioned damage of the cell membrane [221]. Moreover, cells that were damaged due to too high suction strength often showed reduced sealing resistance or atypical electric behavior [232]. On the other hand, suction pressure below 150 mbar had a negative impact on cell capture rate which could be most likely due to the insufficient contact between outer cell membrane and rim of the aperture causing the membrane, if captured, to flutter increasing the risk of the cell to be torn off from the aperture [221].

After capturing the cell, the next modification step was to drop the suction strength to mechanically preserve the cell membrane from rupture [232]. Therefore, the suction strength for holding the cell at the aperture, the so called cell holding pressure, was lowered from – 70 mbar to – 50 mbar revealing an enhanced cell hold rate of another 4 % (Figure 15 B). As in case of the cell capture rate optimized by adjustment of the suction strength of the cell capture pressure, the increased cell holding success rate after adjustment of the cell holding pressure was presumably due to a high enough stability of the cell at the aperture without causing damage to the membrane [3, 221, 232].

Subsequently to the establishment of the whole-cell configuration described in section 2.4.2 and 2.4.3, a seal enhancer was applied to the upper compartment and was then replaced by external solution just before starting the recording. By this additional step, the enhancement of the gigaseal formation rate and seal stability rate over a 5 point measurement was markedly supported and the mode of action by the seal enhancer was presumably based on the neutralization of the negative charge of the borosilicate glass mediated by the high  $\text{Ca}^{2+}$  concentration of the seal enhancer (Figure 15 D) [46, 99]. Final optimization of the seal success rate including gigaseal formation and seal stability over a 5 point measurement was carried out by elaborating the seal rate of cells at different passages revealing that seals were robust from passage 13 to 25 whereas seal rate decreased at higher cell passages (Figure

15 C; Table 14). This cell passage dependency on seal success rate is not completely understood yet, but may be associated with the composition of the phospholipids of the plasma membrane which is dynamic in terms of that other membrane constituents are embedded over time in the cell membrane leading to stabilization or destabilization of the membrane [52, 221]. However, further elucidation of cell membrane components of difference cell passages is needed to gain more insight into the relation between cell membrane composition with respect to its stability and seal success rate.

In total, seal success rate after adjustment of cell capture and hold pressure as well as addition of seal enhancer and limiting the use of cell passage resulted in a total increase of gigaseal formation by a factor of 4.6, increase of stable seals over a five point measurement by a factor of 1.3 and a reduction of run down over a five point measurement by a factor of 0.7 (Figure 15 A-D; Table 14). No more than 5 points per measurement were routinely recorded in experiments of this study in order to not have any compromise in seal stability over time.

Regarding the cell physiology of CHO-K1 cells, this epithelial-like cell line was well suited for planar patch clamping according to the manufacturer's protocol [1, 46]. The reported seal success rate provided by Nanion (60 – 80 %) showed a good concordance with the seal success rate obtained in this study (65 %; Table 14) after adjustment of cell parameters which were modified from standard cellular parameters used by the company (Table 11). Similarly, the automated patch clamp system provided by Sophion Bioscience (QPatc, Ballerup, Denmark) yielded a comparable seal success rate [203].

#### **4.3.2 Current signal rate - Perfusion and application procedures**

Patch clamp investigation of  $\alpha 7$ -nAChR function in the whole-cell configuration required a defined flow rate of test compound application to CHO/RIC-3/ $\alpha 7$ -nAChR cells in order to achieve a high open channel probability of the fast activating and inactivating  $\alpha 7$ -nAChR of the entire cell [148, 377]. Considering the mode of test compound application in the planar patch clamp system of the present study, the solution that flows past the cell was not exposed to the entire cell surface but rather passed the cell undulatory (Figure 28; see section 2.4.3) [46, 99]. Therefore, it was assumed that by a rather slow exposure of agonist to the CHO/RIC-3/ $\alpha 7$ -nAChR cells, some of the receptors have already transitioned from the agonist-induced open into the non-conductible desensitized state before the entire receptor population was exposed to agonist [46, 99, 148, 377]. Therefore, agonist-induced current signal would be decreased as only a small proportion of the  $\alpha 7$ -nAChR population of a cell would be activated simultaneously [46, 99, 148, 377].



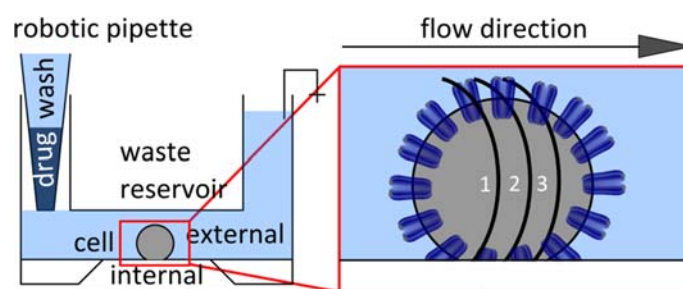


**Figure 28: Schematic representation of the sequential undulatory passing test solution at a CHO/RIC-3/α7-nAChR cell (right) in the recording chamber of a planar patch clamp set-up (left).**

In order to identify the flow rate evoking a high probability of open channel configuration of α7-nAChR which was directly proportional to current size, different flow rates from 16 μl/l to 314 μl/s using a total volume of 40 μl of 100 μM of the agonist nicotine was exposed to CHO-K1/RIC-3/α7-nAChR cells for nAChR activation (see section 2.4.7). A flow rate of 171 μl/s exposing the cell to test solution for 233 ms was found to induce most profound current amplitudes of  $5.81 \pm 2.79 \cdot 10^{-10}$  A by α7-nAChR activation of CHO/RIC-3/α7-nAChR cells (Figure 16 A-B; Table 15). With respect to the course of the current traces, a very rapid onset of nicotine-induced current signal at 171 μl/s and fast decline of such indicated the rapid kinetics of the conformational transition states of activation and inactivation proceeding only within a few milliseconds [148, 377]. Hence, it was reasonable that a rather fast flow rate was needed to have a high probability of simultaneously open α7-nAChR to detect a current signal due to the fast kinetics of conformational changes of α7-nAChR [148, 377].

In contrast to the fast transition from the closed to the open state and vice versa, transition from non-conductible desensitization due to prior overstimulation by an excess of agonist, to the closed conductible state did not occur until desensitizing agonist concentrations were withdrawn from the receptor (Figure 3 D) [148, 221, 377]. Given these desensitization kinetics, critical parameters in patch clamp investigations of α7-nAChR function were to consider enough time and adequate number of wash out steps of agonists for recovery of receptors from desensitization (Figure 17 A-B). Full regeneration of receptors was particularly essential in patch clamp measurements acquiring several recordings from a single cell to avoid run down of the current signal by α7-nAChR desensitization [221]. Therefore, variation of time from 1 to 3 min in combination with different number of washing steps required to fully “resensitize” the receptors, i.e. reverting the receptors from desensitization into the closed conductible state, was investigated (see section 3.4). Hereby, investigation of the slow onset of desensitization induced by an excess agonist concentration rather than fast onset of desensitization occurring immediately after activation upon agonist application was of most interest [377]. Hence, after activation of α7-nAChR with 100 μM nicotine, slow onset desensitization was evoked by an excess of nicotine at 1 mM (Figure 17 A-B). By subsequent application of 100 μM nicotine after 1 to 2

min of induced desensitization without any washing step in between, a current signal was not detectable verifying that time interval was too short to recover receptors from desensitization (Table 16). Furthermore, these results confirmed that 1 mM nicotine was a sufficiently high concentration to achieve a high probability of desensitization as the current signal was fully depleted (Figure 17 A-B; Table 16) [16–18]. Contrarily, if receptors were in a closed, conductible state, nicotine should produce a current signal after inducing desensitization that is comparable in amplitude with the initially applied signal induced with 100  $\mu$ M nicotine while this current signal should decrease with increasing probability of receptors to conduct the desensitized state [16–18, 148, 377]. In the following, washing steps were included in the experimental set-up after desensitization was induced. Thereby, residual nicotine was washed out that may otherwise bind to receptors and lead to a longer persistence of slow onset desensitization as observed by the absence of current signal when 100  $\mu$ M nicotine was applied for activation after desensitization without applying any wash out steps (Figure 17 A-B). By applying one or two washing steps prior to application of 100  $\mu$ M nicotine to activate receptors after 1, 2 or 3 min after desensitization, a time interval of at least 3 minutes and two washing steps comprising external solution were required to completely reverse receptors from a non-conductible desensitized state into the activated conductible state (Figure 17 A-B; Table 16). Notably, it was essential to keep time interval and washing steps to a minimum at the same time to avoid compromise in viability of the cells due to extensively long measurement and to avoid mechanical stress by an excessive large number of washing steps [3, 221, 232]. Consequently, an imbalance of both parameters would cause run down of current signal over time in the 5 point measurement set up used in this study [3, 221, 232].

#### **4.4 Conformational transitions and positive allosteric modulation of human $\alpha$ 7-nAChR**

Dose-response relations of h $\alpha$ 7-nAChR activation, desensitization and modulation were investigated in CHO/RIC-3/h $\alpha$ 7-nAChR cells in order to verify activation and modulation profiles as well as desensitization kinetics that were characteristic for the  $\alpha$ 7-subtype [148]. First of all, dose-response profiles of classical nAChR agonists including the endogenous neurotransmitter ACh, nicotine, carbamoylcholine and epibatidine were determined to validate differences of agonist induced h $\alpha$ 7-nAChR current responses (Figure 19 A-D and I-J). A common feature of all agonist-induced current responses was the course of the individual current records which proceeded in rapidly activating and fast decaying inward currents as illustrated by brief short time constants of decay depicted in Figure 19 A-D and Table 17.

In compliance with the physiological properties of  $\alpha 7$ -nAChR, it could be assumed that rise of currents was related to nAChR activity by an enhanced open channel probability of nAChR while decline of currents was related to an increasing probability of a non-conductible desensitized state of the receptor population of a cell [148, 152, 395]. The fast gating transition from the agonist-bound open to a deactivating state was consistent with other studies proclaiming a low affinity of agonists towards nAChR to activate them and allowing for very fast dissociation from the binding site resulting in the deactivated state within a few milliseconds [148, 152, 395]. The rapid decay of nAChR activation leading to deactivation of receptors was rather due to transition into a non-conductible state denoted as fast onset desensitization than a conductible deactivated state which was in concordance by other studies [9, 115, 206]. Apart from similarities in short-lived activation, the course of dose-response curves elicited by agonists showed a biphasic relation with increasing current amplitudes elicited at low concentrations (nicotine  $\leq 100 \mu\text{M}$ ; ACh  $\leq 100 \mu\text{M}$ ; carbamoylcholine  $\leq 300 \mu\text{M}$ ; epibatidine  $\leq 5 \mu\text{M}$ ) indicating that the probability of receptors to convert into the open configuration increased and a decline at higher concentrations (Figure 19 A-D, I-J) [148, 152, 155, 395]. While ascending dose-response curves of ACh, nicotine and carbamoylcholine showed comparable  $\text{EC}_{50}$  values as depicted in Table 17, the  $\text{EC}_{50}$  value of epibatidine was significantly reduced which is in line with studies in which epibatidine was described as an extremely potent agonist of neuronal nAChR compared to carbamoylcholine or nicotine presumably due to its higher binding affinity towards nAChR [109, 229, 395]. Due to differences in affinity, concentrations of agonists at which the maximum current amplitudes ( $I_{\text{max}}$ ) were reached varied and were markedly lower for epibatidine at  $5 \mu\text{M}$  compared to the other agonists tested (Figure 19 A-D, I-J; Table 17). Furthermore the current amplitude of  $I_{\text{max}}$  was significantly lower in case of epibatidine compared to the other agonists which showed comparable size in  $I_{\text{max}}$  (Figure 19 A-D; I-J; Table 17). These differences in  $I_{\text{max}}$  could be due to agonists binding to different sites within the orthosteric binding site, which was shown for epibatidine on the muscle type nAChR [37, 312]. At concentrations of the corresponding agonists that were higher than those evoking  $I_{\text{max}}$ , current amplitudes declined concentration-dependently (Figure 19 A-D, I-J; Table 17). As aforementioned, this implied that at high agonist concentrations the continuous decrease of signal underlies an increasing probability of the receptor to transition into a non-conducting, slow onset desensitized state [148]. Hereby, determination of  $\text{IC}_{50}$  revealed a high inhibitory potency by epibatidine compared to other agonists (Table 17). Thereby, aforementioned particular binding affinities of epibatidine leading to differences in kinetics of epibatidine-induced responses compared to other agonists could favor a premature desensitized conformational state and thus a stronger inhibitory potency compared to the other agonists [109].

The mechanism of desensitization has not yet been fully clarified, however, energy profiles of the receptor states showed that type II positive allosteric modulators (PAM), such as PNU-120596 which

is a  $\alpha 7$ -specific type II PAM, could increase the energy barrier between the active and desensitized state when binding to the activated receptor state while binding to the receptor in the desensitized state destabilizes this state [33, 62, 148]. By this assumption, positive type II PAMs would both delay entry into desensitization and resensitize receptors from desensitization and therefore might be useful in pathological situations associated with excessive ACh concentrations leading to receptor desensitization and cholinergic crisis [9, 149, 372]. The effect of PNU-120596 on  $\alpha 7$ -nAChR activation was investigated in order to gain more insight into its proposed mode of action. Thereby application of a constant agonist concentration ( $EC_{100}(\text{nicotine}) = 100 \mu\text{M}$ ,  $EC_{100}(\text{ACh}) = 100 \mu\text{M}$ ;  $EC_{100}(\text{carbamoylcholine}) = 300 \mu\text{M}$ ;  $EC_{100}(\text{epibatidine}) = 5 \mu\text{M}$ ) together with increasing concentrations of the  $\alpha 7$ -subtype selective positive allosteric modulator PNU-120596 led to an amplification of the maximum current amplitude ( $I_{\text{max}}$ ), prolongation of current response and a high potency of dose-response relations ( $EC_{50}$ ) (Figure 19 E-H, K-L; Table 17). The mode of action underlying this long persisting current signal could be explained by the mechanism of PNU-120965 which changes energy barriers of conformational states so that the receptor remained in the open channel conformation for an extended period of time [33, 62, 148]. Thus, prolonged activation of  $\alpha 7$ -nAChR indicated a prevention of agonist-induced desensitization due to an increased opening duration of the PNU-120596 modulated nAChR [9, 27, 33, 62, 148, 149]. In line with this, potentiation of the current amplitude observed in all PNU-120596 dose-response curves in the presence of agonist could be due to the fact that a prolonged open state of the receptors may lead to increased cationic influx of  $\text{Na}^+$  and  $\text{Ca}^{2+}$  resulting in a higher net current influx than without modulator [33, 62, 148, 149]. Considering classification of positive allosteric modulators in type I and type II depending on whether they reduced the level of agonist-induced desensitization (type II-PAM) or not (type I-PAM), type I modulators only potentiate activation of receptors displayed by an increase in current amplitude while type II modulators additionally elongate opening time of receptors displayed by prolonged current response [62, 148, 149]. Concluding, mechanistic profile of PNU-120596 potentiating current amplitude and duration of response confirmed that this modulator is a type II-PAM consistent with previous reports and findings of this study [62, 149].

Moreover, the allosteric mechanism by PNU-120596 rather than an agonistic action was verified in this study because application of PNU-120596 without any agonist failed to activate receptors excluding that PNU-120596 was able to activate receptors (data not shown) [148].

Interestingly, comparing the degree of the potentiated current responses induced by different agonists (Figure 19 E-H, K-L; Table 17), increase in current amplitude recorded with nicotine, ACh and carbamoylcholine in the presence of PNU-120596 was significantly more pronounced than with epibatidine whereas duration of current responses with nicotine and carbamoylcholine were significantly more pronounced than with epibatidine and ACh in the presence of PNU-120596 (Figure 19 E-H, K-L; Table 17). As indicated above, differences in binding within the orthosteric binding sites

and in binding affinities by various agonists as reported for epibatidine may favor or alleviate the conformational change by an allosteric mechanism of action by PNU-120596 which may explain alternate amplitude and duration of current response modulated by PNU-120596 [109, 153, 395]. Moreover, a markedly weaker half maximum efficacy ( $EC_{50}$ ) of current response by carbamoylcholine modulated by PNU-120596 in comparison to  $EC_{50}$  of modulated current responses by the other agonists was shown and may also account to these binding differences as an alternate binding mechanism of carbamoylcholine to the orthosteric binding site was reported [37, 153, 312].

At high PNU-120596 concentrations, current responses declined concentration-dependently (Figure 19 E-H, K-L). Thereby, comparable inhibitory potency ( $IC_{50}$ ) of agonist modulated current responses by high PNU-120596 concentrations were recorded with the exception of  $IC_{50}$  of carbamoylcholine current responses modulated by high concentrations of PNU-120596 which was profoundly weaker and could be associated with the alternate binding mechanism of carbamoylcholine to the orthosteric binding site (Table 17) [37, 312]. The mechanism of the additional inhibitory action by high PNU-120596 concentrations is not clarified yet. A hypothesis for the biphasic course of the dose-response relationship with PNU-120596 could be that at high PNU-120596 concentrations the positive allosteric binding sites are occupied and the modulator still possesses other binding sites, for example within the ion channel mediating a steric inhibition through a nonselective block of the pore after initial binding sites are saturated [303, 394, 395]. However, this hypothesis would have to be validated by future studies.

#### 4.5 Electrophysiological characteristics of CHO/RIC-3/ $\alpha 7$ -nAChR cells

Analogous to wildtype CHO-K1 cells, CHO-K1 cells stably transfected with the  $\alpha 7$ -nAChR (CHO/RIC-3/ $\alpha 7$ -nAChR) were electrophysiologically characterized by voltage-step protocols in order to verify that upon stable transfection, electrophysiological endogenous membrane properties of VGIC conductance remained unchanged and, in addition, to verify  $\alpha 7$ -specific properties including ion species permeant to  $\alpha 7$ -nAChR by current-voltage relations (see section 3.6). Current responses measured at different voltages between - 100 and + 80 mV at 20 mV intervals without stimulation, i.e. application of external solution to the cells, showed small increasing currents between - 100 and + 200 pA with increasing voltage indicating a low background by VGIC so that activation of interfering endogenous VGIC disrupting patch clamp measurements could be excluded (Figure 20 A-C; Table 18) [106]. Moreover, current-voltage relations of unstimulated CHO/RIC-3/ $\alpha 7$ -nAChR cells corresponded to the previously results of current-voltage relations of unstimulated CHO-K1 wildtype cells verifying that genes which are determining for the physiological function of the cell were not functionally altered

by integration of  $\alpha 7$ -nAChR cDNA in the genomic DNA of CHO-K1 cells during the stable transfection process (compare Figure 13 B-C).

Application of the voltage-step pulse protocol upon activation of  $\alpha 7$ -nAChR by agonists nicotine or ACh and potentiation by PNU-120596 co-applied with 100  $\mu$ M agonist showed inwardly rectifying currents differing in size of current amplitude that decreased with increasing depolarization from -100 mV to 0 mV (Figure 20 D-F). Inwardly rectifying currents induced by nicotine were approx. enhanced by 2-fold in amplitude compared to amplitude induced by ACh (Figure 20 D-F; Table 18). The currents by the modulation of the receptors with 10  $\mu$ M PNU-120596 in the presence of agonists (nicotine, ACh) were significantly amplified which was manifested in the increase of the maximum current amplitude and in an extension of the duration of the current responses (Figure 20 D-F; Table 18). As obtained from previous results, co-application of agonist and positive allosteric modulator PNU-120596 implied a larger open probability of receptors as well as larger duration of open probability augmenting current amplitude and elongation of response [33, 62, 148, 149]. This potentiation was, as detected by previously determined current traces, more pronounced in current responses of PNU-120596 co-applied with nicotine than with ACh, possibly due to differences in binding mechanisms of agonists within the orthosteric binding sites leading to differences in the degree of the potentiating effect by PNU-120596 [37, 109, 312, 394, 395]. Furthermore, the less pronounced potentiating effect of ACh could be explained by its low stability in aqueous solution as ACh undergoes spontaneous non-enzymatic hydrolysis to acetate and choline in aqueous solution. As a result, degradation of ACh before applied to the  $\alpha 7$ -nAChR of the cell due to hydrolysis may have mitigated the current response.

Further depolarization showed that in all voltage-current relations of agonist-induced activation in the absence and presence of PNU-120596, no significant current responses were detectable between 0 and +40 mV (Figure 20 D-F). Given that this range of the equilibrium potential did not show a clear cut reversal of currents represented that equilibrium potential was caused by a mixed composition of ion species permeability revealing a Nernst potential lying between those ion species involved (see section 2.4.1) [48]. Because  $\alpha 7$ -nAChR were known to be permeable to  $\text{Na}^+$  and  $\text{Ca}^{2+}$ , it was very likely that the equilibrium potential derived from  $\text{Na}^+$  and  $\text{Ca}^{2+}$  permeability indicated by an equilibrium potential range of 0 and +40 mV that was close to the Nernst potential of  $\text{Na}^+$  at +66 mV [232]. The determination of Nernst potential of  $\text{Ca}^{2+}$  was not feasible as no intracellular  $\text{Ca}^{2+}$  was applied, a concentration necessary to calculate the Nernst potential of an ion species [3, 48, 221]. Nevertheless, assuming a very low physiological intracellular  $\text{Ca}^{2+}$  concentration, a positive Nernst potential would be expected that indicated also a contribution of  $\text{Ca}^{2+}$  besides  $\text{Na}^+$  in permeability through  $\alpha 7$ -nAChR [48, 232]. Depolarization above +40 mV up to +80 mV induced minor outward currents that were more pronounced than by control and likely derived from an efflux of  $\text{K}^+$  ions through  $\alpha 7$ -nAChR

corresponding to the electrochemical gradient of  $K^+$  and, in addition, as  $\alpha 7$ -nAChR are described to be bidirectional ion channels that are also permeable to  $K^+$  [149, 232].

Besides verification of VGIC, the investigation of LGIC, most important those nAChR subtypes other than  $\alpha 7$ -subtype, was essential to verify that patch clamp investigations of  $\alpha 7$ -nAChR function were not disrupted by simultaneously activated VGIC or LGIC (see section 3.6).

In order to elucidate if current responses exclusively derived from  $\alpha 7$ -selective nAChR activity rather than from expression of further nAChR subtypes and LGIC functionally interacting with nicotine, nicotine-induced and PNU-120596-modulated currents were inhibited by the  $\alpha 7$ -selective nAChR antagonist methyllycaconitine (MLA). Thereby, inhibitory potency of antagonization of nicotine-induced activation was comparable to that reported by Ward and coworkers ( $IC_{50} = 0.83$  nM) (Figure 21 A-B; Table 18) [364]. MLA antagonization of the potentiation of nicotine-induced activation by the  $\alpha 7$ -specific PAM PNU-120596 significantly reduced the inhibitory effect of MLA, whereas the current signal was completely inhibited at high MLA concentrations. This yielded that PNU-120596 preserves nAChR open probability to a certain degree under the presence of an inhibitor until inhibition increased due to a concentration-dependent displacement effect of PNU-120596 with augmenting MLA concentrations (Figure 21 A, C; Table 18). Consequently, endogenous sources of CHO-K1 cells, such as other nAChR subtypes, functionally interacting with nicotine or PNU-120596 were not detectable and the expression of  $\alpha 7$ -specific nAChR on the CHO-K1 host cell line was confirmed by full antagonization of nAChR activation by nicotine and of  $\alpha 7$ -specific nAChR potentiation by PNU-120596 (Figure 21 A-C). Therefore, a functional interaction of nAChR subtypes other than  $\alpha 7$ -specific nAChR contributing to the nicotine-induced current response could be excluded. In conclusion, the low background of voltage-activated components and the absence of different nAChR subtypes have proven that the CHO-K1 host system served as a reliable system for nAChR investigation [106, 151].

#### **4.6 Effect of structurally different bispyridinium non-oximes on human $\alpha 7$ -nAChR function**

Investigation of  $\alpha 7$ -nAChR function revealed multiple conformational states of the nAChR whereas the equilibria among these states were regulated upon agonist binding in a concentration dependent manner accounting for a closed, open and desensitized state as illustrated by the model in Figure 3 D [53, 92, 377]. In brief, the probability of converting the conformational state from the closed, unbound to the open nAChR increases with the agonist binding sites occupied whereas the agonist binds with low affinity to the orthosteric binding site [83, 148, 276, 322, 371, 377]. After a few milliseconds, the receptor inactivates either by conveying the inactivated or the fast onset desensitized state (see

section 1.7.3) [83, 148, 276, 322, 371, 377]. At higher agonist concentrations, more binding sites are occupied by agonist and this leads from an overstimulation of receptors to the non-conducting slow onset desensitized state which is either conveyed from the activated, the fast onset desensitized or the closed state of the receptors [14, 148, 322, 351]. Transferring the conformational states of the nAChR into physiological means, binding of the neurotransmitter ACh to nAChR under physiological conditions leads to controlled activation and inactivation of receptors and is associated with a normal neuronal and neuromuscular transmission of stimuli (see section 1.3) [9, 11, 121, 260, 389]. However, when nAChR dysfunction occurs by initial overstimulation induced by an excess of ACh and subsequent slow onset desensitization, most severe symptoms are caused including skeletal muscle fasciculation due to overstimulation and subsequent weakness, bronchoconstriction and finally central respiratory depression due to receptor desensitization (Table 1) [11, 25, 29, 260]. Hence, such a desensitization contributes to the cholinergic crises in intoxications with OP compounds, including nerve agents and pesticides, which derives from accumulation of ACh in the synaptic cleft of the neuronal and neuromuscular system due to irreversible AChE inhibition (see section 1.4) [11, 142]. If untreated, nAChR desensitization leads to disturbance of multiples body functions and poses a severe life endangering event by central and peripheral respiratory depression [76, 142, 389]. Consequently, prevention and recovery of desensitized nAChR in respiratory muscles and in the synaptic cleft of the nervous system after OP poisoning may preserve the life-threatening collapse of the central and peripheral respiratory drive (see section 1.6) [62, 117, 290, 322, 372]. To this end, nAChR active substances intended to restore the loss of function of nAChR and thus to counteract the effects of accumulated ACh appears to be a promising therapeutic strategy [208, 296, 330, 377]. As described in section 1.7.3, nAChR ligands acting as type II positive allosteric modulators (PAM) were of interest due to their low intrinsic activity compared to agonists and thus type II PAM may be useful to reduce toxicity and other off-target effects [33, 61, 62, 141, 149]. In particular, the cholinergic tone by neuronal and neuromuscular neurotransmission can be regulated by PAM in the presence of ACh accumulation in the synaptic cleft [33, 149]. Research concerning the identification of those compounds postulated that the bispyridinium (BP) non-oxime compound MB327, a 4-*tert*-butyl-BP, may act as a PAM at nAChR deriving from *Torpedo californica* and proved to recover neuromuscular transmission of soman-impaired muscle-force of human intercostal muscles and rat diaphragms *in vitro* [229, 230, 290]. Although having a positive therapeutic effect, the relatively high concentrations of MB327 required for this effect *in vitro* are likely to be outside of the therapeutic window and may provoke toxic effects *in vivo* [229, 230, 290].

In this study, a series of structurally-related BP non-oxime compounds (PTM compounds) with various groups at different positions of the pyridinium rings analogues to the lead structure MB327 were tested for their ability to modulate  $\alpha 7$ -nAChR function by an allosteric type II mechanism to identify



their structural requirements capable to treat nAChR desensitization after OP poisoning (Figure 4; Table 6). These results are valuable basics for the development of potent PAM of h $\alpha$ 7-nAChR as they allow determination of initial structure-activity relationships of test compounds on h $\alpha$ 7-nAChR function requested for predictive drug design.

Based on the findings of the results of the present study comprising the verified conformational states of the receptor including the closed, activated and desensitized states which were found to transition concentration-dependently, the effect of PTM compounds could be investigated at different conformational states of the receptor (see section 3.7; 3.8). Therefore, the commonly used hydrolysis-stable agonist nicotine was selected for activation and desensitization of receptors instead of ACh because ACh would undergo a non-enzymatic hydrolysis to acetate and choline during the measurement. Analysis of dose-response curves of nicotine revealed a transfer from the closed conductible state of h $\alpha$ 7-nAChR under control condition (external solution) to augmenting h $\alpha$ 7-nAChR activation with increasing nicotine concentrations up to 100  $\mu$ M (see section 3.5; Figure 19 A, I) [322, 371]. With respect to individual current traces, they decayed rapidly after a few milliseconds whereas without enough time and washing steps before next agonist application, current response was not completely regenerated which reflected that fast decay of current response was due to fast desensitization and not inactivation which would be still conductible to h $\alpha$ 7-nAChR activation (data not shown) [83, 148, 276, 322, 371, 377]. Thereby, application of PTM compounds to h $\alpha$ 7-nAChR co-applied with 100  $\mu$ M nicotine enabled the examination of the effect of PTM compounds on activation and on fast onset of desensitization of h $\alpha$ 7-nAChR given that PTM compounds were present throughout the nicotine-induced current response from activation to fast onset desensitization represented by the decay of current trace (see section 3.7). Moreover, the effect of PTM compounds on slow onset desensitization of h $\alpha$ 7-nAChR was investigated in the present study (see section 3.8). The full non-conductible slow onset desensitization induced by excessive agonist concentrations was conveyed with 1 mM nicotine (see section 3.5; Figure 19 I) [14, 148, 351]. This desensitized state was followed by co-application of 1 mM nicotine and PTM compound to examine the ability of these compounds to recover desensitized h $\alpha$ 7-nAChR (see section 3.8).

#### **4.6.1 Structure-activity relations of bispyridinium compounds on activation of human $\alpha$ 7-nAChR**

Analysis of structure-activity relations of PTM compounds on nAChR activity obtained by nAChR activation with 100  $\mu$ M nicotine co-applied with PTM compounds showed that compounds bearing a *tert*-butyl- (MB327, PTM0001, PTM0002) or methoxy-group (PTM0008, PTM0009, PTM0010) were able to potentiate the nicotinic response (Figure 22 A-H). Thereby, both, current amplitude and duration of current response were enhanced most pronounced by MB327 (Figure 22 A, G; Figure 24;

Table 19). Regarding the degree of enhancement of PTM compounds, the position of the substituted group appeared to determine the extent of potentiation as PTM compounds with a substituted group at 3- (*tert*-butyl-, methoxy-) and 4-position (*tert*-butyl-, methoxy-) demonstrated most pronounced enhancement with respect to amplification of current amplitude and duration of nAChR activation compared to a moderate potentiation by test compounds with a substituted group at 2-position (*tert*-butyl-, methoxy-group) (Figure 22 A-H; Figure 24; Table 19). Given that test compounds (MB327 and PTM compounds) did not activate receptors in the absence of nicotine, it was indicative that the potentiation by these compounds was mediated by a direct allosteric interaction with the receptors (data not shown) [148].

When comparing the type II PAM PNU-120596 modulated current traces to modulated current traces induced by MB327 as well as PTM compounds, MB327 and PTM compounds resembled a similar pattern of potentiation although significantly less pronounced than PNU-120596 which is augmentation of current amplitude of nAChR activation and a prolonged activation of  $\alpha 7$ -nAChR (compare Figure 22 E, K; Table 17). Under the assumption that the observed similarities in current response profiles were associated with a common mechanism, the underlying mode of action by the PAM PNU-120596 may be extrapolated to MB327 and PTM compounds [33, 62]. Thus, considering mechanistic profiles of positive allosteric modulators classified in type I and type II depending on whether they reduced the level of agonist-induced desensitization (type II-PAM) or not (type I-PAM), MB327 and PTM compounds were found to be at least type I modulators as they potentiated receptor activation and prevented desensitization by binding to the activated state. They may also mediate the mechanism of a type II-PAM like PNU-120596 by recovering desensitization when binding to the desensitized receptor state, which was investigated more precisely in section 3.8 [148].

Also consistent with dose-response curves of modulated responses by PNU-120596 in the presence of 100  $\mu$ M nicotine, high MB327 and PTM concentrations reduced current response in a concentration dependent manner (Figure 22 G-H). As proposed for PNU-120596, inhibition of the biphasic course of the dose-response curves might be either mediated through a nonselective block of the pore after initial binding sites were saturated or by a non-competitive antagonistic mode of inhibition which was suggested by Ring and colleagues [269] although this mechanism is not completely understood yet [297, 303, 395].

It was apparent that ions or other small molecules may affect nAChR function as reported by Vernino and coworkers [358] who found that neuronal nAChR were positively modulated by physiological levels of external  $\text{Ca}^{2+}$  in a dose-dependent manner. Other studies postulated a biphasic potentiation of neuronal nAChR by zinc and cadmium presumably by modulation of nAChR activation with ACh [144, 145]. Taken into account that two different counterions of test compounds including iodide ( $\text{I}^-$ ) or trifluoromethanesulfonate ( $\text{Tfo}^-$ ) used in this study may also act as ligands of  $\alpha 7$ -nAChR, 2- (PTM0002;

PTM0045) and 4-*tert*-butyl BP (PTM0061; MB327) with either Tfo<sup>-</sup> (PTM0002; PTM0061) or I<sup>-</sup> (PTM0045; MB327) as counterion were exemplarily investigated for the effect of different counterions on the modulation of nicotine-induced activation by these compounds (Figure 23 A-B). Current amplitudes of either 2- or 4-*tert*-butyl BP with different counterions did not deviate significantly from each other indicating that different counterions had no effect on current amplitude of  $\alpha 7$ -nAChR activation or modulation, respectively, and thus do not functionally interact with the  $\alpha 7$ -nAChR (Figure 23 A-B). In contrast to the PTM compounds potentiating current response, the majority of the PTM compounds investigated in this study exerted a solely antagonization of nicotine-activated nAChR (Figure 25 A-D). Weakest inhibitory potency was observed with PTM compounds bearing an isopropyl group (PTM0003, PTM0013, PTM0014) (Figure 25 A; Table 20). With respect to the residual PTM compounds (PTM0007, PTM0015 – PTM0022), no distinct relation between substitution pattern and inhibitory potency could be established (Figure 25 B-D; Table 20). Because no clear structure-inhibition relation was apparent by these PTM compounds, the antagonistic action by PTM compounds could be attributed to a non-selective inhibition of the ion channel, for instance by displacing the agonist from its orthosteric binding site or by impeding the ion permeation through the channel through a steric mechanism [268, 297, 303, 395]. A negative allosteric mechanism inducing closure of the ion channel by a conformational change upon binding of PTM compounds could also be mediated by these compounds as this mechanism was already proposed for other nAChR inhibitors and a series of compounds based on a BP structure varying in length of the polyethylene linker between the two pyridinium moieties [14, 269]. These results were intended to find potent positive allosteric modulators able to prevent receptor desensitization and allowed first structure-activity relations of PTM compounds (Figure 22 A-H; Figure 24; Figure 25 A-D). Thereby, two different intrinsic activities by five PTM compounds and MB327 were found comprising a biphasic action by potentiation and inhibition and solely inhibition by further PTM compounds (see section 3.7). Within the biphasic current response curves, first structural requirements of these modulators were identified demonstrating that those compounds bearing a *tert*-butyl-, methoxy- group at 3- or 4-position had largest potency whereas potency of PTM compounds with a *tert*-butyl-, methoxy- group at 2 was less pronounced (Figure 22 A-H; Figure 24; Table 19). Due to the superior potency of MB327 in comparison to all PTM compounds tested, further improvements with respect to potency of these compounds are required for the development of modulators as potential therapeutic drugs against OP-mediated desensitization.

#### 4.6.2 Recovery from desensitization of $\alpha 7$ -nAChR by bispyridinium compounds

A common feature of type I and type II PAM is that they enhance agonist-induced activation of  $\alpha 7$ -nAChR but it is a unique property of the type II modulator to affect desensitization by recovering

receptors from desensitization [33, 115]. It was shown in the present results investigating the effect of PTM compounds on  $\alpha 7$ -nAChR activation and fast onset desensitization that five of the PTM compounds and MB327 reflected at least a type I positive allosteric mechanism (see section 4.6.1) [33, 62, 148]. However, to elucidate more precisely whether those PTM compounds and MB327 also have significant type II PAM properties that is converting the desensitized state into a conductible state, the receptors were first activated by 100  $\mu$ M nicotine followed by an excess of nicotine (1 mM) to induce desensitization, and subsequently increasing concentrations of the test substance in the presence of 1 mM nicotine were applied (see section 3.8).

Notably, when increasing test compound concentrations were applied to cells to test for recovery of  $\alpha 7$ -nAChR, receptors were consistently exposed to 1mM nicotine throughout the measurement to ensure that recovery of receptors due to the action of test compound was not affected by spontaneous recovery of receptors from desensitization. As expected, PTM compounds that were found to inhibit  $\alpha 7$ -nAChR activation as discussed in section 4.6.1 of the present results, those PTM compounds did also not regenerate receptor function when applied to desensitized nAChR as exemplarily shown by PTM0003, PTM0014, PTM0013, bearing an isopropyl-group at 2-, 3- or 4-position (Figure 26 A).

Interestingly, all five compounds that yielded a type I PAM property found in present results (see section 4.6.1) were also found to yield a type II PAM effect (Figure 26 A, C-D) [33, 62, 149]. More precisely, the maximum current amplitude ( $I_{\max}$ ) and duration of the current response was increased with elevating test compound concentrations of MB327, PTM0001, PTM0002, PTM0008, PTM0009 and PTM0010 applied to the desensitized receptors (Figure 26 A, C-D; Figure 27 A-C; Table 21). Hereby, the highest test compound concentration applied (10 mM) showed the greatest effect. It demonstrated that these compounds only partly transferred the receptors from the desensitized to the activated state because current amplitude was still below control of initially applied 100  $\mu$ M nicotine ( $EC_{100}$  nicotine) at the highest concentration of test compound applied (Figure 26 A, C-D; Table 21). By comparison with PNU-120596, type II PAM properties by PNU-120596 were confirmed by full regeneration of receptor function from desensitization and thus, observed current records were used as a representative example for type II PAM mechanism [27, 149].

In addition, this type II PAM showed a bimodal current response relation when used to resensitize the receptors (Figure 26 B). PNU-120596 fully reversed desensitization when applied in the lower micromolar range ( $\leq 10 \mu$ M) and even amplified the current amplitude of the nicotine-induced cholinergic signal when applied at concentrations in the higher micromolar range ( $\geq 10 \mu$ M  $\leq 100 \mu$ M), but concentrations exceeding 100  $\mu$ M of PNU-120596 decreased signal amplification concentration-dependently (Figure 26 B). The mechanism of this additional inhibitory action is not clear, but reduction of the current signal due to binding of PNU-120596 to an agonistic binding site promoting slow onset desensitization of nAChR is unlikely as PNU-120596 itself was found to exhibit no signal deriving from

an agonistic action (data not shown). Another hypothesis relates to an unspecific binding of PNU-120596 after all initial binding sites were occupied at a critical concentration, competitive or non-competitive, leading to decreased receptor activity [269, 297, 303, 395]. Nevertheless, further investigation to refine this hypothesis is needed, but goes beyond the scope of this study. Notably, the well-prescribed PAM PNU-120596 has no potential use as a therapeutic drug in OP poisoning because it is known to be an exclusive  $\alpha 7$ -selective PAM and not effective at different, centrally and peripherally, expressed nAChR subtypes implicated in paralysis of the respiratory system after OP poisoning [27, 149]. Hence, PNU-120596 served as a representative of type II PAMs in this study to compare current responses induced by MB327 and PTM compounds with PNU-120596 in order to gain insight into the mode of action by the test compounds [149].

Among all test compounds investigated, the greatest effect in  $I_{\max}$  used as a measure of total efficacy and potency ( $EC_{50}$ ) of receptor regeneration from desensitization was recorded at highest concentrations of MB327, which almost recovered receptors completely (Table 21). A recovery by approx. half was observed at highest concentrations of PTM0001, PTM0002 and PTM0008 and only minor type II potency was found with highest concentrations of PTM0009 and PTM0010 (Table 21). Slope coefficients ( $n_H$ ) derived from dose-response curves demonstrated a steep  $n_H$  of PNU-120596 mediated nAChR recovery and slightly less steep  $n_H$  of MB327 whereas rather shallow slopes were found in dose-response curves of PTM0001, PTM0002, PTM0008, PTM0009 and PTM0010 (Table 21). In terms of development of a medical therapy against nicotinic dysfunction against OP poisoning, a compound with a steep slope is a rough indication for a rather small therapeutic window and, thus, would require more careful titration of the therapeutic dose [269]. Hence, a shallow Hill slope is favored as it may indicate a broader therapeutic window [269]. For the analysis of the duration of the current response reflecting the degree of prolonged mean open times of  $\alpha 7$ -nAChR, current amplitudes of resensitized receptors were determined at 10, 50 and 100 ms after onset of current signal and compared to the current amplitude induced by 100  $\mu$ M nicotine at 10, 50 and 100 ms after onset of current signal. As examined before, nicotine produced rapid activation of the receptors, which decayed within a few milliseconds due to the fast onset desensitization of the  $\alpha 7$ -nAChR so that approx. three-quarter of the  $I_{\max}$  remained after 10 ms and was depleted after 50 ms (Figure 27 A-B; Table 21). All test compounds including PNU-120596, MB327 and PTM compounds notably extended the duration of current responses compared to the nicotinic response although to a different degree wherein PNU-120596 showed the most pronounced elongation followed by MB327 and subsequently PTM compounds with decreasing duration of current response in the following order: PTM0001 > PTM0002 > PTM0008 > PTM0009 > PTM0010 (Figure 27 A-C; Table 21). Considering that the long-lived steady state current of recovered the  $\alpha 7$ -nAChR by the type II PAM PNU-120596 was also present with PTM compounds and MB327 compared to the short-lived nicotinic response, it was found that

test compounds were able to re-open receptors from the desensitized state by a conformational change of the receptor [27, 122, 149].

All in all, the response profile of PTM compounds PTM0001, PTM0002, PTM0008, PTM0009 and PTM0010 as well as of MB327 showed that they regenerated the initial current amplitude of nicotine-activated receptors to a different degree and that they were able to elongate the mean open time of receptors after recovery from desensitization. Thus, these compounds resembled the response profile of PNU-120596 although less pronounced and thus the hypothesis of a common mode of action of a type II PAM by these compounds was strengthened (Figure 26 A-D; Figure 27 A-C; Table 21) [27, 122, 148].

## 5. Conclusion and future considerations

Desensitization of nAChR resulting in respiratory paralysis is a severe life-threatening event in OP poisoning [121, 389]. Besides oxime therapy and many years of research to find oximes counteracting OP poisoning by a broad range of cholinesterase-inhibiting compounds, such an oxime has not been identified yet and urges the need of alternative treatment strategies to complement oxime therapy [90, 91, 101, 379]. Thereby, the regeneration of the functional activity of desensitized nAChR has become a very promising therapeutic approach for the treatment after OP poisoning to protect victims from death by respiratory arrest [230, 296, 330, 347]. As a starting point for the development of potent compounds able to resensitize receptors which have not been available so far, MB327 was applied as lead structure for the design of a new series of analogues to MB327 (denoted as PTM compounds) (Figure 4; Table 6)

In this context, MB327 has shown to mediate a positive therapeutic effect *in vitro* and thus shown to have the desired pharmacological properties in principle, but still not efficient enough for a therapeutic use [230, 262, 290]. In this study, functional activities of these so called PTM compounds were identified by establishing a patch clamp screening method. Hereby, structure-activity relations of PTM compounds on  $\alpha 7$ -nAChR activation and the ability of PTM compounds to restore desensitized  $\alpha 7$ -nAChR were examined. In total, PTM compounds PTM0001, PTM0002, PTM0008, PTM0009 and PTM0010 as well as MB327 showed that they prevented and recovered receptors from desensitization to a different degree which was likely to be due to a mechanism of a type II PAM. Further, these compounds revealed distinct structure-activity relations, but were still too low in potency to be sufficient in a therapeutic dosage range for efficient prevention and recovery of desensitization.

Based on the findings of the present study, the utility of positive allosteric modulation of the  $\alpha 7$ -nAChR as a novel therapeutic principle for treating acute OP poisoning was testified. Expanding and refinement of structure-activity relations is thus of great importance to improve pharmacophore models for the identification of new ligands and thus for the long-term goal to develop potential drugs effective against OP poisoning. Further requirements for the development of PAM as potential therapeutic drugs against OP-mediated desensitization comprise a sufficiently high stability of the potential drug in solution and a low activity under physiological conditions to avoid undesirable side effects. Moreover, determination of subtype selectivity of such drugs and potential intrinsic toxicity, i.e. by inhibition of AChE as known by other bispyridinium (BP) compounds, present crucial aspects for the evaluation of the therapeutic application of novel drugs against nerve-agent impaired nicotinic function. Collectively, continuation of this study together with complementary pharmacological investigations comprising affinity studies of test compounds towards different subtypes of nAChR, elucidation of intrinsic toxicity, e.g. AChE inhibition and functional assays, for instance on skeletal

muscle tissue, are requested to substantially advance predictive drug design for generation of new nicotinic drugs paving the way for new therapeutic avenues in the treatment of OP poisoning.



## References

- [1] <http://www.nanion.de>. Accessed 14 June 2017.
- [2] [https://en.wikipedia.org/wiki/Membrane\\_potential](https://en.wikipedia.org/wiki/Membrane_potential). Accessed 14 June 2017.
- [3] The Axon Guide. Electrophysiology and Biophysics Laboratory Techniques. *Molecular Devices*. <https://www.moleculardevices.com/axon-guide>. Accessed 14 June 2017.
- [4] The National Research Council's Committee on Toxicology. 1997. The First 50 Years 1947-1997. *National Academies Press*. <https://www.nap.edu/read/9487/chapter/2>. Accessed 14 June 2017.
- [5] Abou-Donia, M. 1981. Organophosphorus ester-induced delayed neurotoxicity. *Annual review of pharmacology and toxicology* 21, 511–548.
- [6] Pereira, E., Burt, D., Aracava, Y., Kan, R., Hamilton, T., Romano Jr., J., Adler, M., and Albuquerque, E. 2007. Novel Medical Countermeasure for Organophosphorus Intoxication: Connection to Alzheimer's Disease and Dementia. In *Chemical Warfare Agents*. John Wiley & Sons.
- [7] Agency for Toxic Substances and Disease Registry. 2008. *ToxFAQs for nerve agents*. <http://www.atsdr.cdc.gov/tfacts166.html>. Accessed 27 March 2017.
- [8] Alberts, B., Johnson, A., Lewis, J., Raff, M., Roberts, K. and Walter, P. 2002. Molecular biology of the cell. *Garland Science*.
- [9] Albuquerque, E., Alkondon, M., Pereira, E., Castro, N., Schrattenholz, A., Barbosa, C., Bonfante-Cabarcas, R., Aracava, Y., Eisenberg, H., and Maelicke, A. 1997. Properties of neuronal nicotinic acetylcholine receptors: pharmacological characterization and modulation of synaptic function. *The Journal of pharmacology and experimental therapeutics* 280, 3, 1117–1136.
- [10] Albuquerque, E., Pereira, E., Aracava, Y., Fawcett, W., Oliveira, M., Randall, W. R., Hamilton, T., Kan, R., Romano, Jr, J., and Adler, M. 2006. Effective countermeasure against poisoning by organophosphorus insecticides and nerve agents. *Proceedings of the National Academy of Sciences of the United States of America* 103, 35, 13220–13225.
- [11] Aldridge, W. and Reiner, E. 1972. Enzyme Inhibitors as Substrates. Interaction of Esterases with Esters of Organophosphorus and Carbamic Acids 13. *North-Holland Publishing Company*.
- [12] Alkondon, M. and Albuquerque, E. 1989. The nonoxime bispyridinium compound SAD-128 alters the kinetic properties of the nicotinic acetylcholine receptor ion channel: a possible mechanism for antidotal effects. *The Journal of pharmacology and experimental therapeutics* 250, 3, 842–852.
- [13] Amato, A., McVey, A., Cha, C., Matthews, E., Jackson, C., Kleingunther, R., Worley, L., Cornman, E., and Kagan-Hallet, K. 1997. Evaluation of neuromuscular symptoms in veterans of the Persian Gulf War. *Neurology* 48, 1, 4–12.
- [14] Arias, H. 1998. Binding sites for exogenous and endogenous non-competitive inhibitors of the nicotinic acetylcholine receptor. *Biochimica et biophysica acta* 1376, 2, 173–220.
- [15] Arias, H. 2000. Localization of agonist and competitive antagonist binding sites on nicotinic acetylcholine receptors. *Neurochemistry international* 36, 7, 595–645.
- [16] Arias, H. 2010. Positive and negative modulation of nicotinic receptors. *Advances in protein chemistry and structural biology* 80, 153–203.
- [17] Arias, H., de Rosa, M., Bergé, I., Feuerbach, D., and Bouzat, C. 2013. Differential pharmacological activity of JN403 between  $\alpha 7$  and muscle nicotinic acetylcholine receptors. *Biochemistry* 52, 47, 8480–8488.

- [18] Arias, H., Feuerbach, D., Targowska-Duda, K., Aggarwal, S., Lapinsky, D., and Jozwiak, K. 2012. Structural and functional interaction of ( $\pm$ )-2-(N-tert-butylamino)-3'-iodo-4'-azidopropiophenone, a photoreactive bupropion derivative, with nicotinic acetylcholine receptors. *Neurochemistry international* 61, 8, 1433–1441.
- [19] Ariel, N., Ordentlich, A., Barak, D., Bino, T., Velan, B., and Shafferman, A. 1998. The 'aromatic patch' of three proximal residues in the human acetylcholinesterase active centre allows for versatile interaction modes with inhibitors. *The Biochemical journal* 335, 1, 95–102.
- [20] Asa, S., Kovacs, K., Horvath, E., Losinski, N., Laszlo, F., Domokos, I., and Halliday, W. 1988. Human fetal adenohypophysis. Electron microscopic and ultrastructural immunocytochemical analysis. *Neuroendocrinology* 48, 4, 423–431.
- [21] Ashani, Y., Bhattacharjee, A., Leader, H., Saxena, A., and Doctor, B. 2003. Inhibition of cholinesterases with cationic phosphonyl oximes highlights distinctive properties of the charged pyridine groups of quaternary oxime reactivators. *Biochemical pharmacology* 66, 2, 191–202.
- [22] Ashani, Y., Radić, Z., Tsigelny, I., Vellom, D., Pickering, N., Quinn, D., Doctor, B., and Taylor, P. 1995. Amino acid residues controlling reactivation of organophosphonyl conjugates of acetylcholinesterase by mono- and bisquaternary oximes. *The Journal of biological chemistry* 270, 11, 6370–6380.
- [23] Bajgar, F., Jakl, A., and Hrdina, V. 1971. Influence of trimedoxime and atropine on acetylcholinesterase activity in some parts of the brain of mice poisoned by isopropylmethyl phosphonofluoridate. *Biochemical pharmacology* 20, 11, 3230–3233.
- [24] Bajgar, J., Fusek, J., Kuca, K., Bartosova, L., and Jun, D. 2007. Treatment of organophosphate intoxication using cholinesterase reactivators: facts and fiction. *Mini reviews in medicinal chemistry* 7, 5, 461–466.
- [25] Bajgar, J., Patocka, J., Jakl, A., and Hrdina, V. 1975. Antidotal therapy and changes of acetylcholinesterase activity following isopropyl methylphosphonofluoridate intoxication in mice. *Acta biologica et medica Germanica* 34, 6, 1049–1055.
- [26] Baldit, G. 1958. Amiton—a new acaricide and scalicide. *Journal of the Science and Food Agriculture*. 9, 8, 516–524.
- [27] Barron, S., McLaughlin, J., See, J., Richards, V., and Rosenberg, R. 2009. An allosteric modulator of  $\alpha 7$  nicotinic receptors, N-(5-Chloro-2,4-dimethoxyphenyl)-N'-(5-methyl-3-isoxazolyl)-urea (PNU-120596), causes conformational changes in the extracellular ligand binding domain similar to those caused by acetylcholine. *Molecular pharmacology* 76, 2, 253–263.
- [28] Bauer, C., Meyerhof, W., and Schwarz, J. 1990. An inward-rectifying K<sup>+</sup> current in clonal rat pituitary cells and its modulation by thyrotrophin-releasing hormone. *The Journal of physiology* 429, 169–189.
- [29] Benschop, H. and de Jong, L. 2000. Toxicokinetics of Nerve Agents. In *Chemical Warfare Agents*. John Wiley & Sons.
- [30] Benschop, H. and de Jong, L. 1988. Nerve agent stereoisomers: analysis, isolation and toxicology. *Accounts of Chemical Research*. 21, 10, 368–374.
- [31] Bernstein, J. 1912. Elektrobiologie. Die Lehre von den Elektrischen Vorgängen im Organismus auf moderner Grundlage dargestellt. *Vieweg & Sohn*.
- [32] Bertolote, J., 2006. Deaths from pesticide poisoning: a global response. *The British Journal of Psychiatry* 189, 3, 201–203.
- [33] Bertrand, D. and Gopalakrishnan, M. 2007. Allosteric modulation of nicotinic acetylcholine receptors. *Biochemical pharmacology* 74, 8, 1155–1163.

- [34] Bigley, A., Xu, C., Henderson, T., Harvey, S., and Raushel, F. 2013. Enzymatic Neutralization of the Chemical Warfare Agent VX: Evolution of Phosphotriesterase for Phosphorothiolate Hydrolysis. *Journal of the American Chemical Society* 135, 28, 10426–10432.
- [35] Bisset, N. 1992. War and hunting poisons of the New World. Part 1. Notes on the early history of curare. *Journal of ethnopharmacology* 36, 1, 1–26.
- [36] Black, R. 2016. Development, Historical Use and Properties of Chemical Warfare Agents. In *Chemical Warfare Toxicology: Volume 1: Fundamental Aspects. Issues in Toxicology*. Royal Society of Chemistry 1, 1–28.
- [37] Blum, A., Lester, H., and Dougherty, D. 2010. Nicotinic pharmacophore: the pyridine N of nicotine and carbonyl of acetylcholine hydrogen bond across a subunit interface to a backbone NH. *Proceedings of the National Academy of Sciences of the United States of America* 107, 30, 13206–13211.
- [38] Bonner, T., Buckley, N., Young, A., and Brann, M. 1987. Identification of a family of muscarinic acetylcholine receptor genes. *Science* 237, 4814, 527–532.
- [39] Bonner, T., Young, A., Brann, M., and Buckley, N. 1988. Cloning and expression of the human and rat m5 muscarinic acetylcholine receptor genes. *Neuron* 1, 5, 403–410.
- [40] Boonyapisit, K., Kaminski, H., and Ruff, R. 1999. Disorders of neuromuscular junction ion channels. *The American journal of medicine* 106, 1, 97–113.
- [41] Bosse, E., Bottlender, R., Kleppisch, T., Hescheler, J., Welling, A., Hofmann, F., and Flockerzi, V. 1992. Stable and functional expression of the calcium channel alpha 1 subunit from smooth muscle in somatic cell lines. *The EMBO journal* 11, 6, 2033–2038.
- [42] Brams, M., Gay, E., Sáez, J., Guskov, A., van Elk, R., van der Schors, R. C., Peigneur, S., Tytgat, J., Strelkov, S., Smit, A., Yakel, J., and Ulens, C. 2011. Crystal structures of a cysteine-modified mutant in loop D of acetylcholine-binding protein. *The Journal of biological chemistry* 286, 6, 4420–4428.
- [43] Brown, M. and Brix, K. 1998. Review of health consequences from high-, intermediate- and low-level exposure to organophosphorus nerve agents. *Journal of applied toxicology* 18, 6, 393–408.
- [44] Brown, J. and Laiken, N. 2011. Muscarinic receptor agonists and antagonists. In *Goodman and Gilman's The Pharmacological Basis of Therapeutics*. McGraw-Hill Companies Inc.
- [45] Brüggemann, A., Farre, C., Haarmann, C., Haythornthwaite, A., Kreir, M., Stoelzle, S., George, M., and Fertig, N. 2008. Planar patch clamp: advances in electrophysiology. *Methods in molecular biology* 491, 165–176.
- [46] Brüggemann, A., Stoelzle, S., George, M., Behrends, J., and Fertig, N. 2006. Microchip technology for automated and parallel patch-clamp recording. *Small* 2, 7, 840–846.
- [47] Buckley, N. 2004. Overcoming apathy in research on organophosphate poisoning. *British Medical Journal* 329, 7476, 1231–1233.
- [48] Bullock, H., Orkand, R., Grinnell, A., Freeman W. 1978. Introduction to nervous systems. *Experimental Physiology* 63, 2, 203–204.
- [49] Bunnelle, W., Dart, M., and Schrimpf, M. 2004. Design of ligands for the nicotinic acetylcholine receptors: the quest for selectivity. *Current Topics in Medicinal Chemistry* 4, 3, 299–334.
- [50] Burgen, A. 1949. The mechanism of action of anticholinesterase drugs. *British Journal of Pharmacology and Chemotherapy* 4, 3, 219–228.
- [51] Busker, R., Zijlstra, J., van der Wiel, H., Melchers, B., and van Helden, H. 1991. Organophosphate poisoning: a method to test therapeutic effects of oximes other than acetylcholinesterase reactivation in the rat. *Toxicology* 69, 3, 331–344.

- [52] Campbell, N. and Reece, J. 2002. Biology (6<sup>th</sup> Edition). *Benjamin Cummings*.
- [53] Campling, B., Kuryatov, A., and Lindstrom, J. 2013. Acute activation, desensitization and smoldering activation of human acetylcholine receptors. *PloS one* 8, 11, e79653.
- [54] Carpentier, P., Delamanche, I., le Bert, M., Blanchet, G., and Bouchaud, C. 1990. Seizure-related opening of the blood-brain barrier induced by soman: possible correlation with the acute neuropathology observed in poisoned rats. *Neurotoxicology* 11, 3, 493–508.
- [55] Casida, J. and Durkin, K. 2013. Anticholinesterase insecticide retrospective. *Chemico-Biological Interactions* 203, 1, 221–225.
- [56] Casida J. 1956. Mode of action of pesticides, Metabolism of Organophosphorus Insecticides in Relation to their Antiesterase Activity, Stability, and Residual Properties. *Journal of Agricultural and Food Chemistry*, 4, 772–785.
- [57] Caulfield, M. and Birdsall, N. 1998. International Union of Pharmacology. XVII. Classification of muscarinic acetylcholine receptors. *Pharmacological reviews* 50, 2, 279–290.
- [58] Cetković, S., Cvetković, M., Jandrić, D., Cosić, M., and Bosković, B. 1984. Effect of PAM-2 Cl, HI-6, and HGG-12 in poisoning by tabun and its thiocholine-like analog in the rat. *Fundamental and applied toxicology : official journal of the Society of Toxicology* 4, 2, 116–23.
- [59] Chambers, H., Meek, H. and Chambers, J. 2001. Chemistry of Organophosphorus Insecticides. In *Handbook of Pesticide Toxicology*. Elsevier, 913–917.
- [60] Chang, F., Foster, R., Beers, E., Rickett, D., and Filbert, M. 1990. Neurophysiological concomitants of soman-induced respiratory depression in awake, behaving guinea pigs. *Toxicology and applied pharmacology* 102, 2, 233–250.
- [61] Changeux, J. and Edelstein, S. J. 2001. Allosteric mechanisms in normal and pathological nicotinic acetylcholine receptors. *Current opinion in neurobiology* 11, 3, 369–377.
- [62] Chatzidaki, A. and Millar, N. 2015. Allosteric modulation of nicotinic acetylcholine receptors. *Biochemical pharmacology* 97, 4, 408–417.
- [63] Chavez-Noriega, L., Crona, J., Washburn, M., Urrutia, A., Elliott, K., and Johnson, E. 1997. Pharmacological characterization of recombinant human neuronal nicotinic acetylcholine receptors h alpha 2 beta 2, h alpha 2 beta 4, h alpha 3 beta 2, h alpha 3 beta 4, h alpha 4 beta 2, h alpha 4 beta 4 and h alpha 7 expressed in *Xenopus* oocytes. *The Journal of pharmacology and experimental therapeutics* 280, 1, 346–356.
- [64] Childs, A., Davies, D., Green, A., and Rutland, J. 1955. The reactivation by oximes and hydroxamic acids of cholinesterase inhibited by organo-phosphorus compounds. *British journal of pharmacology and chemotherapy* 10, 4, 462–465.
- [65] Clement, J. 1981. Toxicology and pharmacology of bispyridium oximes--insight into the mechanism of action vs Soman poisoning in vivo. *Fundamental and applied toxicology : official journal of the Society of Toxicology* 1, 2, 193–202.
- [66] Clement, J. 1982. HI-6: reactivation of central and peripheral acetylcholinesterase following inhibition by soman, sarin and tabun in vivo in the rat. *Biochemical pharmacology* 31, 7, 1283–1287.
- [67] Cole, K. S. 1979. Mostly membranes (Kenneth S. Cole). *Annual review of physiology* 41, 1–24.
- [68] Coleman, K. 2005. A history of chemical warfare (1<sup>st</sup> Edition). *Palgrave Macmillan*.
- [69] Colović, M., Krstić, D., Lazarević-Pašti, T., Bondžić, A., and Vasić, V. 2013. Acetylcholinesterase inhibitors: pharmacology and toxicology. *Current neuropharmacology* 11, 3, 315–335.
- [70] Conti-Fine, B., Navaneetham, D., Lei, S., and Maus, A. 2000. Neuronal nicotinic receptors in non-neuronal cells: new mediators of tobacco toxicity? *European journal of pharmacology* 393, 1–3, 279–294.

- [71] Corringer, P., Le Novère, N., and Changeux, J. 2000. Nicotinic receptors at the amino acid level. *Annual review of pharmacology and toxicology* 40, 431–458.
- [72] Craig, F., Cummings, E., and Sim, V. 1977. Environmental temperature and the percutaneous absorption of a cholinesterase inhibitor, VX. *The Journal of investigative dermatology* 68, 6, 357–361.
- [73] Cronin, A. 2004. Terrorist motivations for chemical and biological weapons use: Placing the threat in context\*. *Defense & Security Analysis* 20, 4, 313–320.
- [74] Czarnecki, A., Vaur, S., Dufy-Barbe, L., Dufy, B., and Bresson-Bepoldin, L. 2000. Cell cycle-related changes in transient K(+) current density in the GH3 pituitary cell line. *American journal of physiology. Cell physiology* 279, 6, C1819-28.
- [75] Dale, H. 1914. The action of certain esters and ethers of choline and their relation to muscarine. *The Journal of Pharmacology and Experimental Therapeutics* 6, 147–190.
- [76] Dawson, R. 1994. Review of oximes available for treatment of nerve agent poisoning. *Journal of applied toxicology* 14, 5, 317–331.
- [77] de Bleeker, J. 2006. Intermediate Syndrome in Organophosphate Poisoning. In *Toxicology of Organophosphate & Carbamate Compounds*. Elsevier, 371-380.
- [78] de Clermont P. 1854. Note sur la preparation de quelques ethers. *Comptes Rendus de l'Académie des Sciences*, 39, 338–340.
- [79] de Jong, L., Verhagen, M., Langenberg, J., Hagedorn, I., and Löffler, M. 1989. The bispyridinium-dioxime HLö-7. A potent reactivator for acetylcholinesterase inhibited by the stereoisomers of tabun and soman. *Biochemical pharmacology* 38, 4, 633–640.
- [80] Doctor, B., and Saxena, A. 2005. Bioscavengers for the protection of humans against organophosphate toxicity. *Chemico-Biological Interactions* 157-158, 167–171.
- [81] Dumas, D., Durst, H., Landis, W., Raushel, F., and Wild, J. 1990. Inactivation of organophosphorus nerve agents by the phosphotriesterase from *Pseudomonas diminuta*. *Archives of biochemistry and biophysics* 277, 1, 155–159.
- [82] Dunn, M. A. and Sidell, F. R. 1989. Progress in medical defense against nerve agents. *JAMA* 262, 5, 649–652.
- [83] Dutertre, S. and Lewis, R. J. 2006. Toxin insights into nicotinic acetylcholine receptors. *Biochemical pharmacology* 72, 6, 661–670.
- [84] Dwyer, M., Javor, S., Ryan, D., Smith, E., Wang, B., Zhang, J., and Cashman, J. R. 2014. Novel Human Butyrylcholinesterase Variants: Toward Organophosphonate Detoxication. *Biochemistry* 53, 27, 4476–4487.
- [85] Edelstein, S. J. and Changeux, J. P. 1998. Allosteric transitions of the acetylcholine receptor. *Advances in protein chemistry* 51, 121–184.
- [86] Ehrich, M. and Jortner, B. 2001. Organophosphorus-Induced Delayed Neuropathy. In *Handbook of Pesticide Toxicology*. Elsevier, 987–1012.
- [87] Eto, M. 1975. Organophosphorus pesticides. Organic and biological chemistry (1<sup>st</sup> Edition). *CRC Press*.
- [88] Eyer, P. 2003. The role of oximes in the management of organophosphorus pesticide poisoning. *Toxicological reviews* 22, 3, 165–190.
- [89] Eyer, P., Hagedorn, I., Klimmek, R., Lippstreu, P., Löffler, M., Oldiges, H., Spöhrer, U., Steidl, I., Szinicz, L., and Worek, F. 1992. HLö 7 dimethanesulfonate, a potent bispyridinium-dioxime against anticholinesterases. *Archives of toxicology* 66, 9, 603–621.

- [90] Eyer, P., Szinicz, L., Thiermann, H., Worek, F., and Zilker, T. 2007. Testing of antidotes for organophosphorus compounds: experimental procedures and clinical reality. *Toxicology* 233, 1-3, 108–119.
- [91] Eyer, P. and Worek, F. 2007. Oximes. In *Chemical Warfare Agents*. John Wiley & Sons, 305–329.
- [92] Faghieh, R., Gopalakrishnan, M., and Briggs, C. 2008. Allosteric modulators of the  $\alpha 7$  nicotinic acetylcholine receptor. *Journal of medicinal chemistry* 51, 4, 701–712.
- [93] FAO Statistics Division. 2013. *Pesticide use*. <http://www.fao.org/faostat/en/>. Accessed 23 March 2017.
- [94] Farre, C. and Fertig, N. 2012. HTS techniques for patch clamp-based ion channel screening - advances and economy. *Expert opinion on drug discovery* 7, 6, 515–524.
- [95] Farre, C., Haythornthwaite, A., Haarmann, C., Stoelzle, S., Kreir, M., George, M., Brüggemann, A., and Fertig, N. 2009. Port-a-patch and patchliner: high fidelity electrophysiology for secondary screening and safety pharmacology. *Combinatorial chemistry & high throughput screening* 12, 1, 24–37.
- [96] Farre, C., Stoelzle, S., Haarmann, C., George, M., Brüggemann, A., and Fertig, N. 2007. Automated ion channel screening: patch clamping made easy. *Expert opinion on therapeutic targets* 11, 4, 557–565.
- [97] Feldmann, R. and Maibach, H. 1974. Percutaneous penetration of some pesticides and herbicides in man. *Toxicology and applied pharmacology* 28, 1, 126–132.
- [98] Fertig, N. and Farre, C. 2010. Renaissance of ion channel research and drug discovery by patch clamp automation. *Future medicinal chemistry* 2, 5, 691–695.
- [99] Fertig, N., George, M., Klau, M., Meyer, C., Tilke, A., Sobotta, C., Blick, R. H., and Behrends, J. 2003. Microstructured apertures in planar glass substrates for ion channel research. *Receptors & channels* 9, 1, 29–40.
- [100] Field, M., and Wymore, T. 2014. Multiscale modeling of nerve agent hydrolysis mechanisms: a tale of two Nobel Prizes. *Phys. Scr.* 89, 10, 108004.
- [101] Fleisher, J. H. and Harris, L. W. 1965. Dealkylation as a mechanism for aging of cholinesterase after poisoning with pinacolyl methylphosphonofluoridate. *Biochemical pharmacology* 14, 5, 641–650.
- [102] Fleming, C., Edwards, C., Kirby, S., Maxwell, D., Potter, P., Cerasoli, D., and Redinbo, M. 2007. Crystal structures of human carboxylesterase 1 in covalent complexes with the chemical warfare agents soman and tabun. *Biochemistry* 46, 17, 5063–5071.
- [103] Frawley, L., Boockfor, F., and Hoeffler, J. 1985. Identification by plaque assays of a pituitary cell type that secretes both growth hormone and prolactin. *Endocrinology* 116, 2, 734–737.
- [104] Gahring, L., and Rogers, S. 2006. Neuronal nicotinic acetylcholine receptor expression and function on nonneuronal cells. *The AAPS journal* 7, 4, E885-94.
- [105] Galzi, J. L. and Changeux, J. P. 1995. Neuronal nicotinic receptors: molecular organization and regulations. *Neuropharmacology* 34, 6, 563–582.
- [106] Gamper, N., Stockand, J., and Shapiro, M. 2005. The use of Chinese hamster ovary (CHO) cells in the study of ion channels. *Journal of pharmacological and toxicological methods* 51, 3, 177–185.
- [107] Geerts, H. 2005. Indicators of neuroprotection with galantamine. *Brain research bulletin* 64, 6, 519–524.
- [108] Geisse, S., Gram, H., Kleuser, B., and Kocher, H. 1996. Eukaryotic expression systems: a comparison. *Protein expression and purification* 8, 3, 271–282.

- [109] Gerzanich, V., Peng, X., Wang, F., Wells, G., Anand, R., Fletcher, S., and Lindstrom, J. 1995. Comparative pharmacology of epibatidine: a potent agonist for neuronal nicotinic acetylcholine receptors. *Molecular pharmacology* 48, 4, 774–782.
- [110] Ghosh, R. and Newman, J. 1955. A new group of organophosphorus pesticides. *Chemistry and Industry*.
- [111] Glassmeier, G., Hauber, M., Wulfsen, I., Weinsberg, F., Bauer, C., and Schwarz, J. 2001. Ca<sup>2+</sup> channels in clonal rat anterior pituitary cells (GH3/B6). *Pflugers Archiv : European journal of physiology* 442, 4, 577–587.
- [112] Goebel, G. 2008. A history of chemical warfare. [http://www.vectorsite.net/twgas\\_1.html](http://www.vectorsite.net/twgas_1.html). Accessed on May 25 2017.
- [113] Goldman, M., Wilson, T., Kawakami, L., Rosenblatt, M., Culbertson, J., Schreider, J., and Remsen, and M. Shifrine. 1988. Toxicity Studies on Agent VX. Final Report. DTIC AD-A201397. Prepared by the Laboratory for Energy-Related Health Research. *University of California, Davis, Calif., for the U.S. Army Medical Research and Development Command, Fort Detrick, Frederick, Md.*
- [114] Goldsmith, M., Ashani, Y., Simo, Y., Ben-David, M., Leader, H., Silman, I., Sussman, J., and Tawfik, D. 2012. Evolved Stereoselective Hydrolases for Broad-Spectrum G-Type Nerve Agent Detoxification. *Chemistry & Biology* 19, 4, 456–466.
- [115] Gopalakrishnan, M., Buisson, B., Touma, E., Giordano, T., Campbell, J., Hu, I., Donnelly-Roberts, D., Arneric, S., Bertrand, D., and Sullivan, J. 1995. Stable expression and pharmacological properties of the human alpha 7 nicotinic acetylcholine receptor. *European journal of pharmacology* 290, 3, 237–246.
- [116] Gordon, J., Inns, R., Johnson, M., Leadbeater, L., Maidment, M., Upshall, D., Cooper, G., and Rickard, R. 1983. The delayed neuropathic effects of nerve agents and some other organophosphorus compounds. *Archives of toxicology* 52, 2, 71–82.
- [117] Gotti, C. and Clementi, F. 2004. Neuronal nicotinic receptors: from structure to pathology. *Progress in neurobiology* 74, 6, 363–396.
- [118] Gotti, C., Zoli, M., and Clementi, F. 2006. Brain nicotinic acetylcholine receptors: native subtypes and their relevance. *Trends in pharmacological sciences* 27, 9, 482–491.
- [119] Grando, S. 1997. Biological functions of keratinocyte cholinergic receptors. *The journal of investigative dermatology. Symposium proceedings* 2, 1, 41–48.
- [120] Grange-Messent, V., Bouchaud, C., Jamme, M., Lallement, G., Foquin, A., and Carpentier, P. 1999. Seizure-related opening of the blood-brain barrier produced by the anticholinesterase compound, soman: new ultrastructural observations. *Cellular and molecular biology* 45, 1, 1–14.
- [121] Grob, D. and Harvey, A. M. 1953. The effects and treatment of nerve gas poisoning. *The American journal of medicine* 14, 1, 52–63.
- [122] Grønlien, J., Håkerud, M., Ween, H., Thorin-Hagene, K., Briggs, C., Gopalakrishnan, M., and Malysz, J. 2007. Distinct profiles of alpha7 nAChR positive allosteric modulation revealed by structurally diverse chemotypes. *Molecular pharmacology* 72, 3, 715–724.
- [123] Grubic, Z. and Tomazic, A. 1989. Mechanism of action of HI-6 on soman inhibition of acetylcholinesterase in preparations of rat and human skeletal muscle; comparison to SAD-128 and PAM-2. *Archives of toxicology* 63, 1, 68–71.
- [124] Grutter, T., Le Novère, N., and Changeux, J. 2004. Rational understanding of nicotinic receptors drug binding. *Current topics in medicinal chemistry* 4, 6, 645–650.

- [125] Gunnell, D., Eddleston, M., Phillips, M., and Konradsen, F. 2007. The global distribution of fatal pesticide self-poisoning: systematic review. *BMC public health* 7, 357.
- [126] Gupta, R. 2006. Introduction. In *Toxicology of Organophosphate & Carbamate Compounds*. Elsevier, 3–4.
- [127] Gupta, R. 2009. Introduction. In *Handbook of Toxicology of Chemical Warfare Agents*. Elsevier, 3–5.
- [128] Hamilton, M. and Lundy, P. 1989. HI-6 therapy of soman and tabun poisoning in primates and rodents. *Archives of toxicology* 63, 2, 144–149.
- [129] Harris, L., Heyl, W., Stitcher, D., and Broomfield, C. 1978. Effects of 1,1'-oxydimethylene bis-(4-tert-butylpyridinium chloride) (SAD-128) and decamethonium on reactivation of soman- and sarin-inhibited cholinesterase by oximes. *Biochemical pharmacology* 27, 5, 757–761.
- [130] Harris, R. and Paxman, J. 2002. A higher form of killing. The secret history of chemical and biological warfare. *Random House Trade Paperbacks*.
- [131] Hawrami, S. and Ibrahim, N. 2004. Experiencing chemical warfare: two physicians tell their story of Halabja in Northern Iraq. *Canadian journal of rural medicine: the official journal of the Society of Rural Physicians of Canada* 9, 3, 178–181.
- [132] Hayes, W. 1971. Studies on exposure during the use of anticholinesterase pesticides. *Bulletin of the World Health Organization* 44, 1-3, 277–288.
- [133] Heath, A. and Meredith, T. 1992. Atropine in the management of anticholinesterase poisoning. In *Clinical and Experimental Toxicology of Organophosphates and Carbamates*. Butterworth Heinemann, 543–554.
- [134] Hemmert, A., Otto, T., Wierdl, M., Edwards, C., Fleming, C., MacDonald, M., Cashman, J., Potter, P., Cerasoli, D., and Redinbo, M. 2010. Human carboxylesterase 1 stereoselectively binds the nerve agent cyclosarin and spontaneously hydrolyzes the nerve agent sarin. *Molecular pharmacology* 77, 4, 508–516.
- [135] Hibbs, R. and Gouaux, E. 2011. Principles of activation and permeation in an anion-selective Cys-loop receptor. *Nature* 474, 7349, 54–60.
- [136] Hille, B. 1992. Ionic channels of excitable membranes (2<sup>nd</sup> Edition). *Sinauer Associates*.
- [137] Hobbiger, F. 1963. Reactivation of Phosphorylated Acetylcholinesterase. In *Cholinesterases and Anticholinesterase Agents*. Handbook of Experimental Pharmacology. Springer, 921–988.
- [138] Hobbiger, F. 1976. Pharmacology of Anticholinesterase Drugs. In *Neuromuscular Junction*. Springer, 487–581.
- [139] Hobbiger, F., O'Sullivan, D., and Sadler, P. 1958. New potent reactivators of acetochoinesterase inhibited by tetraethyl pyrophosphate. *Nature* 182, 4648, 1498–1499.
- [140] Hodgkin, A. and Keynes, R. 1955. Active transport of cations in giant axons from Sepia and Loligo. *The Journal of physiology* 128, 1, 28–60.
- [141] Hogg, R., Buisson, B., and Bertrand, D. 2005. Allosteric modulation of ligand-gated ion channels. *Biochemical pharmacology* 70, 9, 1267–1276.
- [142] Holmstedt, B. 1959. Pharmacology of organophosphorus cholinesterase inhibitors. *Pharmacological reviews* 11, 567–688.
- [143] Holmstedt, B. 1963. Structure-Activity Relationships of the Organophosphorus Anticholinesterase Agents. In *Cholinesterases and Anticholinesterase Agents*. Handbook of Experimental Pharmacology. Springer, 428–485.
- [144] Hsiao, B., Dweck, D., and Luetje, C. 2001. Subunit-dependent modulation of neuronal nicotinic receptors by zinc. *The Journal of neuroscience: the official journal of the Society for Neuroscience* 21, 6, 1848–1856.



- [145] Hsiao, B., Mihalak, K., Repicky, S., Everhart, D., Mederos, A., Malhotra, A., and Luetje, C. 2006. Determinants of zinc potentiation on the  $\alpha 4$  subunit of neuronal nicotinic receptors. *Molecular pharmacology* 69, 1, 27–36.
- [146] Huang, Y. J., Huang, Y., Baldassarre, H., Wang, B., Lazaris, A., Leduc, M., Bilodeau, A., Bellemare, A., Côté, M., Herskovits, P., Touati, M., Turcotte, C., Valeanu, L., Lemée, N., Wilgus, H., Bégin, I., Bhatia, B., Rao, K., Neveu, N., Brochu, E., Pierson, J., Hockley, D., Cerasoli, D., Lenz, D., Karatzas, C., and Langermann, S. 2007. Recombinant human butyrylcholinesterase from milk of transgenic animals to protect against organophosphate poisoning. *Proceedings of the National Academy of Sciences of the United States of America* 104, 34, 13603–13608.
- [147] Huang, Y., Lundy, P., Lazaris, A., Huang, Y., Baldassarre, H., Wang, B., Turcotte, C., Côté, M., Bellemare, A., Bilodeau, A., Brouillard, S., Touati, M., Herskovits, P., Bégin, I., Neveu, N., Brochu, E., Pierson, J., Hockley, D., Cerasoli, D., Lenz, D., Wilgus, H., Karatzas, C., and Langermann, S. 2008. Substantially improved pharmacokinetics of recombinant human butyrylcholinesterase by fusion to human serum albumin. *BMC biotechnology* 8, 50.
- [148] Hurst, R., Rollema, H., and Bertrand, D. 2013. Nicotinic acetylcholine receptors: from basic science to therapeutics. *Pharmacology & therapeutics* 137, 1, 22–54.
- [149] Hurst, R., Hajós, M., Raggenbass, M., Wall, T., Higdon, N., Lawson, J., Rutherford-Root, K., Berkenpas, M., Hoffmann, W., Piotrowski, D., Groppi, V., Allaman, G., Ogier, R., Bertrand, S., Bertrand, D., and Arneric, S. P. 2005. A novel positive allosteric modulator of the  $\alpha 7$  neuronal nicotinic acetylcholine receptor: in vitro and in vivo characterization. *The Journal of neuroscience : the official journal of the Society for Neuroscience* 25, 17, 4396–4405.
- [150] Inns, R. and Leadbeater, L. 1983. The efficacy of bispyridinium derivatives in the treatment of organophosphonate poisoning in the guinea-pig. *The Journal of pharmacy and pharmacology* 35, 7, 427–433.
- [151] Jayapal, K., Wlaschin, K., and Hu, W. 2007. Recombinant Protein Therapeutics from CHO cells - 20 Years and Counting. CHO consortium. *Chemical Engineering Progress* 103, 10, 40–47.
- [152] Jensen, A., Frølund, B., Liljefors, T., and Krogsaard-Larsen, P. 2005. Neuronal nicotinic acetylcholine receptors: structural revelations, target identifications, and therapeutic inspirations. *Journal of medicinal chemistry* 48, 15, 4705–4745.
- [153] Jensen, A., Mikkelsen, I., Frølund, B., Bräuner-Osborne, H., Falch, E., and Krogsaard-Larsen, P. 2003. Carbamoylcholine homologs: novel and potent agonists at neuronal nicotinic acetylcholine receptors. *Molecular pharmacology* 64, 4, 865–875.
- [154] Jensen, A., Mikkelsen, I., Frølund, B., Bräuner-Osborne, H., Falch, E., and Krogsaard-Larsen, P. 2003. Carbamoylcholine homologs: novel and potent agonists at neuronal nicotinic acetylcholine receptors. *Molecular pharmacology* 64, 4, 865–875.
- [155] Jensen, A., Mikkelsen, I., Frølund, B., Frydenvang, K., Brehm, L., Jaroszewski, J. W., Bräuner-Osborne, H., Falch, E., and Krogsaard-Larsen, P. 2004. Carbamoylcholine homologs: synthesis and pharmacology at nicotinic acetylcholine receptors. *European journal of pharmacology* 497, 2, 125–137.
- [156] Kandel, E., Schwartz, J., Jessell, T., Siegelbaum, S., and Hudspeth, A. 2012. Principles of neural science (5<sup>th</sup> Edition). *McGraw-Hill*.
- [157] John, H., Balszuweit, F., Kehe, K., Worek, F., and Thiermann, H. 2009. Toxicokinetics of Chemical Warfare Agents. In *Handbook of Toxicology of Chemical Warfare Agents*. Elsevier 755–790.

- [158] Jokanović, M. and Stojiljković, M. 2006. Current understanding of the application of pyridinium oximes as cholinesterase reactivators in treatment of organophosphate poisoning. *European journal of pharmacology* 553, 1-3, 10–17.
- [159] Jones, S. 1993. Muscarinic receptor subtypes: modulation of ion channels. *Life sciences* 52, 5-6, 457–464.
- [160] Josse, D., Lockridge, O., Xie, W., Bartels, C., Schopfer, L., and Masson, P. 2001. The active site of human paraoxonase (PON1). *Journal of applied toxicology : JAT* 21 Suppl 1, S7-11.
- [161] Josse, D., Xie, W., Masson, P., and Lockridge, O. 1999. Human serum paraoxonase (PON1): identification of essential amino acid residues by group-selective labelling and site-directed mutagenesis. *Chemico-Biological Interactions* 119-120, 71–78.
- [162] Kalamida, D., Poulas, K., Avramopoulou, V., Fostieri, E., Lagoumintzis, G., Lazaridis, K., Sideri, A., Zouridakis, M., and Tzartos, S. J. 2007. Muscle and neuronal nicotinic acetylcholine receptors. Structure, function and pathogenicity. *The FEBS journal* 274, 15, 3799–3845.
- [163] Karlin, A. 2002. Emerging structure of the nicotinic acetylcholine receptors. *Nature reviews. Neuroscience* 3, 2, 102–114.
- [164] Kassa, J., Jun, D., and Kuca, K. 2006. The reactivating and therapeutic efficacy of oximes to counteract Russian VX poisonings. *International journal of toxicology* 25, 5, 397–401.
- [165] Kassa, J., Pohanka, M., Timperley, C., Bird, M., Green, A. C., and Tattersall, J. 2016. Evaluation of the benefit of the bispyridinium compound MB327 for the antidotal treatment of nerve agent-poisoned mice. *Toxicology Mechanisms and Methods* 26, 5, 334–339.
- [166] Kawashima, K. and Fujii, T. 2003. The lymphocytic cholinergic system and its biological function. *Life sciences* 72, 18-19, 2101–2109.
- [167] Khare, S., Kipnis, Y., Greisen, P., Takeuchi, R., Ashani, Y., Goldsmith, M., Song, Y., Gallaher, J. L., Silman, I., Leader, H., Sussman, J., Stoddard, B., Tawfik, D., and Baker, D. 2012. Computational redesign of a mononuclear zinc metalloenzyme for organophosphate hydrolysis. *Nature chemical biology* 8, 3, 294–300.
- [168] Kiderlen, D., Eyer, P., and Worek, F. 2005. Formation and disposition of diethylphosphoryl-obidoxime, a potent anticholinesterase that is hydrolyzed by human paraoxonase (PON1). *Biochemical pharmacology* 69, 12, 1853–1867.
- [169] Kloog, Y., Galron, R., Balderman, D., and Sokolovsky, M. 1985. Reversible and irreversible inhibition of rat brain muscarinic receptors is related to different substitutions on bisquaternary pyridinium oximes. *Archives of toxicology* 58, 1, 37–39.
- [170] Koelle, G. 1994. Pharmacology of organophosphates. *Journal of applied toxicology*. 14, 2, 105–109.
- [171] Koplovitz, I. and Stewart, J. 1992. Efficacy of oxime plus atropine treatment against soman poisoning in the atropinesterase-free rabbit. *Drug and chemical toxicology* 15, 2, 117–126.
- [172] Kubo, T., Fukuda, K., Mikami, A., Maeda, A., Takahashi, H., Mishina, M., Haga, T., Haga, K., Ichiyama, A., and Kangawa, K. 1986. Cloning, sequencing and expression of complementary DNA encoding the muscarinic acetylcholine receptor. *Nature* 323, 6087, 411–416.
- [173] Kubo, T., Maeda, A., Sugimoto, K., Akiba, I., Mikami, A., Takahashi, H., Haga, T., Haga, K., Ichiyama, A., and Kangawa, K. 1986. Primary structure of porcine cardiac muscarinic acetylcholine receptor deduced from the cDNA sequence. *FEBS letters* 209, 2, 367–372.
- [174] Kuca, K., Jun, D., Cabal, J., Hrabínova, M., Bartosova, L., and Opletalova, V. 2006. Russian VX: inhibition and reactivation of acetylcholinesterase compared with VX agent. *Basic & clinical pharmacology & toxicology* 98, 4, 389–394.

- [175] Kuhnlen-Clausen, D. 1972. Structure-activity relationship of mono- and bisquaternary pyridines in regard to their parasympholytic effects. *Toxicology and applied pharmacology* 23, 3, 443–454.
- [176] Kuryatov, A., Mukherjee, J., and Lindstrom, J. 2013. Chemical chaperones exceed the chaperone effects of RIC-3 in promoting assembly of functional  $\alpha 7$  AChRs. *PloS one* 8, 4, e62246.
- [177] Kusić, R., Bosković, B., Vojvodić, V., and Jovanović, D. 1985. HI-6 in man: blood levels, urinary excretion, and tolerance after intramuscular administration of the oxime to healthy volunteers. *Fundamental and applied toxicology : official journal of the Society of Toxicology* 5, 6, 89-97.
- [178] Lange, W., and von Krueger, G. 1932. Über Ester der Monofluorophosphorsäure. *Berichte der Deutschen Chemischen Gesellschaft* 9, 1598–1601.
- [179] Leadbeater, L., Inns, R., and Rylands, J. 1985. Treatment of poisoning by soman. *Fundamental and applied toxicology : official journal of the Society of Toxicology* 5, 6 Pt 2, S225-31.
- [180] Legay, C. 2000. Why so many forms of acetylcholinesterase? *Microscopy research and technique* 49, 1, 56–72.
- [181] Leicester, H. 1958. Some Aspects of the Chemistry and Toxic Action of Organic Compounds Containing Phosphorous and Fluorine (Saunders, Bernard Charles). *Journal of Chemical Education* 35, 5, A235.
- [182] Léna, C. and Changeux, J. 1998. Allosteric nicotinic receptors, human pathologies. *Journal of physiology, Paris* 92, 2, 63–74.
- [183] Lenz, D., Maxwell, D., Koplovitz, I., Clark, C., Capacio, B., Cerasoli, D., Federko, J., Luo, C., Saxena, A., Doctor, B., and Olson, C. 2005. Protection against soman or VX poisoning by human butyrylcholinesterase in guinea pigs and cynomolgus monkeys. *Chemico-Biological Interactions* 157-158, 205–210.
- [184] Lewis, N., Liu, X., Li, Y., Nagarajan, H., Yerganian, G., O'Brien, E., Bordbar, A., Roth, A., Rosenbloom, J., Bian, C., Xie, M., Chen, W., Li, N., Baycin-Hizal, D., Latif, H., Forster, J., Betenbaugh, M. J., Famili, I., Xu, X., Wang, J., and Palsson, B. O. 2013. Genomic landscapes of Chinese hamster ovary cell lines as revealed by the *Cricetulus griseus* draft genome. *Nature biotechnology* 31, 8, 759–765.
- [185] Li, X., Shimada, K., Showalter, L., and Weinman, S. A. 2000. Biophysical properties of CIC-3 differentiate it from swelling-activated chloride channels in Chinese hamster ovary-K1 cells. *The Journal of biological chemistry* 275, 46, 35994–35998.
- [186] Lindstrom, J. 2000. Acetylcholine receptors and myasthenia. *Muscle & nerve* 23, 4, 453–477.
- [187] Liu, Y., and Wu, S. 2003. Block of erg current by linoleoylamide, a sleep-inducing agent, in pituitary GH3 cells. *European journal of pharmacology* 458, 1-2, 37–47.
- [188] Lleó, A., Greenberg, S., and Growdon, J. 2006. Current pharmacotherapy for Alzheimer's disease. *Annual review of medicine* 57, 513–533.
- [189] Löffler M. 1986. Quartäre Salze von Pyridin-2,4- Diallyloxim als Gegenmittel für Organophosphat- Vergiftungen. *PhD Thesis, Albert Ludwigs Universität*.
- [190] Lotti, M. 1991. The pathogenesis of organophosphate polyneuropathy. *Critical reviews in toxicology* 21, 6, 465–487.
- [191] Lotti, M. and Moretto, A. 2005. Organophosphate-induced delayed polyneuropathy. *Toxicological reviews* 24, 1, 37–49.
- [192] Luettringhaus, A. and Hagedorn, I. 1964. Quartäre Hydroxyiminomethyl-Pyridiniumsalze. *Arzneimittel-Forschung* 14, 1–5.

- [193] Lukas, R. J., Changeux, J., Le Novère, N., Albuquerque, E., Balfour, D., Berg, D., Bertrand, D., Chiappinelli, V., Clarke, P., Collins, A., Dani, J., Grady, S., Kellar, K., Lindstrom, J., Marks, M., Quik, M., Taylor, P., and Wonnacott, S. 1999. International Union of Pharmacology. XX. Current status of the nomenclature for nicotinic acetylcholine receptors and their subunits. *Pharmacological reviews* 51, 2, 397–401.
- [194] Lundy, P., Goulet, J., and Hand, B. 1989. Hormone- and dose schedule-dependent protection by HI-6 against soman and tabun poisoning. *Fundamental and applied toxicology : official journal of the Society of Toxicology* 12, 3, 595–603.
- [195] Macilwain, C. 1993. Study proves Iraq used nerve gas. *Nature* 363, 6424, 3.
- [196] Macklin, K., Maus, A., Pereira, E., Albuquerque, E., and Conti-Fine, B. 1998. Human vascular endothelial cells express functional nicotinic acetylcholine receptors. *The Journal of pharmacology and experimental therapeutics* 287, 1, 435–439.
- [197] Maelicke, A., Samochocki, M., Jostock, R., Fehrenbacher, A., Ludwig, J., Albuquerque, E., and Zerlin, M. 2001. Allosteric sensitization of nicotinic receptors by galantamine, a new treatment strategy for Alzheimer's disease. *Biological psychiatry* 49, 3, 279–288.
- [198] Maksimovic', M., Kovacevic', V., Binenfeld, Z. 1989. Protective and reactivating effects of HI-6-Toxogonin mixture in rats and guinea-pigs poisoned by nerve agents. *Acta Pharm. Jugosl.*, 39, 27–33.
- [199] Marrs, T. 2007. Toxicology of Organophosphate Nerve Agents. In *Chemical Warfare Agents*. John Wiley & Sons 191–221.
- [200] Marrs, T., Maynard, R., and Sidell, F. 2007. Chemical warfare agents. Toxicology and treatment. John Wiley & Sons.
- [201] Masson, P. 2016. Nerve Agents: Catalytic Scavengers as an Alternative Approach for Medical Countermeasures. In *Chemical Warfare Toxicology*, Worek, F., Jenner, J., and Thiermann, H. Royal Society of Chemistry 43–81.
- [202] Masson, P., Josse, D., Lockridge, O., Viguié, N., Taupin, C., and Buhler, C. 1998. Enzymes hydrolyzing organophosphates as potential catalytic scavengers against organophosphate poisoning. *Journal of physiology, Paris* 92, 5-6, 357–362.
- [203] Mathes, C. 2006. QPatch: the past, present and future of automated patch clamp. *Expert opinion on therapeutic targets* 10, 2, 319–327.
- [204] Maxwell, D. 1992. The specificity of carboxylesterase protection against the toxicity of organophosphorus compounds. *Toxicology and applied pharmacology* 114, 2, 306–312.
- [205] Maynard, R. and Beswick, F. 1992. Organophosphorus compounds as chemical warfare agents. In *Clinical and Experimental Toxicology of Organophosphates and Carbamates*. Elsevier, 373–385.
- [206] Mazurov, A., Hauser, T., and Miller, C. 2006. Selective alpha7 nicotinic acetylcholine receptor ligands. *Current medicinal chemistry* 13, 13, 1567–1584.
- [207] McCauley, L. 2009. Epidemiology of Chemical Warfare Agents. In *Handbook of Toxicology of Chemical Warfare Agents*. Elsevier, 33–39.
- [208] McDonough, J. and Shih, T. 1993. Pharmacological modulation of soman-induced seizures. *Neuroscience and biobehavioral reviews* 17, 2, 203–215.
- [209] McDonough, J. and Shih, T. 2007. Atropine and Other Anticholinergic Drugs. In *Chemical Warfare Agents*. John Wiley & Sons 287–303.
- [210] McDonough, J., Zoeffel, L., McMonagle, J., Copeland, T., Smith, C., and Shih, T. 2000. Anticonvulsant treatment of nerve agent seizures: anticholinergics versus diazepam in soman-intoxicated guinea pigs. *Epilepsy research* 38, 1, 1–14.

- [211] Melchers, B., van der Laaken, A., and van Helden, H. 1991. On the mechanism whereby HI-6 improves neuromuscular function after oxime-resistant acetylcholinesterase inhibition and subsequent impairment of neuromuscular transmission. *European journal of pharmacology* 200, 2-3, 331–337.
- [212] Mesic', M., Deljac, A., Deljac, V., Binenfeld, Z., Kilbarda, V., Maksimovic', M., Kovacevic', V. 1991. Reactivations of acetylcholinesterase inhibited by organophosphorus compounds. Imidazole derivatives. II. *Acta Pharm. Jugosl.*, 41, 203–210.
- [213] Michaelis C. 1903. Über die organischen Verbindungen des Phosphors mit Sauerstoff. *Liebigs Annalen der Chemie*, 326, 129–258.
- [214] Michel, H., Hackley, B., Berkowitz, L., List, G., Hackley, E., Gillilan, W., and Pankau, M. 1967. Ageing and dealkylation of Soman (pinacolylmethylphosphonofluoridate)-inactivated eel cholinesterase. *Archives of biochemistry and biophysics* 121, 1, 29–34.
- [215] Mihalak, K., Carroll, F., and Luetje, C. 2006. Varenicline is a partial agonist at  $\alpha 4\beta 2$  and a full agonist at  $\alpha 7$  neuronal nicotinic receptors. *Molecular pharmacology* 70, 3, 801–805.
- [216] Mikler, J., Tenn, C., Worek, F., Reiter, G., Thiermann, H., Garrett, M., Bohnert, S., and Sawyer, T. W. 2011. Immobilization of Russian VX skin depots by localized cooling: Implications for decontamination and medical countermeasures. *Toxicology letters* 206, 1, 47–53.
- [217] Milatović, D. and Jokanović, M. 2009. Pyridinium Oximes as Cholinesterase Reactivators in the Treatment of OP Poisoning. In *Handbook of Toxicology of Chemical Warfare Agents*. Elsevier, 985–996.
- [218] Millard, C., Kryger, G., Ordentlich, A., Greenblatt, H., Harel, M., Raves, M., Segall, Y., Barak, D., Shafferman, A., Silman, I., and Sussman, J. 1999. Crystal Structures of Aged Phosphorylated Acetylcholinesterase: Nerve Agent Reaction Products at the Atomic Level †,‡. *Biochemistry* 38, 22, 7032–7039.
- [219] Milligan, C., Li, J., Sukumar, P., Majeed, Y., Dallas, M., English, A., Emery, P., Porter, K., Smith, A., McFadzean, I., Beccano-Kelly, D., Bahnasi, Y., Cheong, A., Naylor, J., Zeng, F., Liu, X., Gamper, N., Jiang, L., Pearson, H., Peers, C., Robertson, B., and Beech, D. 2009. Robotic multiwell planar patch-clamp for native and primary mammalian cells. *Nature protocols* 4, 2, 244–255.
- [220] Mishina, M., Takai, T., Imoto, K., Noda, M., Takahashi, T., Numa, S., Methfessel, C., and Sakmann, B. 1986. Molecular distinction between fetal and adult forms of muscle acetylcholine receptor. *Nature* 321, 6068, 406–411.
- [221] Molleman, A. 2002. Patch Clamping. *John Wiley & Sons*.
- [222] Monjaraz, E., Navarrete, A., Lopez-Santiago, L., Vega, A., Arias-Montaña, J., and Cota, G. 2000. L-type calcium channel activity regulates sodium channel levels in rat pituitary GH3 cells. *The Journal of physiology* 523 Pt 1, 45–55.
- [223] Morita, H., Yanagisawa, N., Nakajima, T., Shimizu, M., Hirabayashi, H., Okudera, H., Nohara, M., Midorikawa, Y., and Mimura, S. 1995. Sarin poisoning in Matsumoto, Japan. *Lancet* 346, 8970, 290–293.
- [224] Moshiri, M., Darchini-Maragheh, E., and Balali-Mood, M. 2012. Advances in toxicology and medical treatment of chemical warfare nerve agents. *Daru : journal of Faculty of Pharmacy, Tehran University of Medical Sciences* 20, 1, 81.
- [225] Mumford, H., Docx, C., Price, M., Green, A., Tattersall, J., and Armstrong, S. 2013. Human plasma-derived BuChE as a stoichiometric bioscavenger for treatment of nerve agent poisoning. *Chemico-Biological Interactions* 203, 1, 160–166.

- [226] Nagao, M., Takatori, T., Matsuda, Y., Nakajima, M., Iwase, H., and Iwadate, K. 1997. Definitive Evidence for the Acute Sarin Poisoning Diagnosis in the Tokyo Subway. *Toxicology and applied pharmacology* 144, 1, 198–203.
- [227] Neher, E. and sakmann, B. 1976. Single-channel currents recorded from membrane of denervated frog muscle fibres. *Nature* 260, 5554, 799–802.
- [228] Nelson, D. and Cox, M. 2013. *Lehninger Principles of biochemistry*. W.H. Freeman, New York, N.Y.
- [229] Niessen, K., Seeger, T., Tattersall, J., Timperley, C., Bird, M., Green, C., Thiermann, H., and Worek, F. 2013. Affinities of bispyridinium non-oxime compounds to [(3)H]epibatidine binding sites of *Torpedo californica* nicotinic acetylcholine receptors depend on linker length. *Chemico-Biological Interactions* 206, 3, 545–554.
- [230] Niessen, K., Tattersall, J., Timperley, C., Bird, M., Green, C., Seeger, T., Thiermann, H., and Worek, F. 2011. Interaction of bispyridinium compounds with the orthosteric binding site of human  $\alpha 7$  and *Torpedo californica* nicotinic acetylcholine receptors (nAChRs). *Toxicology letters* 206, 1, 100–104.
- [231] Nozaki, H., Aikawa, N., Fujishima, S., Suzuki, M., Shinozawa, Y., Hori, S., and Nogawa, S. 1995. A case of VX poisoning and the difference from sarin. *Lancet* 346, 8976, 698–699.
- [232] Numberger, M. and Draguhn, A. 1996. Patch-clamp-Technik. Labor im Fokus. *Spektrum*.
- [233] O'Brien, R. 1960. Toxic phosphorus esters. Chemistry, metabolism, and biological effects. *Academic Press*.
- [234] Oda, Y. 1999. Choline acetyltransferase: the structure, distribution and pathologic changes in the central nervous system. *Pathology international* 49, 11, 921–937.
- [235] Okonjo, K., Kuhlmann, J., and Maelicke, A. 1991. A second pathway of activation of the *Torpedo* acetylcholine receptor channel. *European journal of biochemistry* 200, 3, 671–677.
- [236] Okudera, H., Morita, H., Iwashita, T., Shibata, T., Otagiri, T., Kobayashi, S., and Yanagisawa, N. 1997. Unexpected nerve gas exposure in the city of Matsumoto: report of rescue activity in the first sarin gas terrorism. *The American journal of emergency medicine* 15, 5, 527–528.
- [237] Okumura, T., Takasu, N., Ishimatsu, S., Miyanoki, S., Mitsuhashi, A., Kumada, K., Tanaka, K., and Hinohara, S. 1996. Report on 640 victims of the Tokyo subway sarin attack. *Annals of emergency medicine* 28, 2, 129–135.
- [238] Oldiges, H. and Schoene, K. 1970. Pyridinium- und Imidazoliumsalze als Antidote gegenüber Soman- und Paraoxonvergiftungen bei Mäusen. *Archiv für Toxikologie* 26, 4, 293–305.
- [239] O'Leary, C. A. 2002. The Kurds of Iraq: recent history, future prospects. *Middle East Review of International Affairs Journal*, 6, 4, 17–29.
- [240] Ooi, G., Tawadros, N., and Escalona, R. 2004. Pituitary cell lines and their endocrine applications. *Molecular and cellular endocrinology* 228, 1-2, 1–21.
- [241] OPCW - Organization for the prohibition of chemical weapons. *Conference of the States Parties of the Organisation for the Prohibition of Chemical Weapons (OPCW)*. <https://www.opcw.org/about-opcw/conference-of-the-states-parties>. Accessed 22 April 2017.
- [242] OPCW - Organization for the prohibition of chemical weapons. *Internal Vision*. <https://www.opcw.org/about-opcw/opcw-internal-vision>. Accessed 22 April 2017.
- [243] OPCW - Organization for the prohibition of chemical weapons. *Member States of the Organisation for the Prohibition of Chemical Weapons (OPCW)*. <https://www.opcw.org/about-opcw/member-states>. Accessed 22 April 2017.

- [244] OPCW - Organization for the prohibition of chemical weapons. 1993. *Convention on the Prohibition the Development, Production, Stockpiling and use of Chemical Weapons and on their destruction*, The Hague.
- [245] OPCW - Organization for the prohibition of chemical weapons. 2002. *Report of the OPCW on the implementation of the convention on the prohibition of the development, production, stockpiling and use of chemical weapons and on their destruction, in the year 2001. (C-7/3, Annex 6, OPCW)*, The Hague.
- [246] OPCW - Organization for the prohibition of chemical weapons. 2006. *Basic facts on chemical disarmament. 6th edn*, The Hague.
- [247] Ortells, M. and Lunt, G. 1995. Evolutionary history of the ligand-gated ion-channel superfamily of receptors. *Trends in neurosciences* 18, 3, 121–127.
- [248] Ozawa, S. and Sand, O. 1986. Electrophysiology of excitable endocrine cells. *Physiological reviews* 66, 4, 887–952.
- [249] Patocka, J., Kuca, K., and Jun, D. 2004. Acetylcholinesterase and butyrylcholinesterase--important enzymes of human body. *Acta medica* 47, 4, 215–228.
- [250] Pavlov, V. and Tracey, K. 2005. The cholinergic anti-inflammatory pathway. *Brain, behavior, and immunity* 19, 6, 493–499.
- [251] Peralta, E., Ashkenazi, A., Winslow, J., Smith, D., Ramachandran, J., and Capon, D. J. 1987. Distinct primary structures, ligand-binding properties and tissue-specific expression of four human muscarinic acetylcholine receptors. *The EMBO journal* 6, 13, 3923–3929.
- [252] Pereira, E., Alkondon, M., Reinhardt, S., Maelicke, A., Peng, X., Lindstrom, J., Whiting, P., and Albuquerque, E. 1994. Physostigmine and galanthamine: probes for a novel binding site on the alpha 4 beta 2 subtype of neuronal nicotinic acetylcholine receptors stably expressed in fibroblast cells. *The Journal of pharmacology and experimental therapeutics* 270, 2, 768–778.
- [253] Pereira, E., Reinhardt-Maelicke, S., Schratzenholz, A., Maelicke, A., and Albuquerque, E. 1993. Identification and functional characterization of a new agonist site on nicotinic acetylcholine receptors of cultured hippocampal neurons. *The Journal of pharmacology and experimental therapeutics* 265, 3, 1474–1491.
- [254] Peter, J., Sudarsan, T., and Moran, J. 2014. Clinical features of organophosphate poisoning: A review of different classification systems and approaches. *Indian journal of critical care medicine : peer-reviewed, official publication of Indian Society of Critical Care Medicine* 18, 11, 735–745.
- [255] Pita, R. and Domingo, J. 2014. The Use of Chemical Weapons in the Syrian Conflict. *Toxics* 2, 3, 391–402.
- [256] Poziomek, E. J., Hackley, B. E., and Steinberg, G. M. 1958. Pyridinium Aldoximes 1. *Journal of Organic Chemistry* 23, 5, 714–717.
- [257] Price, M., Docx, C., Rice, H., Fairhall, S., Poole, S., Bird, M., Whiley, L., Flint, D., Green, A., Timperley, C., and Tattersall, J. 2016. Pharmacokinetic profile and quantitation of protection against soman poisoning by the antinicotinic compound MB327 in the guinea-pig. *Toxicology letters* 244, 154–160.
- [258] Puck, T., Cieciura, S., and Robinson, A. 1958. Genetics of somatic mammalian cells. III. Long-term cultivation of euploid cells from human and animal subjects. *The Journal of experimental medicine* 108, 6, 945–956.
- [259] Quinn, D. 1987. Acetylcholinesterase: enzyme structure, reaction dynamics, and virtual transition states. *Chemistry Review.* 87, 5, 955–979.

- [260] Radic Z. and Taylor P. 2006. Esterases, Receptors, Mechanisms, & Tolerance Development. In *Toxicology of Organophosphate and Carbamate Compounds*. Elsevier, 161–270.
- [261] Raftery, M., Hunkapiller, ., Strader, C., and Hood, L. 1980. Acetylcholine receptor: complex of homologous subunits. *Science* 208, 4451, 1454–1456.
- [262] Rappenglück, S., Niessen, K., Seeger, T., Worek, F., Thiermann, H., Wanner K. 2017. Regioselective and Transition-Metal-Free Addition of *tert* - Butyl Magnesium Reagents to Pyridine Derivatives: A Convenient Method for the Synthesis of 3-Substituted 4-*tert*-Butylpyridine Derivatives. *Synthesis*, 24.
- [263] Redinbo, M., Bencharit, S., and Potter, P. 2003. Human carboxylesterase 1: from drug metabolism to drug discovery. *Biochemical Society transactions* 31, 620–624.
- [264] Reiter, G., Mikler, J., Hill, I., Weatherby, K., Thiermann, H., and Worek, F. 2008. Chromatographic resolution, characterisation and quantification of VX enantiomers in hemolysed swine blood samples. *Journal of chromatography. B, Analytical technologies in the biomedical and life sciences* 873, 1, 86–94.
- [265] Rice, H. 2016. Toxicology of Organophosphorus Nerve Agents. In Chemical Warfare Toxicology, Worek, F., Jenner, J., and Thiermann, H. *Royal Society of Chemistry*, 81–116.
- [266] Rickett, D., Glenn, J., and Beers, E. 1986. Central respiratory effects versus neuromuscular actions of nerve agents. *Neurotoxicology* 7, 1, 225–236.
- [267] Rider, J., Moeller, H., Puletti, E., and Swader, J. 1969. Toxicity of parathion, systox, octamethyl pyrophosphoramidate, and methyl parathion in man. *Toxicology and applied pharmacology* 14, 3, 603–611.
- [268] Ring, A., Strom, B., Turner, S., Timperley, C., Bird, M., Green, A., Chad, J., Worek, F., and Tattersall, J. 2015. Bispyridinium Compounds Inhibit Both Muscle and Neuronal Nicotinic Acetylcholine Receptors in Human Cell Lines. *PloS one* 10, 8, e0135811.
- [269] Ring, A., Strom, B., Turner, S., Timperley, C., Bird, M., Green, A., Chad, J., Worek, F., and Tattersall, J. 2015. Bispyridinium Compounds Inhibit Both Muscle and Neuronal Nicotinic Acetylcholine Receptors in Human Cell Lines. *PloS one* 10, 8, e0135811.
- [270] Roberts, D., Karunarathna, A., Buckley, N., Manuweera, G., Sheriff, M., and Eddleston, M. 2003. Influence of pesticide regulation on acute poisoning deaths in Sri Lanka. *Bulletin of the World Health Organization* 81, 11, 789–798.
- [271] Robertson, B. and Owen, . 1993. Pharmacology of a cloned potassium channel from mouse brain (MK-1) expressed in CHO cells: effects of blockers and an 'inactivation peptide'. *British journal of pharmacology* 109, 3, 725–735.
- [272] Rochu, D., Chabrière, E., and Masson, P. 2007. Human paraoxonase: a promising approach for pre-treatment and therapy of organophosphorus poisoning. *Toxicology* 233, 1-3, 47–59.
- [273] Rollema, H., Chambers, L., Coe, J., Glowa, J., Hurst, R., Lebel, L., Lu, Y., Mansbach, R., Mather, R., Rovetti, C., Sands, S., Schaeffer, E., Schulz, D., Tingley, F., and Williams, K. 2007. Pharmacological profile of the alpha4beta2 nicotinic acetylcholine receptor partial agonist varenicline, an effective smoking cessation aid. *Neuropharmacology* 52, 3, 985–994.
- [274] Rollema, H., Coe, J., Chambers, L., Hurst, R., Stahl, S., and Williams, K. 2007. Rationale, pharmacology and clinical efficacy of partial agonists of alpha4beta2 nACh receptors for smoking cessation. *Trends in pharmacological sciences* 28, 7, 316–325.
- [275] Romanelli, M., Gratterer, P., Guandalini, L., Martini, E., Bonaccini, C., and Gualtieri, F. 2007. Central nicotinic receptors: structure, function, ligands, and therapeutic potential. *ChemMedChem* 2, 6, 746–767.



- [276] Romanelli, M. and Gualtieri, F. 2003. Cholinergic nicotinic receptors: competitive ligands, allosteric modulators, and their potential applications. *Medicinal research reviews* 23, 4, 393–426.
- [277] Romano, C. and Goldstein, A. 1980. Stereospecific nicotine receptors on rat brain membranes. *Science* 210, 4470, 647–650.
- [278] Rosenbaum, C. and Bird, S. 2010. Non-muscarinic therapeutic targets for acute organophosphorus poisoning. *Journal of medical toxicology : official journal of the American College of Medical Toxicology* 6, 4, 408–412.
- [279] Rosenberg, Y., Luo, C., Ashani, Y., Doctor, B., Fischer, R., Wolfe, G., and Saxena, A. 2002. Pharmacokinetics and immunologic consequences of exposing macaques to purified homologous butyrylcholinesterase. *Life sciences* 72, 2, 125–134.
- [280] Rosenberg, Y., Saxena, A., Sun, W., Jiang, X., Chilukuri, N., Luo, C., Doctor, B., and Lee, K. 2010. Demonstration of in vivo stability and lack of immunogenicity of a polyethyleneglycol-conjugated recombinant CHO-derived butyrylcholinesterase bioscavenger using a homologous macaque model. *Chemico-Biological Interactions* 187, 1-3, 279–286.
- [281] Rueter, L., Donnelly-Roberts, D., Curzon, P., Briggs, C., Anderson, D., and Bitner, R. 2006. A-85380: a pharmacological probe for the preclinical and clinical investigation of the alphabeta neuronal nicotinic acetylcholine receptor. *CNS drug reviews* 12, 2, 100–112.
- [282] Santos, M., Alkondon, M., Pereira, E., Aracava, Y., Eisenberg, H., Maelicke, A., and Albuquerque, E. 2002. The nicotinic allosteric potentiating ligand galantamine facilitates synaptic transmission in the mammalian central nervous system. *Molecular pharmacology* 61, 5, 1222–1234.
- [283] Saxena, A. and Luo, C., Chilukuri, N. Novel approaches to medical protection against chemical warfare nerve agents. In *Chemical Warfare Agents. John Wiley & Sons* 145–173.
- [284] Schlumberger, S., Kristan, K., Ota, K., Frangež, R., Molgó, J., Sepčić, K., Benoit, E., and Maček, P. 2014. Permeability characteristics of cell-membrane pores induced by ostreolysin A/pleurotolysin B, binary pore-forming proteins from the oyster mushroom. *FEBS letters* 588, 1, 35–40.
- [285] Schoene, K., Steinhanses, J., and Oldiges, H. 1976. Protective activity of pyridinium salts against soman poisoning in vivo and in vitro. *Biochemical pharmacology* 25, 17, 1955–1958.
- [286] Schrader, G. 1950. Organische Phosphor-Verbindungen als neuartige Insektizide (Auszug). *Angewandte Chemie* 62, 20, 471–473.
- [287] Schrader, G. 1952. Die Entwicklung neuer Insektizide auf Grundlage organischer Fluor- und Phosphor-Verbindungen. Monographien zu Angewandte Chemie und Chemieingenieur-Technik. *Chemie*.
- [288] Schrattenholz, A., Pereira, E., Roth, U., Weber, K., Albuquerque, E., and Maelicke, A. 1996. Agonist responses of neuronal nicotinic acetylcholine receptors are potentiated by a novel class of allosterically acting ligands. *Molecular pharmacology* 49, 1, 1–6.
- [289] Schwendimann, R., Burton, E., and Minagar, A. 2005. Management of myasthenia gravis. *American journal of therapeutics* 12, 3, 262–268.
- [290] Seeger, T., Eichhorn, M., Lindner, M., Niessen, K., Tattersall, J., Timperley, C., Bird, M., Green, A., Thiermann, H., and Worek, F. 2012. Restoration of soman-blocked neuromuscular transmission in human and rat muscle by the bispyridinium non-oxime MB327 in vitro. *Toxicology* 294, 2-3, 80–84.

- [291] Seeger, T., Niessen, K., Langer, P., Gerhardus, J., Worek, F., Friess, H., Bumm, R., Mihaljevic, A. L., and Thiermann, H. 2011. Restoration of nerve agent inhibited muscle force production in human intercostal muscle strips with HI 6. *Toxicology letters* 206, 1, 72–76.
- [292] Senanayake, N. and Karalliedde, L. 1987. Neurotoxic effects of organophosphorus insecticides. An intermediate syndrome. *The New England journal of medicine* 316, 13, 761–763.
- [293] Shafferman, A., Ordentlich, A., Barak, D., Stein, D., Ariel, N., and Velan, B. 1996. Aging of phosphorylated human acetylcholinesterase: catalytic processes mediated by aromatic and polar residues of the active centre. *The Biochemical journal* 318, 3, 833–840.
- [294] Shaw, K., Aracava, Y., Akaike, A., Daly, J., Rickett, D., and Albuquerque, E. 1985. The reversible cholinesterase inhibitor physostigmine has channel-blocking and agonist effects on the acetylcholine receptor-ion channel complex. *Molecular pharmacology* 28, 6, 527–538.
- [295] Sherby, S. M., Eldefrawi, A., Albuquerque, E., and Eldefrawi, M. 1985. Comparison of the actions of carbamate anticholinesterases on the nicotinic acetylcholine receptor. *Molecular pharmacology* 27, 3, 343–348.
- [296] Sheridan, R., Smith, A., Turner, S., and Tattersall, J. 2005. Nicotinic antagonists in the treatment of nerve agent intoxication. *Journal of the Royal Society of Medicine* 98, 3, 114–115.
- [297] Sheridan R., Beeson D., and Tattersall J. 2000. Non-competitive block of the human muscle adult nicotinic acetylcholine receptor ion channel by the bispyridinium compounds, SAD-128 (SAD), toxogonin (TOX) and HI-6. *European Journal of Neuroscience*, 12, 36.
- [298] Shih, T., Duniho, S., and McDonough, J. 2003. Control of nerve agent-induced seizures is critical for neuroprotection and survival. *Toxicology and applied pharmacology* 188, 2, 69–80.
- [299] Sidell, F. 1974. Soman and sarin: clinical manifestations and treatment of accidental poisoning by organophosphates. *Clinical toxicology* 7, 1, 1–17.
- [300] Sidell, F. 1997. Nerve agents. In *Textbook of Military Medicine. Medical Aspects of Chemical and Biological Warfare. Office of the Surgeon General*, 129–179.
- [301] Sidell, F. 2007. A History of Human Studies with Nerve Agents by the UK and USA. In *Chemical Warfare Agents. John Wiley & Sons* 223–239.
- [302] Sim, V., and Stubbs, J. 1960. VX Percutaneous Studies in Man. Army, Chemical. In U.S. Department of the Research and Development Laboratories. *Army Chemical Center*.
- [303] Sine, S., and Engel, A. 2006. Recent advances in Cys-loop receptor structure and function. *Nature* 440, 7083, 448–455.
- [304] Skryma, R., Prevarskaia, N., Vacher, P., and Dufy, B. 1994. Voltage-dependent Ca<sup>2+</sup> channels in Chinese hamster ovary (CHO) cells. *FEBS letters* 349, 2, 289–294.
- [305] Smith, M. 1930. The Pharmacological Action of Certain Phenol Esters, with Special Reference to the Etiology of So-Called Ginger Paralysis (Second Report). *Public Health Reports (1896-1970)* 45, 42, 2509.
- [306] Smythies, J. and Golomb, B. 2004. Nerve gas antidotes. *Journal of the Royal Society of Medicine* 97, 1, 32.
- [307] Somani, S., Solana R., and Dube S. 2000. Toxicodynamics of nerve agents. In *Chemical Warfare Agents: Toxicity at Low Levels. CRC Press*.
- [308] Standen, N., Davies, N., and Langton, P. 1994. Separation and analysis of macroscopic currents. The Plymouth Workshop Handbook. Microelectrode techniques. *The company of biologist*.
- [309] Stark, I. 1968. Versuche zur Darstellung eines LÜH6 (Toxogonin) überlegenen Acetylcholinesterase- Reaktivators. *Albert Ludwigs Universität*.
- [310] Stein, W. and Lieb, W. 1986. Transport and diffusion across cell membranes. *Elsevier*.

- [311] Steinbach, H. and Spiegelman, S. 1943. The sodium and potassium balance in squid nerve axoplasm. *Journal of Cellular and Comparative Physiology* 22, 2, 187–196.
- [312] Stock, P., Ljaschenko, D., Heckmann, M., and Dudel, J. 2014. Agonists binding nicotinic receptors elicit specific channel-opening patterns at  $\alpha\gamma$  and  $\alpha\delta$  sites. *The Journal of physiology* 592, 12, 2501–2517.
- [313] Stoelzle, S., Obergrussberger, A., Brüggemann, A., Haarmann, C., George, M., Kettenhofen, R., and Fertig, N. 2011. State-of-the-Art Automated Patch Clamp Devices: Heat Activation, Action Potentials, and High Throughput in Ion Channel Screening. *Frontiers in pharmacology* 2, 76.
- [314] Storch, A., Schrattenholz, A., Cooper, J. C., Abdel Ghani, E M, Gutbrod, O., Weber, K., Reinhardt, S., Lobron, C., Hermsen, B., and Soskić, V. 1995. Physostigmine, galanthamine and codeine act as 'noncompetitive nicotinic receptor agonists' on clonal rat pheochromocytoma cells. *European journal of pharmacology* 290, 3, 207–219.
- [315] Su, C., Tang, C., Ma, C., Shih, Y., Liu, C., and Wu, M. 1983. Quantitative structure-activity relationships and possible mechanisms of action of bispyridinium oximes as antidotes against pinacolyl methylphosphonofluoridate. *Fundamental and applied toxicology : official journal of the Society of Toxicology* 3, 4, 271–277.
- [316] Sullivan, J., Donnelly-Roberts, D., Briggs, C., Anderson, D., Gopalakrishnan, M., Piattoni-Kaplan, M., Campbell, J., McKenna, D., Molinari, E., Hettinger, A., Garvey, D., Wasicak, J., Holladay, M., Williams, M., and Arneric, S. 1996. A-85380 [3-(2(S)-azetidylmethoxy) pyridine]: in vitro pharmacological properties of a novel, high affinity alpha 4 beta 2 nicotinic acetylcholine receptor ligand. *Neuropharmacology* 35, 6, 725–734.
- [317] Sussman, J., Harel, M., and Silman, I. 1993. Three-dimensional structure of acetylcholinesterase and of its complexes with anticholinesterase drugs. *Chemico-Biological Interactions* 87, 1-3, 187–197.
- [318] Suzuki, J., Kohno, T., Tsukagosi, M., Furuhashi, T., and Yamazaki, K. 1997. Eighteen cases exposed to sarin in Matsumoto, Japan. *Internal medicine* 36, 7, 466–470.
- [319] Suzuki, T., Morita, H., Ono, K., Maekawa, K., Nagai, R., Yazaki, Y., Nozaki, H., Aikawa, N., Shinozawa, Y., Hori, S., Fujishima, S., Takuma, K., and Sagoh, M. 1995. Sarin poisoning in Tokyo subway. *The Lancet* 345, 8955, 980–981.
- [320] Szinicz, L. 2005. History of chemical and biological warfare agents. *Toxicology* 214, 3, 167–181.
- [321] Talbot, B., Anderson, D., Harris, L., Yarbrough, L., and Lennox, W. 1988. A comparison of in vivo and in vitro rates of aging of soman-inhibited erythrocyte acetylcholinesterase in different animal species. *Drug and chemical toxicology* 11, 3, 289–305.
- [322] Taly, A., Corringer, P., Guedin, D., Lestage, P., and Changeux, J. 2009. Nicotinic receptors: allosteric transitions and therapeutic targets in the nervous system. *Nature reviews. Drug discovery* 8, 9, 733–750.
- [323] Tammelin, L. 1958. Organophosphorylcholines and cholinesterases. *Ark Kemi*, 12, 287–298.
- [324] Tan, K. and Tashjian, A. 1984. Voltage-dependent calcium channels in pituitary cells in culture. I. Characterization by  $^{45}\text{Ca}^{2+}$  fluxes. *The Journal of biological chemistry* 259, 1, 418–426.
- [325] Tansey, E. 2006. Henry Dale and the discovery of acetylcholine. *Comptes rendus biologiques* 329, 5-6, 419–425.
- [326] Tashjian, A. 1979. Clonal strains of hormone-producing pituitary cells. *Methods in enzymology* 58, 527–535.
- [327] Tashjian, A., Bancroft, F., and Levine, L. 1970. Production of both prolactin and growth hormone by clonal strains of rat pituitary tumor cells. Differential effects of hydrocortisone and tissue extracts. *The Journal of cell biology* 47, 1, 61–70.

- [328] Tashjian, A., Yasumura, Y., Levine, L., Sato, G., and Parker, M. 1968. Establishment of clonal strains of rat pituitary tumor cells that secrete growth hormone. *Endocrinology* 82, 2, 342–352.
- [329] Tattersall J. 1993. Ion channel blockade by oximes and recovery of diaphragm muscle from soman poisoning in vitro. *British journal of pharmacology* 108, 4, 1006–1015.
- [330] Tattersall, J. 2016. Nicotinic Receptors as Targets for Nerve Agent Therapy. In *Chemical Warfare Toxicology: Volume 2: Management of Poisoning. Issues in Toxicology. Royal Society of Chemistry*, 82–119.
- [331] Taylor, P. and Lappi, S. 1975. Interaction of fluorescence probes with acetylcholinesterase. The site and specificity of propidium binding. *Biochemistry* 14, 9, 1989–1997.
- [332] Taylor, P., Radic, Z., Hosea, N., Camp, S., Marchot, P., and Berman, H. 1995. Structural bases for the specificity of cholinesterase catalysis and inhibition. *Toxicology letters* 82-83, 453–458.
- [333] Taylor, P., Wong, L., Radić, Z., Tsigelny, I., Brüggemann, R., Hosea, N., and Berman, H. 1999. Analysis of cholinesterase inactivation and reactivation by systematic structural modification and enantiomeric selectivity. *Chemico-Biological Interactions* 119-120, 3–15.
- [334] The American Society of Health-System Pharmacists. "Atropine". <https://www.drugs.com/monograph/atropine.html>. Accessed on 13 August 2015.
- [335] Thiermann, H., Aurbek, N., and Worek, F. 2016. Treatment of Nerve Agent Poisoning. In *Chemical Warfare Toxicology: Volume 2: Management of Poisoning. Issues in Toxicology. Royal Society of Chemistry*, 1–42.
- [336] Thiermann, H., Worek, F., and Kehe, K. 2013. Limitations and challenges in treatment of acute chemical warfare agent poisoning. *Chemico-Biological Interactions* 206, 3, 435–443.
- [337] Timmermann, D., Grønlien, J., Kohlhaas, K., Nielsen, E., Dam, E., Jørgensen, T., Ahring, P., Peters, D., Holst, D., Christensen, J., Chrsitensen, J., Malysz, J., Briggs, C., Gopalakrishnan, M., and Olsen, G. 2007. An allosteric modulator of the alpha7 nicotinic acetylcholine receptor possessing cognition-enhancing properties in vivo. *The Journal of pharmacology and experimental therapeutics* 323, 1, 294–307.
- [338] Timperley, C., Bird, M., Green, C., Price, M., Chad, J., Turner, S., and Tattersall, J. 2012. 1,1'-(Propane-1,3-diyl)bis(4-tert-butylpyridinium) di(methanesulfonate) protects guinea pigs from soman poisoning when used as part of a combined therapy. *Medicinal Chemical Communications* 3, 3, 352–356.
- [339] Tonini, R., Ferroni, A., Valenzuela, S., Warton, K., Campbell, T., Breit, S., and Mazzanti, M. 2000. Functional characterization of the NCC27 nuclear protein in stable transfected CHO-K1 cells. *FASEB journal : official publication of the Federation of American Societies for Experimental Biology* 14, 9, 1171–1178.
- [340] Törnquist, K. and Ekokoski, E. 1993. Intracellular free sodium concentrations in GH4C1 cells. *Journal of cellular physiology* 154, 3, 608–614.
- [341] Tougu, V. 2001. Acetylcholinesterase: Mechanism of Catalysis and Inhibition. *CMCCNSA* 1, 2, 155–170.
- [342] Tsai, P., Fox, N., Bigley, A., Harvey, S., Barondeau, D., and Raushel, F. 2012. Enzymes for the homeland defense: optimizing phosphotriesterase for the hydrolysis of organophosphate nerve agents. *Biochemistry* 51, 32, 6463–6475.
- [343] Tsuchihashi, H., Katagi, M., Nishikawa, M., and Tatsuno, M. 1998. Identification of metabolites of nerve agent VX in serum collected from a victim. *Journal of analytical toxicology* 22, 5, 383–388.
- [344] Tu, A. 2002. Chemical terrorism. Horrors in Tokyo subway and Matsumoto City. *Alaken*.

- [345] Tucker, J. 2006. War of nerves. Chemical warfare from World War I to al-Qaeda. *Pantheon Books*.
- [346] Tuovinen, K., Kaliste-Korhonen, E., Raushel, F., and Hänninen, O. 1999. Success of pyridostigmine, physostigmine, eptastigmine and phosphotriesterase treatments in acute sarin intoxication. *Toxicology* 134, 2-3, 169–178.
- [347] Turner, S., Chad, J., Price, M., Timperley, C., Bird, M., Green, A., and Tattersall, J. 2011. Protection against nerve agent poisoning by a noncompetitive nicotinic antagonist. *Toxicology letters* 206, 1, 105–111.
- [348] UK Ministry of Defence. 1987. Medical manual of defence against chemical agents. JSP 312. *HMSO*.
- [349] United Nations Treaty Collection. 1997. Convention on the prohibition of the development, production, stockpiling and use of chemical weapons and on their destruction. [https://treaties.un.org/pages/ViewDetails.aspx?src=TREATY&mtdsg\\_no=XXVI-3&chapter=26&clang=\\_en](https://treaties.un.org/pages/ViewDetails.aspx?src=TREATY&mtdsg_no=XXVI-3&chapter=26&clang=_en). Accessed 22 April 2017.
- [350] Unwin, N. 2005. Refined structure of the nicotinic acetylcholine receptor at 4 Å resolution. *Journal of molecular biology* 346, 4, 967–989.
- [351] Uteshev, V., Meyer, E., and Papke, R. 2002. Activation and inhibition of native neuronal alpha-bungarotoxin-sensitive nicotinic ACh receptors. *Brain research* 948, 1-2, 33–46.
- [352] Vaca, L. and Sampieri, A. 2002. Calmodulin modulates the delay period between release of calcium from internal stores and activation of calcium influx via endogenous TRP1 channels. *The Journal of biological chemistry* 277, 44, 42178–42187.
- [353] Vale, J., Rice, P., and Marrs, T. 2007. Managing Civilian Casualties Affected by Nerve Agents. In *Chemical Warfare Agents*. John Wiley & Sons, 249–260.
- [354] van der Schans, M., Benschop, H., and Whalley, C. 2007. Toxicokinetics of Nerve Agents. In *Chemical Warfare Agents*. John Wiley & Sons 97-118.
- [355] van der Schans, M., Lander, B., van der Wiel, H., Langenberg, J., and Benschop, H. 2003. Toxicokinetics of the nerve agent (+/-)-VX in anesthetized and atropinized hairless guinea pigs and marmosets after intravenous and percutaneous administration. *Toxicology and applied pharmacology* 191, 1, 48–62.
- [356] van Helden, H., Busker, R., Melchers, B., and Bruijnzeel, P. 1996. Pharmacological effects of oximes: how relevant are they? *Archives of toxicology* 70, 12, 779–786.
- [357] van Helden, H., Van Der Wiel, H., de Lange, J., Busker, R., Melchers, B., and Wolthuis, O. 1992. Therapeutic efficacy of HI-6 in soman-poisoned marmoset monkeys. *Toxicology and applied pharmacology* 115, 1, 50–56.
- [358] Vernino, S., Amador, M., Luetje, C., Patrick, J., and Dani, J. 1992. Calcium modulation and high calcium permeability of neuronal nicotinic acetylcholine receptors. *Neuron* 8, 1, 127–134.
- [359] Veterans Today. 2015. *ISIS stole sarin gas from Lybia & has already used it, Gaddafi's cousin*. <http://www.veteranstoday.com/2015/12/19/isis-stole-sarin-gas-from-libya-stores-has-already-used-it-gaddafis-cousin>. Accessed 22 April 2017.
- [360] Wadia, R., Sadagopan, C., Amin, R., and Sardesai, H. 1974. Neurological manifestations of organophosphorous insecticide poisoning. *Journal of neurology, neurosurgery, and psychiatry* 37, 7, 841–847.
- [361] Wang, H., Yu, M., Ochani, M., Amella, C., Tanovic, M., Susarla, S., Li, J., Yang, H., Ulloa, L., Al-Abed, Y., Czura, C., and Tracey, K. 2003. Nicotinic acetylcholine receptor alpha7 subunit is an essential regulator of inflammation. *Nature* 421, 6921, 384–388.

- [362] Wang, X. and Li, M. 2003. Automated electrophysiology: high throughput of art. *Assay and drug development technologies* 1, 5, 695–708.
- [363] Wanner, K., Rappenglück, S., Sichler, S., Scheffel, C., Seeger, T., and Niessen, K. V. 2016. Zwischenbericht - Wirkstoffsuche. *Institut für Pharmakologie und Toxikologie der Bundeswehr*.
- [364] Ward, J., Cockcroft, V., Lunt, G., Smillie, F. S., and Wonnacott, S. 1990. Methyllycaconitine: a selective probe for neuronal alpha-bungarotoxin binding sites. *FEBS letters* 270, 1-2, 45–48.
- [365] Watson, A., Bakshi, K., Opresko, D., Young, R., Hauschild, V., and King, J. 2006. Cholinesterase Inhibitors as Chemical Warfare Agents. In *Toxicology of Organophosphate & Carbamate Compounds*. Elsevier, 47–68.
- [366] Watson, A., Opresko, D., Young, R., Hauschild, V., King, J., and Bakshi, K. 2009. Organophosphate Nerve Agents. In *Handbook of Toxicology of Chemical Warfare Agents*. Elsevier, 43–67..
- [367] Waxman, S. 2007. Molecular neurology. *Elsevier*.
- [368] Weiser, T. 2006. Comparison of the effects of four Na<sup>+</sup> channel analgesics on TTX-resistant Na<sup>+</sup> currents in rat sensory neurons and recombinant Nav1.2 channels. *Neuroscience letters* 395, 3, 179–184.
- [369] Wessely, S., Hotopf, M., and Sharpe, M. 1999. Chronic fatigue and its syndromes. *Oxford University Press*.
- [370] Willems, J., Langenberg, J., Verstraete, A., de Loose, M., Vanhaesebroeck, B., Goethals, G., Belpaire, F., Buylaert, W., Vogelaers, D., and Colardyn, F. 1992. Plasma concentrations of pralidoxime methylsulphate in organophosphorus poisoned patients. *Archives of toxicology* 66, 4, 260–266.
- [371] Williams, D., Wang, J., and Papke, R. 2011. Investigation of the molecular mechanism of the  $\alpha 7$  nicotinic acetylcholine receptor positive allosteric modulator PNU-120596 provides evidence for two distinct desensitized states. *Molecular pharmacology* 80, 6, 1013–1032.
- [372] Williams, D., Wang, J., and Papke, R. 2011. Positive allosteric modulators as an approach to nicotinic acetylcholine receptor-targeted therapeutics: Advantages and limitations. *Biochemical pharmacology* 82, 8, 915–930.
- [373] Williams, M., Burton, B., Urrutia, A., Shcherbatko, A., Chavez-Noriega, L., Cohen, C., and Aiyar, J. 2005. Ric-3 promotes functional expression of the nicotinic acetylcholine receptor alpha7 subunit in mammalian cells. *The Journal of biological chemistry* 280, 2, 1257–1263.
- [374] Wilson, I. and Ginsburg, B. 1955. A powerful reactivator of alkylphosphate-inhibited acetylcholinesterase. *Biochimica et biophysica acta* 18, 1, 168–170.
- [375] Witzemann, V., Barg, B., Nishikawa, Y., Sakmann, B., and Numa, S. 1987. Differential regulation of muscle acetylcholine receptor gamma- and epsilon-subunit mRNAs. *FEBS letters* 223, 1, 104–112.
- [376] Wolfe, A., Rush, R., Doctor, B., Koplovitz, I., and Jones, D. 1987. Acetylcholinesterase prophylaxis against organophosphate toxicity. *Fundamental and applied toxicology : official journal of the Society of Toxicology* 9, 2, 266–270.
- [377] Wonnacott, S. and Barik, J. 2007. Nicotinic ACh Receptors. *Tocris Reviews*, 28.
- [378] Worek, F., Aurbek, N., Wetherell, J., Pearce, P., Mann, T., and Thiermann, H. 2008. Inhibition, reactivation and aging kinetics of highly toxic organophosphorus compounds: pig versus minipig acetylcholinesterase. *Toxicology* 244, 1, 35–41.
- [379] Worek, F., Eyer, P., Aurbek, N., Szinicz, L., and Thiermann, H. 2007. Recent advances in evaluation of oxime efficacy in nerve agent poisoning by in vitro analysis. *Toxicology and applied pharmacology* 219, 2-3, 226–234.

- [380] Worek, F., Eyer, P., Kiderlen, D., Thiermann, H., and Szinicz, L. 2000. Effect of human plasma on the reactivation of sarin-inhibited human erythrocyte acetylcholinesterase. *Archives of toxicology* 74, 1, 21–26.
- [381] Worek, F., Reiter, G., Eyer, P., and Szinicz, L. 2002. Reactivation kinetics of acetylcholinesterase from different species inhibited by highly toxic organophosphates. *Archives of toxicology* 76, 9, 523–529.
- [382] Worek, F., Seeger, T., Goldsmith, M., Ashani, Y., Leader, H., Sussman, J. S., Tawfik, D., Thiermann, H., and Wille, T. 2014. Efficacy of the rePON1 mutant IIG1 to prevent cyclosarin toxicity in vivo and to detoxify structurally different nerve agents in vitro. *Archives of toxicology* 88, 6, 1257–1266.
- [383] Worek, F., Szinicz, L., Eyer, P., and Thiermann, H. 2005. Evaluation of oxime efficacy in nerve agent poisoning: development of a kinetic-based dynamic model. *Toxicology and applied pharmacology* 209, 3, 193–202.
- [384] Worek, F., Thiermann, H., and Wille, T. 2016. Oximes in organophosphate poisoning: 60 years of hope and despair. *Chemico-Biological Interactions* 259, 93–98.
- [385] Worek, F., Wille, T., Aurbek, N., Eyer, P., and Thiermann, H. 2010. Reactivation of organophosphate-inhibited human, Cynomolgus monkey, swine and guinea pig acetylcholinesterase by MMB-4: a modified kinetic approach. *Toxicology and applied pharmacology* 249, 3, 231–237.
- [386] Worek, F., Wille, T., Koller, M., and Thiermann, H. 2016. Toxicology of organophosphorus compounds in view of an increasing terrorist threat. *Archives of toxicology* 90, 9, 2131–2145.
- [387] Wright, L., Pope, C., and Liu, J. 2009. The Nervous System as a Target for Chemical Warfare Agents. In *Handbook of Toxicology of Chemical Warfare Agents*. Elsevier, 463–480.
- [388] Wright, S. 2004. Generation of resting membrane potential. *AJP: Advances in Physiology Education* 28, 4, 139–142.
- [389] Wright, P. 1954. An analysis of the central and peripheral components of respiratory failure produced by anticholinesterase poisoning in the rabbit. *The Journal of physiology* 126, 1, 52–70.
- [390] Wu, S., Ho, L., Li, H., and Chiang, H. T. 2000. Regulation of Ca<sup>2+</sup>-activated K<sup>+</sup> currents by ciglitazone in rat pituitary GH3 cells. *Journal of investigative medicine : the official publication of the American Federation for Clinical Research* 48, 4, 259–269.
- [391] Wu, S., Li, H., and Jan, C. 1998. Regulation of Ca<sup>2+</sup>-activated nonselective cationic currents in rat pituitary GH3 cells: involvement in L-type Ca<sup>2+</sup> current. *Brain research* 812, 1-2, 133–141.
- [392] Wu, S., Li, H., Jan, C., and Shen, A. 1999. Inhibition of Ca<sup>2+</sup>-activated K<sup>+</sup> current by clotrimazole in rat anterior pituitary GH3 cells. *Neuropharmacology* 38, 7, 979–989.
- [393] Xu, X., Nagarajan, H., Lewis, N. E., Pan, S., Cai, Z., Liu, X., Chen, W., Xie, M., Wang, W., Hammond, S., Andersen, M., Neff, N., Passarelli, B., Koh, W., Fan, H., Wang, J., Gui, Y., Lee, K. H., Betenbaugh, M., Quake, S., Famili, I., Palsson, B., and Wang, J. 2011. The genomic sequence of the Chinese hamster ovary (CHO)-K1 cell line. *Nature biotechnology* 29, 8, 735–741.
- [394] Yang, H., Zhang, G., and Cui, J. 2015. BK channels: multiple sensors, one activation gate. *Frontiers in Physiology* 6, 532, 746.
- [395] Zhang, J., Xiao, Y., Abdrakhmanova, G., Wang, W., Cleemann, L., Kellar, K. J., and Morad, M. 1999. Activation and Ca<sup>2+</sup> permeation of stably transfected alpha3/beta4 neuronal nicotinic acetylcholine receptor. *Molecular pharmacology* 55, 6, 970–981.

